Development, Characterization and Transcriptional Profiling of a Mouse Model of Fatal Infectious Diarrhea and Colitis.

by

Diana Borenshtein

M.Sc. Nutritional Sciences, 1999
B.Sc. Nutritional Sciences, 1995
The Hebrew University of Jerusalem, Israel

SUBMITTED TO THE DEPARTMENT OF BIOLOGICAL ENGINEERING IN PARTIAL FULFILLMENT OF THE REQUIREMENTS FOR THE DEGREE OF

DOCTOR OF PHILOSOPHY IN MOLECULAR AND SYSTEMS TOXICOLOGY

at the

MASSACHUSETTS INSTITUTE OF TECHNOLOGY
February 2007

Signature of Author _____
Biological Engineering Division
December 1, 2006

Certified by _____
David B. Schauer
Professor of Biological Engineering
Thesis Supervisor

Accepted by _____
Ram Sasisekharan
Professor of Biological Engineering
Chairman, Committee for Graduate Students

This doctoral thesis has been examined by a committee of the department of Biological Engineering as follows:

Certified by _____

Professor James G. Fox, MIT
Chairman

Certified by _____

Professor James L. Sherley, MIT

Certified by _____

Professor Eric J. Rubin, Harvard School of Public Health

Development, Characterization and Transcriptional Profiling of a Mouse Model of Fatal Infectious Diarrhea and Colitis

by

Diana Borenshtein

Submitted to the Biological Engineering Division on December 1, 2006
in Partial Fulfillment of the Requirements
for the Degree of Doctor of Philosophy in Molecular and Systems Toxicology

Abstract

Citrobacter rodentium is a naturally occurring murine bacterial pathogen which is used to model human diarrheagenic *E. coli* (EPEC and EHEC) infections in mice. *C. rodentium* causes colonic hyperplasia and a variable degree of colitis and mortality in the majority of inbred and outbred lines of mice. Differences in *C. rodentium*-induced disease are determined by the genetic background of the host.

Here, *C. rodentium* infection in resistant outbred Swiss Webster (SW) mice was compared with infection in the cognate inbred FVB strain for the first time. In contrast to subclinical infection in SW mice, adult FVB mice developed overt disease with significant weight loss, severe colitis, and over 75% mortality. Fluid therapy intervention completely prevented mortality in FVB mice, and expression of pro-inflammatory and immunomodulatory genes in the colon was similar in both lines of mice, suggesting that mortality in *C. rodentium*-infected FVB mice is due to hypovolemia resulting from severe dehydration.

To identify host factors responsible for the development of mortality, gene expression in the distal colon of FVB and SW mice was investigated using a whole mouse genome Affymetrix array. Transcripts represented by 1,547 probe sets (3.4%) were differentially expressed between FVB and SW mice prior to infection and at 4 and 9 days post-inoculation. Data analysis suggested that intestinal ion disturbances rather than immune-related processes are responsible for susceptibility in *C. rodentium*-infected FVB mice. Marked impairment in intestinal ion homeostasis predicted by microarray analysis was confirmed by quantitative RT-PCR and serum electrolyte measurements that showed hypochloremia and hyponatremia in susceptible FVB mice.

C. rodentium infection was next characterized in additional inbred strains of Swiss origin. SWR and SJL mice developed minimal morbidity and no mortality in response to the pathogen, demonstrating resistance to disease. Furthermore, C3H mice developed severe diarrhea and gene expression changes comparable to those in infected FVB mice, suggesting common pathogenic mechanisms in susceptible strains.

In conclusion, *C. rodentium* infection in FVB mice is a useful model for fatal infectious diarrhea. These studies contribute to our understanding of *C. rodentium* pathogenesis and identify possible candidates for susceptibility to fatal enteric bacterial infection.

Thesis supervisor: David B. Schauer
Title: Professor of Biological Engineering

Acknowledgements

I dedicate my Ph.D to my lovely husband, whose support and inspiration were so vital for me. I cannot explain how much his love, patience, and support mean to me. I am grateful for his understanding of my needs and accepting my chosen path. I hope he felt (at least most of the time) that he and our family are still my first priority. We have wonderful kids and, being a busy Ph.D student mother, I've enjoyed every moment I spent with my family. I am in deep debt to my parents, who raised me and made all the possible (and impossible) for my education. I also want to recognize my sister, a great friend and which hopefully will follow my steps.

I was very fortunate to have a wonderful advisor, Prof. David Schauer. David has guided me in my research and was an excellent mentor the past 5 years of my life at MIT. David's knowledge and experience were always there for me. Thanks for suffering my annoyance, supporting my crazy ideas and providing the freedom to conduct experiments the way I did. I also thank him for understanding the needs of a mother-student and supporting me during my complicated pregnancy. This meant a lot to me and I am grateful for that.

I express my gratitude to my thesis committee members Prof. James Fox, Prof. James Sherley, and Prof. Eric Rubin for giving me their time and input. Their suggestions throughout my dissertation time were valuable and helped to increase the depth of understanding in my research field.

I had an opportunity to collaborate with many distinguished scientists. I thank Prof. Leona Samson, Dr. Lisiane Meira, and Dr. Rebecca Fry for their time and fruitful discussions. Selected parts of our collaborative work are presented here and hopefully will be published soon. I've become such good friends with Lisi and Becky, and their help and support was valuable to me. I also enjoyed working with Dr. Elena Gostjeva. We found interesting observations and our long chats in the corridors were always interesting to me. Also, I thank Dr. Michael B. Sporn, Dartmouth Medical School for providing anti-inflammatory compounds for our dietary intervention project. In addition, I had an exciting experience collaborating with Dr. Stephen Collins from McMaster University Medical Center, Canada, though not presented in this thesis. I have to recognize help from the microarray facilities of the Whitehead Institute including Tom Volker, the manager, and especially Jen Love, who processed all my microarray samples. Also, I appreciate time and effort of Dr. Sampsa Hautaniemi from BE, MIT, Prof. Vincent Carey from Harvard Medical School, and Prof. Ernest Fraenkel from BE, MIT, who consulted in analysis of the microarray data.

One of the very important things in graduate student life is your lab. My time in MIT has flown past with such a pleasure thanks to many past and present members of the Schauer Lab including Jane Sohn, Ming Chen, Katie Schlieper, Hilda "Scooter" Holcombe, Liz Groff (Colgan), Claude Nagamine, Nancy Guillen, Alex Sheh, Rongcong Wu, Allison Vitsky, Kristen Jellison, Steven Luperchio, and Petra Bertilsson. Thanks to their professional expertise and the fun time we all had together. I thank UROP students, Yuri Matsumoto, Maya Hasan, Joanne Lai, Kriti Jain, and Patricia Zheng. I learned a lot from you and my experience working with you. Kim Knox, in addition of being a highly professional technician and lab manager, we spent time being pregnant

together and I wish you and all your family happiness and great health. Special thanks to Solveig Ravnum and Megan McBee – my dear chatting friends, you made my life in the lab really enjoyable.

I would like to recognize the staff of DCM, especially our veterinary pathologists Dr. Prashant Nambiar, Dr. Barry Rickman and Dr. Arlin Rogers, who collaborated with me on the work presented here. I highly appreciate the professionalism and hard work of the histology lab, managed by Kathy Cormier and staffed with Kate Rydstrom, Chakib Boussahmain, Ernie Smith, Jeff Bajko, Erinn Stefanich, and Bobi Young. I also recognize the hard work and tremendous help by animal facility crew including Gladys Valeriano (Martinez), Kevin Milne, Herber Villanueva, Jarlin Lemus and Melissa Topolszki, Leslie Hopper, Kris Hewes, Kibibi Rwayitare and Jennifer Statile. Other people in DCM that assisted me along the way were Dr. Yan Feng, Dr. Zhonming Ge, Ellen Buckley, Sue Chow, Jim Yang, Glenda Inciong, Dr. Sam Boutin, and Dr. Laura Lemke.

Our department benefits from the help of wonderful people. I thank Marcia Weir, Olga Parkin, Amy Francis, Pat Brown, Christian Rheault, Kay Walsh, JoAnn Sorrento, Mariann Murray, Roni Dudley-Cowans, Kerry Forristall, Kim Bond Schaefer, Debra Luchanin, and Dalia Gabour for their help, assistance and great time in MIT. None of this would be possible without the guidance and excellent management by the director of ex-Division and now a Department of Biological Engineering, Doug Lauffenburger.

I was privileged to become a Biogen Idec, Inc. fellow in 2004-2005 academic year. Special thanks to Dr. James Green, Dr. David Hutto, my mentor, Sarah Vincent, and Prof. Pete Dedon, the coordinator of the program.

There were many people who helped me in my pre-MIT life. I acknowledge my master thesis advisor Prof. Zecharia Madar and Dr. Aliza Stark from the Faculty of Agriculture, The University of Hebrew University, Israel. Their guidance initiated my scientific career. I thank Prof. Leo Herzenberg and Dr. David Voehringer for allowing me to volunteer at Stanford. This experience was very beneficial to me. I also would like to recognize Prof. Michal Schwartz from Weizmann Institute for a great supervision during my work in her biotech company. She served as a model of female scientist I would like to be.

I want to acknowledge many numerous MIT friends that walked with me through both good and bad times of graduate school. The list is quite long. But in addition to some of the names mentioned above, I would like to acknowledge specially Rouzbeh Taghizadeh, Sundina Nataliya, and Alina Berdichevsky. They have been wonderful friends and I will always keep the memories about our time together in MIT. I also have many friends in Israel and USA that supported me during this time as well. Special thanks to Dr. Larisa Sokolov and Dr. Igor Sokolov, who were my first teachers in science and guided and followed me along this way.

I acknowledge support from PHS grants P01 CA26731, T32 ES07020, and P30 ES02109.

Thanks to everybody and to those I inadvertently neglected to mention, for all their efforts and support!

Table of Contents

List of Figures

List of Tables

Chapter 1: Introduction

Citrobacter rodentium (C. rodentium) is a naturally occurring bacterial pathogen of laboratory mice. It is a murine homolog of enteropathogenic *Escherichia coli (E. coli)* and enterohemorrhagic *E. coli* (EPEC and EHEC, respectively), and hence is highly useful in modeling these human infections in mice. In addition, this organism elicits signal transduction events in host that lead to cell cytoskeletal rearrangements, changes in epithelial proliferative capacity and inflammatory responses of the host. Therefore, studies evolving *C. rodentium* are indispensable for elucidating the mechanisms of host-pathogen interactions, inflammation and tumor promotion. Below, I discuss recent advances in *C. rodentium* infection research [reviewed in details in Luperchio and Schauer, 2001 and Mundy et al., 2005].

C. rodentium causes transmissible murine colonic hyperplasia

C. rodentium encompasses all of the isolates previously designated as atypical *C. freundii, C. freundii* biotype 4280, and mouse pathogenic *E. coli* (MPEC) [Luperchio and Schauer, 2001]. This organism was originally isolated in the 1960-1970s during outbreaks of diarrhea and rectal prolapse in mouse colonies in the United States and Japan [Barthold et al., 1976; Brennan et al., 1965; Ediger et al., 1974; Itoh et al., 1978; Muto et al., 1969; Nakagawa et al., 1969; Silverman et al., 1979]. The disease caused by *C. rodentium* is primarily characterized by epithelial cell hyperproliferation and, hence, named transmissible murine colonic hyperplasia (TMCH). The degree of inflammation is variable in mice of different ages, strains, and microbiota, and therefore is not considered a main feature of the disease (Luperchio and Schauer, 2001]. Infection in most adult mice is self-limiting and accompanied by little or no clinical signs and minimal mortality. In contrast, suckling mice and substrains of C3H mice are more susceptible and develop severe morbidity and high mortality rate [Barthold et al., 1976; Barthold et al., 1977; Barthold et al., 1978; Barthold, 1980; Muto et al., 1969; Nakagawa et al., 1969]. Clinical signs usually include retarded growth, diarrhea, dehydration, coat ruffling, hunched posture, reluctance to move, recumbency, and in some cases rectal prolapse (Figure 1-1). A

detailed description of the progression of infection is summarized in [Luperchio and Schauer, 2001].

C. rodentium infection as a model for proliferative bowel disease

The ability of the pathogen to induce hyperplasia in the distal colon can be explained by alterations in cell kinetics of colonic epithelium of infected mice. *C. rodentium*-infected animals demonstrate expansion of the proliferative zone and 2- to 4-fold increase in labeling index in distal colon, which are similar to alterations observed in idiopathic inflammatory bowel diseases (IBD) [Barthold, 1979; Barthold and Beck, 1980; Barthold et al., 1977; Barthold et al., 1978]. Moreover, colon tumorigenesis is promoted in DMH-treated animals or *Apc*$^{Min/+}$ mice infected with *C. rodentium* [Barthold and Beck, 1980; Barthold and Jonas, 1977; Newman et al., 2001]. In addition, alterations in β-catenin pathway [Sellin et al., 2001] and increased mutation rate [Sohn, 2005] are observed in infected mice. Therefore, *C. rodentium* infection can serve as a good model for human diseases with predisposition to colorectal cancers, such as IBD [Bernstein et al., 2001; Riddel et al., 1983; Rutter et al., 2004].

C. rodentium as a model for human attaching and effacing pathogenic *E. coli*

The new era in TMCH research started with the discovery of attaching and effacing (A/E) lesions in the distal colon of infected mice and responsible virulence factors [Schauer and Falkow, 1993a; Schauer and Falkow, 1993b]. A/E lesions are characterized by intimate attachment of bacteria to the host epithelium, effacement of microvilli and production of pedestal-like structures beneath the adherent bacteria (Figure 1-2, panels A-C) [Frankel et al., 1998; Nataro and Kaper, 1998; Schauer and Falkow, 1993a; Schauer and Falkow, 1993b]. This ascribed *C. rodentium* to the family of diarrheagenic A/E bacterial pathogens comprised of EPEC, an important cause of infant diarrhea in developing countries, EHEC, which causes hemorrhagic colitis, hemolytic uremic syndrome and outbreaks of food- and water-borne disease, as well as the rabbit enteropathogenic *E. coli* (REPEC) [Nataro and Kaper, 1998; Vallance and Finlay, 2000]. Since EPEC and EHEC do not readily infect laboratory mice [Frankel et al., 1996; Klapproth et al., 2005; Mundy et al., 2006], studies with *C. rodentium* in mice are highly valuable for elucidating the mechanisms of human EPEC and EHEC infections. *E. coli* in rabbits, pigs and cattle can produce similar diseases, but the cost of these studies, as well as the

limited genetic and immunological reagents available for these animals constrain the use of these host species [Vallance and Finlay, 2000]. In this respect, *C. rodentium* offers an advantage as a murine pathogen, providing a relevant and practical animal model with a wide array of available reagents, including antibodies, recombinant cytokines, and gene knockout strains.

Virulence factors in A/E pathogenesis

Development of A/E lesions depends on a type III secretion system apparatus (TTSS), a common virulence mechanism for many human and plant pathogens [reviewed in Frankel et al., 1998; Garmendia et al., 2005]. TTSS allows translocation of bacterial effector proteins into host epithelial cells, altering signaling processes (Figure 1-2D, Table 1-1). The TTSS is encoded by the locus of enterocyte effacement (LEE), which is shared by all A/E pathogens and contains all of the genes necessary for A/E lesion formation and intimate attachment [Deng et al., 2001; Deng et al., 2004; Frankel et al., 1998; Luperchio et al., 2000; Nataro and Kaper, 1998]. This includes the main structural components of the bacterial TTSS, such as EspA, EspB, and EspD; the outer membrane adhesin intimin and its translocated intimin receptor (Tir), effector proteins, including EspB, EspF, Map and others, as well as transcriptional regulators, and other polypeptides of currently unknown functions (Figure 1-2E, Table 1-1) [Deng et al., 2001; Deng et al., 2003; Deng et al., 2004; Garmendia et al., 2005; Newman et al., 1999; Schauer and Falkow, 1993b]. A number of non-LEE-encoded (Nle) proteins were recently identified as potential effectors, of which NleA and NleB were defined as important virulence determinants [Deng et al., 2004; Gruenheid et al., 2004; Kelly et al., 2006]. In addition, all A/E pathogens including *C. rodentium* have been shown to suppress *in vitro* host immune responses via a novel toxin lymphostatin, alternatively known as EHEC factor for adherence, which is encoded by *lifA*/*efa1* gene outside of LEE [Klapproth et al., 2000; Malstrom and James, 1998]. *In vivo* analysis of *lifA*/*efa1* mutants suggests the possible role of lymphostatin in bacterial colonization, clinical manifestation of disease, epithelial cell proliferation and colonic inflammation [Klapproth et al., 2005]. Signature-tagged transposon mutagenesis and proteomic analysis were performed to identify *C. rodentium*-specific virulence factor(s). Homologs of NleG effector protein, previously found in *C. rodentium* proteome only [Deng et al., 2004], were recently discovered in EPEC and EHEC as well [Tobe et al., 2006]. The *cfc* (colonization factor *Citrobacter*) encodes for the CFC type IV pilus and is the only *C. rodentium*-specific gene

known for today [Mundy et al., 2003]. CFC was suggested to play a role in colonization, infection, transmission or host specificity. Although the gene is absent from EHEC, its product shares identity to proteins of the type IV COF pilus of enterotoxigenic *E. coli* (ETEC), the toxin co-regulated pilus (TCP) of *Vibrio cholerae* and the bundle-forming pilus (BFP) of EPEC [Mundy et al. 2003], demonstrating again high conservation of virulence determinants among diarrheagenic pathogens.

C. rodentium and host defense

The advances in genome manipulations allowed production of various knockout/ transgenic mouse strains that facilitated research in immune-related aspects of *C. rodentium* infection (summarized in Table 1-2) [reviewed in MacDonald et al., 2003; Mundy et al., 2005]. In wild-type animals, the bacteria colonize the colon reaching ~10^9 CFU/g tissue around 7-14 days post-infection (DPI). The infection is cleared by about 3-4 weeks thereafter [Luperchio and Schauer, 2001; MacDonald et al., 2003]. Mice that recover from infection are generally resistant to rechallenge with the pathogen [Ghaem-Maghami et al., 2001; Maaser et al., 2004]. $CD4^+$ T cells, B cells, and IgG, but not secretory IgA or IgM, are critical for the protection against this infection [Bry et al., 2006; Bry and Brenner, 2004; ; Maaser et al., 2004; MacDonald et al., 2003; Simmons et al., 2003; Vallance et al., 2002b]. Innate immunity is also vital, as mast cell-deficient animals develop septicemia and rapidly succumb in response to *C. rodentium* [Wei et al., 2005]. This effect is not mediated by murine cathelicidin-related antimicrobial peptide expressed by mast cells because *Cnlp*-knockout mice are comparable to their wild-type counterparts [Iimura et al., 2005]. In contrast to mast cell-deficient mice, animals lacking TNF-α, IFN-γ, iNOS and IL-12 signaling usually clear the infection from colon and extra-intestinal tissues [Bry et al., 2006; Goncalves et al., 2001; Simmons et al., 2002; Vallance et al., 2002a], indicating that these components of the innate immunity are not required for survival, though important for development of clinical signs and colonic lesions. The Th1 response elicited by the pathogen as well as changes in cell kinetics, which are comparable to those seen in colitis patients, make *C. rodentium* infection an attractive animal model for studying the mechanisms of IBD.

C. rodentium as a model for diarrhea

Acute infectious diarrhea is one of the most common causes of death worldwide, mainly affecting children in developing countries [Kosek et al., 2003; Lopez et al., 2006; WHO, 1999]. Diarrhea may result in rapid dehydration, decreased circulating plasma volume, increased blood viscosity and development of hypovolemic shock [Guyton, 1991; Mello et al., 2004]. Blood losses of more than 10% diminish cardiac output and pressure, which stimulates sympathetic vasoconstrictor system throughout the body in order to prevent deterioration of the circulation. These compensatory mechanisms make tissues more susceptible to local ischemia and may fail when volume loss is higher than 25%. Eventually, systemic activation of inflammatory cascade when volume losses exceed 40% results in irreversible multiple organ failure and death [Guyton, 1991; Mello et al., 2004]. With the exception of intestinal pathogens that possess enterotoxins, the mechanisms responsible for intestinal dysfunction during infections with many bacteria remain largely unestablished. Mice are generally considered inappropriate for studying watery diarrhea induced by many human pathogens. Thus, EPEC, EHEC, enterotoxigenic *E. coli* (ETEC), *Vibrio cholera*, *Campylobacter jejuni, Shigella* and *Salmonella* spp., as well as rotavirus, either fail to efficiently colonize mice or rarely cause appreciable diarrhea, unless young mice (newborn and suckling) or manipulated mice (fasted, germ-free, pretreated with antibiotics, iron, and acidity reducing agents) are used [Allen et al., 2006; Baqar et al., 2000; Frankel et al., 1996; Klapproth et al., 2005; Kordasti et al., 2006; Mundy et al., 2006; Okuda et al., 1997; Santos et al., 2003; Shimamura et al., 1981; Singer and Sansonetti, 2004; Zhang et al., 2003]. Therefore, exploring the pathogenesis of acute diarrheal illness is complicated due to lack of suitable small animal model.

Although initial outbreaks of *C. rodentium* were associated with diarrhea-like symptoms [Barthold et al., 1976; Brennan et al., 1965; Ediger et al., 1974; Itoh et al., 1978; Muto et al., 1969; Nakagawa et al., 1969; Silverman et al., 1979], studies elucidating the pathogenesis of this microorganism for many years have focused on signal transduction and host immune responses. Only recently, modeling of diarrhea using *C. rodentium*-infected mice have received greater attention. The mechanisms of diarrhea development in TMCH, as well as in infection with pathogenic *E. coli,* are not clear. The working hypothesis for EPEC and EHEC infections [Vallance and Finlay, 2000; Garmendia et al., 2005] consists of loss of absorptive epithelium, alterations in tight junction integrity, changes in ion transport, especially of chloride and

bicarbonate, and increased permeability and tissue damage as a consequence of the inflammatory response (Figure 1-3). Similarly, disruption of tight junctions is found in *C. rodentium*-infected mice. The effect does not depend on the inflammatory status of the host and is mediated by EspF and Map effector proteins [Guttman et al., 2006a; Guttman et al., 2006b; Ma et al., 2006]. Recent results from the same lab indicate involvement of water channels, aquaporins, in *C. rodentium*-induced pathogenesis [Guttman et al., 2007]. In addition, interaction of bacterial effector Map with host Na^+/H^+ exchanger regulatory factor 1 (NHERF1), responsible for regulation of ion channels in the intestine [Simpson et al., 2006], further implicates *C. rodentium*-induced transport changes in the development of diarrhea in infected animals. Considering the severe consequences of diarrhea, *C. rodentium*-infected mice may serve as indispensable model for this life-threatening condition.

Factors affecting disease outcome

C. rodentium infection is influenced by age, diet, genetic background and microbiota status, but not by gender. Thus, the disease is more severe in young mice and rapidly fatal in suckling animals [Barthold, 1980; Barthold et al., 1976; Barthold et al., 1978; D'Arienzo et al., 2006; Muto et al., 1969; Nakagawa et al., 1969]. This is particularly significant when infections are performed in immune-knockout mice. Weanling mice develop high mortality most likely due to overwhelming sepsis [Bry and Brenner, 2004; Vallance et al., 2002b]. Adult animals with same immune deficiencies, though fail to clear the infection properly, mainly develop diarrhea and little or no mortality [Maaser et al., 2004; Simmons et al., 2003].

The role of diet was addressed in only two reports. In the first, infected animals on different diets developed significantly different hyperplastic responses. However, the composition of the diets was unknown, and factor(s) mediating distinct proliferating responses were not discussed [Barthold et al., 1977]. The second more recent study investigated molecular consequences of calcium and the soluble fiber pectin administration to *C. rodentium*-inoculated mice [Umar et al., 2003]. Although clinical disease was not affected by dietary intervention, both high-calcium and pectin-rich diets inhibited proliferation and crypt length increases in colonic epithelium. Moreover, a pectin-rich diet inhibits increases in cellular β-catenin, cyclin D1 and c-myc levels, further supporting the anti-proliferative effects of pectin in *C. rodentium*-infected mice [Umar et al., 2003].

TMCH is also sensitive to intestinal flora and different disease outcomes were reported in germ-free, specific pathogen free (barrier), antibiotics-pretreated and conventionally maintained animals [Bathold et al., 1977; Itoh et al., 1978; Itoh et al., 1979; Itoh et al., 1980; Luperchio and Schauer, 2001]. More recently, the protective effects of prophylactic administration of probiotics on *C. rodentium* colonization, translocation, colonic hyperplasia and inflammation were shown [Chen et al., 2005b; D'Arienzo et al., 2006; Johnson-Henry et al., 2005; Varcoe et al., 2003]. On the other hand, concurrent infection with intestinal helminths was reported to augment *C. rodentium*-induced disease [Chen et al., 2005a; Chen et al., 2006]. Therefore, host colonic microflora can define the disease outcome and manipulating the mice with probiotics and concurrent infection with other organisms may ameliorate or exacerbate the disease progress.

Finally, susceptibility to *C. rodentium* infection is highly dependent on the genetic background of the host [Barthold et al., 1977; Itoh et al., 1979; Itoh et al., 1980; Itoh et al., 1988; Khan et al., 2006; Vallance et al., 2003]. Among many strains used for modeling TMCH (Figure 1-4), outbred Swiss Webster (NIH Swiss), and inbred C57BL/6 and C3H mice are the best characterized. Outbred Swiss mice show subclinical infection with primarily significant hyperplasia and little or no evidence of inflammation. C57BL/6 mice, used as a common control strain in transgenic studies, are relatively resistant. Infected C57BL/6 mice do not exhibit profound hyperplastic response, but develop clinical signs and have more substantial colitis. Substrains of C3H mice, regardless of their TLR4 (LPS responsiveness) status, are highly susceptible to *C. rodentium*, develop necrotic colitis and severe mortality that was proposed to be caused by disseminated infection [Barthold et al., 1977; Itoh et al., 1988; Khan et al., 2006; Vallance et al., 2003]. Because outbred mice are genetically heterogeneous compared with inbred animals, and C57BL/6 and C3H mice belong to different genealogic families, distinct disease outcomes between those strains can be explained by genetic polymorphisms. Therefore, we sought an appropriate inbred mouse strain derived from Swiss stock that could be used to compare disease outcomes with outbred Swiss Webster mice.

Genealogy of Swiss mice

In 1926, Clara J. Lynch from the Rockefeller Institute for Medical Research imported nine mice from André de Coulon, Switzerland, to the US, establishing the "Swiss" outbred colony [Chia et al., 2005] (Figure 1-5). Mice from that colony were sent by Lynch to other

researchers, including Leslie Webster in 1932, who passed them to academic and commercial breeders which then founded "Swiss Webster" outbred stock. In addition, in 1935, Lynch sent her animals to the National Institute of Health who established NIH stock of outbred Swiss mice. In 1966, the animals from this colony were selected for sensitivity and resistance to histamine challenge following pertussis vaccination resulting in HSFS/N and HSFR/N mice, respectively. In the early 1970s, histamine-sensitive mice at the eighth generation of inbreeding were found to carry the *Fv1*^{b} allele which confers sensitivity to the B strain of Friend leukaemia virus. Homozygous mice were then inbred as strain FVB/N (referred to hereafter as FVB) (Figure 1-5) [Taketo et al., 1991]. Based on the comparison of 44 common biochemical and coat color markers located on 15 chromosomes (Table 1-3 and data not shown from [Taketo et al., 1991]), strains such as BDP/J, P/J, I/St, and *Mus molossinus* are most distant from FVB/N (<55% of the markers matching), whereas strains such as HSFS/N, NFS/N, and SWR/J are most closely related (>75% matching). The main advantages of the FVB strain are large and prominent pronuclei beneficial for DNA microinjections, and vigorous reproductive performance with large litters [Taketo et al., 1991]. Due to these unique characteristics, FVB mice are widely used for production of transgenic animals on a fully inbred genetic background, which avoids using hybrid animals for that purpose and simplifies genetic manipulation and analysis [Barthold, 2002]. SWR and SJL mice also originated from Lynch's Swiss mice and were inbred at The Jackson Laboratory from 1947 and 1955 respectively. SJL/J mice are useful as a control strain for studying atherosclerosis and immune defects in a mouse model for type 1 diabetes (IDDM), and are susceptible strain to reticulum cell sarcomas. SWR mice are widely used in research as a general purpose strain, and also may be used as a control strain in comparison with autoimmune diabetic NOD mice [Festing, www.informatics.jax.org].

In this thesis, I investigated the impact of host genetic background on the disease associated with *C. rodentium* infection. In the first aim, I developed and characterized the inbred FVB mice infection model for the first time. Compared with closely related resistant outbred Swiss Webster mice, FVB mice demonstrated high mortality which most likely was associated with severe *C. rodentium*-induced diarrhea and consequent dehydration. In the next chapter, I addressed the phenotypic differences between resistant and susceptible mice with similar genetic

background at the genomic levels by applying DNA microarray technology. Results from this experiment were in agreement with the phenotypic observations observed in the first study. The role of genes involved in intestinal ion transport and its regulation in determining the disease outcome in inbred FVB and outbred Swiss Webster mice was proposed. In the last chapter, I confirmed and extended my observations using additional inbred strains of Swiss origin, SWR and SJL mice. These experiments provided the first information on *C. rodentium* infection in SWR and SJL mice, which were resistance to the disease. Furthermore, susceptible C3H mice demonstrated severe diarrhea and comparable changes in transcriptional activity of genes identified as potential candidates for high susceptibility in infected FVB mice, suggesting existence of common mechanisms in development of fatal diarrhea. Although it needs to be shown that comparable changes in genes contributing to electrolyte and fluid imbalance occur in people infected with EPEC and EHEC, my overall results indicate that *C. rodentium*-infected FVB mice can be used to model human acute diarrheal illness (ADI). These studies are very important in elucidating the pathophysiology of infectious diarrhea and identifying host genetic factors for susceptibility.

1.5 Figures and Tables

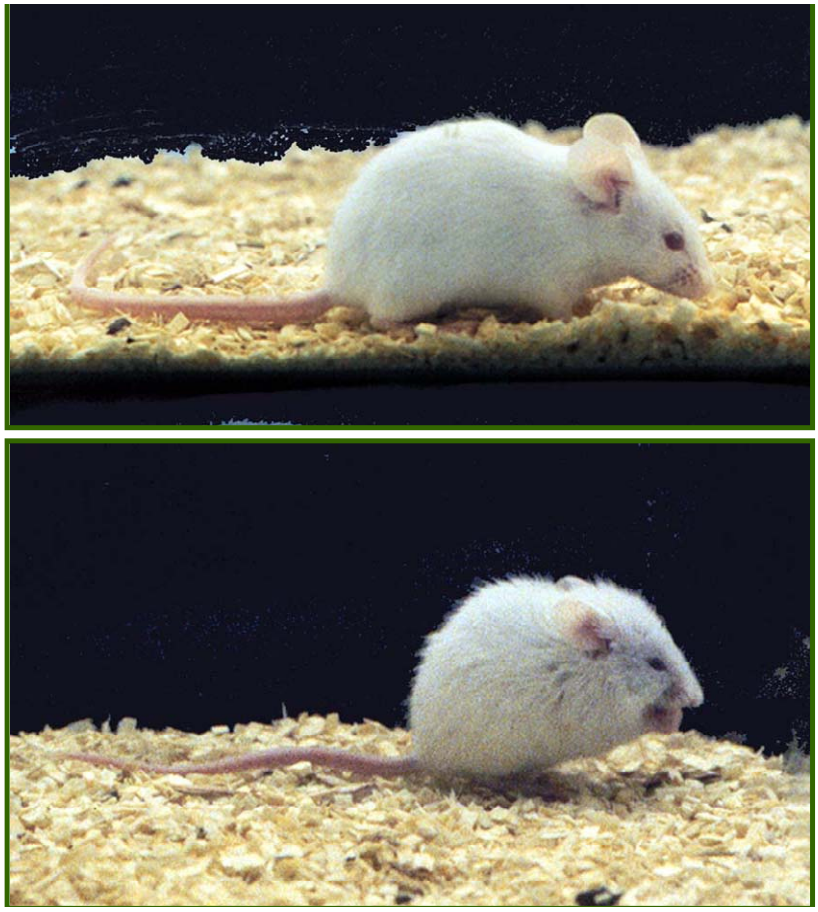

Figure 1-1. Clinical disease in *C. rodentium*-infected weanling SW mice.
Compared with uninoculated control (upper panel), susceptible mice develop signs of retarded growth, diarrhea, dehydration, coat ruffling, hunched posture, reluctance to move, recumbency, and high mortality in response to *C. rodentium* (lower panel). Images are courtesy of David B. Schauer.

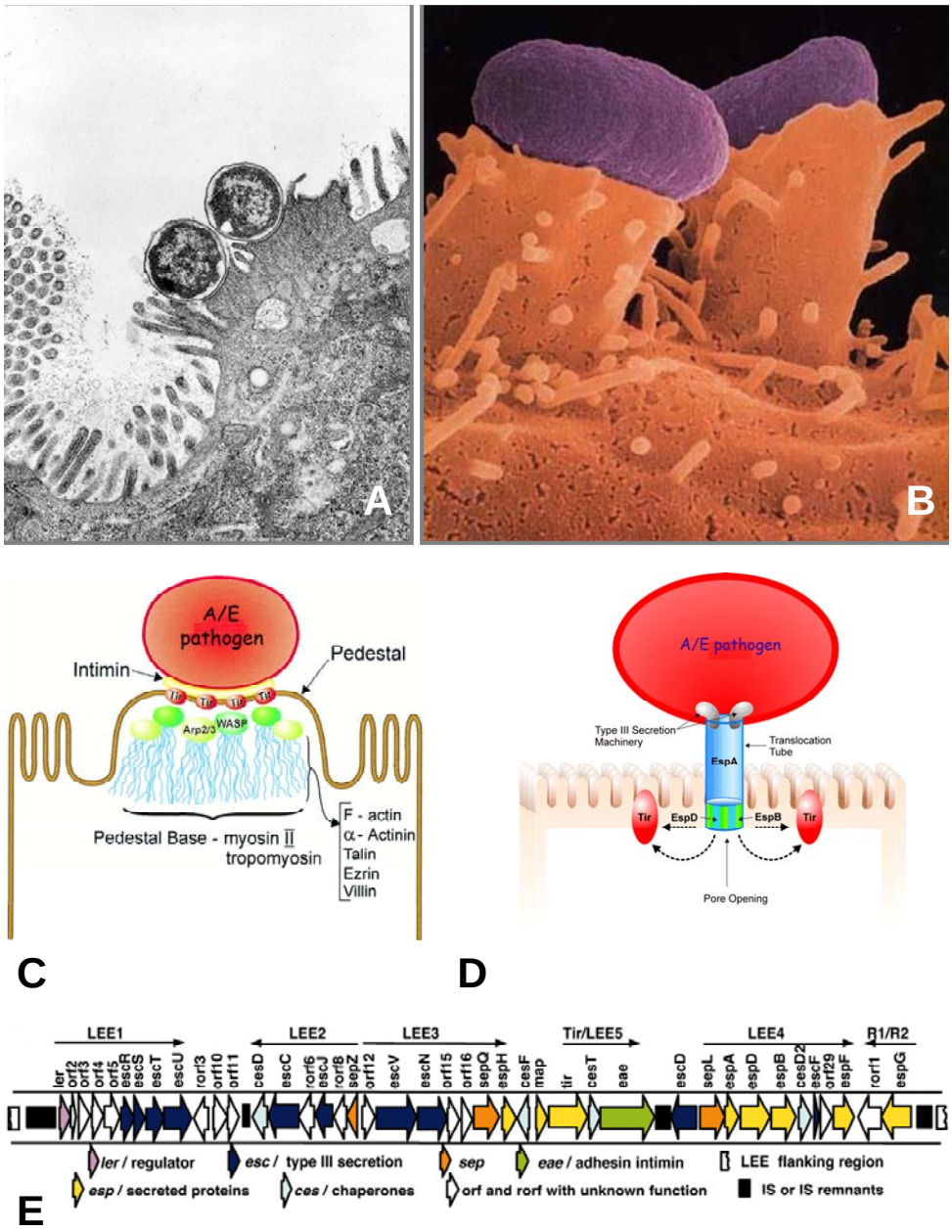

Figure 1-2. Microbial pathogenesis of *C. rodentium*.

(A) transmission electron micrograph of typical A/E lesions characterized by brush border effacement, intimate attachment and pedestal formation in the colon of *C. rodentium*-induced mice [adapted from Luperchio and Schauer, 2001].

(B) comparable A/E lesions induced by EPEC on the host epithelial surface (adapted from http://www.finlaylab.biotech.ubc.ca/research_projects/E.coli.html).

(C) molecular structure of the pedestal formation [modified from Vallance and Finlay, 2000].

(D) type III secretion system allowing translocation of bacteria-secreted proteins (Esps) to a host cell. Once translocated outside the bacteria, EspA forms a filamentous translocation tube whereas EspB and EspD are inserted into the host cell membrane, putatively forming a pore structure, allowing the passage of other effector proteins, such as Tir into the host cell membrane [modified from Vallance and Finlay, 2000].

(E) Genetic organization and assigned functions of *C. rodentium* LEE [adapted from Deng et al., 2004].

TABLE 1-1 List of effector proteins of EHEC, EPEC, and *C. rodentium*

Effector protein	Estimated molecular mass[b] (kDa)	Localization in the genome[c]	Localization in host cells	Function(s)
EPEC/EHEC/ *C. rodentium*				
Tir	56–68*	LEE	Tip of pedestal	Intimate attachment; A/E lesion formation; actin polymerization
Map	20	LEE	Mitochondria	Disruption of TER and mitochondrial membrane potential; filopodium formation
EspF	20–31*	LEE	Mitochondria	Disruption of TER and mitochondrial membrane potential; induction at cell death
EspG	44	LEE	Pedestal/colocalization with tubulin	Destruction of microtubule network
EspH	21	LEE	Underneath microcolony	Cytoskeleton modulation
SepZ	9.5	LEE	Unknown	Unknown
EspB	32	LEE	Bacterial attachment site	Cytoskeleton modulation
EspI/NleA	54	CP-933P	Golgi	Unknown
EspJ	25	CP-933U	Unknown	Regulation of clearance dynamics in vivo
NleB[a]	39	O island 122/CP-933K	Unknown	Unknown
NleC	40	CP-933K	Unknown	Unknown
NleD	28	CP-933K	Unknown	Colonization in calves
NleE	27	O island 122	Unknown	Unknown
NleF	24	O island 71	Unknown	Unknown
NleH[a]	33	nt 2281573–2282484[d]/CP-933K	Unknown	Unknown
EPEC/EHEC				
Cif	32	λ Prophage	Unknown	Cyclomodulin activity
EHEC				
TccP/EspFu	42.4	CP-933U	Tip of pedestal	A/E lesion formation; actin polymerization
EPEC				
EspG2	42	EspC PAI	Pedestal/colocalization with tubulin	Destruction of microtubule network
C. rodentium				
NleG	26		Unknown	Unknown

[a] Several homologous genes found.
[b] Asterisks indicate variations in molecular masses among, proteins of different A/E lesion-forming pathogens.
[c] Localization in the EHEC O157:H7 genome.
[d] Annotated position in EHEC O157:H7 genome. nt, nucleotides.

adapted from [Garmendia et al., 2005].

Table 1-2. Host immune response to *C. rodentium* infection as investigated in genetically-manipulated mice (modified from Mundy et al., 2005).

Gene deleted mice who cannot clear infection	Gene deleted mice with impaired eradication of colonic/systemic infection	Gene deleted mice with no effect on normal progress of infection
• RAG-/- (lacking T and B cells) • TcRβ-/- (lacking αβ T cells) • CD4-/- or depleted mice • CD28-/- (T cell signaling) • CD40L-/- (T cell signaling) • μMT (lacking B cells) • Igh-6^{tm1Cgn} (lacking B cells) • LTβR-/- (lacking the lymphotoxin-β receptor) • W/W^{v} (lacking mast cells)	• J chain-deficient (lacking polymeric immunoglobulins) • MMP3-/- • TcRδ-/- (lacking γδ T cells) • TNFα-/- • IL-12 p40-/- • Interferon-γ -/- • Cnlp-/- (lacking antibacterial mCRAMP)	• SCID-/- (lacking T and B cells) • iNOS-/- • IgG3-deficient • pIgR-/- (lacking the polymeric immunoglobulin receptor on epithelial cells) • IgA-deficient • IgM-deficient • CD8-/- • β7-/- (largely lacking mucosal lymphocytes) • αE-/- (largely lacking mucosal lymphocytes) • PAR2-/- (lacking proteinase activated receptor 2) • IL4-/-
Gene deleted mice who show reduced pathology	**Gene deleted mice who show enhanced pathology**	**Gene deleted mice with no effect on pathology**
• PAR2-/- (lacking proteinase activated receptor 2) • STAT6-/- • young RAG1-/- (lacking T and B cells) • SCID-/- (lacking T and B cells)	• TNFα-/- • IL-12 p40-/- • Interferon-γ -/- • adult RAG1-/- (lacking T and B cells) • RAG2-/- (lacking T and B cells) • LTβR-/- • μMT (lacking B cells) • Igh-6^{tm1Cgn} (lacking B cells) • CD4-/- or depleted mice • CD28-/- (T cell signaling) • CD40L-/- (T cell signaling) • W/W^{v} (lacking mast cells) • TcRβ-/- (lacking αβ T cells)	• iNOS-/- • Cnlp-/- (lacking antibacterial mCRAMP) • IgG3-deficient • J chain-deficient (lacking polymeric immunoglobulins) • pIgR-/- (lacking the polymeric immunoglobulin receptor on epithelial cells) • IgA-deficient • IgM-deficient • MMP3-/- • CD8-/- • TcRδ-/- (lacking γδ T cells) • β7-/- (largely lacking mucosal lymphocytes) • αE-/- (largely lacking mucosal lymphocytes) • IL4-/-

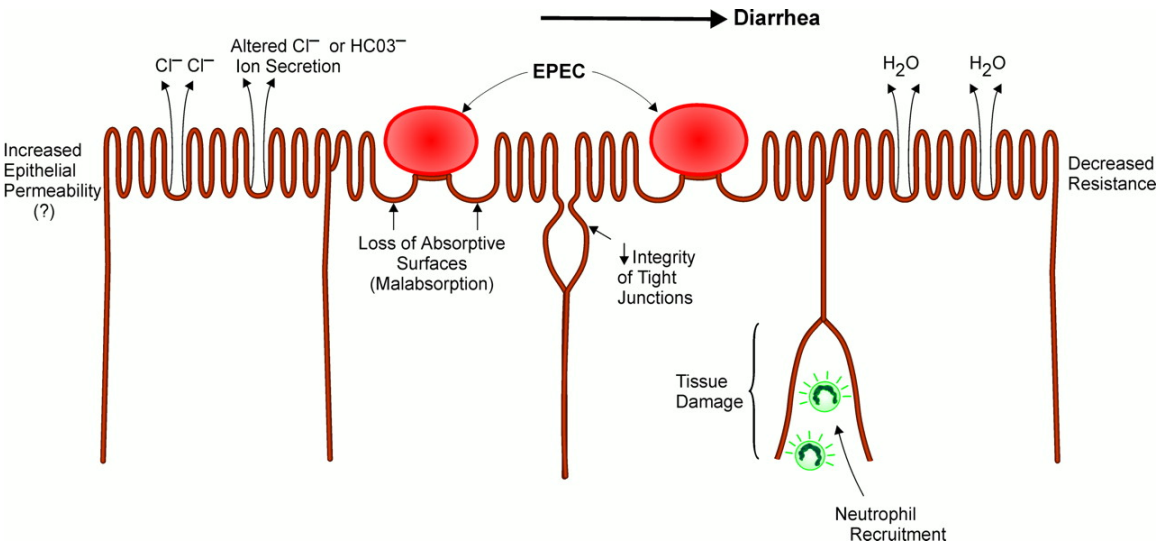

Figure 1-3. Hypothetical mechanisms for development of diarrhea in EPEC infection. Main contributors include increased epithelial permeability and alterations in Cl^- and HCO_3^- ion secretion. Loss of absorptive surfaces, reduced tight junction integrity, and tissue damage may be involved as well [adapted from Vallance and Finlay, 2000].

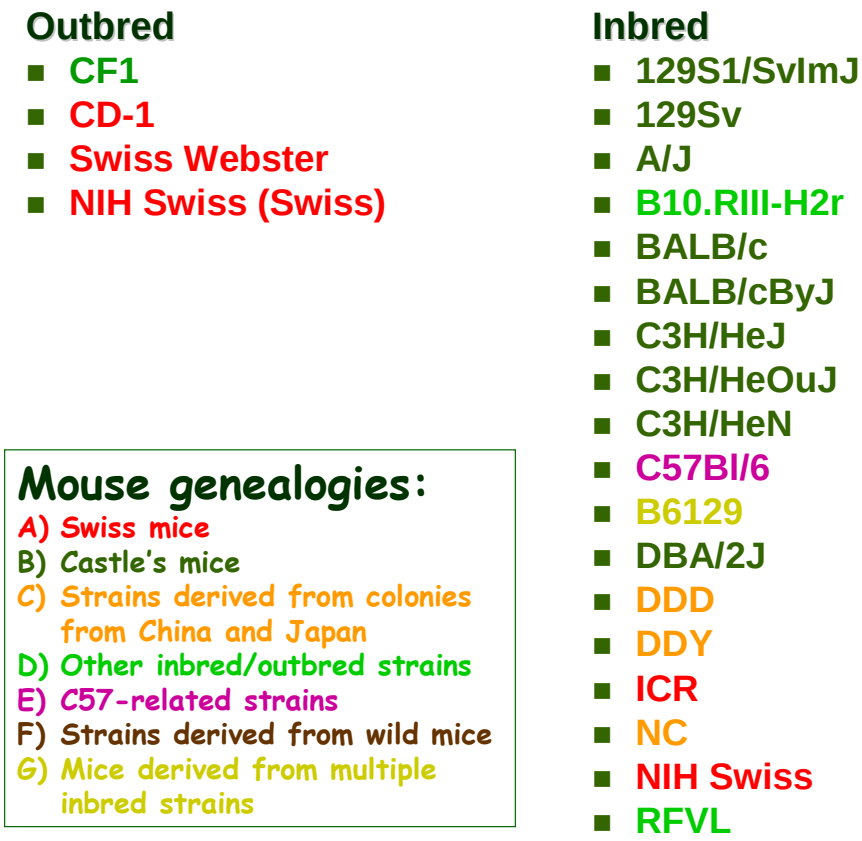

Figure 1-4. Strains/stocks of mice studied for *C. rodentium* infection so far FVB, SWR, and SJL mice reported in this thesis are not included).
Mouse genealogies (color-coded) are adapted from Beck et al., 2000.
In some reports, NIH Swiss and ICR mice appear as outbred, whereas in other studies, inbred mice of the same strain (and name) were used. This factor should be taken in account while comparing literature on *C. rodentium* mouse studies.

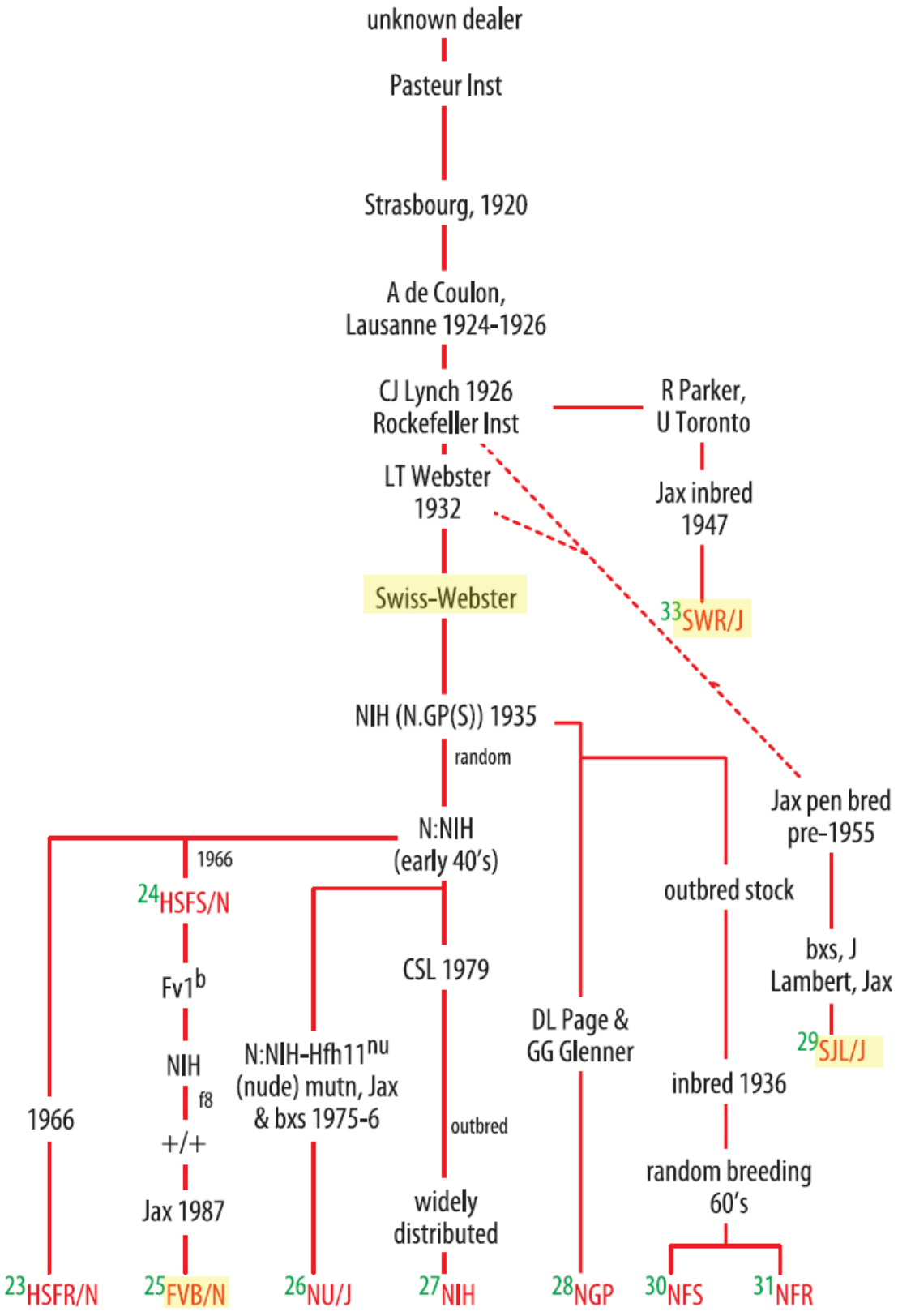

Figure 1-5. Genealogy of Swiss mice (partial, adapted from Beck et al., 2000). Strains and lines of mice used in studies presented in the thesis are highlighted.

Table 1-3. Genetic markers of FVB/N mice and common inbred strains

Symbol	Locus name	Chromosome no.	Allele in strain							
			FVB	129	C3H	C57BL/6	DBA/2	P	SJL/J	SWR
a	Agouti	2	+*	A^w	+	*a*	*a*	*a*	+	+
Ah	Aromatic hydrocarbon responsiveness	12	*b*	*d*	*b*	*b*	*d*	*b*	*d*	*d*
Akp-1	Alkaline phosphatase 1	1	*b**	*b*	*b*	*a*	*a*	*b*	*b*	*b*
Amy-1	Amylase 1	3	*a**	*a*	*a*	*a*	*a*	*a*	*a*	*a*
Apoa-1	Apolipoprotein A1	9	*b**	*b*	*b*	*a*	*b*	*a*	*a*	*b*
b	Brown	4	+*	+	+	+	*b*	*b*	+	+
c	Albino	7	*c**	c^{ch}	+	+	+	+	*c*	*c*
Car-2	Carbonic anhydrase 2	3	*b**	*a*	*b*	*a*	*b*	*a*	*b*	*b*
Ce-2	Kidney catalase	17	*a*	(*b*)	*b*	*a*	*a*	*a*	*a*	*a*
d	Dilute	9	+	+	+	+	*d*	*d*	+	+
Es-1	Esterase 1	8	*b**	*b*	*b*	*a*	*b*	*b*	*b*	*b*
Es-3	Esterase 3	11	*c**	*c*	*c*	*a*	*c*	*a*	*c*	*c*
Es-10	Esterase 10	14	*a**	*b*	*b*	*a*	*b*	*a*	*b*	*a*
Es-11	Esterase 11	8	*a**	*a*	*a*	*a*	*a*	*b*	*a*	*a*
Fv-1	Friend virus susceptibility 1	4	*b**	*n*	*n*	*b*	*n*	*n*	.	*n*
Glo-1	Glyoxylase 1	17	*a**	*a*	*a*	*a*	*a*	*a*	*a*	*b*
Got-2	Glutamate oxaloacetate transaminase 2	8	*a**	*b*	*b*	*b*	*b*	*b*	*b*	*a*
Gpd-1	Glucose-6-phosphate dehydrogenase 1	4	*b**	*a*	*b*	*a*	*b*	*a*	*b*	*b*
Gpi-1	Glucose phosphate isomerase 1	7	*b**	*a*	*b*	*b*	*a*	*a*	*a*	*b*
Gpt-1	Glutamic-pyruvic transaminase 1	15	*a**	*a*	*a*	*a*	*a*	*a*	*a*	*a*
Gr-1	Glutathione reductase 1	8	*a**	*a*	*a*	*a*	*a*	*a*	*b*	*b*
Gus-s	β-Glucuronidase structural	5	*b*	(*b*)	(*h*)	*b*	*b*	*b*	*b*	*b*
H-2	Histocompatibility 2	17	*o**	(*b*)	*k*	*b*	*d*	*p*	*s*	*q*
Hba	Hemoglobin α-chain complex	11	*c*	(*a*)	*c*	*a*	*g*	*h*	*c*	*c*
Hbb	Hemoglobin β-chain complex	7	*d**	*d*	*d*	*s*	*d*	*d*	*s*	*s*
Hc	Hemolytic component (C5)	2	(0*)	(1)	1	1	0	1	1	0
Idh-1	Isocitrate dehydrogenase 1	1	*a**	*a*	(*a*)	*a*	*b*	*b*	*b*	*a*
Ly-1	Lymphocyte antigen 1	19	*b*	*b*	*a*	*b*	*a*	*b*	*b*	*b*
Ly-2	Lymphocyte antigen 2	6	*b*	*b*	*a*	*b*	*a*	.	*b*	*b*
Ly-3	Lymphocyte antigen 3	6	*b*	*b*	*b*	*b*	*b*	*b*	*b*	*b*
Mod-1	Malic enzyme	9	*a**	*a*	*a*	*b*	*a*	*b*	*a*	*a*
Mpi-1	Mannose phosphate isomerase 1	9	*b**	*b*	*b*	*b*	*b*	*b*	*b*	*b*
Mup-1	Major urinary protein 1	4	*c*	*a*	(*a*)	*b*	*a*	*b*	*a*	*a*
Neu-1	Neuraminidase 1	17	*b**	*b*	*b*	*b*	*b*	*b*	*b*	*b*
p	Pink-eyed dilution	7	+*	(*p*)	+	+	+	*p*	*p*	.
Pep-3	Peptidase 3	1	*b**	*b*	*b*	*a*	*b*	*c*	*b*	*b*
Pgm-1	Phosphoglucomutase 1	5	*a**	*a*	(*b*)	*a*	*b*	*b*	*b*	*b*
Pgm-2	Phosphoglucomutase 2	4	*a**	*a*	*a*	*a*	*a*	*a*	*a*	*a*
rd	Retinal degeneration	5	*rd**	+	*rd*	+	+	*rd*	*rd*	*rd*
Thy-1	Thymus cell antigen 1 (θ)	9	*a*	*b*	*b*	*b*	*b*	.	*b*	*b*
Trf	Transferrin	9	*b**	*b*	(*b*)	*b*	*b*	*b*	(*b*)	*b*

Three additional coat color markers were tested but are not listed above because all strains showed the wild-type alleles. They are belted (*bt*) on chromosome 15, leaden (*ln*) on chromosome 1, and piebald (*s*) on chromosome 14. Many of these markers have also been reported in refs. 17 and 18. Data for other strains were obtained from the MATRIX program (12). For the *rd* mutation, see also ref. 19. Inbred strains are shown as composites of their various substrains. When some of their substrains carry different alleles from others or their alleles have not yet been determined, data are placed in parentheses. A complete listing of all substrains is available from the authors. Periods indicate markers not determined.

*Data obtained or confirmed by screening by the authors.

Inbred strains	129	C3H	C57BL/6	DBA/2	P	SJL/J	SWR
% relatedness*	63.64%	72.73%	61.36%	59.09%	52.38%	69.77%	76.74%

*, calculated as percentage of marker alleles similar to FVB/N in all markers tested from the table above (adapted from [Taketo et al., 1991])

Chapter 2: Development of fatal colitis in FVB mice infected with *Citrobacter rodentium*

Diana Borenshtein[1], Prashant R. Nambiar[2], Elizabeth B. Groff[1,2], James G. Fox[1,2], David B. Schauer[1,2]

[1]Biological Engineering Division, [2]Division of Comparative Medicine, Massachusetts Institute of Technology, Cambridge, MA, USA

An abridged version of this chapter was submitted to *Infection and Immunity*.

2.1 Introduction

Diarrheagenic *Citrobacter rodentium* causes transmissible murine colonic hyperplasia (TMCH), a naturally occurring disease of laboratory mice characterized by epithelial cell hyperproliferation in the descending colon [reviewed in Luperchio and Schauer, 2001; Mundy et al., 2005]. *C. rodentium* infection in adult mice of many outbred stocks and inbred strains is self-limiting, with little morbidity or mortality. In contrast, some animals are more susceptible and develop clinical signs of disease, including retarded growth, diarrhea, dehydration, coat ruffling, hunched posture, reluctance to move, recumbency, and high mortality. Susceptibility has been reported for suckling [Muto et al., 1969; Nakagawa et al., 1969; Barthold et al., 1976; Barthold et al., 1978; Barthold, 1980], helminth co-infected [Chen et al., 2005a; Chen et al., 2006], antibiotic pretreated [Luperchio et al., 2000], and adult mice of some inbred strains [Barthold et al., 1977; Itoh et al., 1979; Silverman et al., 1979; Vallance et al., 2003; Khan et al., 2006], as well as genetically engineered mice with varying types of immune defects [Maggio-Price et al., 1998; Vallance et al., 2002b; Vallance et al., 2003; Bry and Brenner, 2004; Spahn et al., 2004; Wei et al., 2005]. The alterations in cell kinetics in TMCH are similar to those seen in idiopathic inflammatory bowel disease (IBD), including a 2- to 4-fold increase in labeling index and expansion of the proliferative zone [Barthold, 1979]. Furthermore, colonic mucosal hyperplasia associated with *C. rodentium* infection in mice serves as a promoter for colon tumorigenesis [Barthold and Jonas, 1977; Newman et al., 2001], analogous to the increased risk for colorectal cancer seen in patients with IBD [Riddell *et al*., 1983; Bernstein *et al*., 2001; Rutter *et al*., 2004]. Therefore, *C. rodentium* was used as an animal model linking bacterial infection, IBD and colorectal cancer.

The importance of host genetic background in TMCH has been demonstrated, but not fully elucidated. First mentioned by Barthold et al., [1977], mouse strain susceptibility to *C. rodentium* infection was further investigated by Itoh et al. [1988], and more recently by Vallance et al. [2003]. Distinct lesions with regard to hyperplasia, inflammation, and mortality can be seen in different outbred stocks and inbred strains in response to bacterial challenge. Diet and indigenous microbiota also play important roles in the outcome of *C. rodentium* infection. Among different stocks and strains of mice, outbred Swiss Webster (SW) mice have been well characterized as a model of TMCH [Ediger et al., 1974; Barthold et al., 1976; Barthold et al., 1977; Barthold et al., 1978; Barthold, 1979; Barthold and Jonas, 1979; Johnson and Barthold,

1979; Barthold, 1980; Barthold and Beck, 1980; Umar et al., 2000; Umar et al, 2003]. FVB mice, widely used for creating transgenic animals, have been inbred from SW mice for homozygosity of the Fv-1^b allele that determines susceptibility to the B strain of Friend leukemia virus [Taketo et al., 1991]. Although FVB mice have been available since the late 1970s, there have been no reports of progression of TMCH in this inbred strain. The aim of this study was to characterize *C. rodentium* infection in adult FVB mice and compare it to disease outcome in cognate outbred SW mice. Marked differences in host response to infection were observed in the two lines. While outbred SW mice developed subclinical disease with classic features of TMCH, FVB mice developed high mortality and severe colitis associated with epithelial atypia. This research characterizes *C. rodentium* infection in FVB mice as a new model for studying fatal infectious colitis.

2.2 Results

FVB mice are highly susceptible to *C. rodentium* infection

As expected, *C. rodentium* infection in adult outbred SW mice failed to produce clinical signs of disease (data not shown). In contrast, 12-week old inbred FVB mice infected with the pathogen developed morbidity by 6 days post-inoculation (DPI), and mortality by 9 DPI with a median survival of 15 days (Figure 2-1). By 21 DPI, only 23% of inoculated FVB mice survived, compared to 100% survival in inoculated SW mice and in uninfected control animals ($p < 0.0001$ by log rank test). The cause of death in these mice is not clear. However, clinical signs, undetectable serum TNF-alpha levels (below the limit of detection by ELISA of 15.6 pg/ml), rare dissemination of bacteria to draining lymph nodes or spleen at 9-12 DPI, and the prevention of mortality by fluid therapy (discussed below), are consistent with hypovolemia as the primary cause of fatality.

Mortality correlated with loss of body weight in infected animals (Figure 2-2A). SW mice stopped gaining weight between 9 and 15 DPI ($p < 0.05$ by paired *t* test), while FVB mice lost weight beginning at 9 DPI ($p < 0.0001$ by paired *t* test). There was a recovery of body weight loss in FVB mice by 21 DPI, although only 23% of the inoculated animals were still alive at that time point, which may have contributed to the apparent increase. Body weight loss was significantly greater in FVB than in SW mice throughout the duration of the experiment ($p < 0.0001$ by two-way ANOVA compared with SW mice); at 9 DPI ($2.8 \pm 1.4\%$ vs. $5.3 \pm 1.2\%$), 12

DPI (5.2 ± 2.1% vs.17.5 ± 1.4%), 15 DPI (6.4 ± 2.3% vs. 20.2 ± 2.7%), and 21 DPI (6.0 ± 3.1% vs. 8.2 ± 1.6%).

Bacterial load of *C. rodentium* in FVB mice

Fecal shedding of *C. rodentium* was detected beginning at 3 DPI, and the levels of fecal shedding were not significantly different between SW and FVB mice through 9 DPI (Figure 2-2B). By 12 DPI, SW mice had reduced bacterial shedding and by 18 DPI the infection was cleared. Although FVB mice cleared the pathogen by 3 weeks post-inoculation (WPI), bacterial counts were higher than in SW mice by 12 DPI, indicating delayed clearance. Furthermore, since the most severely affected FVB mice often did not have any formed feces, the observed fecal counts may have underestimated the actual shedding of *C. rodentium* between 12 and 21 DPI. Fecal shedding correlated with bacterial infection in the cecum and colon of FVB mice (Figure 2-3A). Substantial attachment of *C. rodentium* to epithelial cells was observed in the colon at 6 DPI, with bacterial organisms on the luminal epithelial surface, as well as deeper in crypts (Figure 2-3B panel c). The cecum, although comparable to the colon in level of infection at 6 DPI (Figure 2-3A), did not exhibit *C. rodentium* attachment to epithelial cells (Figure 2-3B panel d). By 12 DPI, *C. rodentium* organisms in the colon were mainly associated with exfoliated cells (Figure 2-3B panel e), while attachment to epithelial cells in the cecum was occasionally observed (Figure 2-3B panel f).

Infected FVB mice develop marked colonic hyperplasia

SW mice develop profound hyperplasia in the descending colon in response to *C. rodentium* infection [Barthold et al., 1977; Barthold, 1979; Johnson and Barthold, 1979; Umar et al., 2000; Umar et al., 2003]. Infected FVB mice were found to have comparable hyperplasia characterized by increased colonic crypt height and changes in proliferation by 6 DPI (Figure 2-4). By 12 DPI, the height of crypts doubled, and the proliferative zone expanded from 29.3 ± 1.2% to 84.3 ± 2.6% of the crypt column ($p < 0.0001$ by ANOVA). Mitotic figures and BrdU-positive cells were found on the surface epithelium (Figure 2-4D), and the labeling index (LI) had increased from 8.9 ± 0.6% to 40.1 ± 2.4% ($p < 0.0001$ by ANOVA). Alterations in the cecum were less pronounced with a 1.5-fold increase in crypt length that was significantly different from uninfected control FVB mice ($p < 0.01$ by Student's *t* test) and a tendency towards

expanded proliferative zone and increased LI by 12 DPI that was not significantly different from uninfected control FVB mice (Figure 2-5).

Apoptosis was analyzed by immunohistochemistry for activated caspase 3 (Figure 2-6). Although occasional apoptotic cells were found in colonic crypts (Figure 2-6B), the majority of activated caspase 3 was associated with exfoliated epithelial cells in the lumen (Figure 2-6C and D), consistent with rapid removal of apoptotic cells from tissue.

Infected FVB mice develop severe inflammation and associated epithelial atypia

In agreement with published reports, SW mice developed limited inflammation in response to infection (Barthold et al., 1978; data not shown). In contrast, infected FVB mice developed substantial inflammation, erosions and ulcers in the descending colon (Figure 2-7A, $p < 0.0001$ using Kruskal-Wallis test with post hoc Dunn's multiple comparison test compared with uninfected controls). By 6 DPI, minimal to mild mucosal infiltrate of granulocytes and mononuclear cells was present. By 12 DPI, infected FVB mice had multifocal coalescing moderate to severe mucosal inflammation with mucosal erosions, ulcers and submucosal edema (Figure 2-7A, $p < 0.001$ compared with uninfected and 3 DPI mice, Figure 2-8). Excessive mucus accompanied the inflammation in the proximal colon, resembling the catarrhal enterocolitis described by Brennan et al. [1965]. Lesions were characteristically most severe in the mid- to distal colon, milder at the cecocolic junction, and typically did not involve the proximal colon or the body of the cecum. Ileitis was rarely observed.

Inflammatory lesions were accompanied by dysplastic changes (Figure 2-7B, $p < 0.0001$ using Kruskal-Wallis test with post hoc Dunn's multiple comparison test compared with uninfected controls) that fit the definition of gastrointestinal intraepithelial neoplasia (GIN) from a recent consensus report [Boivin et al., 2003]. By 6 DPI, infected FVB mice had mild dysplasia in the descending colon, with crypt hyperplasia, minimal alteration of gland shape, and some loss of goblet cell differentiation, although moderate dysplasia was observed in a few animals at this time point (Figure 2-7B, $p < 0.01$ and $p < 0.05$ compared with uninfected and 3 DPI mice respectively). By 12 DPI, a greater fraction of mice had moderate dysplasia (Figure 2-7B, $p < 0.001$ compared with uninfected and 3 DPI mice). The atypical glands were characterized by longer, hypercellular crypts with altered shapes (tortuous, branched), moderate loss of normal crypt orientation, and occasional cystic glands (Figure 2-8E-H). Moderate cellular atypia was

characterized by loss of goblet cell differentiation, plump and elongate nuclei with pseudostratification and nuclear hyperchromatism, loss of cell polarity, dark, elongate to oval, hyperchromatic and anisokaryotic nuclei with pseudostratification. Mice with the most advanced dysplastic changes had high nuclear-to-cytoplasm ratios, crypt branching with irregular buds, and occasional micronests within the abutting lamina propria (Figure 2-8E and F). Approximately 65% of infected FVB mice had atypical crypts that had herniated into the GALT by 12 DPI (Figure 2-8G and H). Dysplastic lesions were positively correlated with inflammation (Spearman $r = 0.87$, $p < 0.0001$). Similar changes, although less dramatic, were observed in the cecum by 12 DPI, and here too dysplasia was positively correlated with inflammation (Spearman $r = 0.729$, $p < 0.0001$, Figure 2-9). These results indicate that FVB mice infected with *C. rodentium* may serve as a new model for studying infectious colitis and associated epithelial atypia.

Chronic studies show reversibility of most of the lesions in FVB mice

Morphologically, the features of regenerative atypia, including prominent crypt branching, occasional villous configuration of the surface, persistent mucus depletion and nuclear changes in the epithelial cells, can resemble GIN. This makes the histopathologic diagnosis more difficult [Riddel et al., 1983]. In order to assess possible progression of the lesions in infected FVB mice to neoplasia, the animals were followed for 16 and 30 WPI. In the first experiment, without therapeutic intervention, only 25% of infected FVB mice survived. These animals were followed to 16 WPI. In a second experiment, fluid therapy was administered to infected FVB mice. Daily subcutaneous administration of fluids beginning at 6 DPI prevented mortality in FVB mice infected with *C. rodentium* without affecting bacterial shedding, or the severity or extent of colonic lesions. Fluid therapy through 15-21 DPI resulted in 100% survival and allowed us to follow the animals through 30 WPI.

The lesions fully resolved in the majority of the mice (Figure 2-10A), although the colonic disease score at 16 WPI was slightly, but significantly, greater than at 30 WPI or uninfected controls ($p < 0.0001$ by Kruskal-Wallis followed by Dunn's multiple comparison test). This observation provides further evidence that the epithelial dysplasia was associated with active inflammation and was reversible. However, one of the mice in each of these two experiments (representing 6.7% and 5% for 16 and 30 WPI respectively) developed chronic

lesions. A mouse at 16 WPI had moderate to marked inflammation and hyperplasia with adjacent areas of normal mucosa that mainly involved the proximal colon and cecum (Figure 2-10B panel a). In a mouse at 30 WPI, similar lesions were found diffusely throughout the large intestine and consisted of significant inflammation and hyperplasia, multiple lymphoid aggregates throughout the mucosa, vascularized lamina propria, and rare crypt abscesses (Figure 2-10 B panels b and c). At these time points the animals were no longer infected with *C. rodentium*, as judged by *eae*-specific PCR (data not shown).

Expression of pro-inflammatory and immunomodulatory genes in SW and FVB mice

Quantitative RT-PCR was performed on RNA isolated from full-thickness descending colon tissue to evaluate the expression of some key genes involved in immune regulation in the intestine, including the pro-inflammatory cytokines IFN-γ and TNF-α and the immunomodulatory cytokine IL-10 (Fig. 2-11). In addition, the expression of inducible nitric oxide synthase (iNOS), which contributes to innate antimicrobial host defense by producing reactive nitrogen species, was determined. The only difference found was in the expression of iNOS prior to infection; uninoculated FVB mice demonstrated 7.5-fold lower expression of iNOS message compared with control SW mice ($p < 0.01$ respectively using one-way ANOVA followed by Tukey's multiple comparison tests). Infection with *C. rodentium* induced expression of INF-γ (12.5-fold, $p < 0.05$), TNF-α (7-fold, $p < 0.001$), and iNOS (19-fold, $p < 0.001$) in SW mice compared with uninoculated controls. IL-10 expression (1.6-fold increase) was not significantly different than in uninfected SW mice. Similarly, infection in FVB mice stimulated expression of proinflammatory genes; INF-γ (4-fold, not significant), TNF-α (7-fold, $p < 0.001$), and iNOS (79-fold, $p < 0.001$) compared with uninfected FVB mice. On the other hand, the expression of IL-10 at 9 DPI had decreased 3-fold in infected FVB mice compared to uninfected controls ($p < 0.05$). By 9 DPI, the transcript levels of all genes were similar in FVB and SW mice.

2.3 Discussion

A number of animal models have been developed to investigate different aspects of IBD, although none of them reproduce human disease completely. Models of intestinal inflammation can be either spontaneous or induced by administration of exogenous agents (chemicals or bacteria), gene targeting (knockout or transgenic rodents), and adoptive transfer of cells into immunodeficient animals [Blumberg et al., 1999; Hendrickson et al., 2002]. Microbiota have profound effects on the host and particularly on the gut, including intestinal epithelium, the enteric nervous system, and mucosal immunity [Elson et al., 2005]. Diarrheagenic *C. rodentium* is a unique murine pathogen that has been used to study important disease processes, including colitis. Infection is characterized by colonic hyperplasia with varying degrees of inflammation, depending on age, diet, microbiologic status and genetic background of the host. Here we report a new model of fatal infectious colitis in adult FVB mice infected with *C. rodentium*.

In contrast to subclinical infection in outbred SW mice, adult inbred FVB mice demonstrated a high degree of susceptibility. The 77% mortality was accompanied by profound inflammatory and erosive changes, including frank lower bowel ulcers, which correlated with morbidity. In contrast to susceptibility to infectious colitis, FVB mice are relatively resistant to DSS colitis, with milder lesions than ICR, C57BL/6, or BALB/c mice, and only 10% mortality 12 days after treatment with 5% DSS in the drinking water [Hahm et al., 2001]. Although they are immunocompetent, the degree of mortality seen in FVB mice infected with *C. rodentium* exceeds that reported in some immunocompromised mice. For example, little to no mortality following *C. rodentium* infection was reported in adult TNFRp55$^{-/-}$, iNOS$^{-/-}$ and IFN-$\gamma^{-/-}$ mice [Goncalves et al., 2001, Simmons et al., 2002] or in adult immunodeficient mice lacking immunoglobulin or T cells [Simmons et al., 2003; Maaser et al., 2004]. In addition, *C. rodentium* infection only caused mortality rates of 5% in adult Rag1$^{-/-}$, 10-15% in IL-12p40$^{-/-}$ and 40% in mast cells-deficient animals [Simmons et al., 2002; Simmons et al., 2003; Wei et al., 2005]. Importantly, adolescent mice between 3 and 5 weeks of age with these same immune defects are highly susceptible to *C. rodentium* infection [Vallance et al., 2002b; Vallance et al., 2003; Bry and Brenner, 2004; Wei et al., 2005]. Furthermore, suckling inbred and outbred mice without such defects are also susceptible and exhibit a high degree of mortality [Muto et al., 1969, Nakagawa et al., 1969; Barthold et al., 1976; Barthold et al., 1978; Barthold 1980]. This suggests that susceptibility in young mice may be independent of innate or adaptive immunity, and may in

fact be due to a failure to adequately compensate for fluid and/or electrolyte losses in the colon during *C. rodentium* infection. Mice lacking functional T and B cells develop chronic *C.* rodentium infection [Vallance et al., 2002b, Simmons et al., 2003; Maaser et al., 2004], demonstrating the importance of adaptive immunity in clearing the infection. Although infected FVB mice exhibited a relative delay in *C. rodentium* clearance compared to SW mice, surviving mice and mice receiving fluid therapy invention did successfully eliminate the infection by 3 WPI. Thus, any intrinsic immune defect that FVB mice have against *C. rodentium* is partial and does not fully explain the susceptibility of this strain to infection.

The only immunocompetent inbred strain of mouse with a high degree of susceptibility to *C. rodentium* infection that has been reported previously is the C3H strain. Different C3H substrains exhibit 50% to 100% mortality by 3 WPI independent of TLR4 status [Barthold et al., 1977; Vallance et al., 2003; Khan et al., 2006]. C3H mice develop high levels of *C. rodentium* in the colon as well as bacterial translocation to mesenteric lymph nodes, consistent with a defect in the clearance of infection. The mechanism of susceptibility of FVB mice to *C. rodentium* infection appears to be different from that of C3H mice. For example, fecal shedding of *C. rodentium* in FVB mice was similar to that seen in resistant SW mice. Furthermore, serum TNF-α was not detectable by ELISA, and dissemination of bacteria to extraintestinal tissues was minimal and not associated with mortality (data not shown), allowing us to exclude bacteremia as the cause of death in infected FVB mice. Sick FVB mice did exhibit signs of severe dehydration [Eliason and Lewan, 1998], including sunken eyes, reluctance to move, and decreased skin turgor. Based on clinical signs and the success of fluid therapy intervention, we suspect hypovolemia was the primary cause of fatality. The relative contribution of malabsorption and decreased fluid uptake, increased ion secretion, compromise of barrier function and/or exudation to *C. rodentium* diarrhea, and the role of altered fluid balance in morbidity and mortality, remains to be determined.

The kinetics of *C. rodentium* infection in FVB mice was comparable to that in other strains of mice. Similar to what has been reported in C57BL/6 mice as measured by bioluminescence imaging [Wiles et al., 2004], FVB mice had 2 logs more *C. rodentium* in the cecum than in the colon at 3 DPI. No *C. rodentium* aggregates were detected in the colon of FVB mice at 3 DPI by IHC, also consistent with the lack of microcolonies made up of $\geq 10^3$ bacteria in the colon of C57BL/6 mice 3 DPI [Wiles *et al.,* 2004]. By 6 DPI, extensive attachment of

bacteria to the epithelial surface of the colon was found in FVB mice. By 12 DPI, the bacteria were no longer attached to the colonic epithelial surface, but were attached to exfoliated cells, which has been previously reported [Johnson and Barthold, 1979; Umar et al., 2000; Umar et al., 2003]. *C. rodentium* were abundant in the cecum of FVB mice by 6 DPI, but attachment to the cecal epithelial surface was not observed until 12 DPI. In contrast, Wiles et al. (2004) reported attachment to the cecal lymphoid patch by 1 DPI in C57BL/6 mice that persisted focally without involving the remainder of the organ. The cecal patch is analogous to the Peyer's patch in the ileum and is present in the apical portion of cecum. Whether these differences are due to differing kinetics of infection in FVB versus C57BL/6 mice or to differences in IHC detection versus bioluminescence imaging of the cecal surface, following removal of cecal contents, remains to be determined. In any case, cecal lesions in FVB mice were associated with *C. rodentium* attachment and not simply the presence of organisms in the lumen of the organ (Figure 2-9).

The increase in crypt column heights in the colon of FVB mice was comparable to that reported for SW mice [Barthold et al., 1977; Barthold, 1979; Johnson and Barthold, 1979; Umar et al., 2000; Umar et al., 2003], as well as in other inbred strains [Higgins et al., 1999, Newman et al., 2001; Vallance et al., 2002a; Vallance et al., 2002b]. Epithelial hyperplasia reflects an imbalance between proliferation and death of cells arising in the crypt. We detected apoptosis by staining for activated caspase 3. Few apoptotic cells were identified in colonic crypt columns most likely due to their rapid removal from the mucosa. Strong activated caspase 3 signal was found primarily in extruded cells in the lumen of the colon. It remains to be determined if *C. rodentium* infection causes apoptosis in epithelial cells which are then shed into the lumen, or if infection and subsequent cytoskeletal rearrangements result in exfoliation of cells that then undergo anoikis, or perhaps both. In any case, some differences that have been reported with regard to the influence of *C. rodentium* infection on apoptosis may be explained by methodology. Evaluation of apoptosis in isolated crypts would exclude exfoliated cells, thus it is not surprising that no increase in colon apoptosis in SW mice was detected by TUNEL 12 DPI using this method [Umar et al., 2000]. In addition, techniques that rely on DNA fragmentation to detect apoptosis, including the TUNEL assay, are not specific but also detect cells with DNA damage resulting from cell injury and other forms of cell death [Grasl-Kraupp et al., 1995, Stadelmann and Lassmann, 2000]. Thus, increases in TUNEL-positive cells in crypts in tissue

sections from C3H mice [Vallance et al., 2003] could correlate with cellular injury and DNA damage as well as apoptosis, which would be expected to exceed the number of apoptotic cells detected by activated caspase 3 staining.

Both FVB and SW mice developed comparable epithelial hyperplasia when infected with *C. rodentium*. FVB mice also developed severe mucosal inflammation associated with epithelial atypia (dysplasia). Inflammatory changes in the colon of FVB mice were similar to those in mouse models of colitis that have been used to study idiopathic IBD [Sartor, 1997]. These lesions included erosions and frank colonic ulcers, infiltration of the lamina propria with neutrophils and mononuclear cells, crypt abscesses and gland atrophy, goblet cell depletion, epithelial hyperplasia, and epithelial atypia and dysplasia. Dysplasia has been identified as a precursor to neoplasia in IBD [Riddell et al., 1983, Ullman et al., 2003], but there can be difficulties in distinguishing true dysplasia from regenerative atypia that can accompany severe inflammation [Riddell et al., 1983]. Consequently, chronic studies were carried out to determine the ultimate fate of these dysplastic changes. The majority of surviving mice in the absence of therapy or mice receiving fluid therapy intervention no longer had epithelial inflammation and dysplasia in the colon by 16 or 30 WPI, consistent with the complete resolution of lesions reported in SW mice [Barthold et al., 1978; Johnson and Barthold, 1979]. However, a small fraction of animals (5-7%) developed chronic colitis. Persistent infection or recurrent infection could be excluded as a cause of these lesions by *eae*-specific PCR. There is also evidence for long-lasting or perhaps life-long immunity against rechallenge in convalescent animals following *C. rodentium* infection [Barthold 1980; Ghaem-Maghami et al., 2001; Maaser et al., 2004].

To test the hypothesis that cytokines could contribute to the dramatically different response of FVB and SW mice to *C. rodentium* infection, colon message levels of some key immunoregulatory cytokines were quantified. Despite initial differences in iNOS expression between uninoculated FVB and SW mice, infection as expected [Higgins et al., 1999; Goncalves et al., 2001; Simmons et al,. 2002; Vallance et al., 2002a; Vallance et al., 2002b] induced expression of proinflammatory genes to comparable levels in the two lines of mice. This suggests that neither IFN-γ nor iNOS or TNF-α play a critical role in determining the differential response of FVB and SW mice to *C. rodentium* infection. As reported in BALB/cByJ mice [Chen et al., 2005b], IL-10 expression in SW mice slightly increased by 9 DPI, consistent with the induction of a regulatory T cell response [Powrie, 2004] by *C. rodentium* infection. However,

IL-10 expression in FVB mice declined 3-fold by 9 DPI, suggesting a reduced capacity to regulate the inflammatory and immune responses directed against the pathogen in these animals. The differential IL-10 expression in the colon of FVB and SW mice could contribute to the distinct morbidity and mortality observed between these two cognate lines of mice. A protective role for IL-10 is in contrast to what has been reported for BALB/cByJ mice co-infected with a helminth *Heligomosomoides polygyrus* and *C. rodentium* [Chen et al., 2005a; Chen et al., 2006]. This may reflect true differences between BALB/cByJ and FVB mice, or it may be that factors other than IL-10 contribute to the increased susceptibility to *C. rodentium* challenge during helminth infection. Studies to further define the role of immunoregulatory cytokines in susceptibility and resistance to *C. rodentium* infection are currently underway.

In a summary, we have developed and characterized a novel mouse model for studying fatal infectious colitis. FVB mice are immunocompetent, yet develop mortality similar to what has been reported in immunodeficient lines of mice that fail to control infection. To our knowledge, this is the first report demonstrating the protective effect of fluid therapy intervention. It remains to be determined if this approach will effectively prevent fatal colitis in immunodeficient lines of mice. The availability of susceptible and resistant lines of mice with very similar genetic backgrounds should facilitate the identification of host factors that determine the outcome of infection with *C. rodentium*.

2.4 Selected Methods

Mouse infections. Specific pathogen free 12-week-old inbred FVB/NTac or outbred Tac:SW mice of both sexes (Taconic Laboratories, Germantown, N.Y.) were housed and maintained as described in Appendix 1: General methods. The experiments included 16 uninfected and 20 infected SW mice. The numbers of FVB mice within each experimental group (except studies with fluid intervention, see below) are given in Table 2-1, and represent 5 independent experiments. Mice were inoculated by oral gavage with 100 µl of a bacterial culture grown overnight and concentrated 1:10 in LB broth (approximately 3-5 x 10^9 CFU/mouse as determined by plate counts on MacConkey lactose agar) or with 100 µl of sterile LB broth. Every three days, fecal shedding of *C. rodentium* was determined as described in Appendix 1. Mice were euthanized and necropsied at 3, 6, 12 DPI and 16 WPI as described in Appendix 1. For the second chronic study, groups of 20 control and infected mice were used. Infected mice

received wet food from the day of inoculation and daily subcutaneous injections with 1 ml of LRS (Lactated Ringer's Injection, USP, Abbott Laboratories, Abbott Park, Illinois) from 6 DPI until 15-21 DPI (depending on body weight loss). At 30 WPI, mice were euthanized and necropsied as described in Appendix 1. As no gender differences were observed, the results for female and male mice were combined.

Histopathology. The tissues were dissected and processed as described in Appendix 1. H&E-stained colonic sections were scored for pathological lesions by a veterinary pathologist (PRN) blinded to experimental groups. Inflammation and epithelial atypia within intestinal tissue sections were graded on a scale of 0 to 4 as described in Appendix 1. In chronic studies, the cumulative disease index was calculated as (inflammation score x distribution score) + (hyperplasia score x distribution score) + (dysplasia score x distribution score). The maximum possible disease index score was 48.

Immunohistochemistry. Immunohistochemical analyses of formalin-fixed paraffin-embedded intestinal sections were performed to assess bacterial attachment to epithelial cells, apoptosis and proliferation *in situ* as previously described [Cahill et al., 1997; Newman et al., 1999; Erdman et al., 2005]. Polyclonal rabbit anti-*C. rodentium* [Newman et al., 1999] and anti–activated caspase 3 (Cell Signaling Technologies, Inc., Beverly, MA) antibodies, and monoclonal anti-BrdU antibodies (Dakopatts, Glostrup, Denmark) were used according to the recommendations of the manufacturer. Primary antibodies were detected with either biotinylated goat anti-rabbit IgG (Sigma) or using Animal Research Kit (DAKO, Carpinteria, CA). Sections were visualized using diaminobenzidine as substrate and counterstained with hematoxylin.

Quantification of epithelial proliferation. Animals received a single intraperitoneal injection of bromodeoxyuridine (BrdU; 50 mg/kg) from a freshly made stock solution of 5 mg/ml dissolved in PBS. The mice were euthanized 1 h later. The distal 4-5 cm of the colon were assessed for crypt length and for BrdU incorporation using quantitative computer-assisted image analysis (KS-400 MACROS). Only crypts visible along their entire length were analyzed. The number of specimen examined were n = 14 for control, n = 6 for 3 and 6 DPI, and n = 12 for 12 DPI colons with mean 21.6 crypts/mouse (n = 3-4 mice for cecum with mean 10 crypts/mouse).

Crypt length was expressed in either cell number per crypt column or in μm. BrdU incorporation was expressed as the labeling index percent (LI%), which was calculated as a percentage ratio of labeled cells out of the total number of cells in the crypt. In addition, the proliferative zone was calculated as height of the highest positive cell to a total length of the crypt.

Endpoint PCR for *C. rodentium*. DNA isolated from frozen tissues using Qiagen DNeasy Tissue kit was amplified with primers specific for *eae* (ECW1, ECW2) as described [Wieler et al., 1996]. DNA isolated from DBS120 and *eae* mutant DBS255 [Schauer and Falkow, 1993] were used as positive and negative controls, respectively.

2.5 Tables and Figures

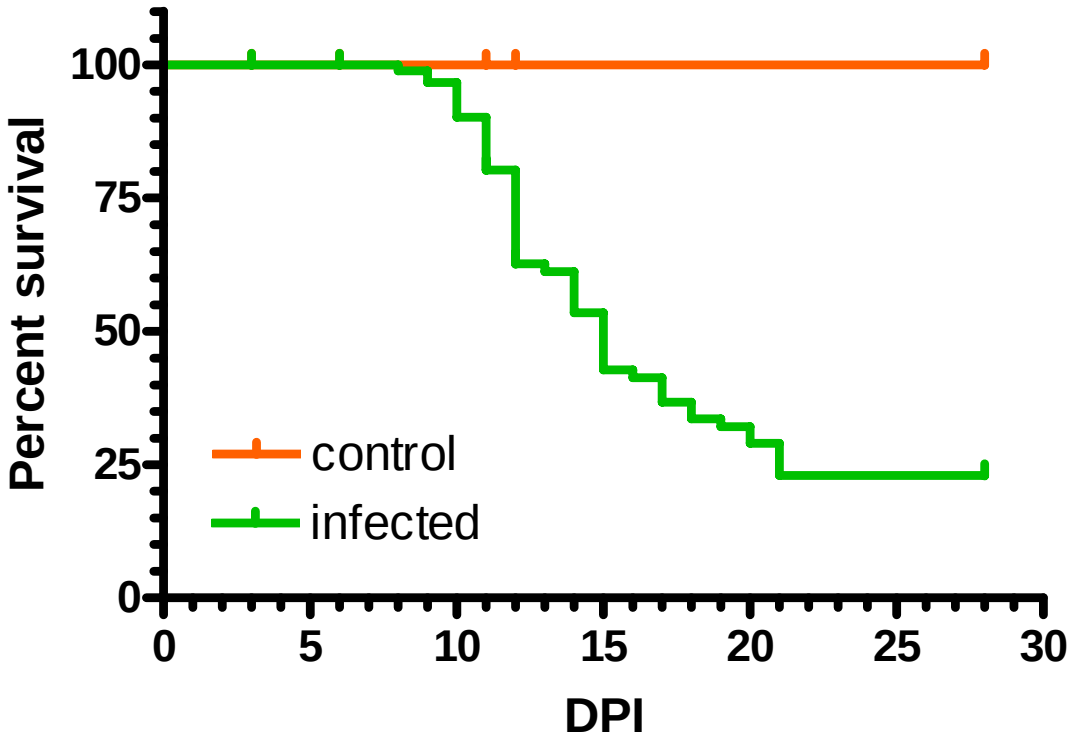

Figure 2-1. Experimental inoculation of FVB mice with *C. rodentium* causes significant mortality beginning by 9 days post-inoculation (DPI).
By 3 weeks only 23% of infected animals survived. Survival curves were generated from 5 independent experiments (n = 41 for control and n = 84 for infected FVB mice). Differences between infected and control animals were significant ($p < 0.0001$ by the Logrank test). There was no mortality in Swiss Webster mice with (n = 20) or without infection (n = 16).

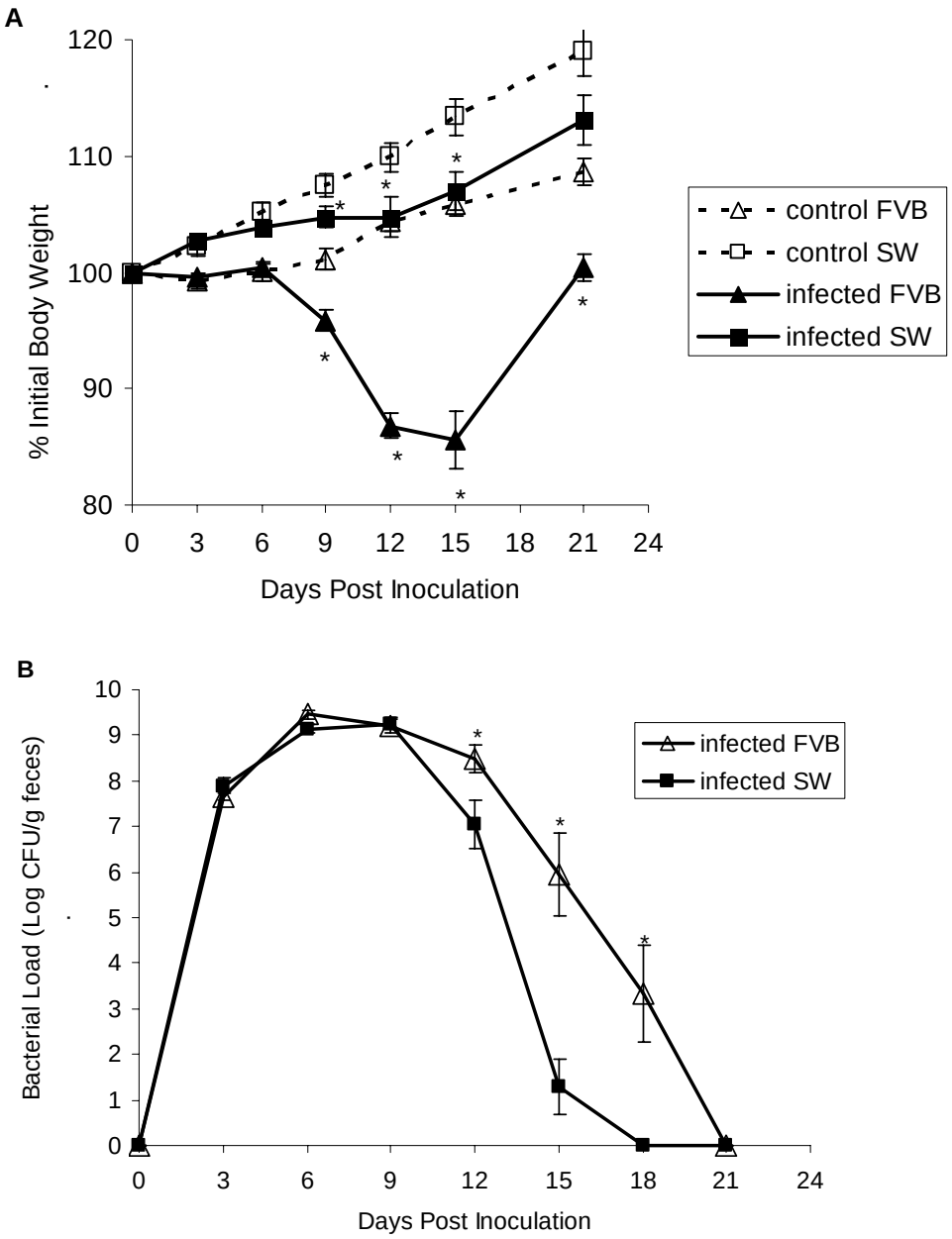

Figure 2-2. *C. rodentium* infection in FVB mice results in body weight loss and delayed bacterial clearance.

A. Body weight loss was greater in FVB mice than in SW mice beginning by 9 DPI ($p < 0.0001$ by two-way ANOVA). Shown are mean ± SEM of percent body weight change compared with initial body weight for surviving mice at each time point, which may overestimate the 21 DPI body weight change for FVB mice (see text). *$p < 0.05$ for SW and $p < 0.0001$ for FVB mice by the paired *t* test.

B. Infection kinetics were similar in both groups through 9 DPI, but bacterial clearance was delayed in FVB mice thereafter. Shown are mean ± SEM log 10 transformed CFU/g feces for surviving animals with feces at each time point, which may underestimate the fecal shedding of *C. rodentium* in FVB mice (see text). *$p < 0.05$ for 12 DPI and $p < 0.0005$ for 15 and 18 DPI by Student's *t* test.

A

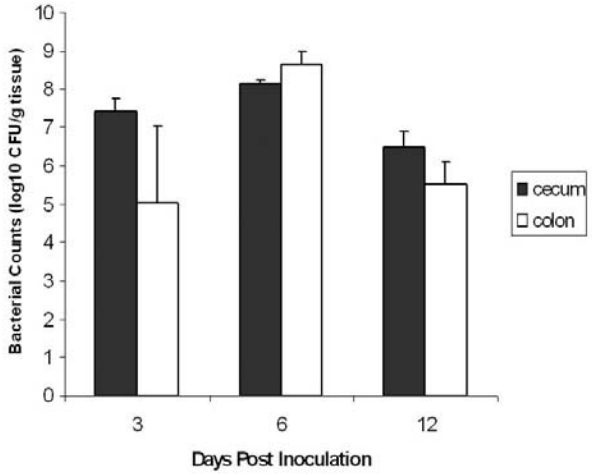
Bacterial Counts (log10 CFU/g tissue)
10
9
8
7
6
5
4
3
2
1
0
3
6
12
Days Post Inoculation
cecum
colon

B

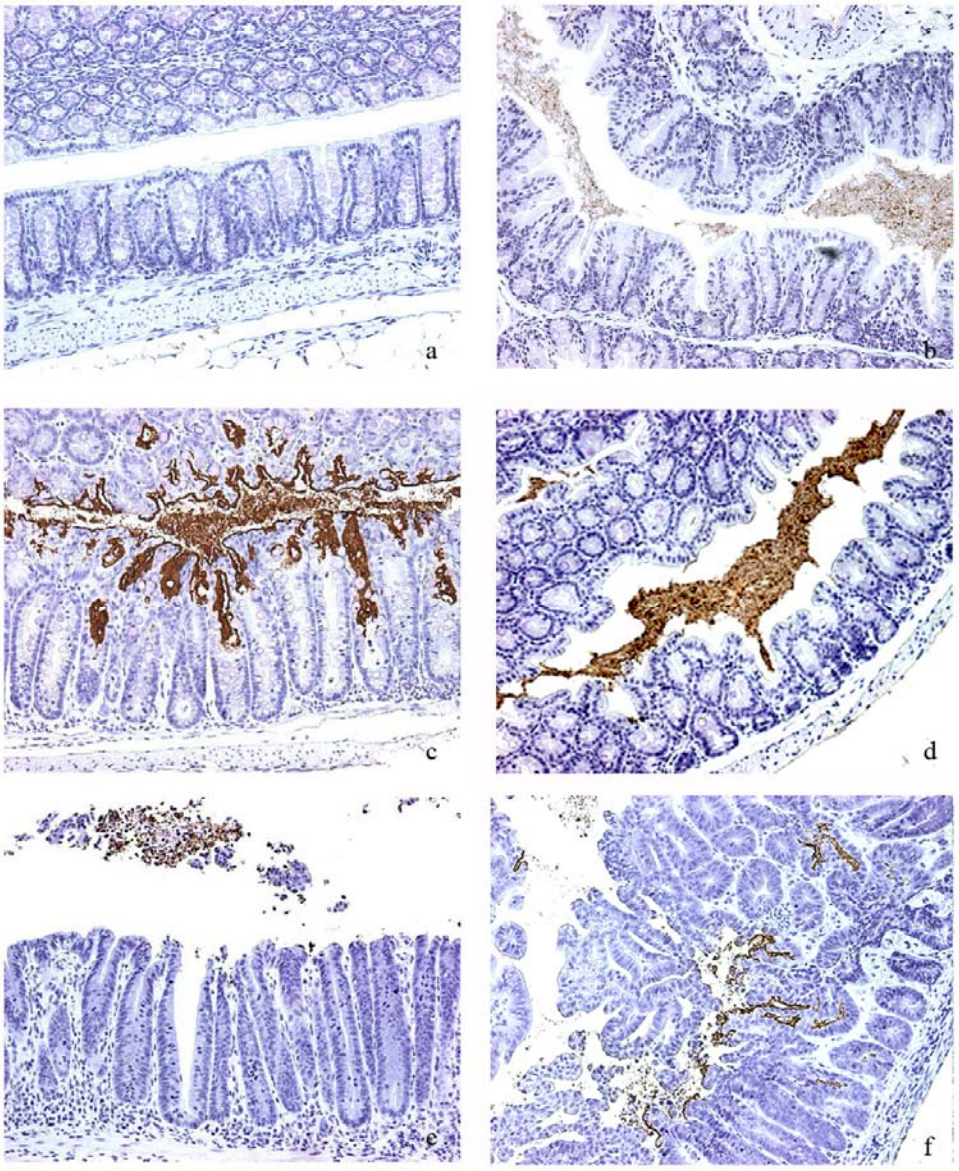
a
b
c
d
e
f

Figure 2-3. Colon and cecum counts of *C. rodentium* do not correlate with bacterial attachment in FVB mice.

A. Tissue homogenates were plated at 3, 6, and 12 DPI. Shown are mean ± SEM log 10 transformed CFU/g tissue.

B. Although high bacterial burden was found at all time points in both cecum and colon, there was no correlation with attachment of bacteria to epithelial cells identified by immunohistochemistry (IHC) for *C. rodentium* (original magnification 200x; panels **a**, c, and **e** are colon; **b**, **d**, and **f** are cecum). No *C. rodentium* was present in control colon or cecum of FVB mice (**a** and **b**). Bacterial attachment was observed in the distal colon beginning by 6 DPI. Bacteria are on the luminal surface, as well as deeper in the crypts (**c**). Although the lumen of the cecum contains bacteria, no attachment to epithelium was observed in the cecum at 6 DPI (**d**). By 12 DPI, most of the positive signal in the colon was associated with exfoliated cells (**f**), though some surface attachment was identified in more proximal regions of the colon (not shown). On the other hand, there were occasional areas of focal bacterial attachment to epithelial cells in the cecum at 12 DPI (**f**).

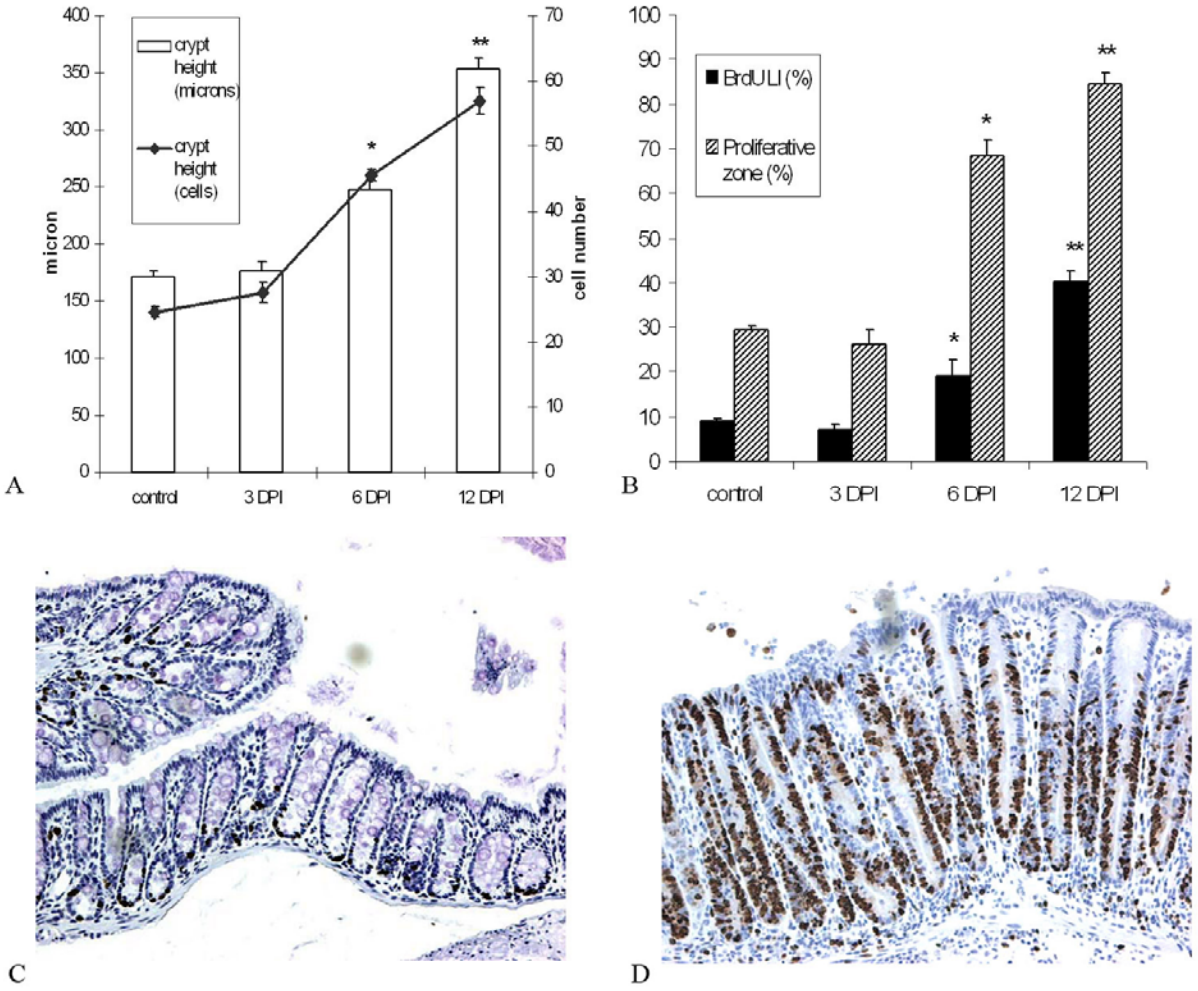

Figure 2-4. *C. rodentium* infection causes epithelial hyperplasia in the colon of FVB mice.
By 6 DPI, there was an increase in crypt column heights and labeling index (**A**) and expansion of the proliferative zone (**B**) in the distal colon of infected animals. Shown are mean ± SEM values, *$p < 0.0001$ by ANOVA with post-hoc Student's *t* test comparisons between the groups. BrdU labeling in control (**C**) and 12-DPI colon (**D**) reveals extensive proliferation of enterocytes throughout the entire crypt including the surface epithelium in infected mice, original magnification 100x.

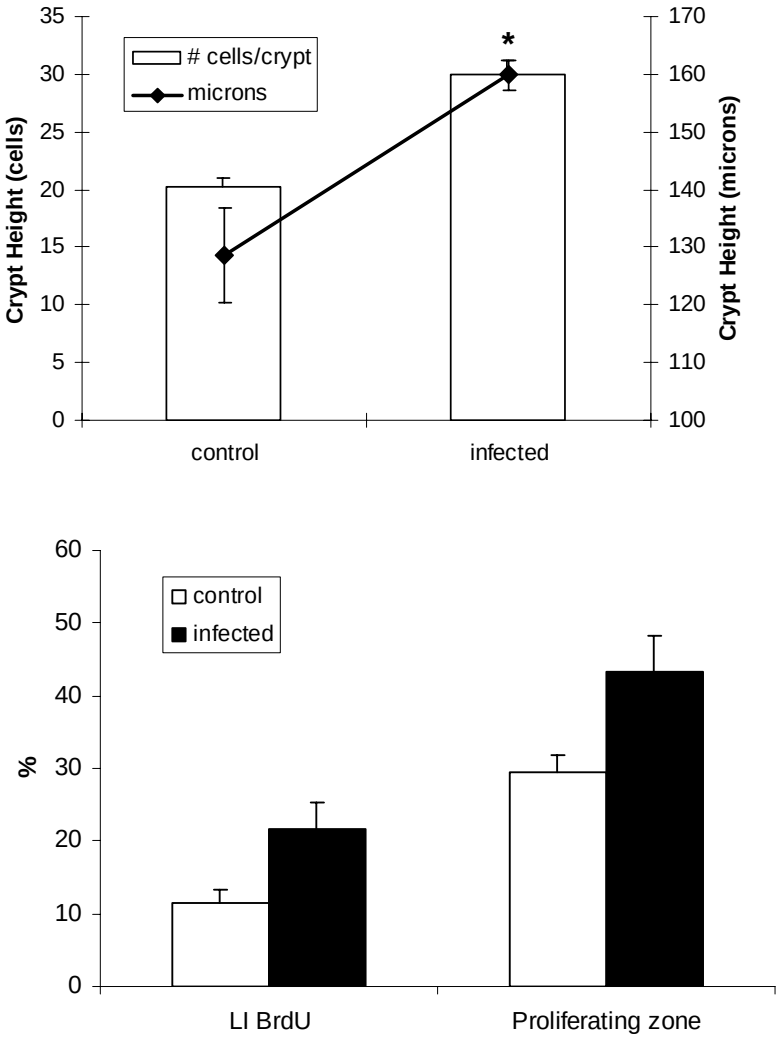

Figure 2-5. Epithelial proliferation in the cecum of *C. rodentium*–infected FVB mice 12 DPI.
Despite the trend for an increase, no significant differences were found for any of the proliferation parameters, except cecum crypt height ($p < 0.01$ by Student's *t* test). The increase in proliferation was less substantial in cecum than in the colon of infected FVB mice (Figure 2-4), which correlated with less bacterial attachment in the cecum than in the colon. Shown are mean $\pm$ SEM values.

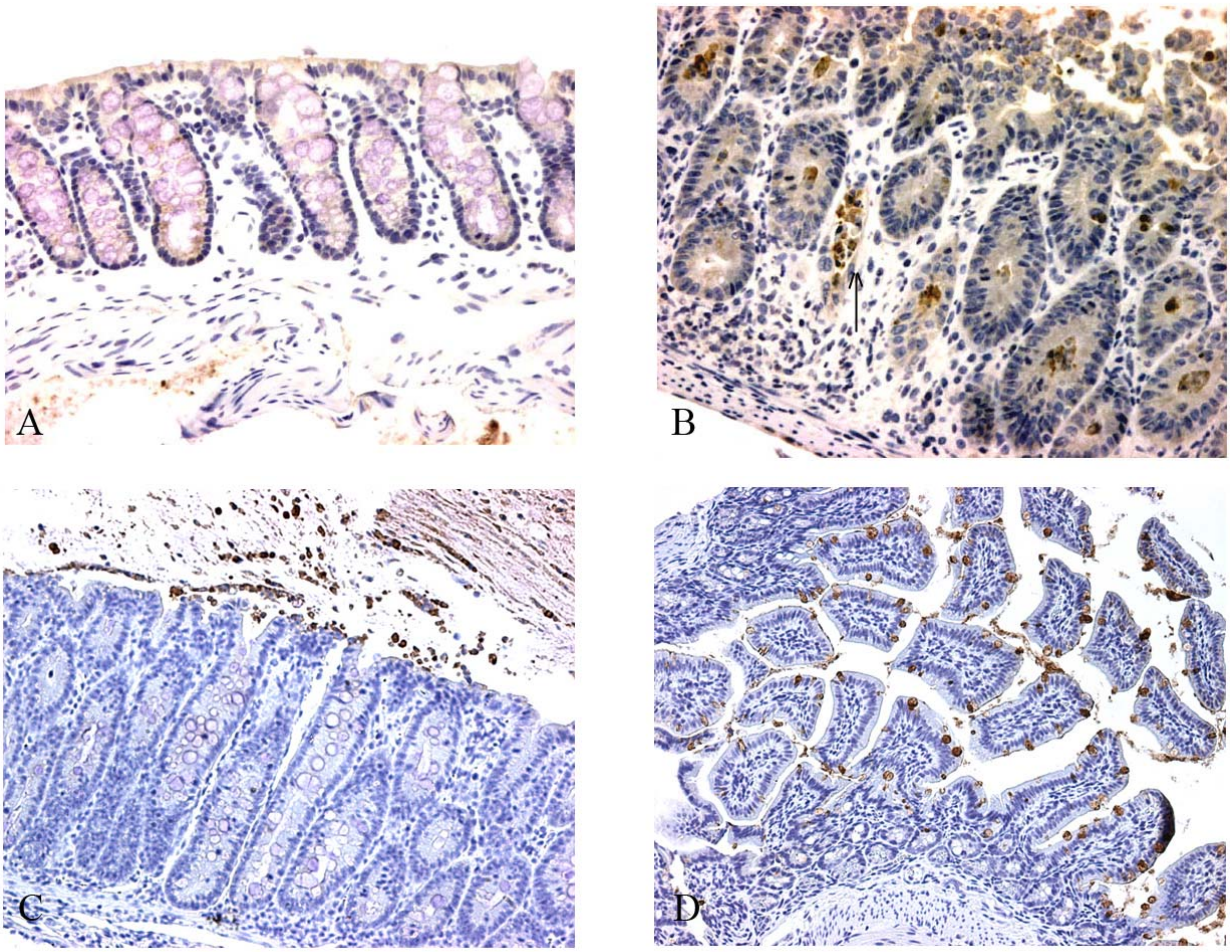

Figure 2-6. Apoptosis in infected FVB mice 12 DPI identified by activated caspase 3 staining.
No apoptosis detected in the colon of uninoculated mice (**A**). Increased apoptosis was observed in dying atrophic crypts (arrow) (**B**). Apoptosis was mainly associated with exfoliated luminal, but not mucosal cells, indicating that apoptotic cells are rapidly removed from the tissues (**C**). Despite the low number of apoptotic cells seen in the colon, substantial staining was observed in the ileum on the same slides (**D**). Original magnification 200x.

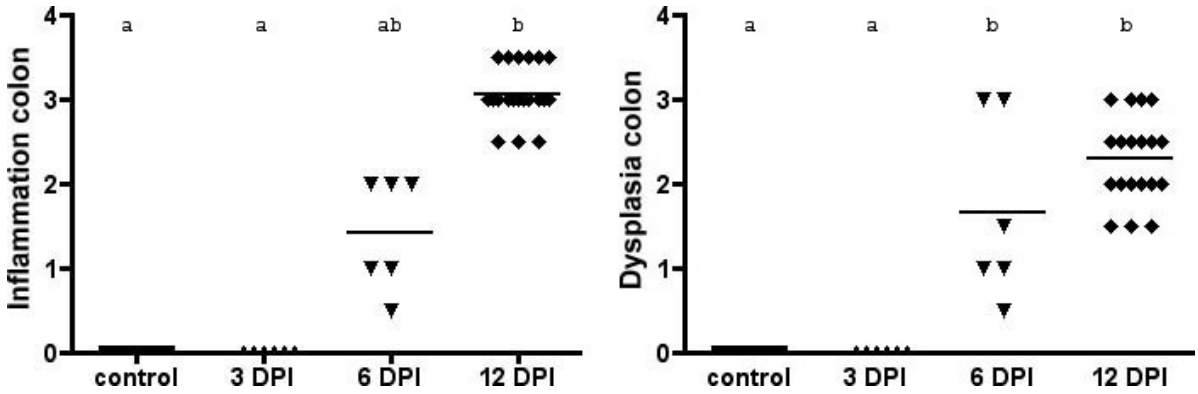

Figure 2-7. Colonic histopathology in FVB mice infected with *C. rodentium.*
FVB mice infected with *C. rodentium* developed colonic inflammation (**A**), by 6 DPI that was more pronounced by 12 DPI. This was accompanied by an increase in epithelial dysplasia (**B**) ($p < 0.0001$ using Kruskal-Wallis non-parametric test with subsequent Dunn's multiple comparison test). Each dot represents one animal. Correlation analysis of inflammation versus dysplasia revealed a strong association between these two factors (Spearman $r = 0.871$, $p < 0.0001$).

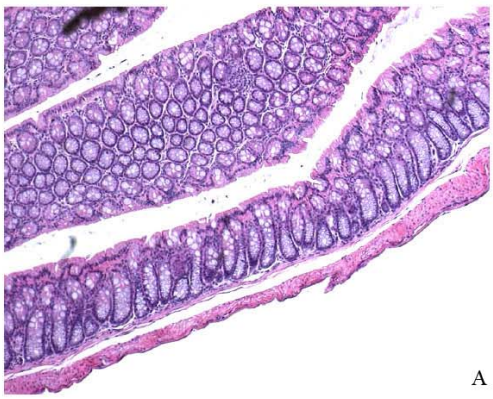
A

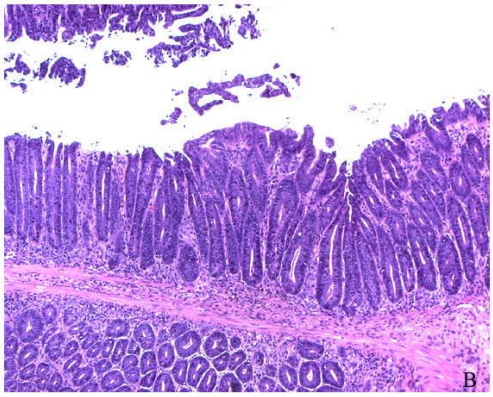
B

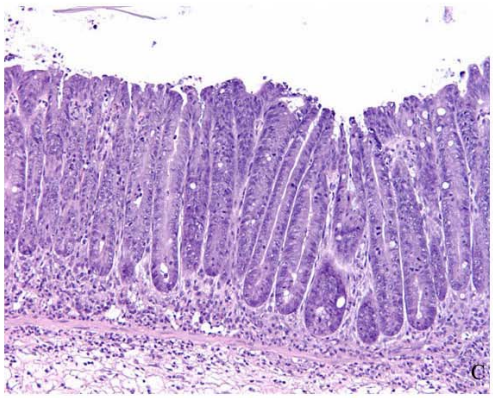
C

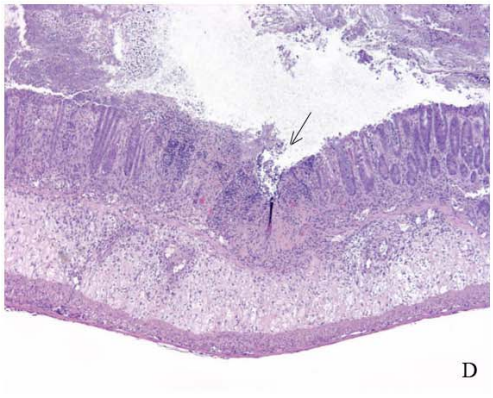
D

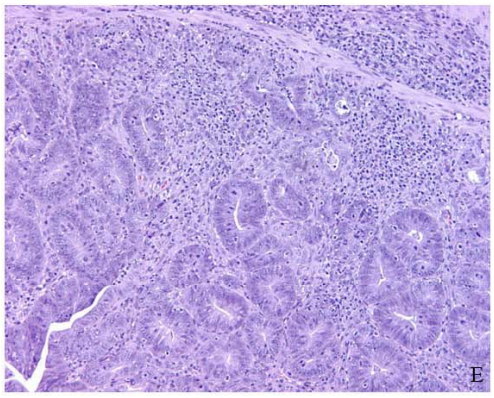
E

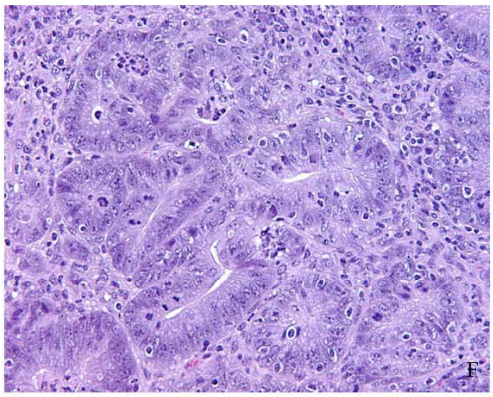
F


G

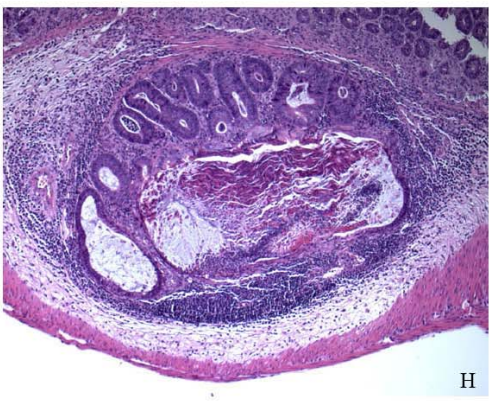
H

Figure 2-8. Microscopic lesions in the colon of FVB mice 12-15 DPI.
A. Normal colon from an uninoculated FVB mouse.
B and C. Hyperplastic crypts with increased numbers of mitotic figures and goblet cell depletion. Note significant infiltrate of inflammatory cells in the mucosa and submucosa.
D. Colitis and ulcer (arrow) with marked transmural inflammation and submucosal edema.
E and F. Epithelial atypia characterized by loss of normal tissue architecture, epithelial cell pleomorphism, gland malformation with splitting, branching and infolding. Some mice with more advanced lesions displayed high nuclear-to-cytoplasm ratio, crypt branching with irregular buds and occasional micronests within the abutting lamina propria.
G and H. GALT-associated atypia with herniated dysplastic crypts and dilated and attenuated cysts in submucosa. H&E stain. Original magnifications are 25x for panel G, 40x for D, 100x for A, B, and H, 200x for C and E, and 400x for F.

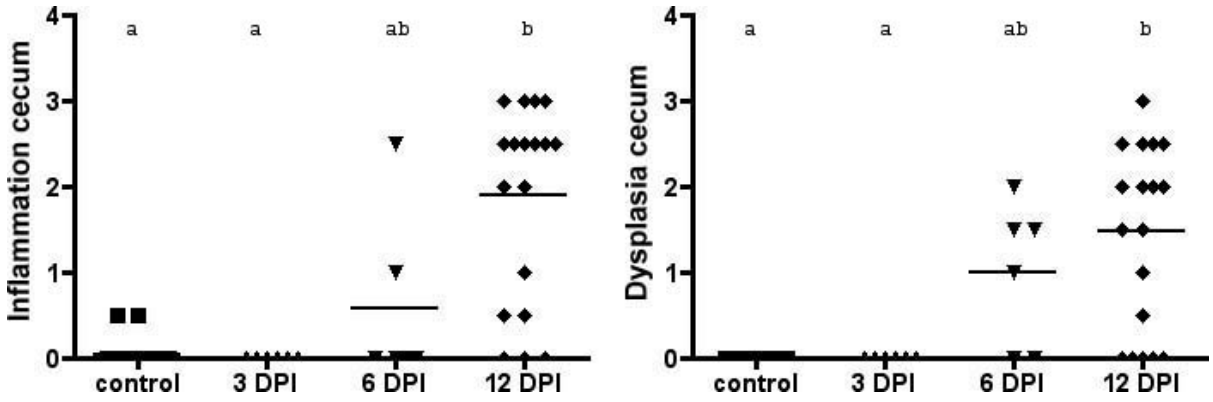

Figure 2-9. Cecal histopathology in FVB mice infected with *C. rodentium.*
Cecal lesions were identified by 12 DPI in infected FVB mice ($p < 0.0001$ using Kruskal-Wallis non-parametric test with subsequent Dunn's multiple comparison test). Inflammation and dysplasia were well correlated (Spearman $r = 0.729$, $p < 0.0001$).

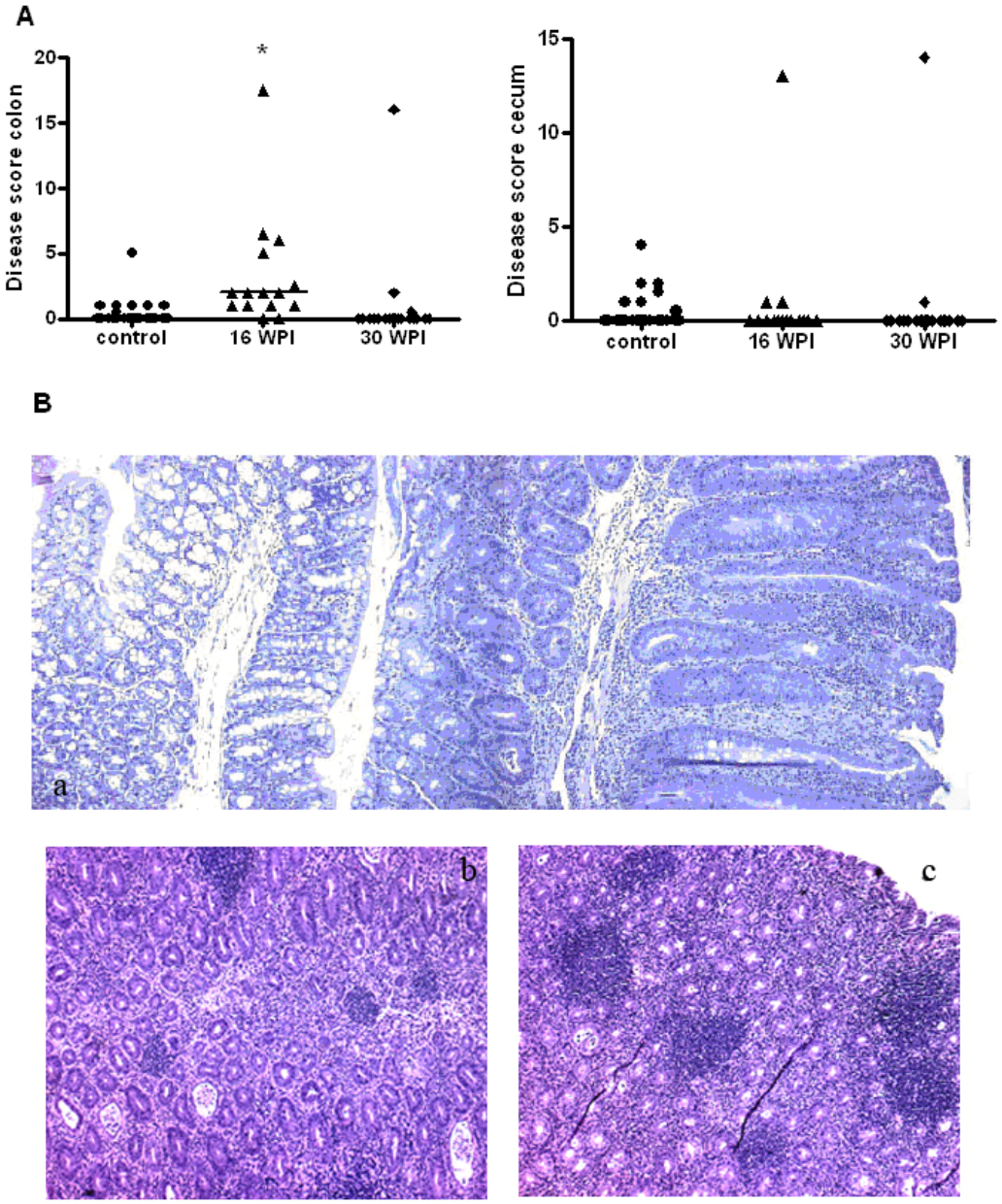

Figure 2-10. A small percentage of mice develop persistent lesions in the large intestine 16 or 30 WPI with *C. rodentium*.
A. Lesion scores in the colon and cecum of uninoculated mice and mice at 16 and 30 WPI. Each dot represents one animal. The colonic disease score was slightly, but significantly, greater at 16 WPI ($p < 0.0001$ by Kruskall-Wallis followed by Dunn's multiple comparison test) compared with uninfected controls and 30 WPI.
B. Photomicrographs of chronic lesions. At 16 WPI, inflamed and hyperplastic tissue, mainly in the proximal colon was segmentally distributed (see adjacent normal mucosa). Original magnification 200x (a). At 30 WPI, diffuse lesions were observed throughout the colon and cecum. Note the numerous lymphoid aggregates, crypt abscesses and dilation. Original magnification 100x (b and c).

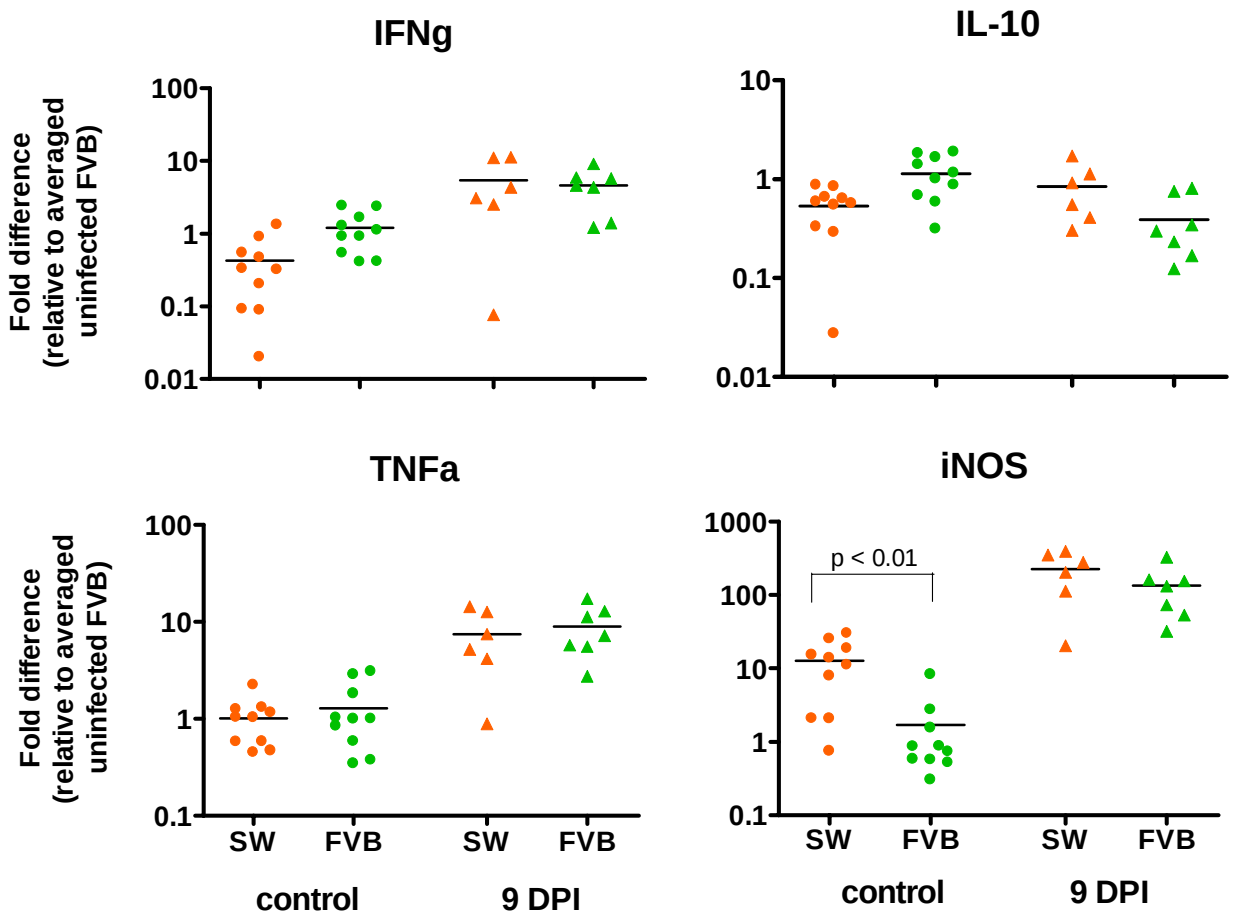

Figure 2-11. Quantitative RT-PCR for expression of immunomodulatory cytokines.
Susceptible FVB and resistant SW mice demonstrated comparable expression of proinflammatory and immunomodulatory genes in response to *C. rodentium* infection. Each dot represents one animal. Mean lines are presented.
$p<0.01$ by one-way ANOVA followed by Tukey's Multiple Comparison Test.

Table 2-1. Number of FVB mice used in the study

Inoculum	3 DPI[a]		6 DPI		12 DPI		16 WPI[b]		Total
	M	F	M	F	M	F	M	F	
Sterile broth	1	2	1	2	7	8	10	10	41
C. rodentium	3	3	3	4	12	19	24	16	84

[a]days post-inoculation, [b]weeks post-inoculation

Chapter 3: Global transcriptome analysis links diarrhea as a cause of mortality in a mouse model of infectious colitis.

Diana Borenshtein[1], Rebecca C. Fry[1,2], Elizabeth B. Groff[3], Prashant R. Nambiar[3], Vincent J. Carey[4], James G. Fox[2,3], David B. Schauer[1,2,3*].

[1]Biological Engineering Division, [2]Center of Environmental Health Sciences, [3]Division of Comparative Medicine, Massachusetts Institute of Technology, Cambridge, Massachusetts, United States, [4]Harvard Medical School, Boston, Massachusetts, United States.

To be submitted to PLOS Pathogens

3.1. Introduction

Acute diarrhea illness is one the most important health problems in the world today, particularly in young children in developing countries. This life-threatening condition occurs in about four billion people per year and causes more than 2 million deaths worldwide each year [Kosek et al., 2003; Lopez et al., 2006; WHO, 1999]. The most common cause of diarrhea is gastrointestinal infection. Infection results in increased intestinal secretion and/or decreased intestinal absorption leading to fluid and electrolyte loss and dehydration that can be fatal if not treated [Casburn-Jones and Farthing, 2004]. Among the most important bacterial causes of diarrhea are enteropathogenic and enterohaemorrhagic *Escherichia coli* (EPEC and EHEC, respectively) [Nataro & Kaper, 1998]. These pathogens produce ultrastructural changes characterized by intimate bacterial adhesion to the apical surface of enterocytes, effacement of microvilli, and pedestal formation, which are called “attaching and effacing” (A/E) lesions. The pathophysiology of diarrhea due to infection with A/E pathogens is not well understood. Proposed mechanisms include decreased absorptive surface epithelium, disruption of tight junction and intestinal barrier function, impaired ion transport, and induction of inflammation [Berkes et al., 2003; Dean et al., 2006; Guttman et al., 2006a; Shifflett et al., 2005; Vallance & Finlay, 2000].

Citrobacter rodentium, a murine A/E pathogen, possess similar virulence factors as EPEC and EHEC, and produces comparable ultrastructural changes in the distal colon of infected mice [reviewed in Luperchio and Schauer, 2001; Mundy et al., 2005]. Typically, this organism causes severe but temporary epithelial hyperplasia with a variable degree of inflammation in the distal colon of most inbred and outbred lines of laboratory mice. Exceptions include suckling animals or C3H substrains (independent of TLR4 status), which demonstrate 60% to 100% mortality by approximately two weeks after infection with *C. rodentium* [Barthold et al., 1976; Barthold et al., 1978; Barthold, 1979; Khan et al., 2006; Vallance et al., 2003]. We recently discovered that adult FVB/N mice (FVB) are also extremely susceptible to *C. rodentium* infection [Borenshtein et al., submitted]. Inbred FVB mice are derived from outbred Swiss Webster (SW) mice and, since SW are known to be resistant, comparative studies between those cognate lines of mice were performed. Twelve-week old FVB mice infected with *C. rodentium* developed high degree of mortality and severe colitis compared with their outbred SW counterparts, which developed more typical subclinical disease in response to infection.

Differences in disease outcome were observed despite comparable expression of TNF-α, IFN-γ, and iNOS in susceptible and resistant animals. The results of our previous study suggested that the cause of death in *C. rodentium*-infected FVB mice was hypovolemia due to dehydration [Borenshtein et al., submitted]. To characterize the mechanistic basis for the striking difference in outcome of infection between two closely related lines of mice, we used microarray technology to determine global patterns of gene expression in susceptible FVB and resistant SW mice infected with *C. rodentium*. Gene Chips from Affymetrix were employed to identify and quantify both strain-dependent and infection-dependent alterations in host gene expression, and results were confirmed by quantitative real-time PCR and serology. We discuss predominant functional categories of differentially regulated genes, potential candidates for susceptibility and implications for future studies of *C. rodentium* pathogenesis. We suggest novel testable hypotheses about newly implicated host genes and their potential role in the development of infectious colitis and diarrhea.

3.2 Results

Infection of FVB and SW mice with *C. rodentium*

To characterize how differentially expressed genes determine susceptibility to *C. rodentium* infection, FVB and SW mice were analyzed before and at two different time points post-inoculation. Time points were selected to reveal differentially expressed genes prior to infection, following establishment of infection but before development of disease (4 dpi), and after the development of colitis but before the development of appreciable mortality (9 dpi). As expected, sham-dosed 12-week old mice were found to be indistinguishable 4 and 9 dpi, therefore, samples from these uninoculated control animals were combined and treated as a single group for each line of mouse (experimental design is presented in Table 3-1).

Details of FVB susceptibility to *C. rodentium* infection were previously reported [Borenshtein et al., submitted]. Here, FVB and SW mice infected with *C. rodentium* developed comparable alterations in body weight, fecal bacterial shedding, and no appreciable colonic lesions at 3-4 dpi (Figure 3-1). By 8 dpi, body weight gain in infected and uninoculated control SW mice was not significantly different (107.5 ± 2.0 % and 106.3 ± 1.8 % of initial body weight respectively, Figure 3-1A), whereas infected FVB mice developed significant weight loss (103.4 ± 1.8 % and 97.6 ± 2.2 % for control and infected mice respectively, $p<0.05$). Likewise, fecal

bacterial shedding was higher in FVB mice than in SW mice at 8 dpi (8.1 ± 0.2 vs. 7.5 ± 0.2 log10 CFU/g feces, respectively, $p<0.05$, Figure 3-1B), although the significance of this difference is not completely clear. At 9 dpi, FVB mice infected with *C. rodentium* developed significant pathological lesions, including colonic inflammation, hyperplasia, and mild dysplasia (Figure 3-1C). Infected SW mice developed comparable hyperplasia, but less inflammation and no dysplasia at 9 dpi ($p<0.0001$). The median lesion scores for infected versus control FVB mice were 2.5 vs. 0 for inflammation, 2 vs. 0 for hyperplasia, and 0.5 vs. 0 for dysplasia. The median lesion scores for infected versus control SW mice were 2 vs. 0 for inflammation, 2 vs. 0 for hyperplasia, and 0 vs. 0 for dysplasia. Samples for microarray analysis were selected based on the clinical signs, infection status, and severity of lesions, and are shown in Figure 3-1.

Gene expression analysis of FVB and SW mice during *C. rodentium* infection

Differential expression analysis of pairwise comparisons (Material and Methods) identified 462 probe sets (1% of the total number of probe sets) significantly different between SW and FVB mice prior to infection (Figure 3-2A). In response to *C. rodentium* inoculation, 5,123 probe sets (11.4%) were either induced or repressed by more than two-fold in one or both of the lines of mice. The number of significantly modulated genes in response to infection was greater in susceptible FVB mice than in resistant SW mice, particularly as disease progressed. Specifically, infected FVB mice had 2,195 and 3,297 differentially expressed probe sets at 4 and 9 dpi, respectively, compared with uninoculated controls, whereas infected SW mice had 1,798 and 1,945 differentially expressed probe sets at 4 and 9 dpi, respectively, compared to uninoculated controls (Figure 3-2A). Overall, alterations in 5,585 (12.4%) probe sets corresponding to 4,257 genes were detected during the course of the experiment. Most of the differences were within +/- 7-fold range (Table 3-S1, available at http://web.mit.edu/diana_b/www/TableS1.xls)

Validation of microarray results by quantitative RT-PCR

To confirm the results obtained with Gene Chips, quantitative real-time fluorigenic RT-PCR (TaqMan) was performed for 35 selected genes. Correlation analysis was performed by comparing expression ratios from microarray results versus ratios determined by TaqMan analysis (Figure 3-2B). Significant correlation was observed between the two assays (Pearson

correlation coefficient r = 0.87, R^2 = 0.75, p<0.0001). Individual Pearson correlation coefficients ranged from 0.67 to 1 in all but two out of 35 genes (*Crry* and *Slc10a2*) (Table 3-2). The overall predictability rate of the microarray results by quantitative real time PCR was 94%, which compares favorable or even exceeds that reported for data processing by dChip [Rosati et al., 2004]. Side-by-side comparisons of microarray and qRT-PCR results are presented in Figure 3-3.

Analysis of genes exhibiting a host effect

To identify genes that were differentially expressed between susceptible FVB mice and resistant SW mice, referred to here as a host effect, comparative analysis of common and unique genes modulated at individual time points was performed (Spvs.Fp or Si4vs.Fi4 or Si9vs.Fi9). Transcripts (1,303) represented by 1,547 probe sets (3.4%), were more than two-fold differentially expressed between the two lines of mice (a complete list of genes with host effects is presented in Table 3-S2, available at http://web.mit.edu/diana_b/www/TableS2.xls).

Principal Component Analysis (PCA) was applied to the resulting data (Figure 3-4A, Table 3-3), yielding distinct groups correlating to the line of mouse and infection status. Consistent with their inbred strain background, there was tighter clustering of uninoculated control FVB mice than uninoculated control outbred SW mice. Discrimination of FVB mice as a function of time during infection was quite good, whereas classification of SW mice as a function of time during infection was less robust, reflecting greater variation between individuals and milder disease overall. Similar results were obtained by hierarchical clustering (Figure 3-5). Distinct branches for uninoculated, 4 dpi, and 9 dpi FVB mice, along with good separation between uninoculated and infected SW mice was in good agreement with the results of PCA.

Differentially expressed genes between SW to FVB mice as a function of time during infection were divided into 7 sub-groups (Figure 3-4B). Group A represents genes that were differentially expressed between the lines of mice at all times. Groups B, C, and D represent genes that were differentially expressed at two time points. Groups E, F, and G represent genes uniquely differentially expressed between uninfected mice, or infected mice at 4 or 9 dpi, respectively. Enrichment analysis was performed to identify, group, and permit further characterization of genes that contribute to specific biological functions. Many transcripts identified by enrichment analysis were uncharacterized genes or expressed sequence tags, but 1,015 (77.9%) transcripts were assigned to a Gene Ontology (GO) node, 347 (26.6%) to a

Protein Domain node, 164 (12.6%) to a Pathway node, and 1,136 (87.2%) to a Chromosome node. The complete list of enriched GO categories, as well as in each sub-groups, is shown in Table 3-S3 (available at http://web.mit.edu/diana_b/www/TableS3.xls).

To analyze GO terms enriched between the two lines of mice for biological function, fast assignment and transference of information GO (FatiGO) was used. After excluding genes with unknown function and redundant probe sets, 902 genes out of 1,547 were used for analysis. Approximately 25% of these genes were assigned to GO "transport" at the fifth level of hierarchical clustering, making it one of the most prevalent categories. On the other hand, only 11% of genes were assigned to "immune response" category (Figure 3-4C).

The most significantly differentially expressed genes are presented in Table 3-4 (hierarchical clustering of those genes is shown in Figure 3-6). A number of these genes were consistently overexpressed in one line of mouse compared to the other line before and at all time points after infection (Group A). These genes included arginase type II (*Arg2*), hypoxia inducible factor alpha (*Hif1a*), interferon activated genes 202b and 203 (*Ifi202b* and *Ifi203*), membrane-spanning 4-domains (*Ms4a4b*, aka *Chandra*), proton-dependent high affinity oligopeptide transporter *Pept2* (*Slc15a2*), sorting nexin 6 (*Snx6*), sialyltransferases *St3gal4* (aka *Siat4c*) and *St6galNac1* (aka *Siat7a*), and ubiquitin carboxyl-terminal esterase L5 (*Uchl5* aka *Uch37*). Other genes, such as angiogenin (*Ang4*), immunoglobulin chains (*IgK*, *Igh-VJ558*), and intelectin (*Intl*) were overexpressed in one line of mouse prior to infection, but became overexpressed in the other line at some point during infection. Some genes were profoundly modulated in one line of mice at a particular time point. Among those transcripts were apolipoprotein C-II (*Apoc2*), aquaporin 8 (*Aqp8*), carbonic anhydrases 1 and 4 (*CA I* and *CA IV*), chloride channel calcium activated 3 (*Clca3*), cytochrome P450 (C*yp2d9*), meprins 1 alpha and beta (*Mep1a* and *Mep1b*), resistin-like beta (*Retnlb*, aka *Fizz2* or *Relmb*), oligopeptide transporter *Pept1* (*Slc15a1)*, and down-regulated in adenoma *Dra* (*Slc26a3*). A few genes, namely *Krt6a, Stfa3, Rptn*, and *Krtdap*, showed variable expression within the group of uninoculated animals in both FVB and SW strains, and hence were excluded from further analysis.

Enrichment analysis of the top genes using the hypergeometric test for establishing a cutoff threshold revealed 9 genes in "transporter activity", 6 genes in "oxidoreductase activity", 5 genes in "carrier activity", and 4 genes in "immune response" categories ($p<0.05$) (Table 3-5).

Most of those genes, including ATP-binding cassette *Abcg5*, *Apoc2*, *Aqp8*, *Clca3*, *Slc15a1*, and *Slc26a3* were substantially down-regulated in FVB mice at 9 dpi. Radial spokehead-like 2 (*Rshl2*) was expressed at higher level in SW mice, especially at 4 dpi. Two other genes, *Slc15a2* and *Snx6*, were expressed at a significantly lower level in FVB mice at all time points (Table 3-4 and Figure 3-6).

To address temporal changes in response to infection, delta eta analysis was performed (see methods). Out of 1,385 probe sets detected by delta eta analysis, 468 were differentially expressed between the lines of mice at 4 dpi, 1,173 transcripts at 9 dpi, and 256 at both time points. The top candidates differentially expressed by more than 8-fold included 36 genes, most of which were also identified by pairwise comparisons described above. Interestingly, delta eta analysis also discovered novel candidates that were not identified by pairwise comparisons (Figure 3-7, Table 3-S4 http://web.mit.edu/diana_b/www/TableS4.xls), including aquaporin 4 (*Aqp4*) which was upregulated in SW mice but not in FVB mice. Enrichment analysis of these transcripts revealed 8 genes in “organismal physiological process”, 7 genes in “transporter activity”, 6 genes in "immune response", 6 genes in “antigen binding”, 4 genes in “channel or pore class transporter activity”, and 4 genes in “carbohydrate binding” categories ($p<0.05$, Table 3-6)

Comparative analytical approach

To independently confirm the results obtained by dChip analysis, Robust Multichip Analysis (RMA) using Bioconductor was also applied to the data. Comparison of uninoculated mice by Limma resulted in 232 host-related genes (Table 3-S5, available at available at http://web.mit.edu/diana_b/www/TableS5.xls).). Temporal changes in infected mice were determined by contrasting linear models for expression with different slopes for the two lines of mice and resulted in 167 host x infection time-related genes (Table 3-S6, available at available at http://web.mit.edu/diana_b/www/TableS6.xls). Only 12 genes were shared between the two sets of genes. GO category “transporter activity” was the most highly enriched functional cluster within genes altered by infection in a host-dependent manner ($p<0.0005$, Table 3-7). Categories with transport functions were markedly overrepresented compared with immune-related clusters as detected by FatiGO analysis (Figure 3-8). When random forest evaluation of gene importance in predicting four classes (host x infection status) was applied, 19 genes appeared to have high

predictive capacity ($p<0.05$) (Figure 3-9). Among them were the transcripts for *Slc26a3* and *Aqp8*, which were as well detected by dChip analysis as most differentially expressed between infected SW and FVB mice.

Differential expression of genes involved in intestinal ion transport and its regulation

The prevalence of transport genes within the set of differentially expressed transcripts detected by different analytical methods supports the hypothesis that high mortality in *C. rodentium*-infected FVB mice results from severe diarrhea and dehydration as a consequence of electrolyte imbalance [Borenshtein et al., submitted]. We next concentrated on genes implicated in intestinal ion transport as well as genes with regulatory and/or signaling functions. GO annotations are not complete for all transcripts. Moreover, some genes involved in intestinal transport, though included in other annotational categories, do not comprise a single distinct "intestinal transport" group in pathway analysis. Therefore, differentially expressed genes to be validated by quantitative RT-PCR (Figure 3-10) and further characterized (Figure 3-11) were selected based on current understanding of colonic ion transport [reviewed in Field, 2003; Kunzelmann and Mall, 2002].

Differential expression of a number of transcripts was observed between the two lines of mice at all time points (Group A). For example, FVB mice had consistently higher expression of the adenosine A2B receptor (*Adora2b*). Other genes were consistently overexpressed in FVB mice compared to SW mice, but also exhibited different expression as a function of time during infection. Sorting nexin *Snx6* (overexpressed in FVB mice by 16 to 31-fold compared with SW mice) had increased expression at 4 dpi by approximately 2-fold in both lines of mice. However, at 9 dpi, expression of *Snx6* remained elevated in FVB mice but returned to normal in SW mice. *Slc15a2* (overexpressed in FVB mice by 50-, 15-, and 2-fold before infection and at 4 and 9 dpi, respectively) had increased expression in infected SW mice by 2-fold, but was downregulated in infected FVB mice by 1.5- and 11-fold at 4 and 9 dpi, respectively.

Some genes were differentially modulated in infected mice as early as 4 dpi, indicating a rapid response and/or involvement in regulation. For example, expression of the Na^+/K^+-ATPase beta 2 subunit (*Atp1b2*) was increased in SW mice by only 2.5- and 6-fold at 4 and 9 dpi, whereas in infected FVB mice it was induced by 10- and 55-fold respectively. Similar changes

were observed in transcription factor FBJ osteosarcoma oncogene B (*Fosb)*, with 3-fold increased expression in infected SW mice at both time points, and 12- and 16-fold changes in FVB mice at 4 and 9 dpi, respectively. The calcium/calmodulin-dependent protein kinase *Camk2b* had 4-fold decreased expression in SW mice at 4 dpi, but 2.5-fold increase in expression in FVB mice at 9 dpi. Expression of the basolateral water channel *Aqp4* was induced in both lines of mice at 4 dpi, but more significantly in SW mice (6- to 7-fold increase compared with 2- to 3-fold increase in FVB mice). At 9 dpi, expression of *Aqp4* remained elevated in SW mice, but returned to baseline in FVB mice, resulting in 6- to 8-fold difference between the lines.

The number of differentially regulated genes between infected FVB and SW mice increased over time. Many of these genes had profound decreases in expression, including *Slc26a3* (1,100- vs. 3-fold change in FVB vs. SW mice at 9 dpi), *Aqp8* (268- vs. 2-fold change), the sodium/hydrogen exchanger *Slc9a2 (NHE2)* (22.5- vs. 6-fold change), the apical iodide transporter (*Slc5a8*) (13- vs. 2-fold-change), and carbonic anhydrases *CA I* and *CA IV* (87- vs. 0.8-, and 586- vs. 2.5-fold change, respectively). Less dramatic changes included more than 2-fold upregulation of the potassium channel *Kcnn4 (SK4)* and the cGMP-dependent protein kinase *Prkg2* in FVB mice without notable change in the expression of these genes in SW mice. Likewise, downregulation of the sodium/hydrogen exchanger *Slc9a3 (NHE3)* (8- vs. 3-fold decrease in FVB vs. SW mice), alpha and beta subunits of the epithelial Na+ channel (ENaC) encoded by *Scnn1a* and *Scnn1b* (2.7-fold decrease in FVB mice vs. 1.8-fold decrease or no change in SW mice, respectively), the sodium-hydrogen exchanger regulatory factor *Slc9a3r1* (*NHERF1* aka *EBP-50)* (2-fold vs. no change) and *2010110P09Rik* encoding the calcineurin B homologous protein Chp2 (8- vs. 2-fold change) was observed. Expression of the ouabain-sensitive H^+, K^+-ATPase *Atp12a* (*cHKA*) had decreased in FVB mice by 2.5-fold, but increased in SW mice by 1.5-fold at 9 dpi (Figure 3-11, Table 3-S1).

In addition to genes identified by array, we verified the expression of cystic fibrosis transmembrane conductance regulator homolog (*Cftr*), which serves as the main chloride transporter in intestine and other tissues. Two transcripts corresponding to this gene showed opposite results by array (Figure 3-11, Table 3-S1), bringing into question the importance of changes in expression of the gene in our model. Nevertheless, to create a clearer picture of intestinal ion transport in *C. rodentium*-infected mice, we analyzed that gene by qRT-PCR and

found no difference in *Cftr* expression between SW and FVB mice, though subtle decrease in mRNA levels was observed at 9 dpi (2- and 4-fold respectively; Figure 3-10).

Alterations in serum electrolytes

Gene expression profiling identified significant differences in expression of ion transporters which could contribute to diarrhea and fluid and electrolyte loss in FVB mice. Because severe alterations in electrolyte homeostasis could be reflected in changes in serum chemistry, we measured serum electrolytes in SW and FVB mice (Figure 3-12). While no changes in electrolytes levels were detected in SW mice during infection, infected FVB mice developed significant hypochloremia and hyponatremia ($p<0.001$). The mean concentrations of serum chloride was 102.4 ± 1.8, 105.5 ± 2.3, and 104.8 ± 2.3 mEq/L in SW mice before infection and at 4 and 9 dpi, respectively; and 102.9 ± 1.8, 99.6 ± 2.1, and 91.5 ± 2.3 mEq/L in FVB mice before infection and at 4 and 9 dpi. Sodium concentration in serum was 146.4 ± 1.5, 144.7 ± 1.9, and 147.2 ± 1.9 mEq/L in SW mice before infection and at 4 and 9 dpi; and 144.2 ± 1.5, 139.6 ± 1.7, and 138.5 ± 1.9 mEq/L in FVB mice before infection and at 4 and 9 dpi. Anion gap, total CO_2 and potassium levels were comparable in all groups at all time points (data not shown), whereas Na^+/K^+ ratios was lower in infected FVB mice at 9 dpi (16.0 ± 0.9 compared with 20.5 ± 0.9 in SW at 9 dpi, $p<0.005$).

3.3 Discussion

Global expression profiling is emerging as a powerful method to characterize host-pathogen interactions [Coombes et al., 2004], although many of the studies to date have been performed on cultured cells rather than *in vivo*. Here we present global expression analysis of host response to infection with an A/E pathogen for the first time. The goal of this study was to characterize the pathophysiologic basis of susceptibility to *C. rodentium* infection in FVB mice. In order to accomplish this, we performed quantitative analysis of the transcriptome of distal colon tissues from FVB and SW mice before and during *C. rodentium* infection. These studies revealed profound differences in response to infection between susceptible FVB mice and resistant SW mice.

Many studies of *C. rodentium* interactions with host cells have focused on immune responses and the actin cytoskeleton [Luperchio and Schauer, 2001; Mundy et al., 2005]. Indeed, a substantial fraction of functional categories of differentially expressed genes that we identified are involved in immune responses and cellular adhesion (Table 3-S3). However, studies from our group as well as others suggest that innate and adaptive immunity, though important in determining the development of morbidity, is not the most important factor in determining mortality. Susceptible FVB mice were able to clear *C. rodentium* infection, were fully protected against mortality by fluid therapy (without affecting the severity or extent of colonic lesions), and demonstrated similar expression of pro-inflammatory and immunomodulatory genes in the colon compared to resistant SW mice [Borenshtein et al., submitted]. Likewise, the status of LPS responsiveness (TLR4 sufficiency) in different substrains of C3H mice infected with high load of *C. rodentium* did not affect the incidence of mortality [Khan et al., 2006; Vallance et al., 2003]. These observations suggest that immune status of the mice does not contribute to ability to survive through the infection, but most likely affects the clearance of the pathogen.

Genes differentially expressed between FVB and SW mice, including the most significant candidate susceptibility genes, were remarkably enriched for transport activity (Figure 3-4C and Table 3-5). These results were confirmed using multiple algorithms and demonstrated a larger fraction of transport genes than immune-related genes in determining susceptibility to *C. rodentium* infection. In addition, serum chemistry analysis showed significant hypochloremia and hyponatremia in infected FVB mice (Figure 3-15), consistent with marked electrolyte losses in animals suffering from severe diarrhea [Al-Majali et al., 2000; George and Lerche, 1990; Schweinfest et al., 2006]. We previously suggested that high mortality in FVB mice infected with *C. rodentium* could be attributed to hypovolemia induced by severe diarrhea [Borenshtein et al., submitted]. Results from this study suggest that intestinal ion disturbances rather than immune-related processes are responsible for dramatic phenotype in *C. rodentium*-infected FVB mice. Here, we discuss potential candidate genes for susceptibility identified in microarray analysis and how they could contribute to mortality in FVB mice infected with *C. rodentium*. Our working hypothesis for the overall mechanism of susceptibility is presented in Figure 3-13.

Candidates for susceptibility – genes involved in ion transport and its regulation.

The main function of the adult colon is to absorb Na^+, Cl^-, short-chain fatty acids (SCFAs) and fluid and to secrete K^+, Cl^-, HCO_3^-, and mucus [reviewed in Field, 2003; Kunzelmann and Mall, 2002] (Figure 3-13A). Osmotic gradient created by active salt transport is the driving force for passive water movement in/out of the lumen. Water transport can also occur actively through specific water channels, aquaporins [Barrett and Keely, 2000]. The absorptive functions of the colon are usually dominant, whereas transport is changed toward more electrolyte secretion and less absorption resulting in loss of fluid into intestinal lumen during diarrhea [Field, 2003; Kunzelmann and Mall, 2002]. Secretion of fluid and mucus into the lumen is an important mucosal defense mechanism that serves to dilute and wash away deleterious substances from the epithelial surface [Hecht, 1999]. However these mechanisms also can lead to hypovolemia, circulatory collapse and multiple organ failure when profound fluid losses result in marked decrease in plasma volume [Mello et al., 2004].

In FVB mice, transcriptional changes in transporters and signaling or regulatory genes were more dramatic than in SW mice during *C. rodentium* infection (Figure 13-3B and C).

Chloride absoprtion. The most striking difference between infected FVB mice and SW mice was in *Slc26a3* which encodes the down-regulated in adenoma (Dra) protein. Dra mediates apical sodium-independent reabsorption of chloride into epithelial cells and excretion of bicarbonate into the lumen [Ko et al., 2002; Makela et al., 2002]. Mutation in Dra is associated with congenital chloride diarrhea (CLD), a recessive inherited intestinal disorder characterized by watery diarrhea and severe dehydration, high levels of fecal chloride, electrolyte disturbances, including hypochloremia and hyponatremia, leading to metabolic alkalosis, hypokalemia, and death if untreated [Hoglund et al., 1996, Holmberg et al., 1975]. *Dra*$^{-/-}$ mice are the only mouse model for intestinal transporter deficiency that develop substantial diarrhea and serum electrolyte imbalances [Schweinfest et al., 2006], whereas *NHE2*$^{-/-}$, *NHE3*$^{-/-}$, *cHKA*$^{-/-}$, *Aqp4*$^{-/-}$ and *Aqp8*$^{-/-}$ mice have subtle if any changes in stool water content and normal serum levels of chloride and sodium [Bachmann et al., 2004; Meneton et al., 1998; Schultheis et al., 1998a; Schultheis et al., 1998b; Wang et al., 2000; Yang et al., 2005]. Remarkable downregulation in *Dra* expression in infected FVB mice (by 1,100-fold at 9 dpi) suggests *Slc26a3* as one of the most plausible candidate genes for susceptibility to mortality.

Chloride secretion. There are conflicting data regarding regulation of *Slc26a3* by CFTR, the major chloride channel [Chernova et al., 2003; Greeley et al., 2001; Simpson et al., 2005; Wheat et al., 2000]. In this study, expression of *Cftr* was only slightly decreased in FVB mice at 9 dpi and was not associated with changes in *Slc26a3* message. Similar observations were made by Umar et al. [2000] who reported subtle changes in *Cftr* expression in whole distal colon from SW mice infected with *C. rodentium*. Although isolated crypts exhibited a greater increase in the levels of *Cftr* mRNA and protein, this did not correlate with large increases in transmucosal cAMP-dependent Cl^- current, suggesting that other factors play an important role in regulating chloride transport during *C. rodentium* infection [Umar et al., 2000]. For example, chloride secretion via CFTR and other chloride channels can be activated by cAMP, cGMP, and calcium [Barrett and Keely, 2000; Berkes et al., 2003]. *Camk2b* and *Prkg2*, which would be expected to be downstream of these signals, were increased in infected FVB but not SW mice. This is consistent with a post-transcriptional mechanism of CFTR involvement in *C. rodentium*-induced diarrhea. Notably, the same signaling pathways are also implicated in inhibition of sodium/proton exchange and electrogenic Na^+ absorption in colon [Kunzelmann and Mall, 2002; Lamprecht et al., 2002; McSwine et al., 1998; Zachos et al., 2005].

Sodium absorption. Expression of *ENaC, NHE2* and *NHE3*, which are the main sodium channels involved in apical electrogenic and electroneutral sodium absorption, pH maintenance and fluid balance in intestine [Kunzelmann and Mall, 2002; Zachos et al., 2005], was decreased by infection in FVB mice, and to a lesser extent in SW mice. Downregulation of the calcineurin B homologous protein (CHP), which is required for Na^+/H^+ antiport activity [Pang et al., 2001] further indicates that intestinal transport is affected at transcriptional and post-transcriptional levels in infected FVB mice. Coupling of DRA, CFTR, and NHE3 activity is mediated by PDZ-binding scaffold proteins [reviewed in Lamprecht and Seidler, 2006]. One such protein, EBP50 encoded by *Slc9a3r1* (*NHERF1),* is required for cAMP-mediated inhibition of NHE3 activity and stimulation of CFTR activity. The interaction of NHERF1 with the type III secretion system effector Map was recently implicated in the pathogenesis of EPEC and *C. rodentium* [Simpson et al., 2006]. The decrease in expression of EBP50 in infected FVB mice may represent an unsuccessful attempt to control diarrhea. It is notable that decreased expression of individual sodium transport genes was mild (2- to 3-fold), but collectively of the failure to reabsorb sodium contributes mortality.

Potassium transport. The driving force for apical Cl^- secretion is provided by means of basolateral potassium recycling through Na^+, K^+-ATPase and K^+ channels [Barrett and Keely, 2000]. Infected FVB mice demonstrated marked increase in expression of *Atp1b2* that encodes Na^+, K^+-ATPase beta-2 isoform at both 4 and 9 dpi, and to a lesser extent stimulated expression of potassium channels *KCNN4* and *NKCC1* at 9 dpi. Furthermore, Na^+, K^+-ATPase activity was recently shown to be indirectly stimulated by SNX6 [Yoon et al., 2006]. This gene was not only consistently overexpressed in FVB mice at all times compares to SW mice, but also was upregulated in FVB mice at 4 and 9 dpi. These changes could potentiate electrogenic Cl^- secretion and, hence, fluid loss. While basolateral potassium transporters were mainly upregulated in infected FVB mice, the luminal ouabain-sensitive H^+, K^+-ATPase (cHKA) encoded by *Atp12a* was downregulated in FVB mice but not in SW mice at 9 dpi. This ATPase was suggested to regulate Dra activity in colons of in NHE3-deficient mice [Melvin et al., 1999]. Furthermore, compensatory increase in intestinal *cHKA* expression was observed in a number of ion transporter gene knockout mouse models [Schultheis et al., 1998b; Schweinfest et al., 2006], indicating its role in maintaining intestinal ion homeostasis. Thus, impaired transcriptional activity of *cHKA* can contribute to the pathogenesis of diarrhea in *C. rodentium*-susceptible animals.

Bicarbonate metabolism and pH regulation. The activity of many intestinal transporters is regulated by intracellular pH. Rapid diffusion and equilibration of protons entering enterocytes at the apical membrane is dependent on carbonic anhydrases (CA), enzymes that catalyze the reversible hydration/dehydration of CO_2 and water [Stewart et al., 1999]. Carbonic anhydrases, especially cytosolic CA I and membrane-associated CA IV, are known to play a role in ion and water transport in the small intestine and distal colon [Alvarez et al., 2003; Charney and Dagher, 1996; Clarke and Harline, 1998; Fonti et al., 1998; Goldfarb et al., 2000; Sterling et al., 2002]. Because inhibition of carbonic anhydrases is associated with marked decrease in sodium, chloride and water absorption as well as bicarbonate secretion [Charney et al., 2002; Charney et al., 2004; Goldfarb et al., 2000], profound downregulation of *CA I* and *CA IV* in infected FVB mice at 9 dpi suggest their critical role in *C. rodentium*-induced mortality.

Additional proteins able to affect intracellular pH include oligopeptide-protons symporters *Pept1* and *Pept2*, whose expression was differentially expressed between FVB and SW mice. Although H^+/dipeptide transport is coupled with Na^+/H^+ exchanger and carbonic

anhydrase activity in Caco-2 cells and mouse enterocytes isolated from small intestine [Stewart et al., 1999; Thwaites et al., 1999], the function of these transporters in distal colon is not clear [Boll et al., 1996; Meredith and Boyd, 2000; Shen et al., 2001].

SCFA transport. Both cytosolic and luminal pH is regulated by butyrate and other SCFAs produced by enteric bacterial fermentation of undigested carbohydrates and dietary fiber. SCFAs, following ileal or colonic absorption by nonionic diffusion or via SCFA/HCO_3^-(OH^-) exchange mechanism, maintain mucosal integrity and stimulate water and electrolyte absorption by acidification of colonocytes and activation of apical Na^+/H^+ and Cl^-/ HCO_3^- exchangers [Borthakur et al., 2006; Charney and Dagher, 1996; Vidyasagar et al., 2005]. Therefore, decreased butyrate/SCFAs availability due to downregulation of Na^+-dependent SCFA transporter *Slc5a8* (*Ait*) in FVB mice at 9 dpi might affect mucosal permeability, disturb acid-base homeostasis, and inhibit ion absorption in colon, thereby contributing to *C. rodentium*-mediated diarrhea in susceptible FVB mice. This is similar to the decreased expression of the epithelial SCFA transporter MCT-1, and subsequent decrease in butyrate uptake reported in Caco-2 cells infected with EPEC [Borthakur et al., 2006]. This inhibitory effect depended on functional type III secretion system (TTSS) (*escN, espA, espB,* or *espD* genes), but did not require known effector proteins encoded by *espF, espG, espH,* and *map* EPEC genes [Borthakur et al., 2006]. These results suggest that intimate attachment is necessary for butyrate uptake in host cells, but yet unidentified bacterial effector proteins are implicated in the process. This further justifies using *C. rodentium* in mice as a model for EPEC infections.

Water transport. As was mentioned above, water passes through cells either passively, following osmotic gradient created by chloride and sodium transport, or can be absorbed by means of specific water channels, aquaporins [reviewed in Ma and Verkman, 1999; and Matsuzaki et al., 2004]. A number of aquaporins were differentially expressed in infected FVB mice compared with SW mice. Apical channel *Aqp8* was profoundly downregulated in FVB mice at 9 dpi, which could interfere with fluid transport from the intestinal lumen in susceptible animals. In resistant SW mice, fluid loss caused by decreased ion reabsorption is compensated by upregulation of basolateral channel *Aqp4,* which prevents fluid accumulation in colon of resistant animals. Although a slight increase in *Aqp4* expression was observed in FVB mice at 4 dpi, the transcripts levels returned to baseline at 9 dpi. These results are consistent with a recent report implicating mislocalization of aquaporins 2 and 3 in *C. rodentium* diarrrhea [Guttman et al.,

2007]. Thus, the function of water channels in *C. rodentium*-infected FVB mice deserves further investigation.

Transcriptional regulation. Among the transcription factors differentially expressed between susceptible and resistant mice, *Fosb* was the most affected by infection at 4 dpi (by 12-fold). Its expression increased in FVB mice at 9 dpi as well (by 16-fold), whereas a subtle 3-fold increase was observed in SW mice at 4 and 9 dpi. FosB is an "immediate-early" nuclear protein from the Fos family of transcription factors. Dimerization of Fos and Jun proteins causes binding to activator protein 1 (AP-1) promoter sites. AP-1 complexes affect expression of a many genes, including ion channels, receptors, cytoskeletal proteins and signaling molecules [Chen et al., 2001; Nestler and Hyman, 2002; Turi et al., 2002]. Within the set of genes with a strain effect, 67% were predicted to have AP-1 binding sites. This included many potential candidates for susceptibility, such as *Aqp4* and *Aqp8, Alox12, cHKA, CA I, Slc26a3, Slc5a8, Slc9a2, NHERF1*, and *Fosb* itself (data not shown). Early upregulation of *Fosb* in infected FVB mice may indicate that FosB contributes to fatal diarrhea independent of and prior to inflammation-mediated effects. Further studies are needed to determine signals that upregulate *Fosb* expression in susceptible mice, FosB partners in DNA binding and FosB target genes.

Inflammatory effectors. Inflammatory mediators are also implicated in pathogenesis of diarrhea. A good example is adenosine, a secretagogue released by polymorphonuclear cells, eosinophils and mast cells in inflammatory conditions [Madara et al., 1993; Marquardt et al., 1984; Strohmeier et al., 1995]. Adenosine released from the breakdown of ATP released from injured cells during infection is an additional possible source, as has been proposed for type-III secretion possessing pathogens such as EPEC, *E. coli* O157:H7, and *Salmonella enterica* [Crane et al., 2002]. Adenosine signaling is mediated by G-protein-coupled receptors of which A2BAR encoded by *Adora2b* is the predominant adenosine receptor in intestinal epithelial cells [Strohmeier et al., 1995]. Downstream signaling by activated A2BAR results in cAMP- and arachidonic acid-dependent activation of potassium channels and intestinal Cl- secretion [Barrett et al., 1990; Barrett and Bigby, 1993; Cobb et al., 2002; Kolachala et al., 2005a; Kolachala et al., 2005b; Madara et al., 1993; Strohmeier et al., 1995; Wang et al., 2004]. The consistently higher *Adora2b* expression in FVB mice may predispose susceptible animals to this diarrhea-inducing pathway and contribute to the susceptibility of FVB mice to *C. rodentium* infection.

Epithelial differentiation. Notably, a number of genes profoundly downregulated in susceptible FVB mice, such as *Slc26a3 (Dra), Aqp8, CAIV,* and *Slc5a8 (Ait),* are also implicated in the development of colonic tumors [Agrawal et al., 2002; Birkenkamp-Demtroder et al., 2005; Croner et al., 2005; Fischer et al., 2001; Haila et al., 2000; Hoglund et al., 1996; Reichling et al., 2005]. Thus, relative loss of differentiated epithelium due to erosions and ulcerations and/or expansion of less well differentiated proliferating cells in the crypt compartment [Borenshtein et al., submitted] could contribute to altered transcriptional activity in infected FVB mice. However, expression of other markers of differentiation, such as *sucrase-isomaltase, alkaline phosphatase, villin, intestinal trefoil factor 3, Kruppel-like factor 4,* [Ho 1992; Mariadason et al., 2005], was unchanged or not altered to the same extent in infected FVB mice, indicating that erosions or hyperplasia alone can not fully account for the dramatic loss of expression of *Dra, Aqp8, CAIV,* and *Ait* in susceptible FVB mice.

Developmental regulation. Expression of many genes identified in our global analysis changes during postnatal development. This includes sodium exchangers, aquaporins and carbonic anhydrases with higher levels of expression and PEPT proteins with lower expression in adults animals compared with suckling or weanling animals [Bates et al., 2002; Bekku et al., 1998; Collins et al., 1997; Collins et al., 1998; Fleming et al., 1993; Purkerson and Schwartz, 2005; Shen et al, 2001]. The results suggest that high mortality in *C. rodentium*-infected adult FVB mice and young mice of all strains and stocks may result from common pathogenic mechanism, such as inadequate apical ion, proton and water transport in distal colon leading to dehydration and hypovolemic shock. Therefore, genes identified by microarray analysis are integral for understanding the mechanisms of susceptibility to fatal infectious diarrhea in young mice and other mammals.

Applications for other models of diarrhea. Ion imbalances are implicated in other non-infectious animal models of diarrhea. Thus, mice with defect in cytoskeletal intermediate filaments, like keratin 8-deficient mice (on FVB/N background), demonstrate ion transport impairment before the onset of colonic hyperproliferation and inflammation. Interestingly, those animals develop diarrhea despite normal tight junction permeability [Toivola et al., 2004], raising the possibility that tight junction abnormalities contribute but do not directly cause mortality in *C. rodentium*-infected FVB mice. In addition, significant impairment of sodium and chloride absorption and bicarbonate secretion is found in colitis-prone IL-$2^{-/-}$ mice [Barmeyer et al.,

2004]. Chemical induction of colitis by treatment with dextran sulfate sodium (DSS) results in substantial downregulation of carbonic anhydrases *CA I* and *CA IV* and aquaporins *Aqp4* and *Aqp8* [Hardin et al., 2004; Mizoguchi et al., 2003; Renes et al., 2002]. These results indicate that infectious diarrhea and noninfectious inflammation-associated diarrhea may have common mechanisms of pathogenesis and further justify the use of our model for studying fluid and electrolyte imbalance.

In a summary, we present the first gene expression profiling of *C. rodentium* infection *in vivo*. The genomic analysis of the host response to infection generated novel testable hypotheses about how this enteric murine pathogen causes disease and mortality in FVB mice. Marked impairment in intestinal ion homeostasis was predicted by microarray analysis and confirmed by quantitative RT-PCR and serum electrolyte measurements. The fact that the majority of genetically manipulated mice with deficiency in ion transporters develop mild if any diarrhea and no appreciable serum electrolyte disturbances indicates the existence of compensatory mechanisms. It is likely that in the disease state (i.e. diarrhea induced by *C. rodentium*) many genes involved in intestinal ion transport, signaling and regulation act together. In that regard, orchestrated alterations, such as down-regulation of main apical colonic transporters, upregulation of basolateral ion channels and other changes in regulatory signals observed in susceptible strain upon *C. rodentium* infection, may provide a basic mechanism for the development of severe diarrhea and fatal dehydration in infected FVB mice compared with the resistant SW mice. Our study identified potential candidate genes for susceptibility that can be used to develop new strategies for preventing and treating intestinal inflammation and fatal diarrhea.

3.4 Selected Methods

Animal infections. Inbred FVB/NTac and outbred Swiss Webster Tac:SW moms with 40 and 36 female two-week-old pups respectively were purchased from Taconic Laboratories (Germantown, N.Y.). Because animals came from different barrier units, mixing of bedding from the weaning till the required age (12 weeks old) was performed twice a week to obtain comparable bacterial background and minimize commensal flora-related bias. The animals were housed in microisolator cages within a specific pathogen-free facility approved by Association

for Assessment and Accreditation of Laboratory Animal Care and maintained on pelleted rodent chow and water *ad libitum*. At 12 weeks of age, infectious colitis was induced by intragastric inoculation with 1.9 x 10^9 CFU of DBS120 as described Appendix 1: General Methods. A total of 37 FVB and 36 SW mice were used in the inoculation study as described in Table 3-1. Animals were weighed and monitored for fecal bacterial shedding prior to inoculation and at 3, 6, and 8 DPI. Fecal bacterial shedding was assessed by plating serial dilutions of feces from individual animals on MacConkey lactose agar supplemented with 40 μg/ml Kan. The lower limit of detection was 1 CFU/mg of feces. Animals were euthanized at 4 and 9 DPI. At necropsy, the colon of each mouse was collected aseptically, cleared of feces, and the distal colon was dissected in half longitudinally. The one half of the distal colon was snap frozen in liquid nitrogen and stored at -80°C until RNA was extracted. The rest of the tissues were fixed, processed and scored as described in Appendix 1. All experiments were approved by the MIT Animal Care and Use Committee.

RNA extraction. Total RNA was extracted from frozen distal colon using Trizol reagent according to the recommendations of the manufacturer (Invitrogen, Carlsbad, CA). The resultant RNA was DNase I treated and purified with RNeasy Clean-up kit as recommended by the manufacturer (Qiagen, Valencia, CA). The total RNA concentration and 260/280 ratio was evaluated spectrophotometrically. Only samples with a 260/280 ratios range of 1.8 to 2.1 were further processed. RNA samples were evaluated by the Agilent 2100 Bioanalyzer (Agilent, Palo Alto, CA) and consistently demonstrated high-quality RNA with distinct 28S and 18S peaks and no evidence of degradation.

Array design and hybridization. Global gene expression analysis was performed on the distal colon with 2-3 mice per group. Because no difference for any parameters was observed in uninfected mice at 4 or 9 dpi, the animals were pooled into uninfected control groups for each line of mouse. The selection of representative samples for microarray analysis was based on known infection status and colonic lesions. The final number of biological replicates for each condition was n = 5 uninfected FVB mice (“Fp” group), n = 4 uninfected SW mice (“Sp” group), and n = 3 infected animals from each stock at each time point (“Fi4”, “Si4”, “Fi9”, and “Si9” respectively, Table 3-1). One-cycle target labeling of isolated RNA, hybridization, washing/staining and scanning was carried out in the Whitehead Institute Center for Microarray Technology (Cambridge, MA) as detailed at http://www.wi.mit.edu/CMT/protocols.html. First-

and second-strand cDNA syntheses were performed using SuperScript double-stranded cDNA synthesis kit (Invitrogen, Carlsbad, CA). The second strand DNA synthesis, the clean-up of the double-stranded cDNA, the synthesis and the clean-up of the biotin-labeled cRNA were completed according to Affymetrix protocols (Santa Clara, CA). Twenty μg of cRNA were fragmented and hybridized as recommended by Affymetrix to the GeneChip Murine Genome 430 2.0 Arrays (Affymetrix, Santa Clara, CA) containing 45,037 probe sets that correspond to over 34,000 well characterized mouse genes. Each sample was hybridized to one array, with 21 total chips used. The arrays were scanned using GeneChip scanner 3000 enabling for high-resolution scanning as recommended (Affymetrix, Santa Clara, CA). The expression output for all the samples met the Quality control requirements (data not shown). The presence call for all the arrays ranged from 58% to 66%. Microarray results were tightly correlated between biological replicates within and between the animal groups (Figure 3-14).

Identifying differentially expressed genes. The cell intensity files (*.cel) containing hybridization signals were generated with GeneChip Operating Software (GCOS 1.2). The normalization and processing of the results were done by DNA-Chip Analyzer (dChip) software (www.dchip.org) implementing model-based expression index (MBEI) analysis using outlier detection algorithm to eliminate potential cross-hybridizing probes [Li and Wong, 2001a, Li and Wong 2001b]. Normalization using invariant set of genes, in which all arrays are normalized to the common baseline array with median intensity, was followed by background correction and log2 transformation. The perfect match-only model was applied in order to reduce noise. A mean value was calculated from signal log2 ratios for each gene and group. Gene expression was considered to be significant when it was changed by more than two-fold (an average log2 ratios of above 1.0 or below -1.0). Genes were clustered by tightness with centroid-linkage method using 1 – r (where r is the Pearson correlation coefficient) as the distance measure while redundant probes were masked. Results were visualized with the help of heat maps showing color-coded expression levels (red = high expression, black = medium expression, and green = low expression) and vertically drawn gene trees. Enrichment analysis was done within dChip software using Hypergeometric test with $p<0.05$ and at least 4 functionally annotated genes if not otherwise indicated. FatiGO (Fast Assignment and Transference of Information using Gene Ontology (GO)) Plus web-based tool [Al-Shahrour et al., 2004; Al-Shahrour et al., 2005, http://fatigo.bioinfo.cipf.es] was used for calculating the prevalence of GO functional groups.

The results of inclusive analysis at the deepness of 5th level and more than 5% of GO categories enrichment were presented. Temporal changes in response to infection were addressed using a "delta eta" analysis to identify significant differential transcript modulation in response to treatment where for each transcript [log2 (FVB infected/FVB uninoculated) – log2 (SW infected/SW uninoculated)] where FC>1.5 For each gene, delta eta values for 4 and 9 dpi were calculated as log2(Si4vs.Sp) – log2(Fi4vs.Fp) and log2(Si9vs.Sp) – log2(Fi9vs.Fp), respectively. The results were processed in Spotfare and subjected to enrichment GO analysis by dChip. All the Affymetrix and GO annotations based on October 2006 datafiles.

Results obtained by dChip data processing were verified by RMA method [Irizarry et al., 2003], available as part of the BioConductor software. Differential expression between the animal groups was assessed by calculating a moderated *t*-statistic for each gene using the Limma package [Smyth, 2005] and 2-fold threshold. Temporal infection-induced trends between the groups were determined by linear model with false discovery rate (FDR) < 0.05 and 2-fold cut off threshold. To discriminate gene behavior, random forest analysis to predict four classes (strain x infection status) was applied with $p<0.05$. Enrichment analysis was performed within dChip with $p<0.0005$, and the prevalence of functional groups was determined with FatiGO as indicated above.

TaqMan quantitative RT-PCR. cDNA generation and qRT-PCR using Applied Biosystems predesigned primers and probes (Table 3-3) were done as described in Appendix 1: General Methods. The resultant ratios were matched with corresponding comparisons from microarray analysis and subjected to Pearson correlation analysis. The number of samples used for TaqMan were n=10 in uninoculated control groups and n=6 to 8 samples for infected groups in each line of mice (Tables 3-1). Each reaction was carried out in duplicates.

Measuring serum electrolyte levels. Electrolytes were detected in serum by IDEXX Preclinical Research Services (IDEXX Laboratories Inc., MA) using electrolyte Panel 957, which included detection of bicarbonate, chloride, potassium, sodium, Na/K ratio and anion gap in 200 μl of serum samples.

3.5 Tables and Figures

Table 3-1. Number of animals used for microarray analysis, quantitative RT-PCR (TaqMan) and experiment

Array sample name	Days post inoculation	Group	Group label	Total number of arrays in a group	Total number of samples for TaqMan	Total number of mice in a group
S4_1 S4_2 S9_1 S9_2	4 4 9 9	SW pooled controls	Sp	4 (2 + 2)	10 (5 + 5)	16 (8 + 8)
F4_1 F4_2 F9_1 F9_2 F9_3	4 4 9 9 9	FVB pooled controls	Fp	5 (2 + 3)	10 (5 + 5)	20 (10 + 10)
Si4_1 Si4_2 Si4_3	4 4 4	SW 4 dpi	Si4	3	6	10
Fi4_1 Fi4_2 Fi4_3	4 4 4	FVB 4 dpi	Fi4	3	8	10
Si9_1 Si9_2 Si9_3	9 9 9	SW 9 dpi	Si9	3	6	10
Fi9_1 Fi9_2 Fi9_3	9 9 9	FVB 9 dpi	Fi9	3	7	7

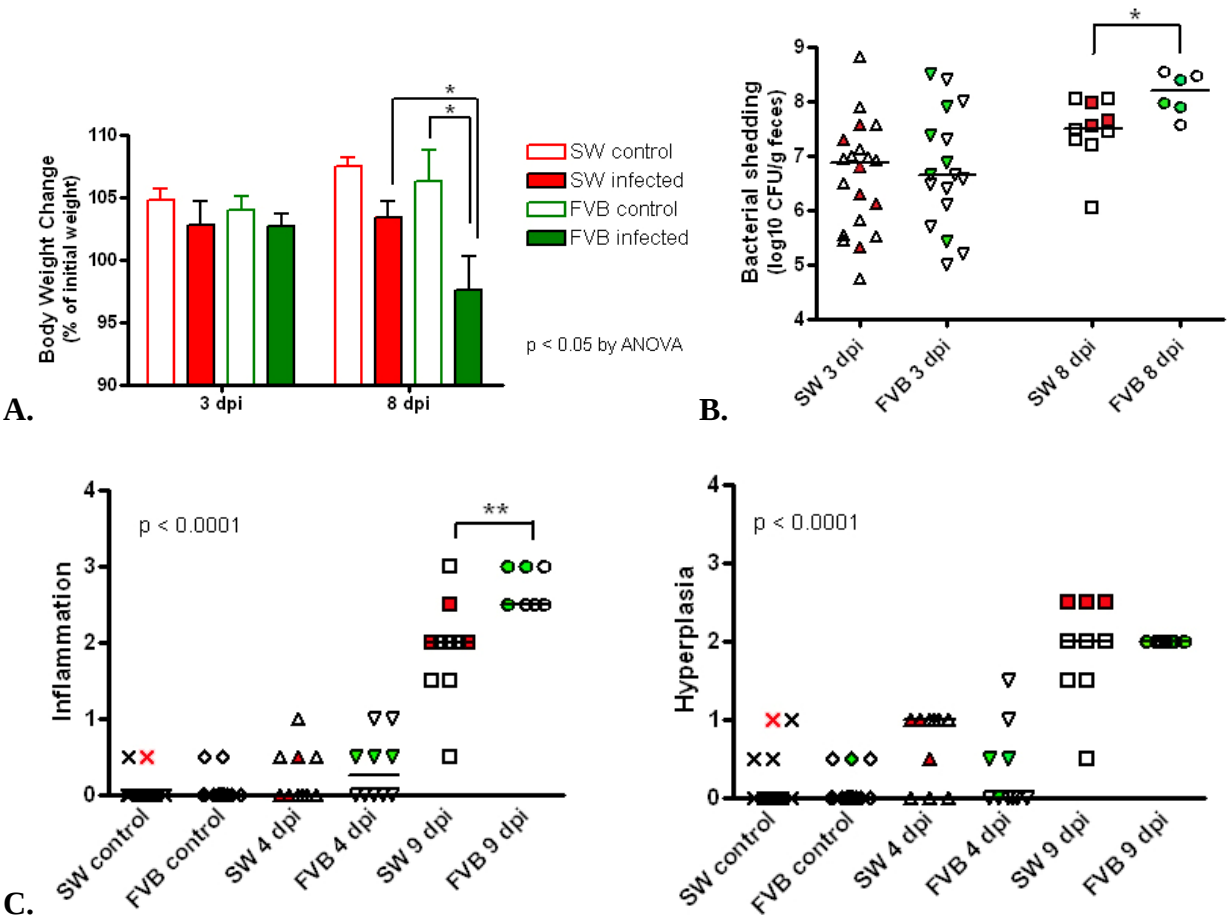

Figure 3-1. *C. rodentium* infection in adult susceptible inbred FVB mice and resistant outbred SW mice.

A. Significant weight loss was observed in infected FVB mice at 8 dpi ($p<0.05$). Weight was normalized and expressed as percent change of initial baseline. Data presented as mean ± SEM.

B. Infection kinetics was similar in both groups at 3 dpi, but higher bacterial shedding was observed in FVB mice at 8 dpi ($p<0.05$). Bacterial counts were log10 transformed. Each dot represents one animal; line indicates mean of the group.

C. FVB mice infected with *C. rodentium* developed significant colonic inflammation and hyperplasia, at 9 dpi. Infected SW mice developed less inflammation ($p<0.0001$), but comparable hyperplasia at 9 dpi. Each dot represents one animal; line indicates median of the group.

Experimental groups included 20, 10, and 7 uninoculated control, 4 dpi, and 9 dpi FVB mice, and 16, 10, and 10 SW mice in the corresponded groups.

Comparisons		Number of altered probe sets	Number of corresponding transcripts
strain - basal effect	Spvs.Fp	462	410
strain – early infection response	Si4vs.Fi4	557	476
strain - late infection / inflammatory response	Si9vs.Fi9	1,065	904
SW 4 dpi response compared with uninfected	Si4vs.Sp	1,798	1,481
SW 9 dpi response compared with uninfected	Si9vs.Sp	1,945	1,523
SW disease progression response 9 dpi compared with 4 dpi	Si9vs.Si4	901	746
FVB 4 dpi response compared with uninfected	Fi4vs.Fp	2,195	1,784
FVB 9 dpi response compared with uninfected	Fi9vs.Fp	3,297	2,490
FVB disease progression response 9 dpi compared with 4 dpi	Fi9vs.Fi4	1,506	1,212
Total	All combined comparisons	5,585	4,257

A.

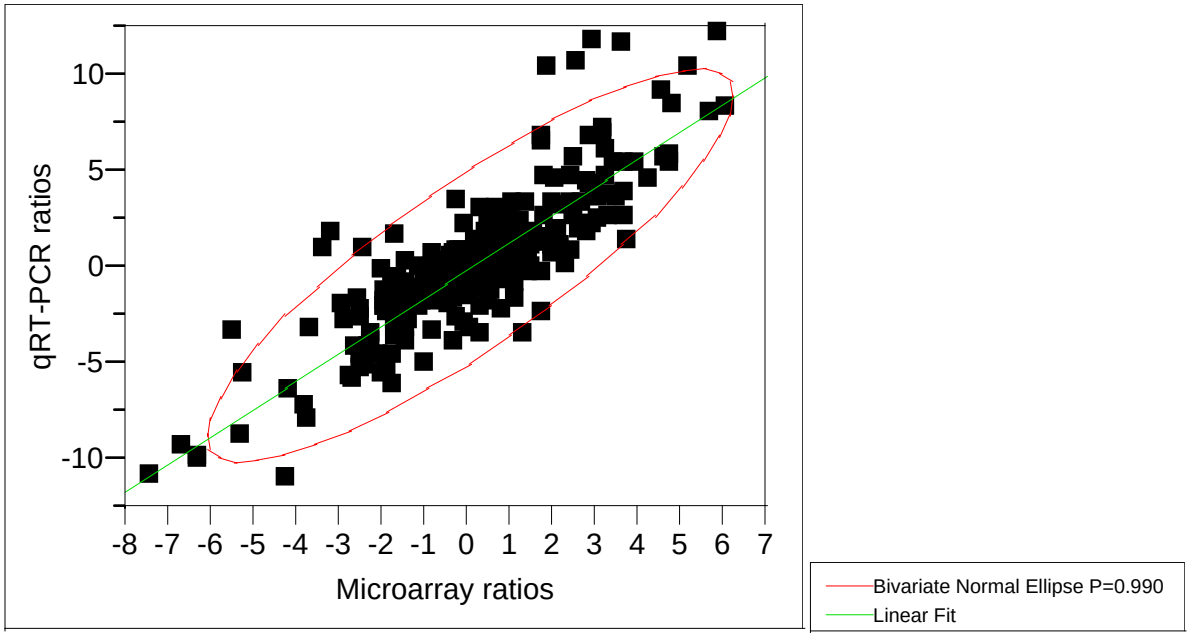

B.

Figure 3-2. Differential expression of genes between and within the strains prior to or in response to *C. rodentium* infection.

A. Summary of transcripts differentially expressed in individual and combined comparisons. The analysis was performed using Affymetrix whole mouse genome oligonucleotide chip (430 2.0 Array), which contains >45,000 probe sets comprising expression levels of >39,000 transcripts and variants from >34,000 well-characterized mouse genes. The normalization and processing of the results were performed using DNA-Chip Analyzer (dChip) software implementing model-based expression analysis. One percent of the total probe sets presented on the array was more than two-fold differentially expressed between SW and FVB

mice prior to infection. In response to *C. rodentium* inoculation, 11.4% of probe sets were either induced or repressed in one or both of the lines of mice. There were more differentially expressed genes in response to infection in susceptible FVB mice than in resistant SW mice, especially as disease progressed. Overall, alterations in 12.4% probe sets were detected throughout the experiment.

B. Validation of microarray results by quantitative real-time PCR (TaqMan) of selected genes. Transcript levels were normalized to the endogenous control GAPDH, and expressed as fold change compared with uninoculated control FVB mice, which were set at 1, using the Comparative Ct method. The resultant log2 ratios were matched with corresponding log2 ratios detected in microarray analysis and subjected to Pearson correlation analysis. Significant correlation was observed between the two assays (Pearson correlation coefficient $r = 0.87$, $R^2 = 0.75$, $p<0.0001$). Pearson correlations for individual genes ranged from 0.67 to 1. Only two out of 35 examined genes did not confirm the array results, yielding a predictability rate of 94% (Table 3-2).

Table 3-2. Validation of microarray results by quantitative RT-PCR (TaqMan) on selected genes

Gene	Gene Symbols	ABI ID for predesigned assay-on-demand	Pearson correlation	P value	R^2 of linear fit
adenosine A2b receptor	Adora2b	Mm00839292_m1	0.91	0.0007	0.83
angiogenin, ribonuclease A family, member 4	Ang4, Rnase5d	Mm01315577_s1	0.97	<0.0001	0.95
aquaporin 8	Aqp8	Mm00431846_m1	0.97	<0.0001	0.95
arachidonate 12-lipoxygenase	Alox12	Mm00545833_m1	0.98	<0.0001	0.96
arginase type I, liver	Arg1	Mm00475988_m1	0.93	0.0002	0.87
arginase type II	Arg2	Mm00477592_m1	0.88	0.0019	0.77
ATPase, Na+/K+ transporting, beta 2 polypeptide	Atp1b2	Mm00442612_m1	0.89	0.0014	0.79
beta galactoside alpha 2,6 sialyltransferase 1	Siat1, ST6GaI1	Mm00486119_m1	0.86	0.0028	0.74
bone morphogenetic protein 5	Bmp5, se	Mm00432091_m1	0.94	0.0001	0.89
carbonic anhydrase 1	Car1, CA I	Mm00486717_m1	0.99	<0.0001	0.99
carbonic anhydrase 4	Car4, CA IV	Mm00483021_m1	1.00	<0.0001	0.99
CD14 antigen	Cd14	Mm00438094_g1	0.91	0.0007	0.83
CD34 antigen	Cd34	Mm00519283_m1	0.90	0.0009	0.81
complement receptor related protein	Crry	Mm00785297_s1	-0.38	0.3123	0.14
cystic fibrosis transmembrane conductance regulator homolog	CFTR, Abcc7	Mm00445197_m1			
extracellular proteinase inhibitor	Expi, WDNM1	Mm00433159_m1	0.98	<0.0001	0.97
FBJ osteosarcoma oncogene B	FosB	Mm00500401_m1	0.89	0.0014	0.79
glyceraldehyde-3-phosphate dehydrogenase	GAPDH	Mm99999915_g1			
histocompatibility 2, class II antigen E beta	H2-Eb1, IIa-4	Mm00439221_m1	0.86	0.0027	0.75
immunoglobulin lambda chain, variable 1	Igl-V1	Mm01627739_g1	0.81	0.0086	0.65
Intelectin	Itln	Mm01616618_g1	0.67	0.0468	0.45
Interferon activated gene 202B	Ifi202b	Mm00839397_m1	0.97	<0.0001	0.93
Interferon activated gene 203	Ifi203	Mm01238610_m1	1.00	<0.0001	0.99
Interferon activated gene 205	Ifi205	Mm01315309_m1	0.75	0.0189	0.57
lectin, galactose binding, soluble 6	Lgals6	Mm02524460_s1	0.92	0.0005	0.85
mucin 2	muc2	Mm00458304_g1	0.98	<0.0001	0.96
myelocytomatosis oncogene	Myc	Mm00487804_m1	0.94	0.0001	0.89
nitric oxide synthase 2, inducible, macrophage	iNOS, Nos-2	Mm00440485_m1	0.69	0.0416	0.47
protein kinase C, mu	Prkcm, PKD1	Mm00435790_m1	0.91	0.0006	0.84
sialyltransferase 4C (beta-galactoside alpha-2,3-sialytransferase)	Siat4c, ST3Gal IV	Mm00501503_m1	0.83	0.0052	0.69
sialyltransferase 7 ((alpha-N-acetylneuraminyl 2,3-betagalactosyl-1,3)-N-acetyl galactosaminide alpha-2,6-sialyltransferase) D	Siat7d, ST6GalNAc IV	Mm00488228_m1	0.94	0.0001	0.89
sialyltransferase 7 (alpha-N-acetylneuraminyl 2,3-beta-galactosyl-1,3)-N-acetyl galactosaminde alpha-2,6-sialyltransferase) A)	Siat7a, ST6GalNAc I	Mm00488218_m1	0.93	0.0003	0.87
solute carrier family 10, member 2	Slc10a2, ASBT	Mm00488258_m1	0.64	0.0661	0.40
solute carrier family 15 (H+/peptide transporter), member 2	Slc15a2, Pept2	Mm00451610_m1	0.75	0.0212	0.56
solute carrier family 26, member 3	Slc26a3, Dra	Mm01291071_m1	1.00	<0.0001	1.00
solute carrier family 5 (iodide transporter), member 8	Slc5a8, Ait	Mm00520629_m1	0.92	0.0005	0.84
tumor necrosis factor	TNFa	Mm00443258_m1	0.92	0.0004	0.85

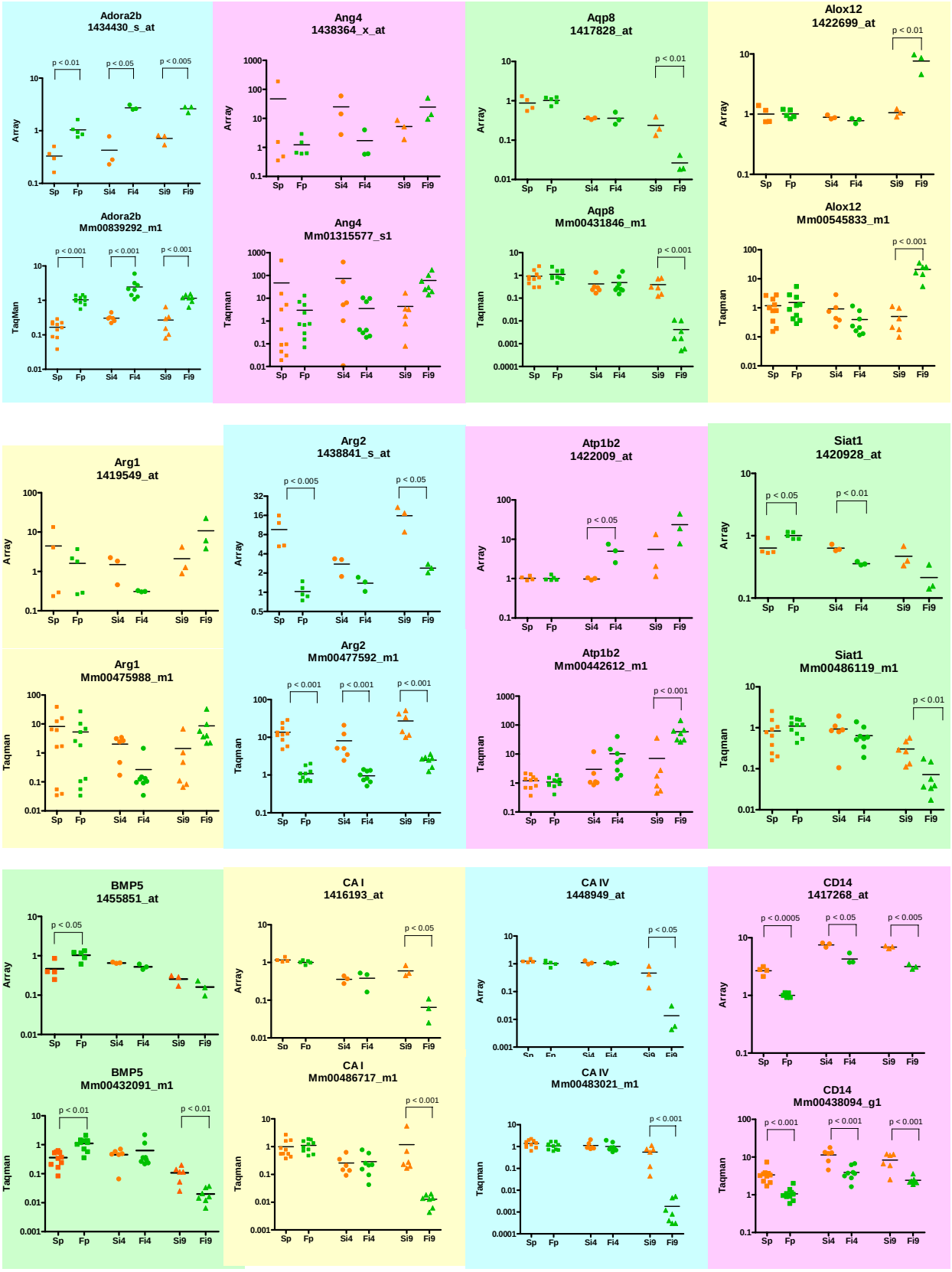

Figure 3-3. Side-by-side comparison of gene expression analyzed by microarray and qRT-PCR

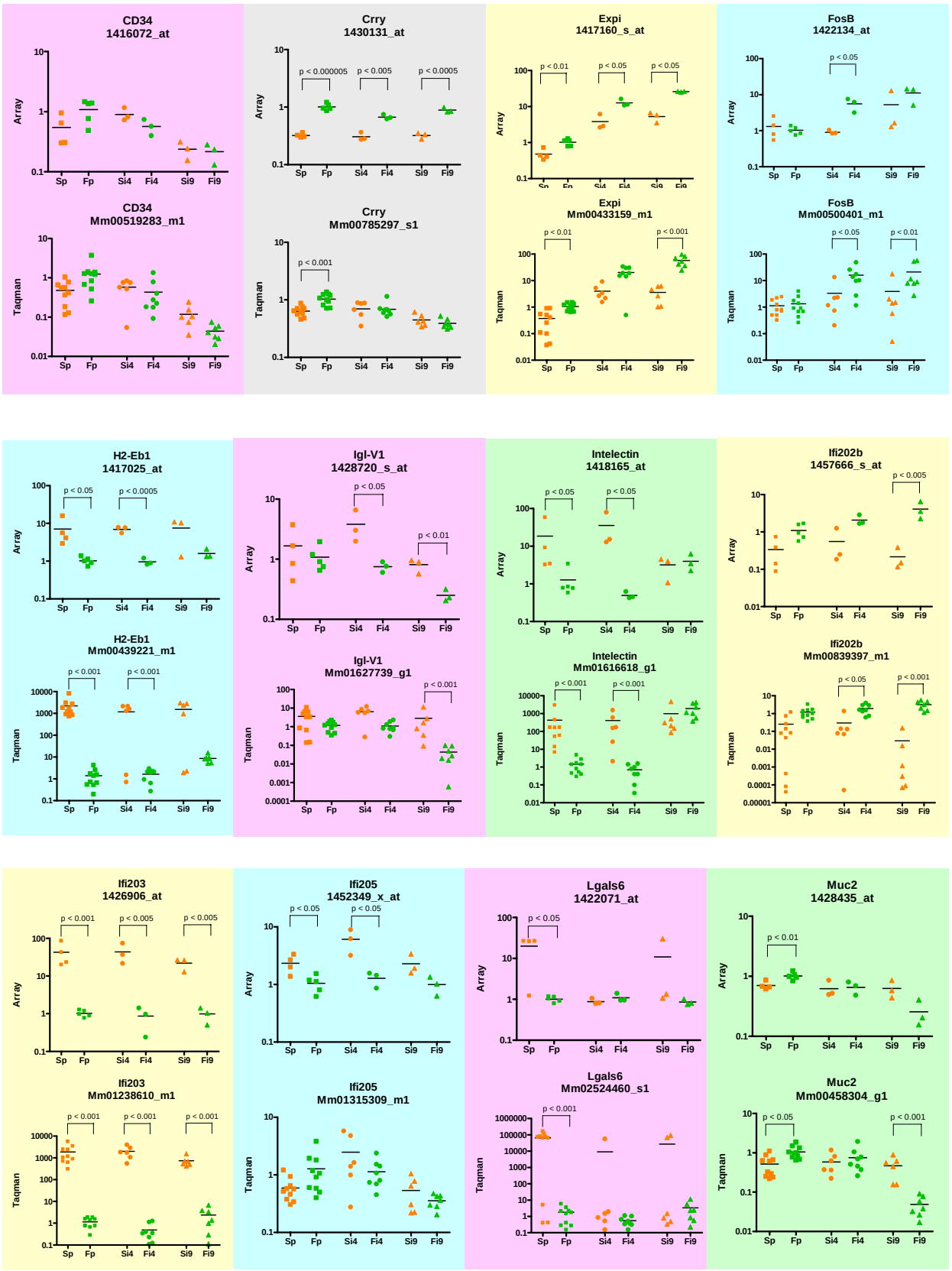

Figure 3-3. Side-by-side comparison of gene expression analyzed by microarray and qRT-PCR (cont.)

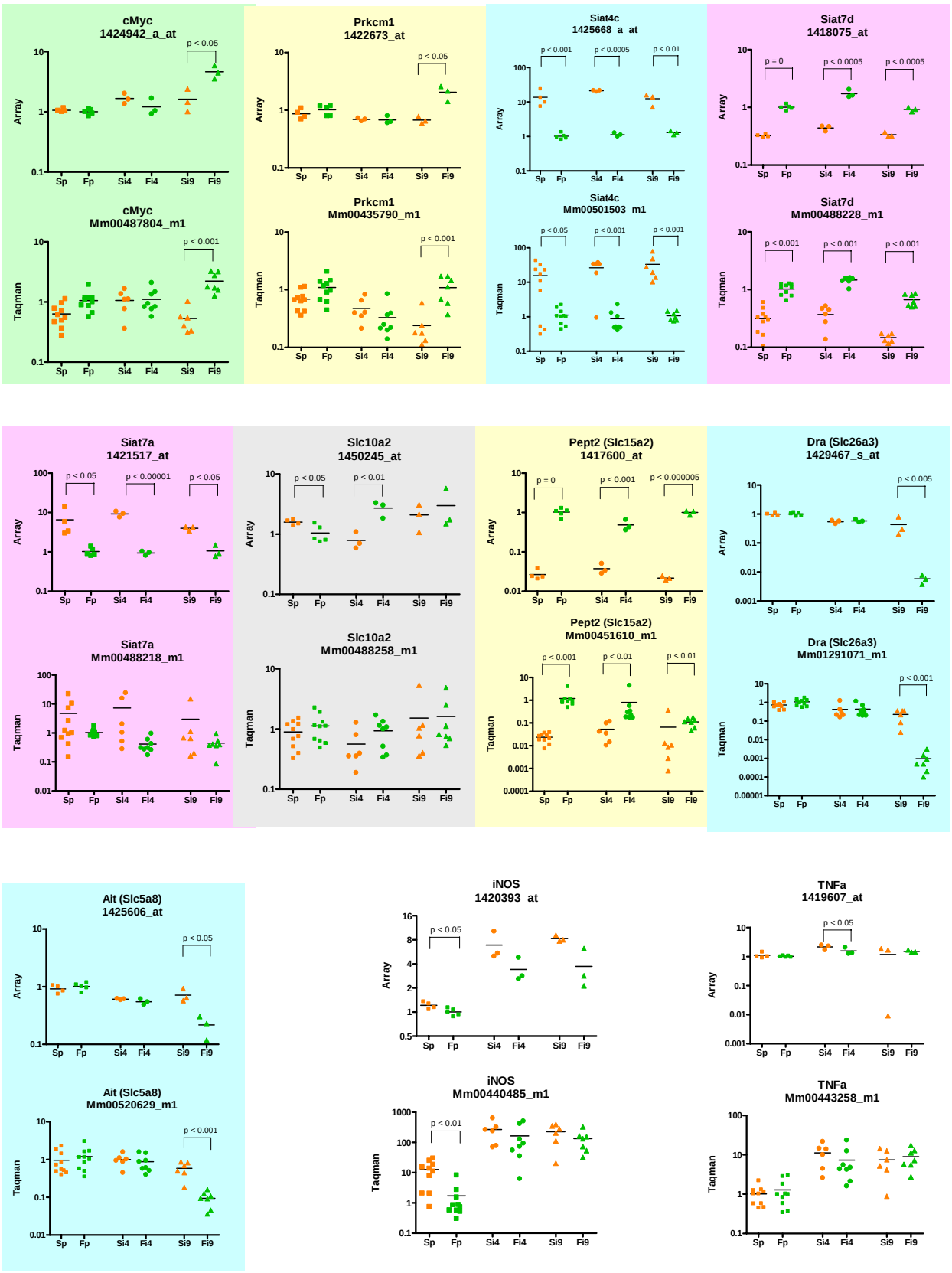

Figure 3-3. Side-by-side comparison of gene expression analyzed by microarray and qRT-PCR (cont.)

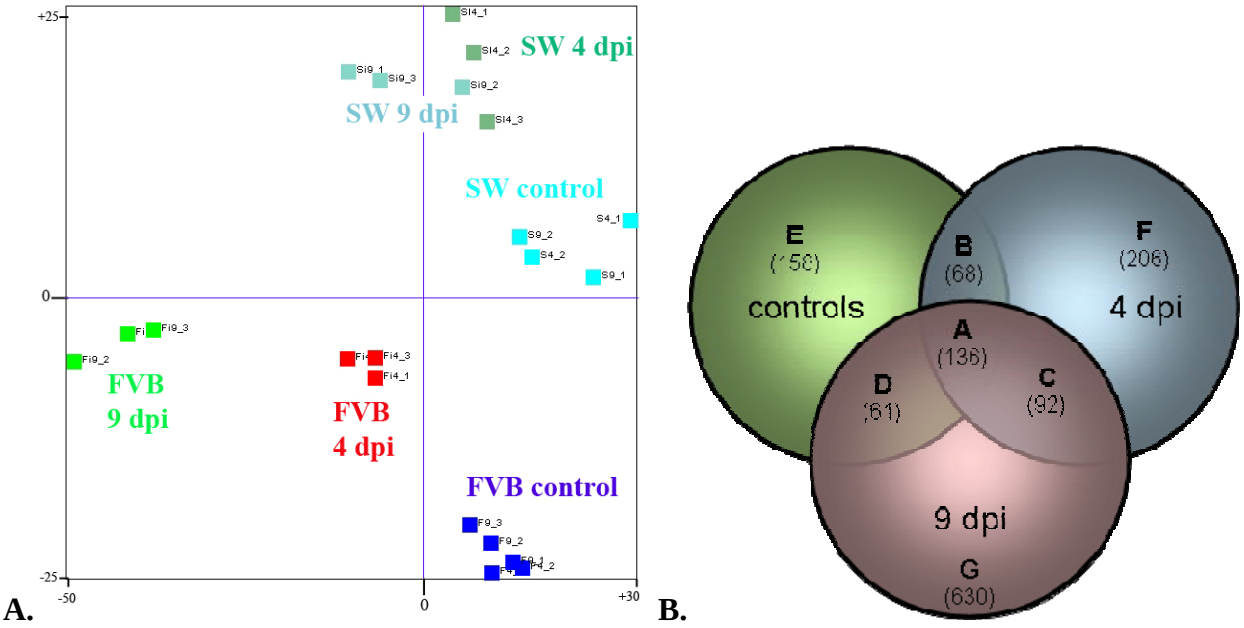

A. B.

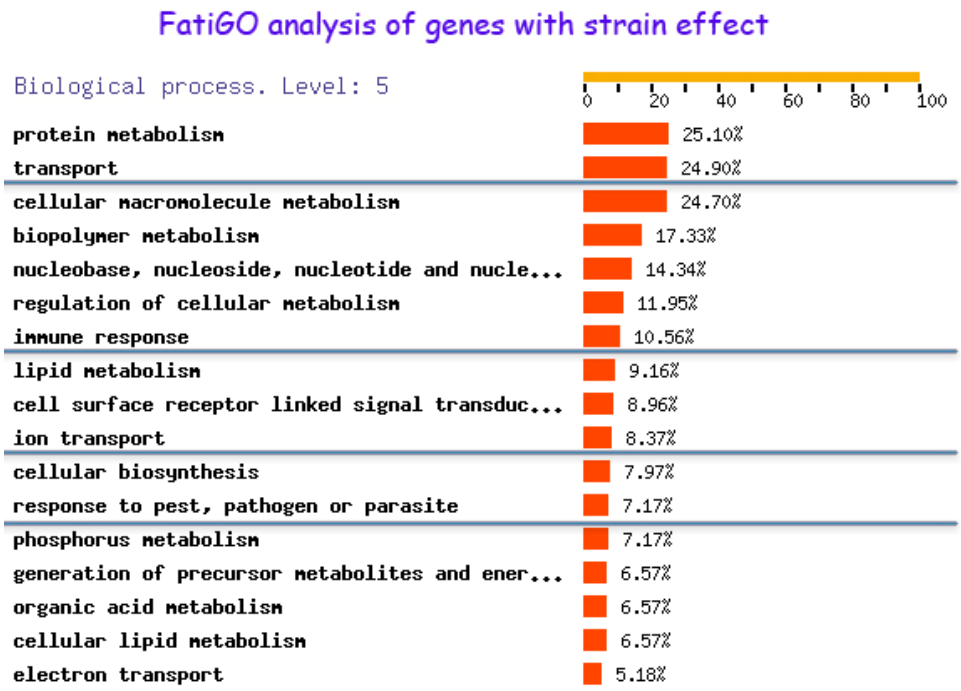

C.

Figure 3-4. Exploring 1,547 genes with the host (strain) effect.

A. Principle Component Analysis (PCA) shows distinct groups correlating to the different lines of mice or status of infection. Less tight clustering of uninoculated SW mice was observed compared with inbred FVB mice, which reflected their heterogeneous outbred nature. Components analyzed were sufficient to distinguish FVB mice throughout infection, whereas the separation between controls and infected SW mice was less robust (smaller distances between the animals, Table 3-3). This result was consistent with more severe disease in the sensitive FVB mice.

B. Sets of differentially expressed SW to FVB genes, as shown in the Venn Diagram, are represented as 7 distinct groups. Group A represented genes that were differentially expressed between the mouse lines at all times. Groups B, C, and D revealed genes that were differentially expressed at 2 conditions/time points.

Groups E, F, and G symbolized genes unique to uninfected status, 4 dpi and 9 dpi respectively. Each circle represents the comparison of resistant outbred SW mice over susceptible inbred FVB mice at three different time points. Numbers in parentheses represent number of genes corresponding to differentially expressed probe sets in each group. Significantly enriched GO clusters for each group and for all set of genes with strain effect are given in Table S2.

C. The prevalence of genes within GO categories was assessed by FatiGO analysis. Only categories containing more than 5% of genes are shown. Genes from transport processes were overrepresented.

Table 3-3. Two-dimensional principal component analysis (PCA) in the subspace of genes differentially regulated between FVB and SW mice.

	Sample	PC1	PC2
FVB uninfected controls (Fp)	F4_1	10.0345	-24.7474
	F4_2	14.3277	-24.3638
	F9_1	12.9357	-23.798
	F9_2	9.91588	-22.0406
	F9_3	6.89841	-20.4539
FVB 4 dpi (Fi4)	Fi4_1	-6.26868	-7.04468
	Fi4_2	-10.0843	-5.28929
	Fi4_3	-6.18853	-5.25129
FVB 9 dpi (Fi9)	Fi9_1	-40.8488	-3.05197
	Fi9_2	-48.3705	-5.546
	Fi9_3	-37.1858	-2.71321
SW uninfected controls (Sp)	S4_1	29.3196	7.28819
	S4_2	15.6219	3.93392
	S9_1	24.2379	2.07921
	S9_2	13.8939	5.7856
SW 4 dpi (Si4)	SI4_1	4.58773	26.0865
	SI4_2	7.49687	22.5136
	SI4_3	9.4241	16.2882
SW 9 dpi (Si9)	Si9_1	-10.0365	20.8283
	Si9_2	5.91621	19.448
	Si9_3	-5.62731	20.0485

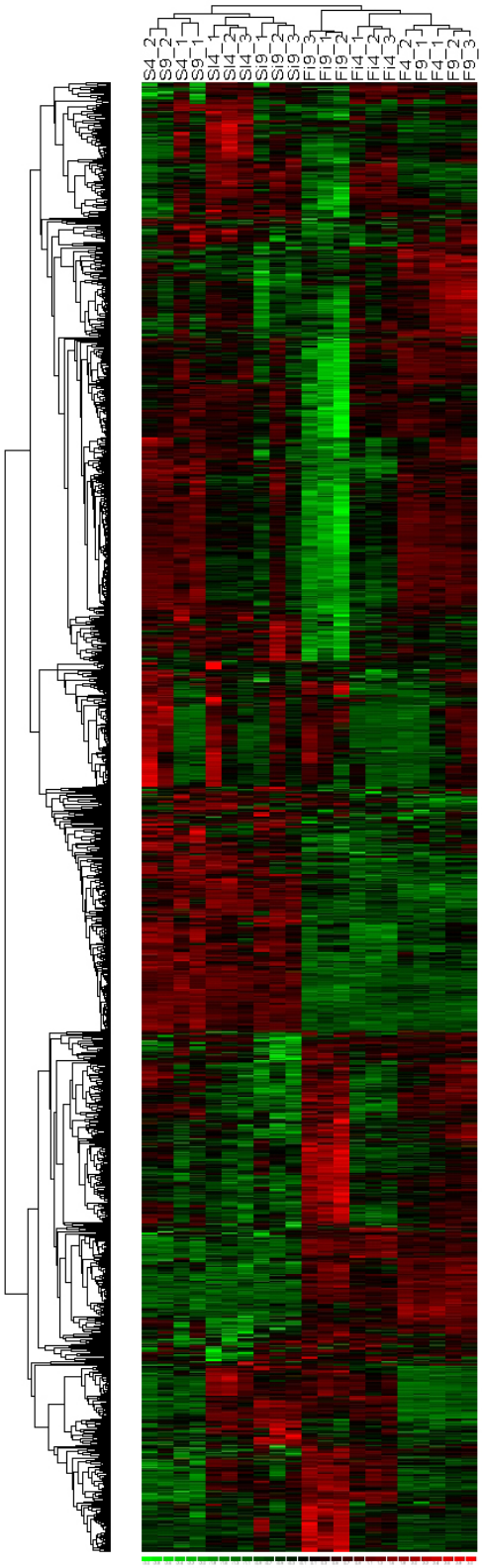

Figure 3-5. Hierarchical clustering of 1,547 genes exhibiting host effect.
Redundant probe sets were excluded from the analysis. The heat map shows color-coded expression levels (red = high expression, black = medium expression, and green = low expression). Gene trees are drawn vertically and sample trees vertically.

Table 3-4. The top genes differentially expressed between susceptible and resistant strains prior to *C. rodentium* infection and/or at 4 and 9 dpi.

Probe set ID	Gene	Gene name/ aliases	Locus Link	SW over FVB, control[a]	SW over FVB, 4 dpi	SW over FVB, 9 dpi	Main functions
1454714_x_at 1456471_x_at	3-phosphoglycerate dehydrogenase	Phgdh	236539	-3.37***	-5.2***	-4.8**	Oxidoreductase activity, amino acid biosynthesis, metabolism
1418979_at	aldo-keto reductase family 1, member C14	Akr1c14	105387			3.06*	Oxidoreductase activity
1417920_at	amnionless	Amn	93835	3.58****	3.06****	1.9	Development, protein localization
1438364_x_at	angiogenin, ribonuclease A family, member 4 [b]	Ang4	219033	1.39	3.56	-2.09	Antimicrobial humoral response, defense response to bacteria
1418069_at	apolipoprotein C-II	Apoc2	11813	0.53		3.61*	Lipid transporter activity
1417828_at	**aquaporin 8** [b]	Aqp8	11833			3.14*	Water channel activity, transport
1438841_s_at	arginase type II [b]	Arg2	11847	3.09**	0.96	2.64*	Arginine metabolism
1419393_at	ATP-binding cassette, sub-family G (WHITE), member 5	Abcg5, sterolin 1	27409	1.02	0.64	3.18***	ATPase activity, transport
1455869_at	**calcium/calmodulin-dependent protein kinase II, beta**	Camk2b	12323	-0.85	-3.39	-2.46	G1/S transition of mitotic cell cycle, calcium ion transport, calcium signaling
1416193_at	**carbonic anhydrase 1** [b]	Car1, CA I	12346			3.4*	one-carbon compound metabolism, maintenance of pH , anion transport
1448949_at 1418094_s_at	**carbonic anhydrase 4** [b]	Car4, CA IV	12351			5.32*	one-carbon compound metabolism, maintenance of pH , anion transport
1416306_at	chloride channel calcium activated 3	Clca3, gob-5	23844		0.65	3.06	Chloride transport
1418626_a_at 1454849_x_at	clusterin	Clu, ApoJ	12759		0.71	-3.17*	Cell death
1419349_a_at	cytochrome P450, family 2, subfamily d, polypeptide 9	Cyp2d9	13105			3.04*	Oxidoreductase activity
1440016_at	dihydrolipoamide branched chain transacylase E2	Dbt	13171	3.63*	2.52	1.37	Metabolism
1458099_at	EST			-3.21*		-1.43	
1446934_at	EST			-3.49*	-2.36*	-2.73	
1451948_at	gene model 1409, (NCBI)	Gm1409, IGKV5-39	620017		2.66*	3.24*	Immunoglobulin-like
1449526_a_at	glycerophosphodiester phosphodiesterase domain containing 3	Gdpd3	68616	-5.1****	-4.35***	-3.98**	Glycerol metabolism
1457231_at	hypoxia inducible factor 1, alpha subunit	Hif1a, MOP1	15251	1.64	2.9*	3.05**	Cell differentiation, signal transduction, transcription factor activity
1460423_x_at	Ig kappa chain	Cr1, IgK	381774	-1.18	2.33*	3.28**	Immune response
1429381_x_at 1421653_a_at 1425763_x_at	immunoglobulin heavy chain (J558 family)	Igh-VJ558, Igh-A	16061	-2.12	1.15*	3.65*	Immune response
1460423_x_at	immunoglobulin heavy chain (V7183 family) /// Ig kappa chain variable 1 (V1) /// Ig kappa chain variable 1-117 /// Ig kappa chain	Igh-V7183 Igk-V1 Igkv1-117 Cr1	16059 /// 16081 /// 16098	-1.18	2.33*	3.28**	
1460423_x_at	Ig kappa chain	Cr1, IgK	381774	-1.18	2.33*	3.28**	Immune response

Table 3-4. Continued

Probe set ID	Gene	Gene name/ aliases	Locus Link	SW over FVB, control[a]	SW over FVB, 4 dpi	SW over FVB, 9 dpi	Main functions
1452577_at	immunoglobulin heavy chain complex	Igh, J558	111507	2.19	4.52*	1.89*	Immune response
1424931_s_at	immunoglobulin lambda chain, variable 1 [b]	Igl-V1	16142	0.83	4.08**	1.28	Antigen binding, humoral immune response
1418165_at	intelectin a [b]	Itlna, Lfr	16429	3.14*	5.67*	-0.44	Sugar binding, response to nematode
1457666_s_at	interferon activated gene 202b[b]	Ifi202b	26388	-2.04	-2.4	-4.3**	Immune response
1426906_at	interferon activated gene 203[b]	Ifi203	15950	5.17**	5.82*	4.52**	Immune response, regulation of transcription
1422071_at	lectin, galactose binding, soluble 6	Lgals6, galectin-6	16857	3.61*		2.05	Sugar binding, immunomodulation
1426573_at	malic enzyme 2, NAD(+)-dependent, mitochondrial	ME2, NAD-ME	107029	2.55****	2.32*	3.08***	Oxidoreductase activity, metabolism
1423467_at	membrane-spanning 4-domains, subfamily A, member 4B	Ms4a4b, Chandra	60361	2.12*	3.15*	3.0*	Immune response, Th1 differentiation
1447252_s_at 1450719_at	meprin 1 alpha	Mep1a	17287	0.71*	0.9*	3.39*	Metallopeptidase activity, proteolysis
1418215_at	meprin 1 beta	Mep1b	17288			3.14*	Metallopeptidase activity, proteolysis
1453070_at	protocadherin 17	Pcdh17	219228	-3.24***	-1.95	-2.09	Calcium ion binding
1432579_at	radial spokehead-like 2	Rshl2a	66832	0.68	3.16***	0.97*	Transporter activity
1418368_at	resistin like beta	Retnlb, Fizz2	57263	-3.1			Hormone activity
1427963_s_at	retinol dehydrogenase 9	Rdh9	103142	0.6		3.14**	Oxidoreductase activity, transport
1424784_at	RIKEN cDNA 1700029I01		433791	-2.75****	-3.15**	-2.54	Zinc ion binding
1428359_s_at 1428358_at 1434137_x_at	RIKEN cDNA 1810010M01	ZG16p	69036			3.94	Sugar binding
1417735_at	RIKEN cDNA 1810030J14		66289	0.57	1.43	4.75**	similar to Serum amyloid P-component precursor (SAP)
1434152_at	RIKEN cDNA 2210421G13		108956	1.53	3.72****	2.01	Lipid binding
1428604_at	RIKEN cDNA 2610305D13		112422	2.5****	3.17***	2.68*	Zinc ion binding, regulation of transcription
1426936_at	RIKEN cDNA 2610305J24		192885	2.91**	2.87***	4.18*	
1429896_at	RIKEN cDNA 5830408B19		74756	-0.87*	-0.76**	-3.71*	
1437128_a_at	RIKEN cDNA A630033E08		240041	-1.76	-2.69**	-3.81***	Zinc ion binding, regulation of transcription
1460147_at	RIKEN cDNA A730009E18		319603	-3.07****	-2.59**	-2.59**	
1439065_x_at	Similar to zinc finger protein 665		626316	2.48*	3.03*	3.58***	Zinc ion binding, regulation of transcription
1417600_at	**solute carrier family 15 (H+/ peptide transporter), member 2** [b]	Slc15a2, Pept2	57738	-5.28****	-3.69**	-5.53****	oligopeptide transport
1419343_at	**solute carrier family 15 (oligopeptide transporter), member 1**	Slc15a1, Pept1	56643		0.59	3.79*	oligopeptide transport
1429467_s_at 1421445_at 1427547_a_at	**solute carrier family 26, member 3** [b]	Slc26a3, Dra	13487			6.04**	Anion exchanger activity, transport
1444057_at	Transcribed locus			3.03****	2.36*	1.11	
1456111_at	Transcribed locus			2.41	4.09***	0.87	
1459649_at	Transcribed locus			4.08****	3.27**	3.44*	
1451602_at	**sorting nexin 6**	Snx6, TFAF2	72183	-3.98****	-4.01	-4.95**	Protein and ion transport

Table 3-4. Continued

Probe set ID	Gene	Gene name/ aliases	Locus Link	SW over FVB, control[a]	SW over FVB, 4 dpi	SW over FVB, 9 dpi	Main functions
1447458_at 1425668_a_at	ST3 beta-galactoside alpha-2,3-sialyltransferase 4, mRNA[b]	Siat4c, St3gal4	20443	6.24****	4.99****	5.65***	Glycosyl transferase activity, protein amino acid glycosylation
1421517_at	ST6 (alpha-N-acetyl-neuraminyl-2,3-beta-galactosyl-1,3)-N-acetylgalactosaminide alpha-2,6-sialyltransferase 1[b]	Siat7a, St6galnac1	20445	2.42*	3.29***	1.95*	Glycosyl transferase activity, protein amino acid glycosylation
1450813_a_at	troponin I, skeletal, slow 1	Tnni1	21952			3.24*	Actin binding, structural constituent of cytoskeleton
1419453_at	ubiquitin carboxyl-terminal esterase L5	Uchl5, Uch37	56207	3.22****	3.56***	3.23***	ubiquitin-dependent protein catabolism

[a], the numbers represent log2 ratios resulted from individual groups comparison. Significance by *t*-test was
*, $p < 0.05$
** $p \leq 0.005$
***, $p \leq 0.0005$
****, $p \leq 0.00005$
[b], gene expression was confirmed by quantitative real-time PCR (TaqMan)
Genes discussed in the text are bolded

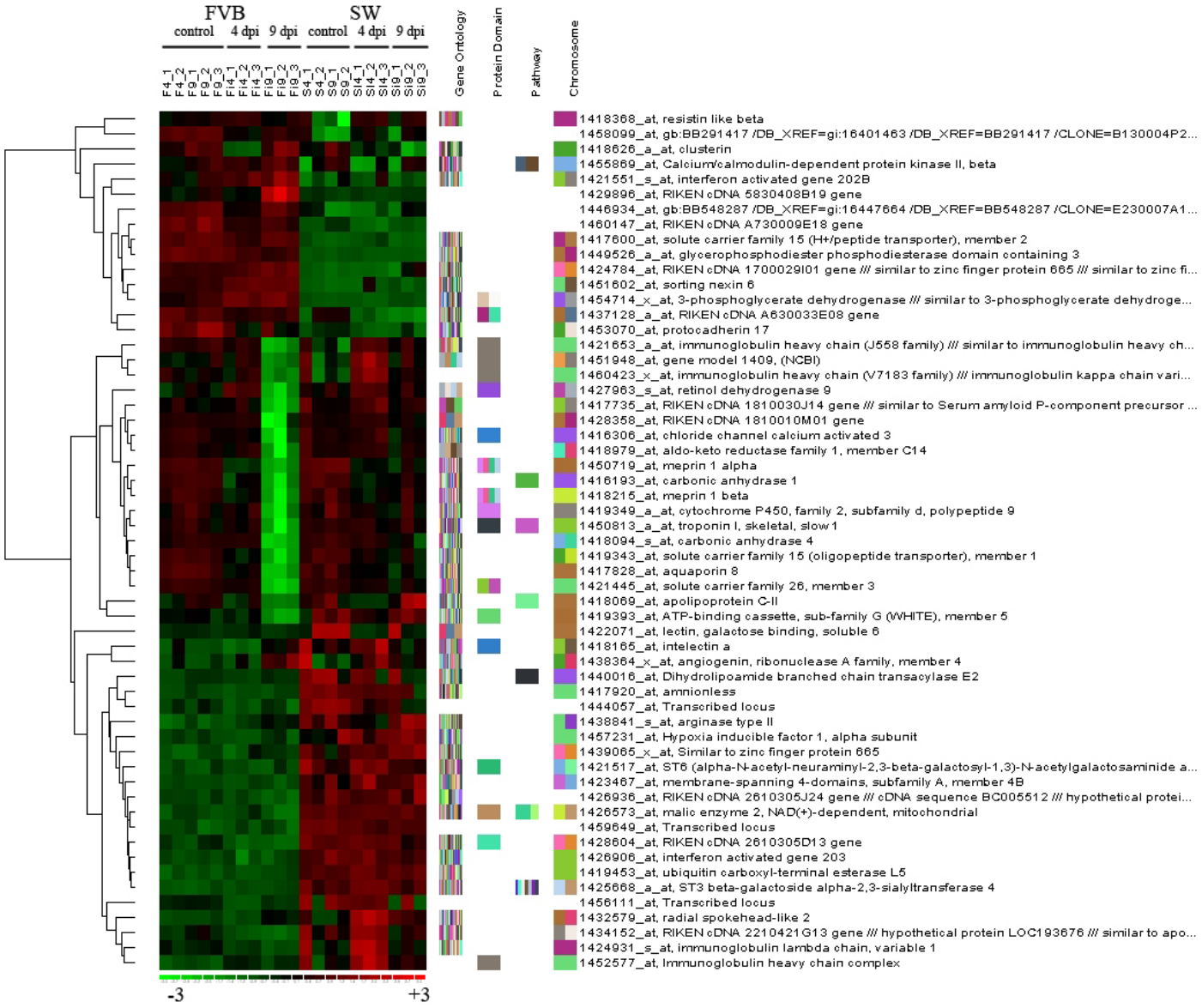

Figure 3-6. Hierarchical clustering of the most differentially expressed genes exhibiting host effect. Redundant probe sets were excluded from the analysis. The heat map shows color-coded expression levels (red = high expression, black = medium expression, and green = low expression). Gene trees are drawn vertically.

Table 3-5. Enrichment of GO categories from analysis of the most differentially expressed genes exhibiting host effect ($p<0.05$ by Hypergeometric test and at least 4 functionally annotated genes)

probe set	gene	LocusLink
Found 9 Gene Ontology "transporter activity" genes in a list with 48 annotated genes (all: 2752/31850, PValue: 0.020300) **		
1416306_at	chloride channel calcium activated 3	23844
1417600_at	solute carrier family 15 (H+/peptide transporter), member 2	57738
1417828_at	aquaporin 8	11833
1418069_at	apolipoprotein C-II	11813
1419343_at	solute carrier family 15 (oligopeptide transporter), member 1	56643
1419393_at	ATP-binding cassette, sub-family G (WHITE), member 5	27409
1421445_at	solute carrier family 26, member 3	13487
1451602_at	sorting nexin 6	72183
1432579_at	radial spokehead-like 2	66832
Found 5 Gene Ontology "carrier activity" genes in a list with 48 annotated genes (all: 761/31850, PValue: 0.005634) ***		
1416306_at	chloride channel calcium activated 3	23844
1417600_at	solute carrier family 15 (H+/peptide transporter), member 2	57738
1419343_at	solute carrier family 15 (oligopeptide transporter), member 1	56643
1421445_at	solute carrier family 26, member 3	13487
1432579_at	radial spokehead-like 2	66832
Found 12 Gene Ontology "extracellular region" genes in a list with 48 annotated genes (all: 3950/31850, PValue: 0.012438) **		
1417735_at	RIKEN cDNA 1810030J14 gene /// similar to Serum amyloid P-component precursor (SAP)	630754 /// 66289
1417920_at	amnionless	93835
1418069_at	apolipoprotein C-II	11813
1418094_s_at	carbonic anhydrase 4	12351
1418165_at	intelectin a	16429
1418215_at	meprin 1 beta	17288
1418368_at	resistin like beta	57263
1418626_a_at	clusterin	12759
1425668_a_at	ST3 beta-galactoside alpha-2,3-sialyltransferase 4	20443
1450719_at	meprin 1 alpha	17287
1434152_at	RIKEN cDNA 2210421G13 gene /// hypothetical protein LOC193676 /// similar to apolipoprotein L, 3 (predicted)	108956 /// 193676 /// 666661
1438364_x_at	angiogenin, ribonuclease A family, member 4	219033
Found 11 Gene Ontology "extracellular space" genes in a list with 48 annotated genes (all: 3531/31850, PValue: 0.014240) **		
1417735_at	RIKEN cDNA 1810030J14 gene /// similar to Serum amyloid P-component precursor (SAP)	630754 /// 66289
1417920_at	amnionless	93835
1418069_at	apolipoprotein C-II	11813
1418094_s_at	carbonic anhydrase 4	12351
1418165_at	intelectin a	16429
1418215_at	meprin 1 beta	17288
1418368_at	resistin like beta	57263
1418626_a_at	clusterin	12759
1425668_a_at	ST3 beta-galactoside alpha-2,3-sialyltransferase 4	20443
1450719_at	meprin 1 alpha	17287
1438364_x_at	angiogenin, ribonuclease A family, member 4	219033

Table 3-5. Continued

probe set	gene	LocusLink
Found 4 Gene Ontology "immune response" genes in a list with 48 annotated genes (all: 667/31850, PValue: 0.017922) **		
1421551_s_at	interferon activated gene 202B	26388
1424931_s_at	immunoglobulin lambda chain, variable 1	16142
1426906_at	interferon activated gene 203	15950
1438364_x_at	angiogenin, ribonuclease A family, member 4	219033
Found 6 Gene Ontology "oxidoreductase activity" genes in a list with 48 annotated genes (all: 1491/31850, PValue: 0.023848) **		
1418979_at	aldo-keto reductase family 1, member C14	105387
1419349_a_at	cytochrome P450, family 2, subfamily d, polypeptide 9	13105
1426573_at	malic enzyme 2, NAD(+)-dependent, mitochondrial	107029
1427963_s_at	retinol dehydrogenase 9	103142
1454714_x_at	3-phosphoglycerate dehydrogenase /// similar to 3-phosphoglycerate dehydrogenase /// similar to 3-phosphoglycerate dehydrogenase /// similar to 3-phosphoglycerate dehydrogenase /// similar to 3-phosphoglycerate dehydrogenase	236539 /// 668771 /// 670155 /// 671972 /// 673015
1457231_at	Hypoxia inducible factor 1, alpha subunit	15251
Found 11 Gene Ontology "extracellular region part" genes in a list with 48 annotated genes (all: 3743/31850, PValue: 0.021262) **		
1417735_at	RIKEN cDNA 1810030J14 gene /// similar to Serum amyloid P-component precursor (SAP)	630754 /// 66289
1417920_at	amnionless	93835
1418069_at	apolipoprotein C-II	11813
1418094_s_at	carbonic anhydrase 4	12351
1418165_at	intelectin a	16429
1418215_at	meprin 1 beta	17288
1418368_at	resistin like beta	57263
1418626_a_at	clusterin	12759
1425668_a_at	ST3 beta-galactoside alpha-2,3-sialyltransferase 4	20443
1450719_at	meprin 1 alpha	17287
1438364_x_at	angiogenin, ribonuclease A family, member 4	219033
Found 4 Protein Domain "Immunoglobulin-like // 3.4E-7" genes in a list with 18 annotated genes (all: 326/10020, PValue: 0.002344) ***		
1421653_a_at	immunoglobulin heavy chain (J558 family) /// similar to immunoglobulin heavy chain variable region /// similar to immunoglobulin mu-chain /// similar to anti-poly(dC) monoclonal antibody heavy chain	16061 /// 238447 /// 544903 /// 544907
1451948_at	gene model 1409, (NCBI)	620017
1452577_at	Immunoglobulin heavy chain complex	111507
1460423_x_at	immunoglobulin heavy chain (V7183 family) /// immunoglobulin kappa chain variable 1 (V1) /// immunoglobulin kappa chain variable 1-117 /// Ig kappa chain	16059 /// 16081 /// 16098 /// 381774
Found 8 Chromosome "12" genes in a list with 49 annotated genes (all: 1367/37379, PValue: 0.000372) ****		
1417920_at	amnionless	93835
1421445_at	solute carrier family 26, member 3	13487
1421653_a_at	immunoglobulin heavy chain (J558 family) /// similar to immunoglobulin heavy chain variable region /// similar to immunoglobulin mu-chain /// similar to anti-poly(dC) monoclonal antibody heavy chain	16061 /// 238447 /// 544903 /// 544907
1438841_s_at	arginase type II	11847
1451602_at	sorting nexin 6	72183
1452577_at	Immunoglobulin heavy chain complex	111507
1460423_x_at	immunoglobulin heavy chain (V7183 family) /// immunoglobulin kappa chain variable 1 (V1) /// immunoglobulin kappa chain variable 1-117 /// Ig kappa chain	16059 /// 16081 /// 16098 /// 381774
1457231_at	Hypoxia inducible factor 1, alpha subunit	15251

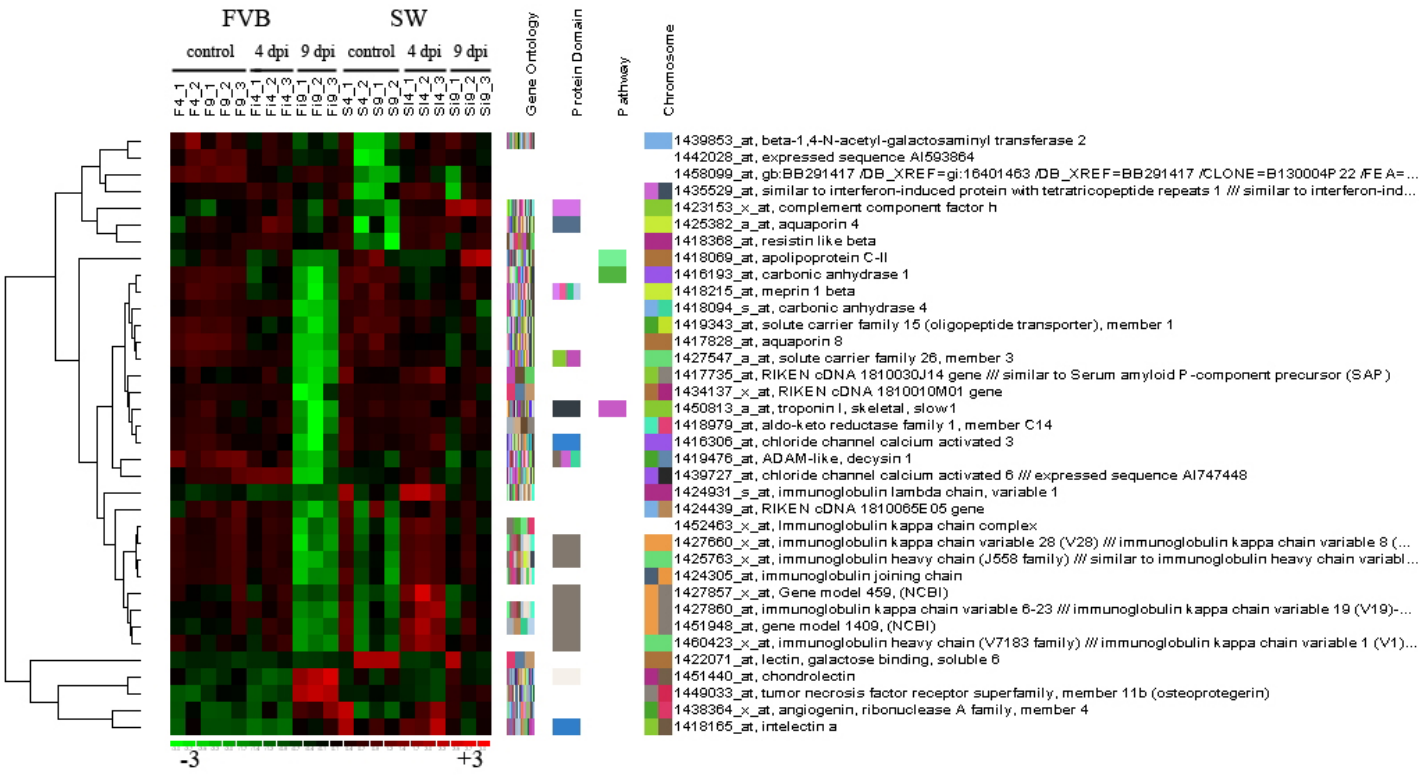

Figure 3-7. Hierarchical clustering of the most differentially expressed genes from delta eta analysis. Red and green colors indicate up- and downregulation respectively.

Table 3-6. Enrichment of GO categories of the most differentially expressed genes from delta eta analysis ($p<0.05$ by Hypergeometric test and at least 4 functionally annotated genes)

gene		LocusLink
Found 7 "transporter activity" genes in a list with 30 annotated genes (all: 2752/31850, PValue: 0.012322) **		
1416306_at	chloride channel calcium activated 3	23844
1417828_at	aquaporin 8	11833
1418069_at	apolipoprotein C-II	11813
1419343_at	solute carrier family 15 (oligopeptide transporter), member 1	56643
1425382_a_at	aquaporin 4	11829
1427547_a_at	solute carrier family 26, member 3	13487
1439727_at	chloride channel calcium activated 6 /// expressed sequence AI747448	99663 /// 99709
Found 6 "immune system process" genes in a list with 30 annotated genes (all: 1101/31850, PValue: 0.000490) ****		
Found 6 "immune response" genes in a list with 30 annotated genes (all: 667/31850, PValue: 0.000032) *****		
Found 6 "humoral immune response" genes in a list with 30 annotated genes (all: 116/31850, PValue: 0.000000) *********		
Found 6 "physiological response to stimulus" genes in a list with 30 annotated genes (all: 1417/31850, PValue: 0.001816) ***		
1423153_x_at	complement component factor h	12628
1424305_at	immunoglobulin joining chain	16069
1424931_s_at	immunoglobulin lambda chain, variable 1	16142
1427660_x_at	immunoglobulin kappa chain variable 28 (V28) /// immunoglobulin kappa chain variable 8 (V8)-16	16114 /// 640340 637227 /// 667881 /// 667899 ///
1427860_at	immunoglobulin kappa chain variable 6-23 /// immunoglobulin kappa chain variable 19 (V19)-14 /// immunoglobulin kappa chain variable 19 (V19)-13 /// similar to Ig kappa chain V-V region MPC11 precursor /// similar to Ig kappa chain V-V region MPC11 precursor /// similar to Ig kappa chain V-V region MPC11 precursor /// similar to Ig kappa chain V-V region MPC11 precursor /// similar to Ig kappa chain V-V region MPC11 precursor	669053 /// 669070 /// 676136 /// 676162 /// 676175
1438364_x_at	angiogenin, ribonuclease A family, member 4	219033
Found 6 "antigen binding" genes in a list with 30 annotated genes (all: 103/31850, PValue: 0.000000) *********		
1424305_at	immunoglobulin joining chain	16069
1424931_s_at	immunoglobulin lambda chain, variable 1	16142
1425763_x_at	immunoglobulin heavy chain (J558 family) /// similar to immunoglobulin heavy chain variable region /// similar to immunoglobulin mu-chain /// similar to anti-poly(dC) monoclonal antibody heavy chain	16061 /// 238447 /// 544903 /// 544907
1427660_x_at	immunoglobulin kappa chain variable 28 (V28) /// immunoglobulin kappa chain variable 8 (V8)-16	16114 /// 640340 637227 /// 667881 /// 667899 ///
1427860_at	immunoglobulin kappa chain variable 6-23 /// immunoglobulin kappa chain variable 19 (V19)-14 /// immunoglobulin kappa chain variable 19 (V19)-13 /// similar to Ig kappa chain V-V region MPC11 precursor /// similar to Ig kappa chain V-V region MPC11 precursor /// similar to Ig kappa chain V-V region MPC11 precursor /// similar to Ig kappa chain V-V region MPC11 precursor /// similar to Ig kappa chain V-V region MPC11 precursor	669053 /// 669070 /// 676136 /// 676162 /// 676175
1452463_x_at	Immunoglobulin kappa chain complex	243469
Found 4 "sugar binding" genes in a list with 30 annotated genes (all: 337/31850, PValue: 0.000272) ****		
Found 4 "carbohydrate binding" genes in a list with 30 annotated genes (all: 500/31850, PValue: 0.001190) ***		
1418165_at	intelectin a	16429
1422071_at	lectin, galactose binding, soluble 6	16857
1434137_x_at	RIKEN cDNA 1810010M01 gene	69036
1451440_at	chondrolectin	246048

Table 3-6. Continued

gene		LocusLink
Found 11 "extracellular region" genes in a list with 30 annotated genes (all: 3950/31850, PValue: 0.000597) ****		
Found 11 "extracellular space" genes in a list with 30 annotated genes (all: 3531/31850, PValue: 0.000224) ****		
Found 11 "extracellular region part" genes in a list with 30 annotated genes (all: 3743/31850, PValue: 0.000374) ****		
1417735_at	RIKEN cDNA 1810030J14 gene /// similar to Serum amyloid P-component precursor (SAP)	630754 /// 66289
1418069_at	apolipoprotein C-II	11813
1418094_s_at	carbonic anhydrase 4	12351
1418165_at	intelectin a	16429
1418215_at	meprin 1 beta	17288
1418368_at	resistin like beta	57263
1419476_at	ADAM-like, decysin 1	58860
1424305_at	immunoglobulin joining chain	16069
1449033_at	tumor necrosis factor receptor superfamily, member 11b (osteoprotegerin)	18383
1438364_x_at	angiogenin, ribonuclease A family, member 4	219033
1439853_at	beta-1,4-N-acetyl-galactosaminyl transferase 2	14422
Found 4 "channel or pore class transporter activity" genes in a list with 30 annotated genes (all: 777/31850, PValue: 0.005817) ***		
Found 4 "alpha-type channel activity" genes in a list with 30 annotated genes (all: 732/31850, PValue: 0.004716) ***		
1416306_at	chloride channel calcium activated 3	23844
1417828_at	aquaporin 8	11833
1425382_a_at	aquaporin 4	11829
1439727_at	chloride channel calcium activated 6 /// expressed sequence AI747448	99663 /// 99709
Found 8 "organismal physiological process" genes in a list with 30 annotated genes (all: 2672/31850, PValue: 0.002650) ***		
1423153_x_at	complement component factor h	12628
1424305_at	immunoglobulin joining chain	16069
1424931_s_at	immunoglobulin lambda chain, variable 1	16142
1425382_a_at	aquaporin 4	11829
1427660_x_at	immunoglobulin kappa chain variable 28 (V28) /// immunoglobulin kappa chain variable 8 (V8)-16	16114 /// 640340
1427860_at	immunoglobulin kappa chain variable 6-23 /// immunoglobulin kappa chain variable 19 (V19)-14 /// immunoglobulin kappa chain variable 19 (V19)-13 /// similar to Ig kappa chain V-V region MPC11 precursor /// similar to Ig kappa chain V-V region MPC11 precursor /// similar to Ig kappa chain V-V region MPC11 precursor /// similar to Ig kappa chain V-V region MPC11 precursor /// similar to Ig kappa chain V-V region MPC11 precursor	637227 /// 667881 /// 667899 /// 669053 /// 669070 /// 676136 /// 676162 /// 676175
1450813_a_at	troponin I, skeletal, slow 1	21952
1438364_x_at	angiogenin, ribonuclease A family, member 4	219033

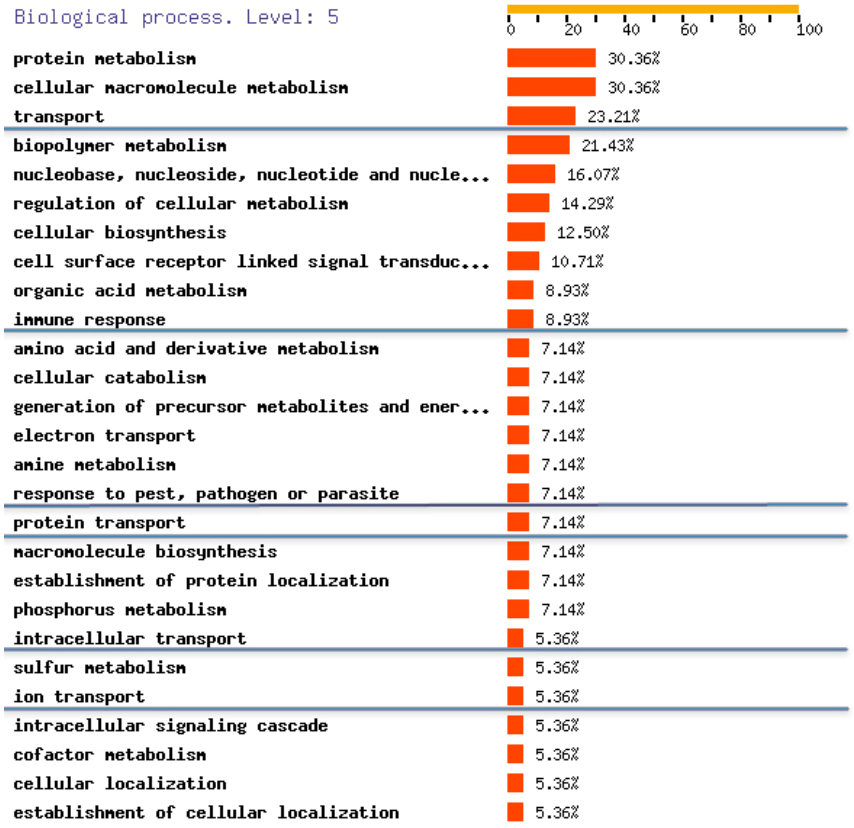

A.

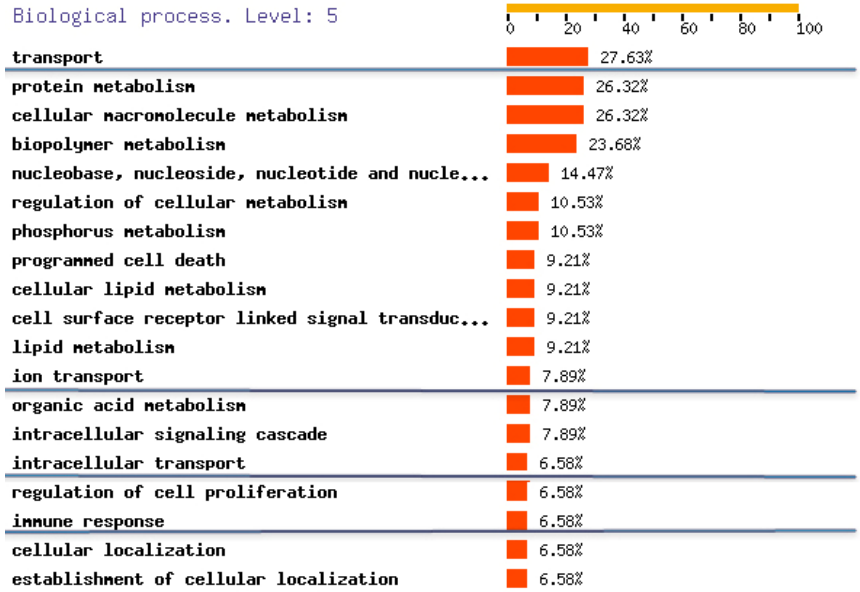

B.

Figure 3-8. FatiGO (fast assignment and transference of information) analysis of genes with strain effect (**A**) and infection x strain effect (**B**) identified by BioConductor analysis. After exclusion of unknown and redundant probe sets, 106 out of 232 genes and 126 out of 167 genes were analyzed respectively. Transport-related categories were markedly overrepresented when compared with immune-related ones, recapitulating the results obtained by dChip analysis.

Table 3-7. Enrichment of genes detected by BioConductor analysis by Hypergeometric test with p<0.0005

Strain effect - Found 232 genes or SNPs; 21 redundant probe sets excluded; 211 left

Finding significant Gene Ontology clusters...

Found 4 "phosphoric ester hydrolase activity" genes in a cluster with 17 annotated genes (all: 687/31850, PValue: 0.000408)
Found 5 "hydrolase activity\, acting on ester bonds" genes in a cluster with 16 annotated genes (all: 1367/31850, PValue: 0.000425)

Finding significant Chromosome clusters...

Found 5 "2 H4" genes in a cluster with 175 annotated genes (all: 118/37379, PValue: 0.000242)

Found 6 "4 E1" genes in a cluster with 175 annotated genes (all: 116/37379, PValue: 0.000019)

Infection effect - Found 167 genes or SNPs; 20 redundant probe sets excluded; 147 left

Finding significant Gene Ontology clusters...

Found 48 "membrane" genes in a cluster with 90 annotated genes (all: 10764/31850, PValue: 0.000106)

Found 39 "membrane part" genes in a cluster with 90 annotated genes (all: 8454/31850, PValue: 0.000419)

Found 5 "lytic vacuole" genes in a cluster with 79 annotated genes (all: 258/31850, PValue: 0.000464)

Found 17 "transporter activity" genes in a cluster with 79 annotated genes (all: 2752/31850, PValue: 0.000353)

1417828_at	aquaporin 8
1422699_at	arachidonate 12-lipoxygenase
1421129_a_at	ATPase, Ca++ transporting, ubiquitous
1428988_at	ATP-binding cassette, sub-family C (CFTR/MRP), member 3
1435613_x_at	cytochrome c oxidase, subunit Vb
1425525_a_at	purinergic receptor P2X, ligand-gated ion channel 4
1424364_a_at	RIKEN cDNA 1110020P15 gene
1452326_at	RIKEN cDNA 1810010G06 gene
1419343_at	solute carrier family 15 (oligopeptide transporter), member 1
1426600_at	solute carrier family 2 (facilitated glucose transporter), member 1
1421445_at	solute carrier family 26, member 3
1428793_at	solute carrier family 36 (proton/amino acid symporter), member 1
1452445_at	solute carrier family 41, member 2
1425606_at	solute carrier family 5 (iodide transporter), member 8
1426069_s_at	solute carrier family 7 (cationic amino acid transporter, y+ system), member 4
1437259_at	solute carrier family 9 (sodium/hydrogen exchanger), member 2
1429240_at	StAR-related lipid transfer (START) domain containing 4
1441927_at	Synaptotagmin VII

Found 5 "lysosome" genes in a cluster with 79 annotated genes (all: 258/31850, PValue: 0.000464)

Found 31 "integral to membrane" genes in a cluster with 70 annotated genes (all: 7545/31850, PValue: 0.000119)

Found 31 "intrinsic to membrane" genes in a cluster with 70 annotated genes (all: 7564/31850, PValue: 0.000125)

Found 5 "vacuole" genes in a cluster with 68 annotated genes (all: 301/31850, PValue: 0.000467)

Found 5 "integral to plasma membrane" genes in a cluster with 18 annotated genes (all: 1199/31850, PValue: 0.000426)

Found 5 "intrinsic to plasma membrane" genes in a cluster with 18 annotated genes (all: 1220/31850, PValue: 0.000462)

Finding significant Chromosome clusters...

Found 5 "10 C1" genes in a cluster with 93 annotated genes (all: 254/37379, PValue: 0.000445)

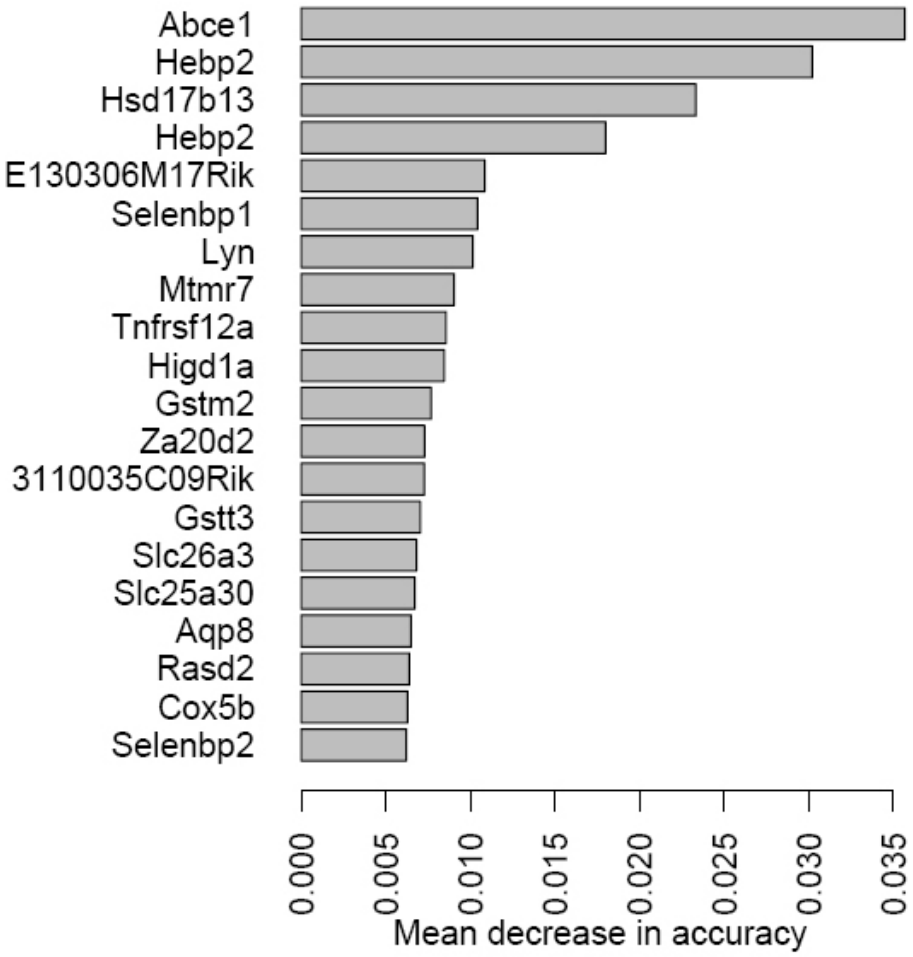

Figure 3-9. Genes with most predictive power obtained from BioConductor analysis.
When random forest evaluation of gene importance in predicting four classes (strain x infection status) was applied, a subset of genes appeared as having high predictive capacity. Genes such as *Slc26a3* and *Aqp8* were identified as most differentially expressed by dChip analysis as well.

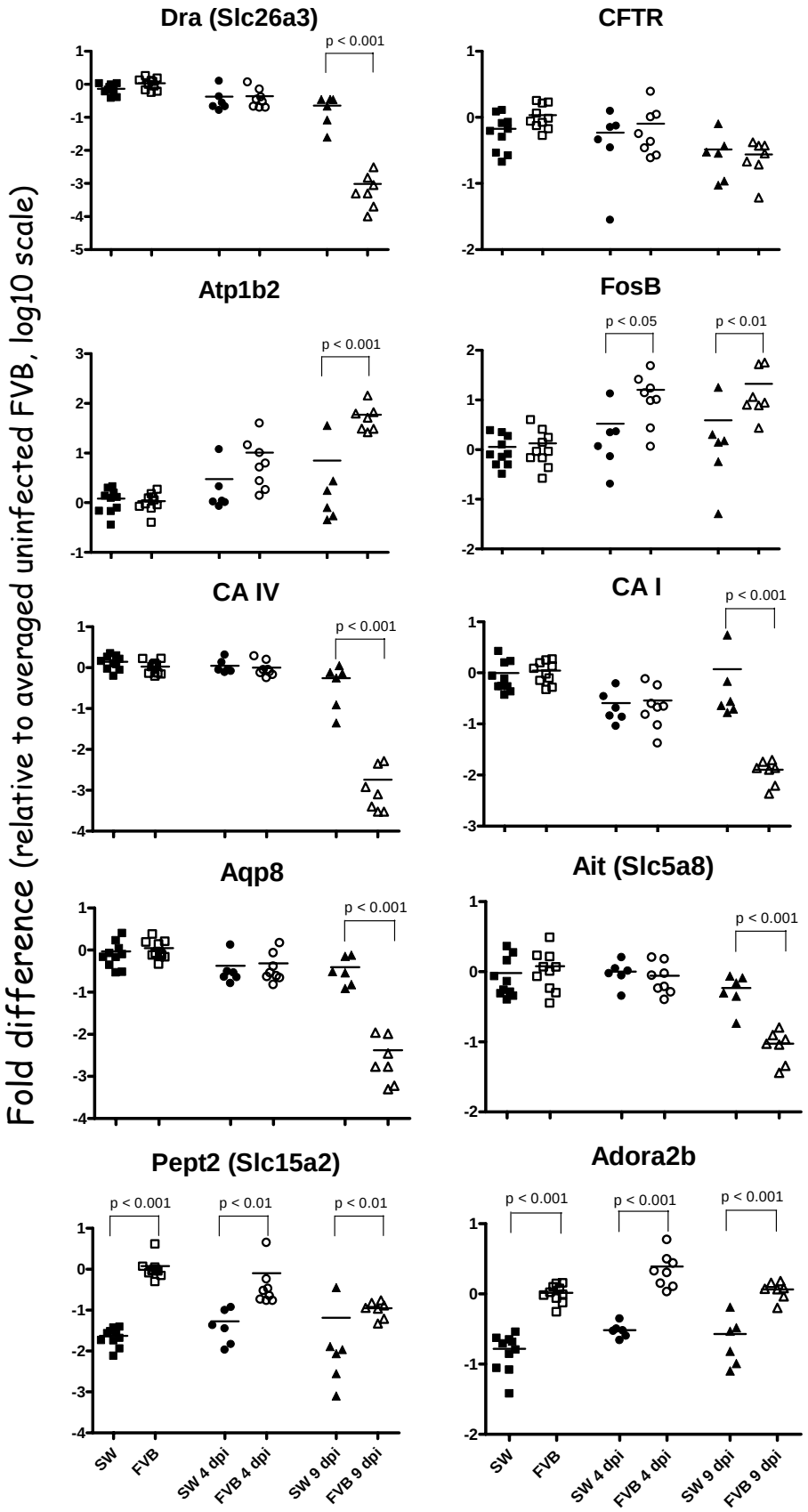

Figure 3-10. Quantitative real-time PCR of genes involved in intestinal transport and its regulation.

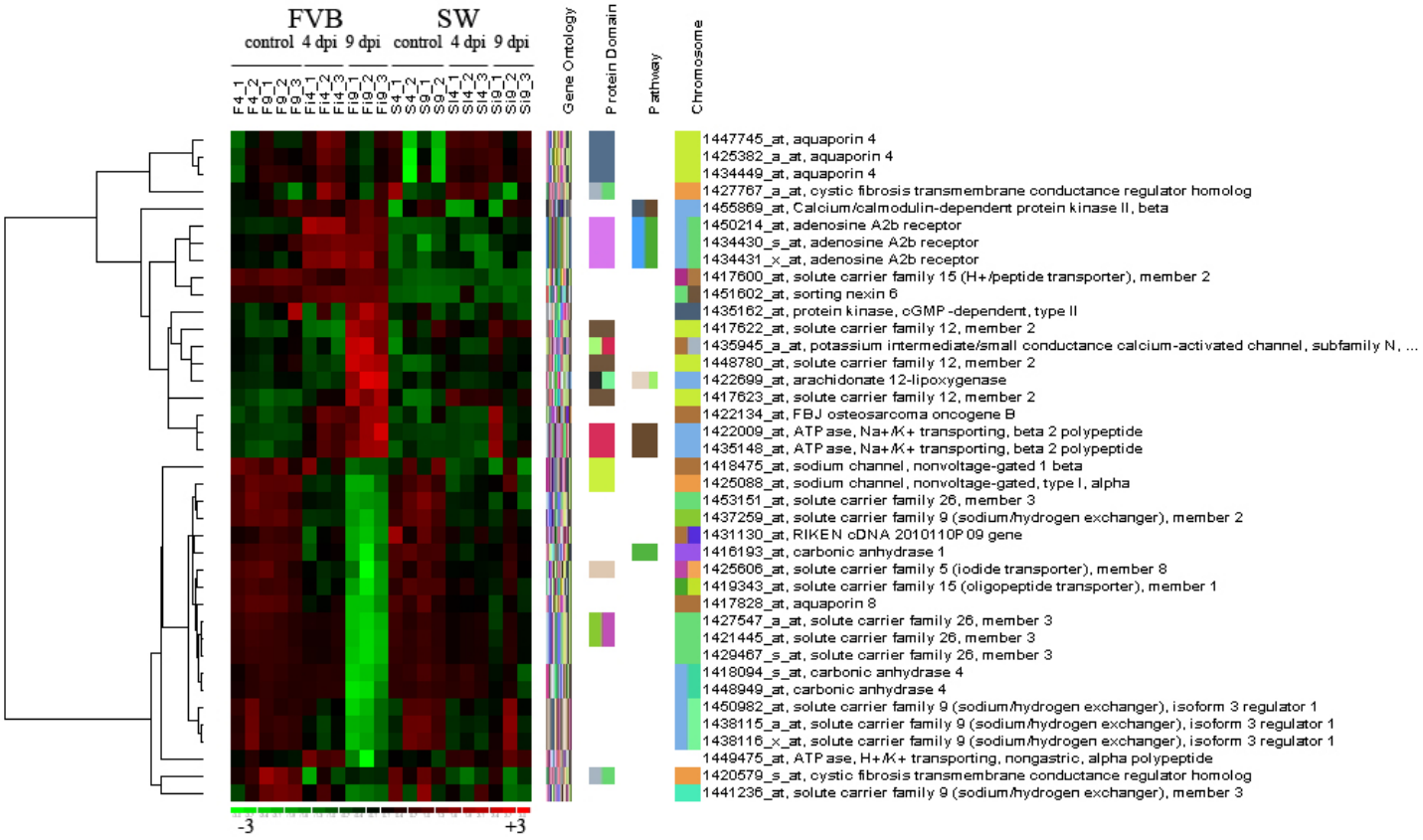

Figure 3-11. Hierarchical clustering of genes discussed in text as potentially contributing to development of intestinal ion disturbances and diarrhea. Red and green colors indicate up- and downregulation respectively.

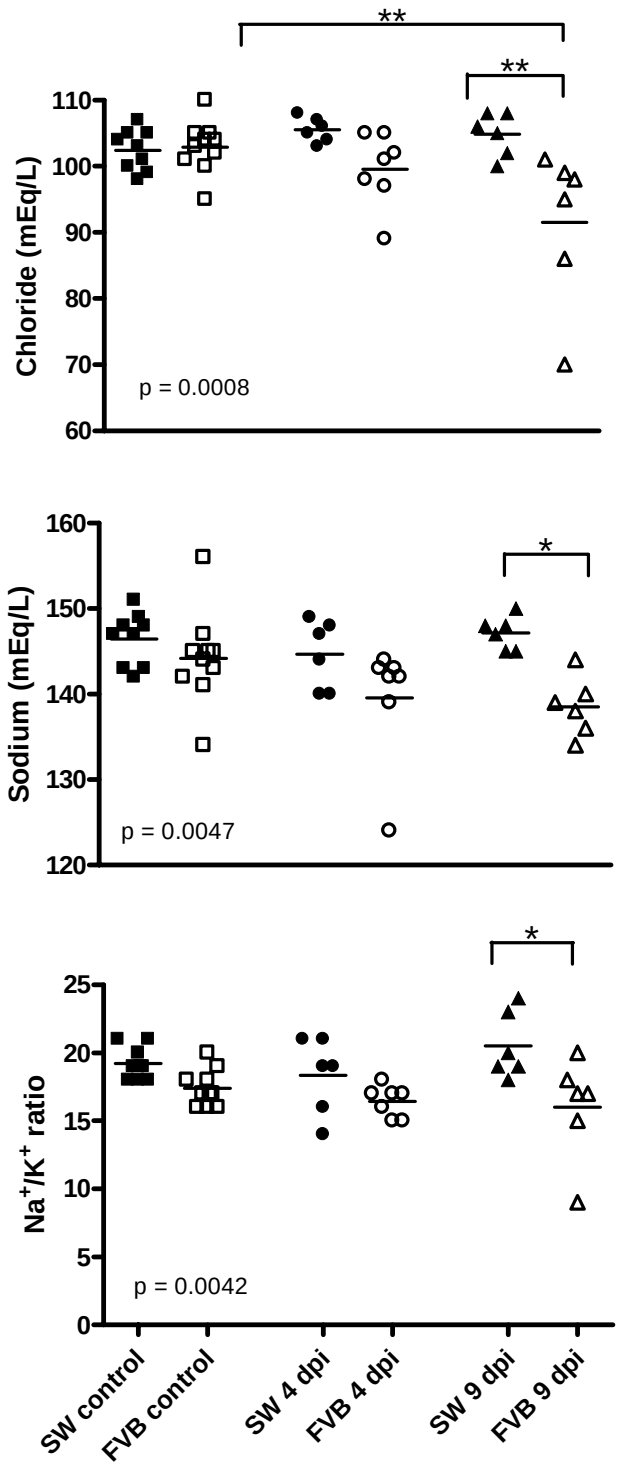

Figure 3-12. Serum electrolyte levels.
Infected FVB mice exhibit hypochloremia (A), hyponatremia (B), and altered Na^+/K^+ ratio in serum compared with infected SW mice. Scattergrams of all measurements are shown; lines indicate means of the groups.
*, $p < 0.05$; ** $p < 0.01$

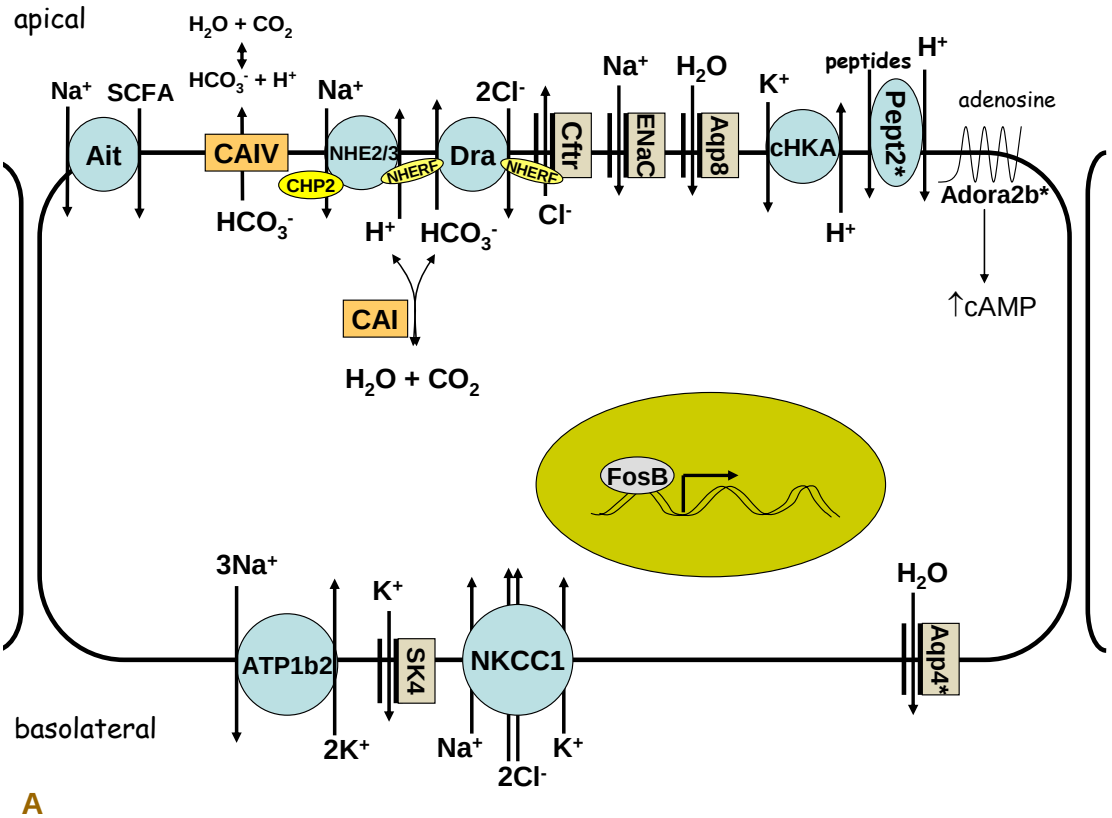
apical
$H_2O + CO_2$
$HCO_3^- + H^+$
Na^+ SCFA
Ait
CAIV
HCO_3^-
Na^+
NHE2/3
CHP2
NHERF
Dra
$2Cl^-$
Cftr
Cl^-
Na^+ H_2O
ENaC
Aqp8
K^+
cHKA
H^+
peptides
H^+
Pept2*
adenosine
Adora2b*
↑cAMP
H^+ HCO_3^-
CAI
$H_2O + CO_2$
FosB
$3Na^+$
K^+
ATP1b2
SK4
NKCC1
H_2O
Aqp4*
basolateral
$2K^+$
Na^+ K^+
$2Cl^-$

A

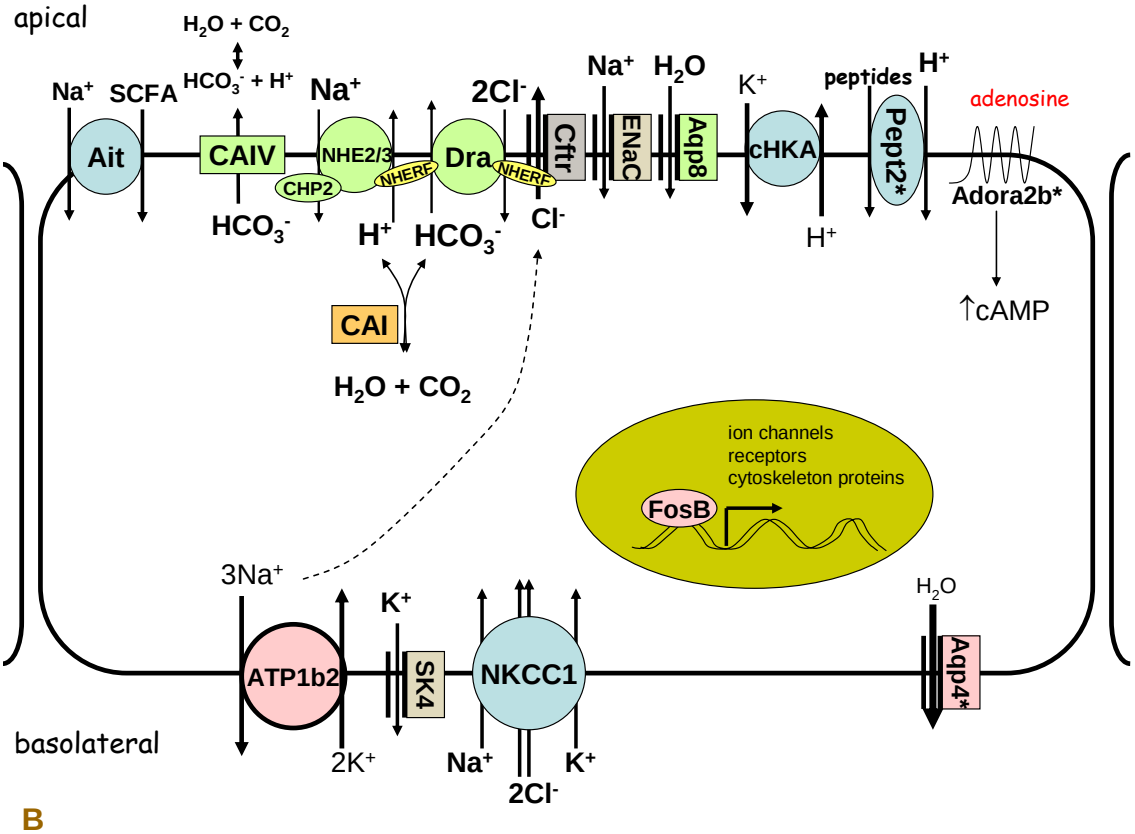
apical
$H_2O + CO_2$
$HCO_3^- + H^+$
Na^+ SCFA
Ait
CAIV
HCO_3^-
Na^+
NHE2/3
CHP2
NHERF
Dra
$2Cl^-$
Cftr
Cl^-
Na^+ H_2O
ENaC
Aqp8
K^+
cHKA
H^+
peptides
H^+
Pept2*
adenosine
Adora2b*
↑cAMP
H^+ HCO_3^-
CAI
$H_2O + CO_2$
ion channels
receptors
cytoskeleton proteins
FosB
$3Na^+$
K^+
ATP1b2
SK4
NKCC1
H_2O
Aqp4*
basolateral
$2K^+$
Na^+ K^+
$2Cl^-$

B

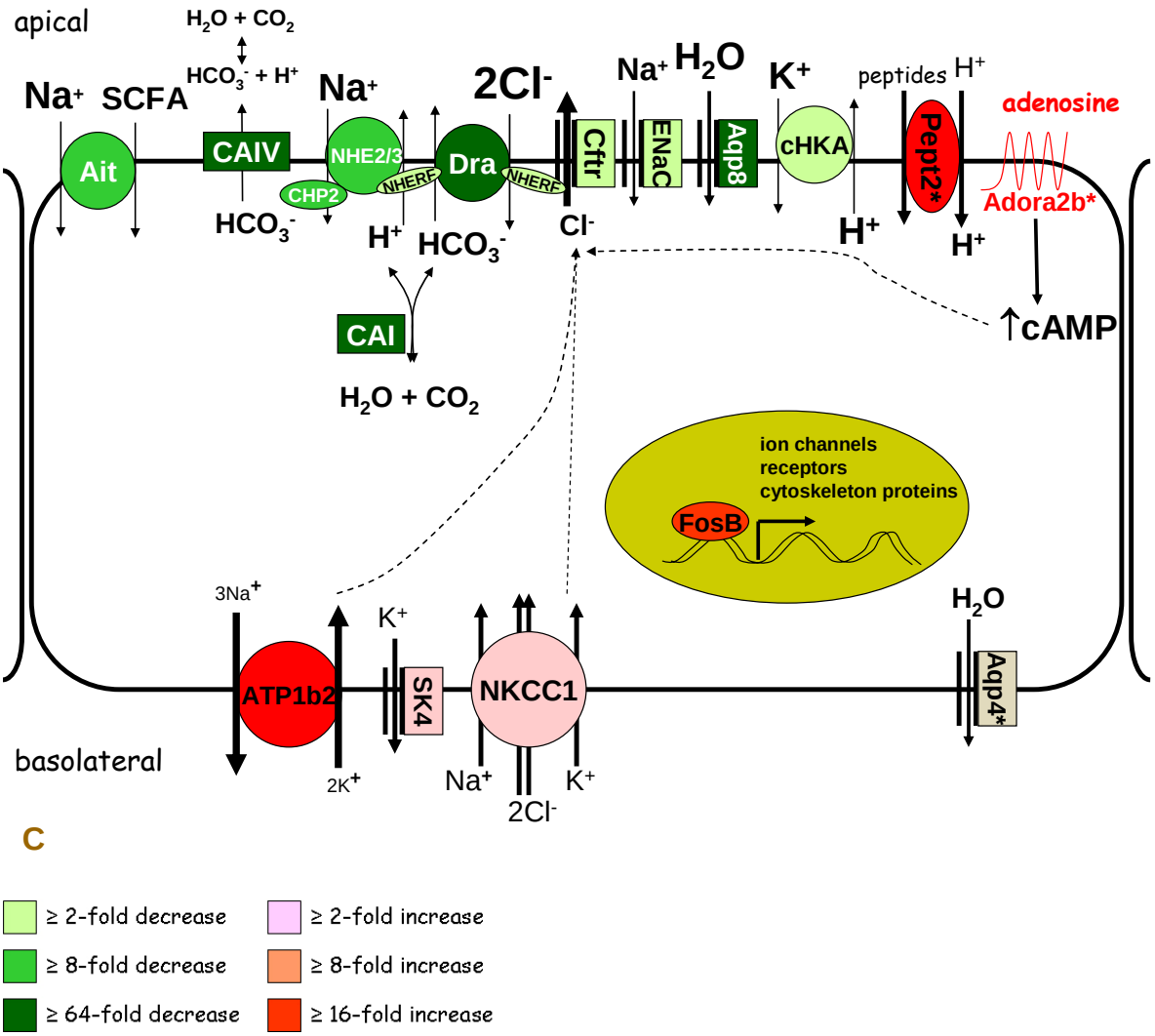

Figure 3-13. Working model for the contribution of alterations in colonic ion transport to fatal diarrhea in *C. rodentium*-infected FVB mice.

A. normal ion transport in large intestine mediated largely by a coupled action of anion exchanger DRA, CFTR, sodium/proton exchangers NHE2/3, potassium transporters and carbonic anhydrases;

B. alterations in ion transport in *C. rodentium*-infected SW mice included subtle decreases in expression of some apical transporters and compensatory increase in basolateral water channel *Aqp4* expression;

C. profound changes in infected FVB consisted of mild to marked downregulation of majority of apical transporters involved in intestinal NaCl absorption and bicarbonate secretion, along with upregulation of basolateral transporters providing driving force for chloride secretion. In addition, constitutively higher levels of *Pept2* and *Adora2b* expression in FVB mice (indicated by *) can contribute to alterations in cytosolic pH and cAMP during infection, thereby further affecting ion exchange. The cumulative effect may ultimately result in severe diarrhea and lead to death in susceptible animals.

Vesicular trafficking of some proteins (i.e. A2B receptor, aquaporins, NHE3, ATPases) and paracellular transport are not addressed here.

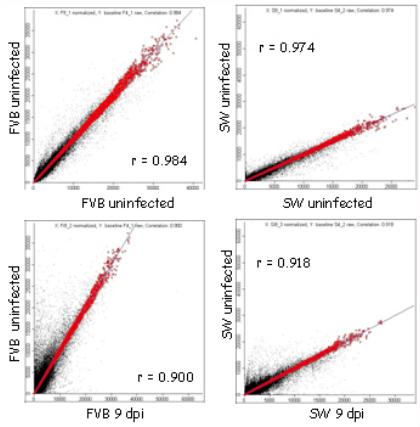

Sample	F4_1	F4_2	F9_1	F9_2	F9_3	Fi4_1	Fi4_2	Fi4_3	Fi9_1	Fi9_2	Fi9_3	S4_1	S4_2	S9_1	S9_2	Si4_1	Si4_2	Si4_3	Si9_1	Si9_2	Si9_3
F4_1	1.00																				
F4_2	0.99	1.00																			
F9_1	0.98	0.99	1.00																		
F9_2	0.98	0.98	0.99	1.00																	
F9_3	0.97	0.96	0.97	0.98	1.00																
Fi4_1	0.93	0.92	0.92	0.90	0.90	1.00															
Fi4_2	0.94	0.94	0.95	0.93	0.93	0.96	1.00														
Fi4_3	0.94	0.95	0.95	0.94	0.93	0.94	0.99	1.00													
Fi9_1	0.91	0.90	0.90	0.91	0.90	0.89	0.94	0.94	1.00												
Fi9_2	0.90	0.89	0.89	0.90	0.89	0.88	0.93	0.92	0.98	1.00											
Fi9_3	0.92	0.91	0.92	0.91	0.91	0.92	0.96	0.95	0.97	0.97	1.00										
S4_1	0.94	0.96	0.96	0.94	0.93	0.89	0.93	0.93	0.87	0.86	0.89	1.00									
S4_2	0.97	0.96	0.96	0.97	0.96	0.89	0.91	0.92	0.91	0.90	0.90	0.92	1.00								
S9_1	0.96	0.97	0.97	0.98	0.96	0.88	0.91	0.92	0.89	0.88	0.89	0.93	0.97	1.00							
S9_2	0.97	0.97	0.97	0.98	0.96	0.89	0.92	0.93	0.92	0.91	0.91	0.93	0.98	0.98	1.00						
Si4_1	0.94	0.94	0.94	0.94	0.93	0.93	0.98	0.98	0.94	0.92	0.94	0.94	0.92	0.92	0.93	1.00					
Si4_2	0.94	0.94	0.94	0.94	0.93	0.95	0.98	0.98	0.93	0.91	0.94	0.94	0.92	0.92	0.93	0.99	1.00				
Si4_3	0.94	0.94	0.94	0.92	0.92	0.97	0.97	0.96	0.91	0.89	0.93	0.94	0.91	0.91	0.91	0.96	0.97	1.00			
Si9_1	0.92	0.92	0.93	0.93	0.92	0.91	0.96	0.96	0.96	0.96	0.96	0.90	0.92	0.93	0.94	0.96	0.95	0.93	1.00		
Si9_2	0.95	0.96	0.96	0.96	0.95	0.92	0.96	0.96	0.92	0.91	0.93	0.93	0.94	0.95	0.96	0.97	0.96	0.94	0.97	1.00	
Si9_3	0.93	0.93	0.93	0.93	0.92	0.92	0.97	0.97	0.96	0.95	0.97	0.92	0.92	0.91	0.93	0.97	0.97	0.95	0.98	0.97	1.00

Figure 3-14. Correlation of raw intensities between biological replicates.
Microarray results were tightly correlated between biological replicates within FVB mice groups (r between 0.96 to 0.99 for controls, 0.94 to 0.99 for 4 dpi, and 0.97 to 0.98 for 9 dpi). Samples from uninoculated SW mice were less tightly correlated in accordance with the outbred nature of the animals (r between 0.92 to 0.98 for controls, 0.96 to 0.99 for 4 dpi, and 0.97 to 0.98 for 9 dpi). The correlations between the control and infected mice were smaller and reflected the severity of the disease progression. Thus, comparison of 4 dpi and 9 dpi FVB mice with the uninoculated controls or between each other resulted in r between 0.90 to 0.95, 0.89 to 0.92, and 0.88 to 0.96 respectively. Similar comparisons in SW mice lead to higher correlations (r between 0.91 to 0. 94, 0.90 to 0.96, and 0.93 to 0. 97 for 4 dpi and 9 dpi mice compared with controls or between each other) in accordance with the subclinical disease in the outbred animals. None of the correlations was substantially low (all r were higher than 0.85) indicating that 9 days of infection did not robustly change global gene expression profile.

- **A.** Representative examples of array-to-array correlations between uninoculated and infected animals within the same genetic group.
- **B.** Correlation matrix with r values for all array-to-array comparisons.

The following code for individual samples was used: F or S correspond to FVB or SW lines; “i” indicates infection status, 4 and 9 represent 4 and 9 dpi respectively, and “_1”, “_2”, and “_3” specify biological replicate.

Chapter 4: Susceptibility to fatal infectious diarrhea in inbred mice of Swiss origin

Diana Borenshtein[1], Katherine A. Schlieper[2], Megan E. McBee[1], Patricia Z. Zheng[1], Barry H. Rickman[2], Arlin B. Rogers[2], James G. Fox[2], David B. Schauer[1,2].

[1]Biological Engineering Division, [2]Division of Comparative Medicine, Massachusetts Institute of Technology, Cambridge, MA, 02139.

Manuscript in preparation

4.1. Introduction

Citrobacter rodentium is a naturally occurring murine pathogen. *C. rodentium* infects large intestine and causes attaching and effacing (A/E) lesions, colonic hyperplasia and variable degrees of colitis in the majority of genetically non-manipulated (referred to hereafter as wild type) mouse strains [reviewed in Luperchio and Schauer, 2001; Mundy et al, 2005]. The disease was initially characterized in outbred Swiss mice [Barthold, 1980; Barthold et al., 1976; Barthold et al., 1977; Barthold et al., 1978; Barthold and Jonas, 1977; Ediger et al, 1974; Johnson and Barthold, 1979] with subsequent characterization in a variety of inbred strains [Barthold et al., 1977; Goncalves et al., 2001; Itoh et al., 1979; Itoh et al., 1988; Khan et al., 2006; Li et al., 2004; Maaser et al., 2004; Okutani et al., 2001; Silverman et al., 1979; Vallance et al., 2003]. Among the lines of mice that have been characterized, C3H mice are the only wild type strain demonstrating fatal infection so far [Barthold et al., 1977; Deng et al., 2004; Gruenheid et al., 2004; Khan et al., 2006; Nagai et al., 2005; Tatsuno et al., 2006; Vallance et al., 2003]. However, C3H mice are genetically distant from C57BL/6 and Swiss mice [Beck et al., 2000]. Therefore, differences in *C. rodentium*-induced disease can be explained by distinct genealogy.

We recently showed different susceptibility to *C. rodentium* infection in closely related outbred Swiss Webster (SW) and inbred FVB/N (FVB) mice [Chapters 2 and 3]. FVB mice demonstrated high mortality rate, profound weight loss, development of severe colitis and substantial downregulation in expression of apical ion transporters, making it a second inbred strain with marked susceptibility to *C. rodentium* infection. Our results are highly important considering extensive use of FVB in transgenic studies [Barthold, 2002]. However, SW mice, used as control animals in our experiments, are randomly bred and, hence, genetically variable [Chia et al., 2005]. To get better insight into the mechanisms of susceptibility to fatal infectious diarrhea and colitis, a genetically defined inbred strain would be desired. SWR and SJL mice, widely used in general and immunology-related research, are both derived from Swiss mice. Based on the genetic comparison of biochemical and coat color markers [Taketo et al., 1991, Table 1-3], FVB mice have the highest degree of relatedness with SWR mice (77% of matching) compared with C57BL/6, SJL, and C3H mice (61%, 70%, and 73%, respectively). However, *C. rodentium* infection was not characterized in SWR and SJL strains yet. The aim of this study was to examine effects of *C. rodentium* infection on gross and microscopic lesions, gene expression,

and diarrhea development in inbred mice from Swiss origin: FVB/NJ, SWR/J, and SJL/J. Two additional control groups, consisting of C57BL/6 and C3H mice that are well-characterized in terms of outcome of *C. rodentium* infection (resistant and susceptible strain, respectively) were used as non-Swiss control strains. The C3H/HeOuJ substrain (endotoxin sensitive) rather than C3H/HeJ (TLR4-deficient) was chosen to avoid the bias of LPS-nonresponsiveness.

4.2. Results

C3H and FVB mice, but not SWR, SJL and C57BL/6 mice, develop fatal *C. rodentium* infection.

As expected, C3H/HeOuJ (referred hereafter as C3H) mice developed overt disease leading to 100% mortality in 8-11 days post *C. rodentium* infection (DPI) (Figure 4-1). FVB mice were also susceptible and demonstrated 61.5% mortality. Median survival rate was 9 and 12 days for C3H/HeOu and FVB mice respectively ($p<0.0001$ by Logrank test). SWR, SJL, and C57BL/6 mice were resistant and survived throughout the two week period post-inoculation.

Severe clinical disease in C3H mice was associated with rapid decline in body weight reaching $26.7 \pm 2.4\%$ loss by 9 DPI ($p<0.001$ by two-way ANOVA followed by Bonferroni posttest) (Figure 4-2). The body weight loss in FVB mice was somewhat less severe but still greater than in resistant strains reaching $18.3 \pm 2.5\%$ by 12 DPI ($p<0.01$ by two-way ANOVA followed by Bonferroni posttest). The changes in body weight in the rest of inbred strains fluctuated within +/-10% range and were not significant in SJL and SWR mice.

Fecal bacterial load in inbred mice infected with *C. rodentium.*

Bacterial counts in feces obtained from susceptible C3H mice and resistant SWR and C57BL/6 mice were similar at all time points (Figure 4-3). The levels of *C. rodentium* in SJL mice at 3 DPI were lower compared with C3H mice, but higher compared with FVB mice ($p<0.01$ by two-way ANOVA followed by Bonferroni posttest). In addition, SJL mice demonstrated delayed clearance and had the highest level of fecal *C. rodentium* shedding at 12 DPI. Susceptibility in FVB mice was not associated with increased bacterial load, as fecal

bacterial counts were lower in FVB mice at 3 and 6 DPI compared with the rest of the strains ($p<0.01$ by two-way ANOVA followed by Bonferroni posttest). Furthermore, 2 out of 15 FVB mice failed to become infected and were excluded from further analysis.

Culturing *C. rodentium* from tissues

C. rodentium load in the colon was highest in C3H mice, intermediate in SJL and FVB mice, and lowest in SWR, FVB and C57BL/6 mice ($p<0.0001$ by one-way ANOVA, Figure 4-4). High bacterial colonization of cecum was comparable in all the strains. High MLN counts of the pathogen were found in all C3H mice ($p=0.0003$ by one-way ANOVA), and in some FVB mice. However, only limited number of animals had *C. rodentium* counts in spleen. These results are somehow inconsistent with fecal shedding found in all the groups by 9-12 dpi. However, because some animals had to be euthanized at different time points post inoculation, the *C. rodentium* load in tissues is not directly comparable. Thus, tissues were collected at 9-10 DPI from C3H mice, at 12-14 DPI from FVB mice, and at 14 DPI from the rest of the groups.

Development of *C. rodentium*–specific humoral immune response in Swiss mice.

Early humoral response represented by IgM titers, developed in all inbred strains from Swiss origin by 12 DPI (Figure 4-5). Although it tended to be highest in SWR/J mice, the difference did not reach statistical significance ($p = 0.058$ by ANOVA). By 12 dpi, earlier than substantial IgG titers would be expected to be seen, SWR/J mice developed IgG1 (NS by ANOVA) and IgG2 ($p = 0.02$) responses specific to the pathogen. There was no difference in IgG1 to IgG2 ratios between the strains. These results suggest that humoral immune response is not likely to account for differences in susceptibility and mortality between the strains.

Measuring diarrhea in inbred mice infected with *C. rodentium.*

C. rodentium infection induced diarrhea in all the animals ($p<0.0001$ by two-way ANOVA, Figure 4-6). One of the most drastic responses was observed in C3H mice. Animals from that group demonstrated increase in fecal water content from $60.4 \pm 1.4\%$ in uninfected state to $81.6 \pm 0.5\%$ and $87.8 \pm 1.6\%$ at 6 and 9 DPI respectively ($p<0.05$ by two-way ANOVA followed by Bonferroni posttest), indicating rapid development of severe diarrhea. The water

content in the rest of the strains has increased from 58-62% in uninfected state to 75-78% at 9 and 12 DPI. Notably, substantial diarrhea in *C. rodentium*-infected FVB mice was associated with the failure to develop well-formed feces, which made quantitative comparison of stool water content with other strains impossible.

Intestinal lesions in inbred mice infected with *C. rodentium.*

Grossly, in the majority of the strains the distal half of the colon was rigid and distended and a prominent cecal patch was observed. The only exception was FVB mice that developed gross lesions in the whole colon, including the proximal parts. No gross cecal changes were seen in infected FVB mice. Histologically, infected mice of all strains developed mild to moderate inflammation and hyperplasia, minimal dysplasia, mild edema, and a wide range of epithelial defects ($p<0.0001$ by Kruskal-Wallis test, Figures 4-7 and 4-8). No significant differences were found between the groups in any of the parameters, although colonic epithelial defects and cumulative disease index tended to be higher in C3H mice ($p>0.05$ by post-hoc Dunn's Multiple Comparison Test). The pathological changes in cecum were milder than in colon in all infected animals (data not shown). Interestingly, the cecal inflammation, hyperplasia, edema and cumulative disease index in C3H mice were more severe than in FVB mice, but comparable to other inbred strains ($p<0.0001$ by Kruskal-Wallis test). The only exception was significantly higher dysplasia in cecum of C3H mice compared with all other strains ($p<0.05$ by post-hoc Dunn’s test, data not shown). The majority of the FVB, C3H and a few of the SWR mice had gland herniation into GALT. Multifocal hepatic lesions, including coagulative necrosis, were observed in 80% of the infected SJL mice. In addition, SJL mice demonstrated profound splenomegaly in response to infection, whereas mild increase in spleen weight was observed in SWR and C57BL/6 mice and no change in C3H and FVB mice ($p<0.0001$ by one-way ANOVA, Figure 4-9). Colon weight was increased in all the animals infected with *C. rodentium* (Figure 4-9). The most significant change was detected in C3H and FVB mice, and the least in SJL and C57BL/6 mice ($p<0.0001$ by one-way ANOVA). Colon weight was positively correlated with inflammation, hyperplasia and disease index scores in distal colon of infected mice ($p<0.05$ by Spearman correlation test, Figure 4-10).

Quantitative real-time RT-PCR on genes involved in intestinal transport and its regulation (validation of the results obtained from microarray analysis)

Expression of the majority of the genes involved in intestinal transport was similar to the previously reported for FVB mice (Chapter 3). Upon infection, the expression of *Slc26a3* (*Dra*), *Aqp8, CA I* and *CA IV* was lower and expression of *Atp1b2* and *Fosb* was higher in susceptible strains compared with resistant strains, though in few cases the differences did not reach statistical significance (Figure 4-11). C3H mice were the most severely affected, whereas FVB mice had intermediate level of differential gene expression. At the same time, FVB mice had constitutively higher expression of *Adora2b* than the rest of the animals at all time points ($p<0.0001$ by ANOVA). The expression profile of *Ait (Slc5a8)* was similar between the groups. In addition, both susceptible FVB and resistant SWR mice had the highest and C3H mice had the lowest levels of *Pept2 (Slc15a2)* expression. *Cftr* was differentially expressed between the infected groups with highest level of transcripts in FVB mice, intermediate in C3H, SWR and SJL mice, and lowest in C57BL/6 mice.

Detection of mast cells in inbred mice infected with *C. rodentium*

Toluidine-positive mast cells were rare in colon tissues from SWR, SJL, C3H and C57BL/6 mice, and ranged from 0 to 4 cells/mm^2 (Figure 4-12). In contrast, dense accumulation of mast cells, mainly in the most distal colorectal area, was observed in FVB mice ($p<0.0001$ by ANOVA). The number of mast cells was 16.3 ± 3.3 cells/mm^2 and 11.0 ± 3.3 cells/mm^2 in uninoculated and infected FVB mice, respectively ($p<0.001$ by post-hoc *t* test compared with the rest of the groups). The highest density was found in close proximity to the rectum reaching 25-27 cells/mm^2 in uninfected FVB mice. The infection was associated with the decrease in number of toluidine-positive cells that was statistically significant for FVB mice only ($p<0.01$ by post-hoc *t* test).

FVB mice from different vendors develop distinct responses to *C. rodentium*.

FVB mice obtained from Taconic Farms and The Jackson Laboratories (FVB/NTac and FVB/NJ, respectively) exhibited differences in disease progression. Thus, clinical signs and mortality in infected FVB/NJ developed later than in FVB/NTac (latent period of 12 DPI vs. 8

DPI, respectively), though no statistical significance in the survival rate was achieved (Figure 4-13A). Body weight loss was also comparable between the Taconic and Jackson FVB substrains, despite lower fecal bacterial shedding in FVB/NJ at 3 and 6 DPI ($p<0.0001$ by *t* test, Figure 4-13B and C). Furthermore, development of colonic inflammation, hyperplasia and dysplasia was more severe in FVB/NTac mice by 12 DPI ($p<0.0005$ by Mann-Whitney test, Figure 4-14).

4.3. Discussion

Here, we characterized the progression of *C. rodentium* infection in two inbred strains of Swiss mice that have not been characterized previously. Infected SWR and SJL mice developed minimal morbidity in response to the pathogen and survived throughout 14 days of the study, indicating their resistance to infection. The results were comparable to C57BL/6 mice, a non-Swiss strain that has been characterized as being resistant to the disease [Barthold et al., 1977; Maaser et al.,2004; Simmons et al., 2003; Vallance et al., 2002al Vallance et al., 2002b; Vallance et al., 2003]. Consistent with our previous studies (Chapter 2), FVB mice developed high morbidity and mortality upon infection, although the response was less dramatic than in C3H/HeOu mice that have been characterized as being *C. rodentium*-susceptible strain [Barthold et al., 1977; Deng et al, 2004; Gruenheid et al., 2004; Khan et al., 2006; Nagai et al., 2005; Tatsuno et al., 2006; Vallance et al., 2003].

Fecal bacterial shedding reached approximately 10^8-10^9 CFU/g feces at 3 DPI and was comparable between susceptible C3H, and resistant SWR and C57BL/6 mice at all time points. This is in contrast with previous report of susceptibility to *C. rodentium* in inbred strains [Vallance et al., 2003], where susceptible C3H mice had high colonic counts of *C. rodentium* at 4 DPI (~10^9 CFU/g colon) compared with poor colonization (≤~10^4 CFU/g colon) in resistant C57BL/6, BALB/c, 129S1/SvImJ, and NIH Swiss mice. Furthermore, at 6 DPI there was a log difference in colonic counts between C3H mice and resistant strains in this study [Vallance et al., 2003]. The reason for such a discrepancy with our results is not clear, though different tissues used for *C. rodentium* culturing (colon vs. feces) may play a role. Strikingly, high mortality rate in FVB mice was not correlated with bacterial burden; an increase in fecal *C. rodentium* counts was lower in this strain at 3 and 6 DPI compared with other groups. To clarify the contribution of immune response to these differences, serum antibody titers were analyzed in inbred mice of Swiss origin (referred to hereafter as Swiss mice). Due to high degree of mortality in FVB mice,

assessment of humoral immune response was done at 12 DPI. At that time point, *C. rodentium*-specific IgM titers were detected in all infected Swiss mice, demonstrating development of early humoral immune responses. However, appreciable *C. rodentium*-specific IgG1 and IgG2 titers were detected in SWR, but not in SJL and FVB mice at that time point. Although inconsistent development of adaptive immunity (IgG responses) in mice within two weeks post *C. rodentium* infection was shown [Simmons et al., 2002; McBee and Schauer, unpublished results], these distinct IgG titers can contribute to delayed bacterial eradication in SJL mice. Nevertheless, the observed humoral immune response cannot account for the differences in mortality between FVB, SJL and SWR mice. Moreover, both resistant SWR and susceptible FVB mice possess the H-2^q haplotype, indicating that polymorphisms in major histocompatibility complex are not responsible for the observed differences in the disease outcome between inbred strains.

Despite similar fecal bacterial load in susceptible C3H/HeOu and resistant SWR and C57BL/6 mice, high *C. rodentium* counts were cultured from colon and MLN of C3H mice compared with other strains. This may be attributable to different day of sample collection. Thus, due to severe morbidity, C3H mice were euthanized and necropsied at 9-10 DPI, representing the peak of infection. Samples from FVB mice and other strains were collected when decline in infection took place, i.e. at 12-14 DPI and at 14 DPI, respectively. Therefore, higher tissue bacterial counts in C3H mice should be interpreted with caution. Furthermore, only a few animals demonstrated limited bacterial counts in spleen (1/10 in SJL, 2/7 in FVB, and 1/8 in C3H infected mice). Although an earlier translocation of bacteria to spleen cannot be denied at this point, the results suggest that *C. rodentium* infection in adult wild-type animals is contained within intestinal/abdominal compartment. This disagrees with the report of disseminated disease in C3H mice [Vallance et al., 2003]. Other factors may be responsible for early and severe mortality in C3H and FVB mice. Based on the studies presented in Chapters 2 and 3, we suggested that fatal *C. rodentium* infection in susceptible animals is caused by hypovolemia due to extensive diarrhea.

Consistent with that hypothesis, analysis of stool water content indicated significant diarrhea in C3H mice beginning as early as 3 DPI, but statistically significant from 6 DPI. The magnitude of diarrhea in this strain was comparable to levels reported in DRA-deficient mice used as a model of congenital chloride diarrhea [Schweinfest et al., 2006]. Moreover, the lack of well-formed feces in moribund FVB mice indicated development of remarkable diarrhea in this

strain as well, though making quantitative analysis of that parameter impossible. This finding suggests that both susceptible strains may suffer from severe dehydration induced by *C. rodentium* infection. Studying effects of fluid therapy in C3H mice would be helpful in clarifying the contribution of fluid loss to the disease outcome in that strain.

Colon weight was positively correlated with histological lesion scores, consistent with other reports using this parameter as a marker of intestinal pathology in *C. rodentium* infection [Deng et al., 2004; Ghaem-Maghami et al., 2001; Goncalves et al., 2001; Khan et al., 2006; Higgins et al., 1999; Mundy et al., 2003; Mundy et al., 2004; Nagai et al., 2005; Simmons et al., 2003; Vallance et al., 2002a; Vallance et al., 2002b; Vallance et al., 2003]. Despite the fact that colon weight was higher in susceptible animals, the lesion grades were comparable between the strains. This is consistent with our hypothesis that susceptibility does not fully depend on degree of intestinal damage (Chapters 2 and 3). However, tissue collection day bias should be taken in account for that parameter as well. Thus, non-significant trend to develop more severe pathology in C3H mice could be much more profound if all the groups were compared at the same date. Therefore, contribution of epithelial damage to *C. rodentium*-induced diarrhea can not be excluded for C3H mice. Additional experiment studying the disease progression with the same end-point for all the strains (9 DPI) should be performed.

We next evaluated contribution of intestinal ion transport to distinct disease phenotypes in susceptible and resistant mice. To accomplish this, we measured the expression of genes predicted by microarray analysis (Chapter 3). Transcriptional activity for the main candidates for susceptibility was comparable to our previous findings. In response to infection, *CA I* and *CA IV* were markedly downregulated, while *Atp1b2* and *Fosb* were significantly upregulated in both susceptible FVB and C3H strains compared with SWR and C57BL/6 mice. This indicates the importance of FosB, Na^+/K^+-ATPase and carbonic anhydrases I and IV in regulating ion homeostasis and mediating susceptibility to *C. rodentium* infection. In addition, the decrease in *Dra (Slc26a3)* expression was remarkable in C3H mice and comparable to the levels in FVB/NTac mice in previous study (Chapter 3). However, decline in *Dra* message was milder in FVB/NJ mice and not different from the levels in the resistant SWR mice. These striking differences in *Dra* expression between current and previous study led us to think about other possible factors affecting gene expression. The most plausible cause for distinct gene behavior can be again different time point for tissue collection. To prove that, we compared side-by-side

C3H/HeOuJ and FVB/NTac mice which were euthanized at the same time point (9 DPI) in current and previous studies. This analysis revealed that expression of majority of genes, including *Dra, Fosb, Atp1b2, Aqp8* and *Slc5a8,* was similar in C3H/HeOuJ and FVB/NTac mice (Figure 4 Supplemental 1). Furthermore, expression of *TNFa*, which increases with the time post-infection [Goncalves et al., 2001; Li et al., 2004; McBee and Schauer, unpublished results], was markedly higher in colons collected from SWR, SJL, and C57BL/6 mice at 14 DPI compared with tissues collected from Swiss Webster, FVB/NTac, and C3H/HeOuJ at 9 dpi. Therefore, the role of predicted genes in mediating fatal infectious diarrhea in FVB and C3H mice needs further evaluation. Conducting a study in which all test subjects are euthanized at a comparable time point would be critical. Nevertheless, the results strongly suggest the possibility of common pathogenic mechanism of *C. rodentium*-induced mortality in susceptible inbred strains of different origins.

SJL mice had slightly different phenotype than the rest of the resistant animals. Compared with susceptible and resistant inbred strains, SJL mice had intermediate expression of majority of the genes involved in intestinal ion transport. Moreover, unlike the rest of the groups, SJL mice had delayed clearance of infection and demonstrated profound splenomegaly and liver pathology despite comparable intestinal lesions. Although SJL mice are considered to be immunocompetent, they have high circulating levels of T cells, defective TCR-induced IL-4 and IgE production, elevated IL-12p40 expression by antigen presenting cells, and a high incidence of spontaneous B-cell type lymphomas [Alleva et al., 2001; Beutner et al., 1997; Festing, 1999; Tang et al., 1998; Yoshimoto et al., 1995]. Considering these facts and the highest degree of relatedness between SWR and FVB/N mice [Taketo et al., 1991, Table 1-3], SWR may serve as better control strain for studying fatal infectious diarrhea in FVB mice.

While most of the expression changes were similar between C3H and FVB mice, overexpression of *Adora2b* was found in FVB mice only. This receptor is activated by adenosine, a secretagogue released by different types of immune cells, and mediates signals suggested to be implicated in diarrhea [Strohmeier et al., 1995]. Activated mast cells secrete adenosine and other inflammatory mediators, and their role in the pathogenesis of diarrhea has long been recognized [Barrett, 1991; Brandt et al., 2003; Crowe et al., 1997; Crowe and Perdue, 1992; Jakate et al., 2006; Marquardt et al., 1984; McDermott et al., 2003; Rijnierse et al., 2006]. We therefore quantified mast cells in colon tissue of inbred strains by toluidine staining. Notably,

FVB mice (both control and *C. rodentium*-inoculated) had remarkably higher counts compared with the rest of the groups. Similar colonic mastocytosis was found in OVA-challenged Balb/c mice, which serve as a model of oral allergen-induced diarrhea [Brandt et al., 2003]. Saline-treated mice in this study did not develop diarrhea [Brandt et al., 2003] and had colonic counts of mast cells comparable to levels we found in SWR, SJL, C3H, and C57BL/6 mice. Infection was associated with the reduction in toluidine-positive cells in all mice, but significant in FVB strain only. Because the efficiency of toluidine blue staining is substantially reduced in degranulated mast cells [Bischoff et al., 1996], this result may be indicative of extensive mast cells activation. Therefore, despite being indispensable for *C. rodentium* clearance [Wei et al., 2005], abundant mast cells in colorectal areas of FVB mice can be activated during *C. rodentium* infection, and release adenosine and other secretagoges which will ultimately contribute to the development of fatal diarrhea in FVB mice. The discovery of enriched mast cell population in colorectal areas of FVB mice may have far-reaching implications. For example, recent reports indicate increased morbidity, mortality, and colitis development in mice co-infected with *C. rodentium* and helminth *Heligomosomoides polygyrus* [Chen et al., 2005]. Although this outcome was attributed to activation of dendritic cells and imbalanced Th1, Th2, and T regulatory cell responses [Chen et al., 2005; Chen et al., 2006], the increased susceptibility of mice coinfected with *C. rodentium* and *H. polygyrus* may also result from mastocytosis, which usually accompanies nematode parasites infections. Considering this and the high susceptibility of FVB mice to allergic diseases [Baker et al., 2000; Knoops et al., 2005; Whitehead et al., 2003], the role of mast cells in pathogenesis of fatal infectious diarrhea in FVB mice needs further investigation.

Another interesting observation from our study was the distinct response of FVB mice supplied from different vendors, which could be an additional factor responsible for differences found in gene expression between this and previous studies (Chapters 2 and 3). Thus, FVB/NJ mice had less morbidity but showed no difference in body weight loss. They also demonstrated longer latent period before the development of clinical signs (i.e. FVB/NTac mice had an earlier onset of disease), though mortality rate was not significantly different between the substrains. Notably, fatal disease was observed in both strains despite significantly lower increase in bacterial counts in FVB/NJ mice, which further supports our conclusion that high bacterial load is not required for development of mortality. At the same time, differences in bacterial load may at least partially account for lower lesion scores and delayed clinical disease found in FVB/NJ

mice. The reasons for those differences are unclear, but distinct microbial flora in animals supplied by different vendors would the possible factor. Also, genetic segregation and/or mutation can not be excluded. To examine the possibility that mastocytosis in the distal colon is unique feature of FVB/NJ mice, we stained the tissues from Swiss Webster and FVB/NTac mice with toluidine as well (Figure 4 Supplemental 2). As in current study, FVB/NTac mice had higher counts of mast cells prior to infection, which went down as infection progressed. However, the levels were comparable to those found in FVB/NJ mice and cannot explain the differences in fecal bacterial burden, latent period until appearance of clinical signs and mortality, and pathological lesions.

In conclusion, this study is the first report on *C. rodentium* infection in SWR and SJL mice, which were found to be resistant to disease. SWR mice will be more suitable as a control strain for studying *C. rodentium* induced fatal disease in FVB mice than random bred Swiss Webster mice because of their genetic uniformity. Our data indicate that susceptible animals die from severe dehydration due to pathogen-induced diarrhea. Solid evidence from our work suggests the existence of common pathologic mechanism in *C. rodentium*-infected C3H and FVB mice despite their different genetic background. To further confirm diarrhea-induced hypovolemia as the main cause of fatality in C3H mice, fluid therapy should be evaluated in those animals. Designing experiment in which all the tissues will be collected at the same time will help to exclude temporal changes in organ culturing, pathology, and gene expression profile. Our studies demonstrate that *C. rodentium* infection in FVB mice can be used for studying the mechanisms of infectious diarrhea. Potential involvement of mast cells and their mediators presents a new paradigm for high susceptibility in *C. rodentium*-infected FVB mice.

4.4. Selected methods

Mouse infections. Specific pathogen free 10-week-old inbred FVB/NJ, SWR/J, SJL/J, C3H.HeOuJ, and C57BL/6J female mice (The Jackson Laboratory, Bar Harbor, Maine) were housed and maintained as described in Appendix 1: General methods. The numbers of mice within each experimental group are given in Table 4-1, and represent 2 independent experiments. Mice were inoculated by oral gavage with 100 µl of a bacterial culture grown overnight and concentrated 1:10 in 3% (w/v) sodium bicarbonate $NaHCO_3$ (approximately 3-5 x 10^9

CFU/mouse as determined by plate counts on MacConkey lactose agar) or with 100 µl of sterile vehicle. Every three days, fecal shedding of *C. rodentium* was determined as described in Appendix 1. On the same days feces were collected for measuring water content as a marker for diarrhea. The animals were euthanized and necropsied as described in Appendix 1 at 14 DPI, or earlier if moribund. At necropsy, spleen, MLN, liver, colon and cecum were collected, cleaned of feces (in the case of the large intestine), weighed and plated or subjected for histopathological scoring. Tissue weight was expressed as a percentage of body weight. Small pieces of distal colon were also snap-frozen for subsequent RNA isolation and qRT-PCR analysis.

Detection of humoral response in serum. Titers against *C. rodentium* were determined on serum samples by ELISA, as recommended by manufacturer (http://www.bdbiosciences.com) ELISA Immulon II plates (Thermo Labsystems, Franklin, MA) were coated with *C. rodentium* diluted 1/20 in PBS. Coated plates were washed in PBS plus 0.5% Tween 20, blocked for 1 h in 1% BSA in PBS, and washed before addition of serially diluted standards, namely mouse monoclonal purified IgG1, IgM (BD PharMingen, San Diego, CA), IgG2a (Southern Biotechnology Associates, Birmingham, AL), and standardized sera with 55 µg/ml mouse IgG2c (Bethyl Laboratories, Montgomery, TX), or unknowns. Plates were washed 3 times in PBS plus 0.5% Tween 20. Ig isotypes were detected with biotin-conjugated rabbit anti-mouse IgM, IgG1, IgG2a (BD PharMingen), or goat anti-mouse IgG2c (Southern Biotechnology), incubated with extravidin peroxidase (Sigma, St. Louis, MO) and 2,2'-azinobis-(3-ethylbenzothiazoline-6-sulfonic acid), diammonium salt (ABTS) substrate (Kirkegaard & Perry Laboratories, Gaithersburg, MD) for color development. Absorbance development at at OD_{450} was recorded by an ELISA plate reader (Dynatech MR7000, Dynatech Laboratories, Inc., Chantilly, VA) and quantity was determined against the standard curve for each plate.

Detection of water content in stool. Feces were weighed immediately after collection to define “wet weight” (WW). Following the incubation at 37ºC for 72 hours, feces were weighed to define “dry weight” (DW). The water content in stool was expressed as percentage of (WW-DW)/WW.

Histopathology. The 10% formalin-fixed and paraffin embedded tissues were processed as described in Appendix 1. H&E-stained colonic sections were scored for pathological lesions by veterinary pathologists (BHR, ABR) blinded to experimental groups. Inflammation, hyperplasia, dysplasia, edema and epithelial defects within intestinal tissue sections were graded on a scale of 0 to 4 as described in Appendix 1. The cumulative disease index was calculated as sum of all grades with 20 as a maximal possible score.

Mast cells detection. Formalin-fixed paraffin-embedded intestinal sections from 3 mice per group were stained with 0.1% toluidine blue. Mast cells appear as deep violet cells on a blue background. The positive cells in distal colon were counted in five to ten microscope fields (x200), averaged and expressed as number of cells per mm^2.

Real-time quantitative RT-PCR. Total RNA was isolated as described in Appendix 1. The qRT-PCR was performed as described in Appendix 1 and Chapter 3 with predesigned ABI probe and primer sets (see Table 3-2).

4.5 Tables and Figures

Table 4-1. Number of animals used in the experiments

Mouse strain	Uninfected	Infected
FVB/NJ	9	13[a]
SWR/J	9	15
SJL/J	9	15
C3H/HeOuJ	6	10
C57BL/6J	6	10

[a], two out of 15 FVB/NJ mice failed to become infected and have been excluded from the study.

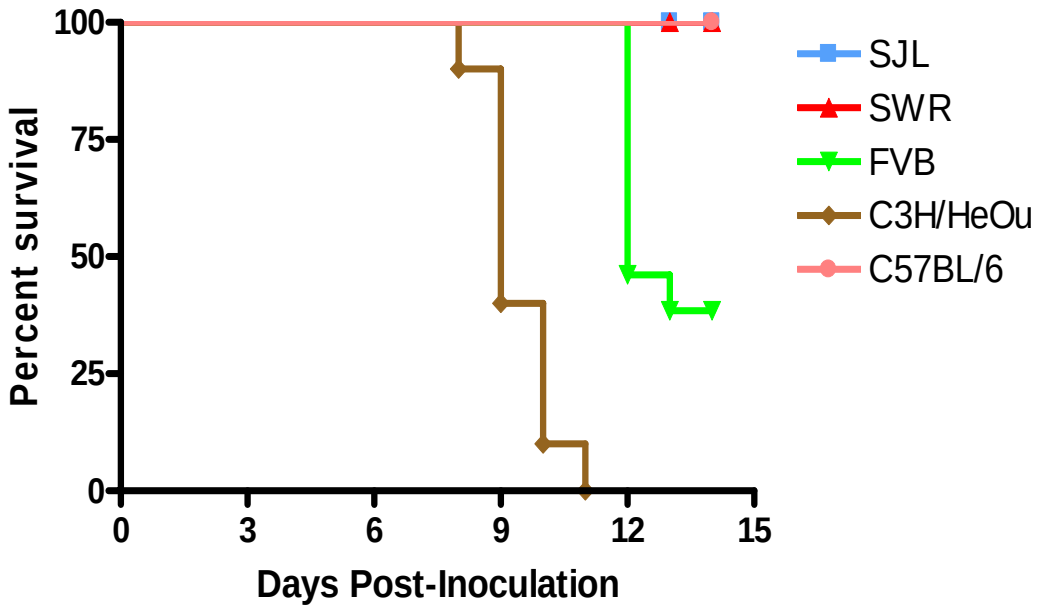

Figure 4-1. Survival of inbred mice in response to *C. rodentium* infection.
Two strains demonstrated susceptible phenotype; 100% of C3H mice died in between 8 and 11 DPI, and 61.5% FVB mice died from 12 DPI. SWR, SJL, and C57BL/6 mice were resistant and showed 100% survival in two weeks post-inoculation ($p<0.0001$ by Logrank test).

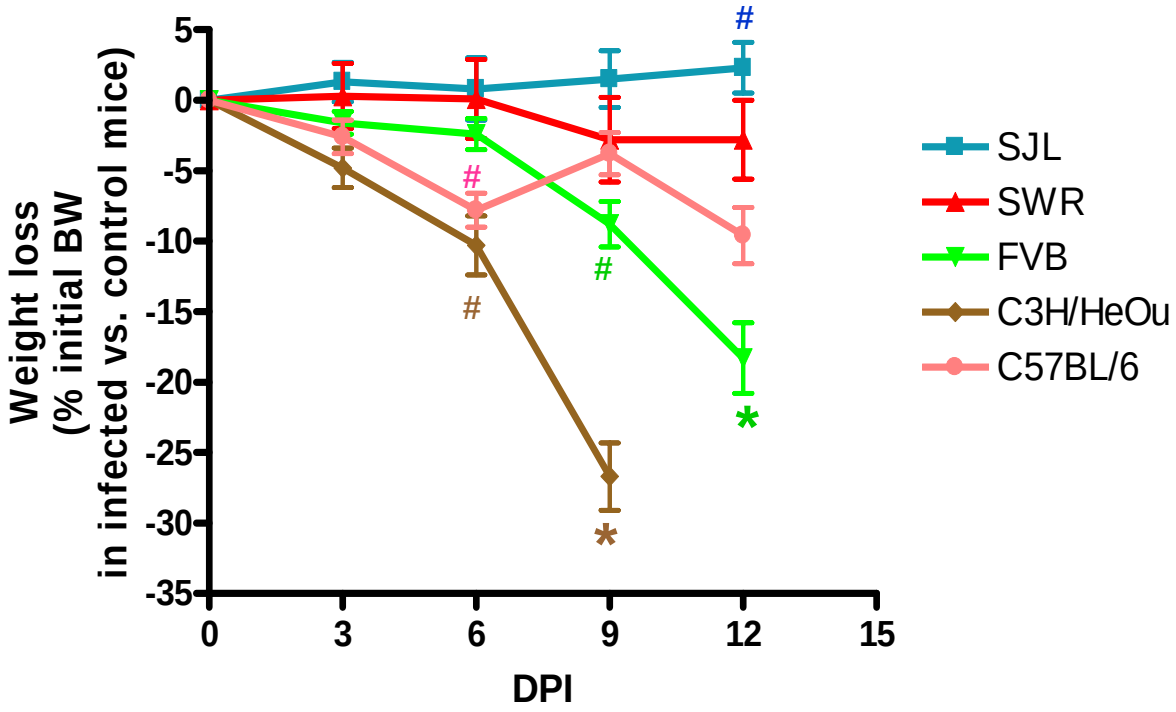

Figure 4-2. *C. rodentium* effects on body weight in inbred strains.
Severe clinical disease was observed in C3H mice that lost >25% of body weight by 9 DPI, and FVB mice that lost >15% of body weight by 12 DPI ($p<0.0001$ by two-way ANOVA). The changes in body weight in resistant SJL, SWR, and C57BL/6 mice fluctuated within +/-10% range and were not significant in Swiss mice.
The weight loss was calculated as % of initial body weight in infected mice subtracted from control mice. Data presented as mean ± SEM.
*, $p<0.01$ by Bonferroni posttest compared with the rest of the groups.
#, $p<0.05$ by Bonferroni posttest compared with one, two or three groups.

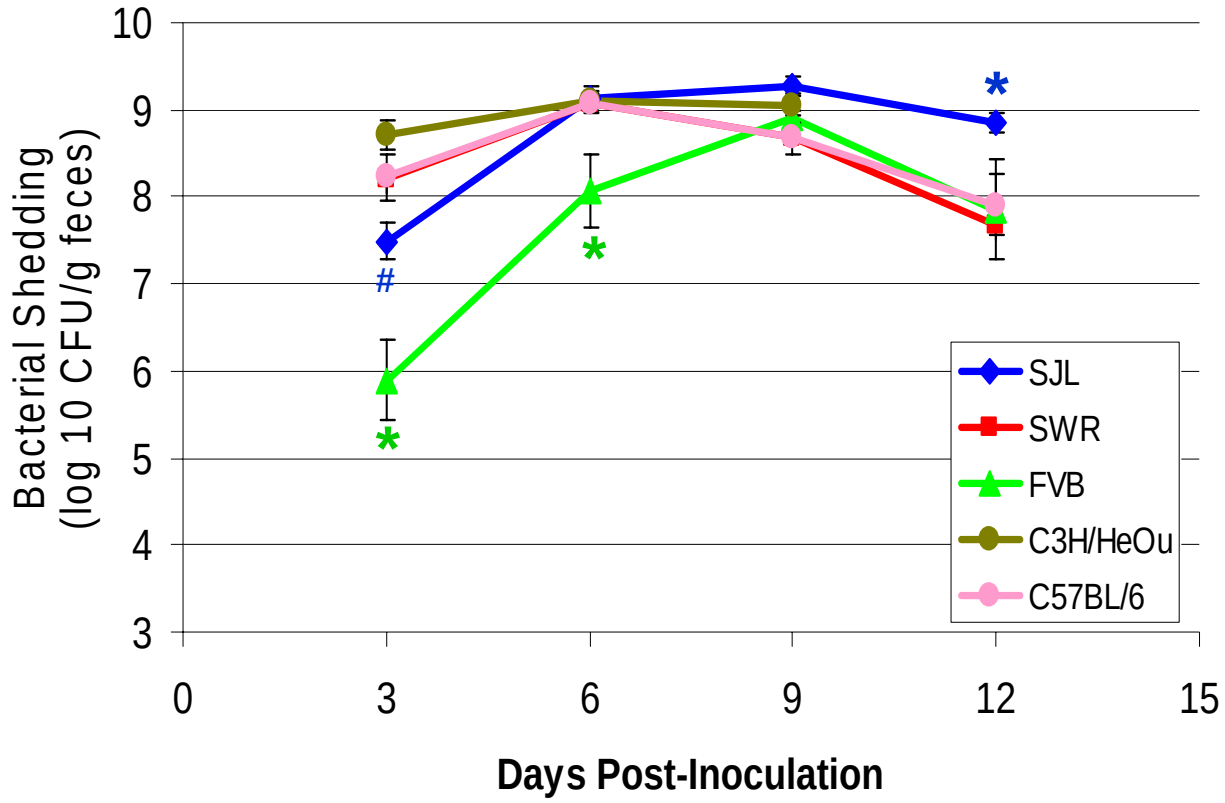

Figure 4-3. Fecal bacterial shedding in inbred mice infected with *C. rodentium*.
FVB mice, compared with other strains used in the study, demonstrated lower bacterial counts at 3 and 6 DPI ($p<0.0001$ by two-way ANOVA). SJL mice had lower bacterial load than in C3H mice at 3 DPI, but higher fecal counts compared with other groups at 12 DPI.
Fecal bacterial counts in susceptible C3H mice were not different from those in resistant SWR and C57BL/6 mice. The limit of detection was 10^3 CFU/g feces. Data was log10 transformed and presented as mean ± SEM.
*, $p<0.01$ by Bonferroni posttest compared with the rest of the groups.
#, $p<0.01$ by Bonferroni posttest compared with one, two or three groups.

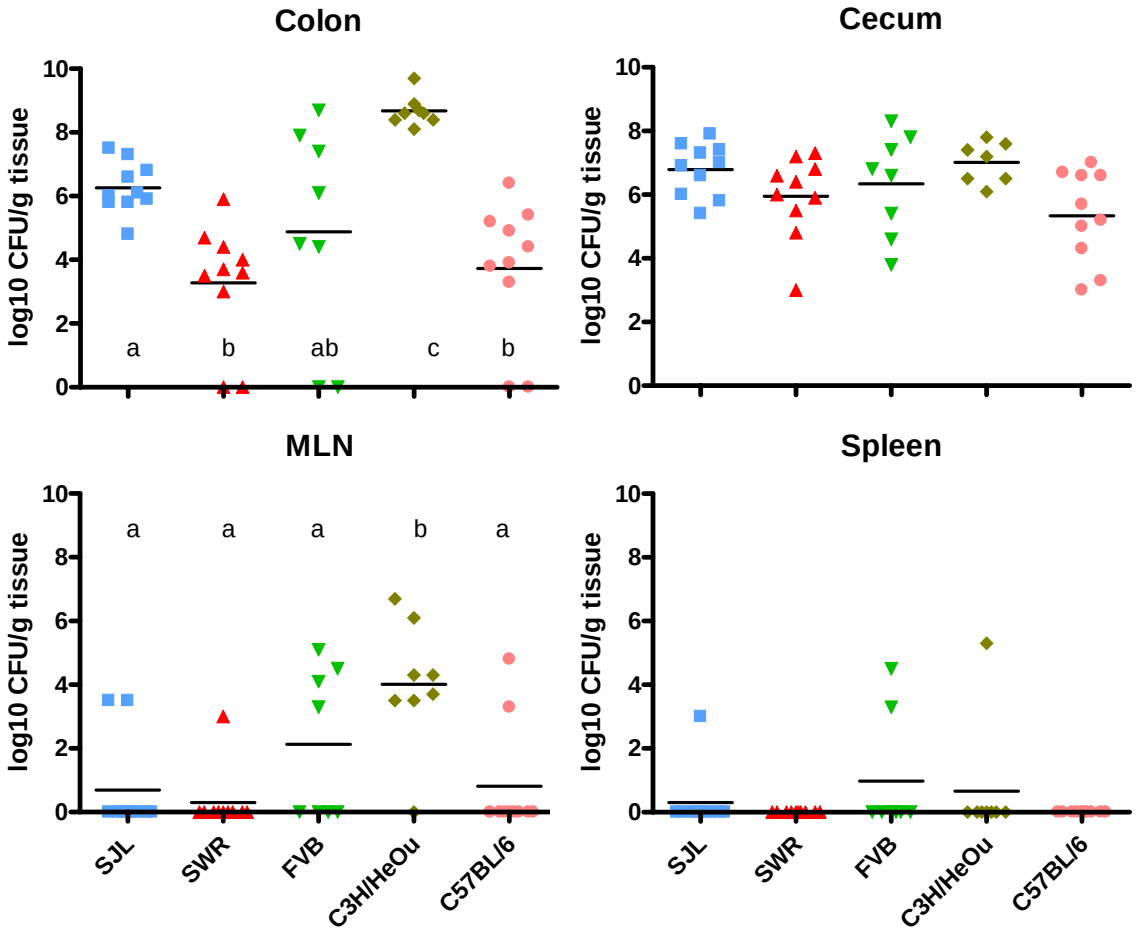

Figure 4-4. *C. rodentium* counts in tissues.
The bacterial load in colon was highest in C3H mice, intermediate in SJL and FVB mice, and lowest in SWR, and C57BL/6 mice ($p<0.0001$ by one-way ANOVA). High colonization of cecum was comparable in all the strains. C3H mice demonstrated high bacterial counts in mesenteric lymph nodes (MLN) ($p=0.0003$ by one-way ANOVA). However dissemination of *C. rodentium* to spleen was rare in all the strains. The interpretation of these results is confounded by different end points; tissue were collected at 9-10 DPI from C3H mice, at 12-14 DPI from FVB mice, and at 14 DPI from the rest of the groups.
The limit of detection was 10^3 CFU/g feces. Data was log10 transformed. Each dot represents one animal. Lines indicate mean of the group. Letters indicate significant differences as detected by post-hoc *t* test.

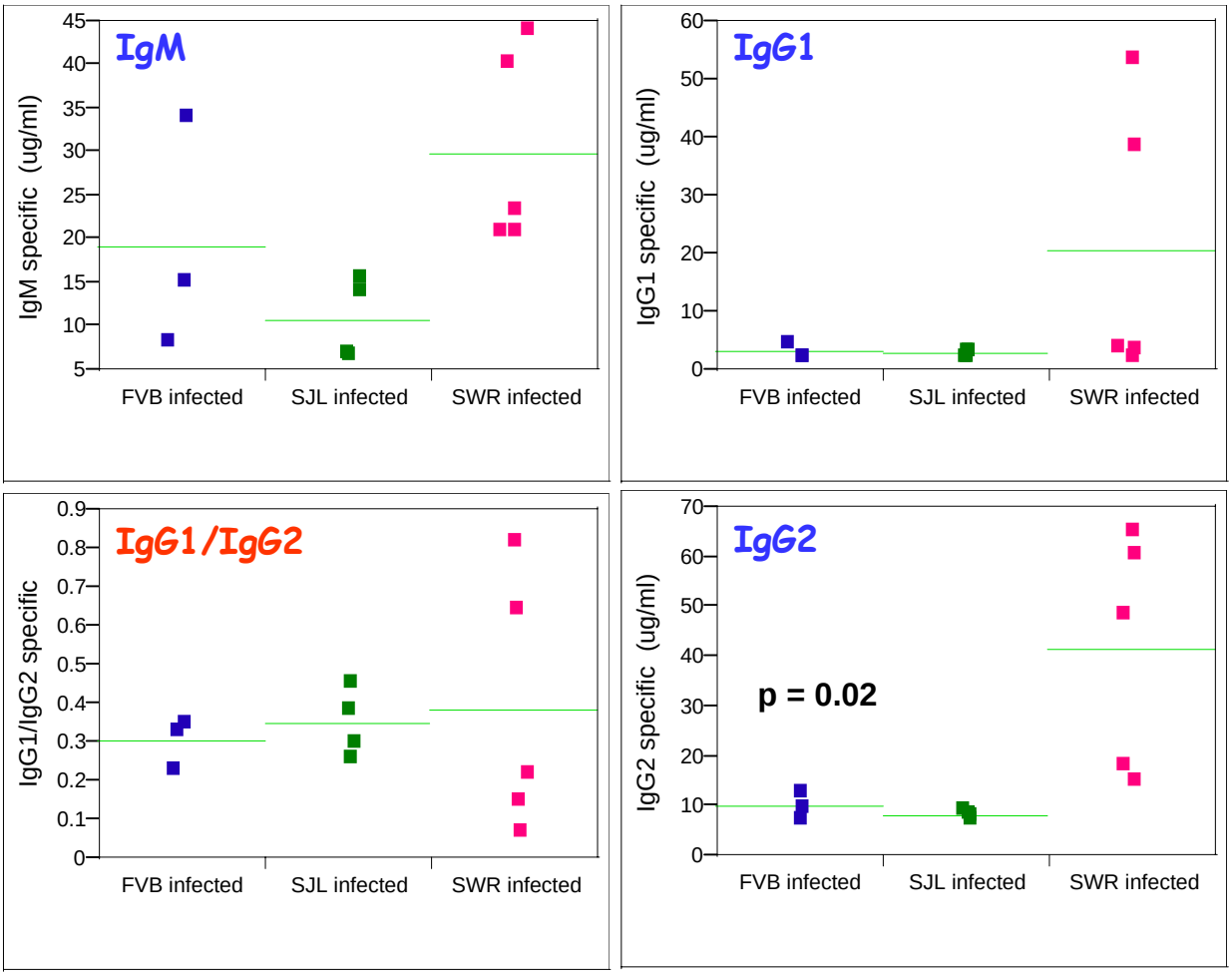

Figure 4-5. Development of humoral *C. rodentium*-specific response in Swiss mice.
C. rodentium-specific IgM titers were detected by ELISA in all inbred strains by 12 DPI but not significantly different ($p = 0.058$ by ANOVA). The levels of IgG1 and IgG2 were higher in SWR mice at 12DPI (NS and $p = 0.02$ by ANOVA, respectively). However, the IgG1 to IgG2 ratios were comparable between the groups.

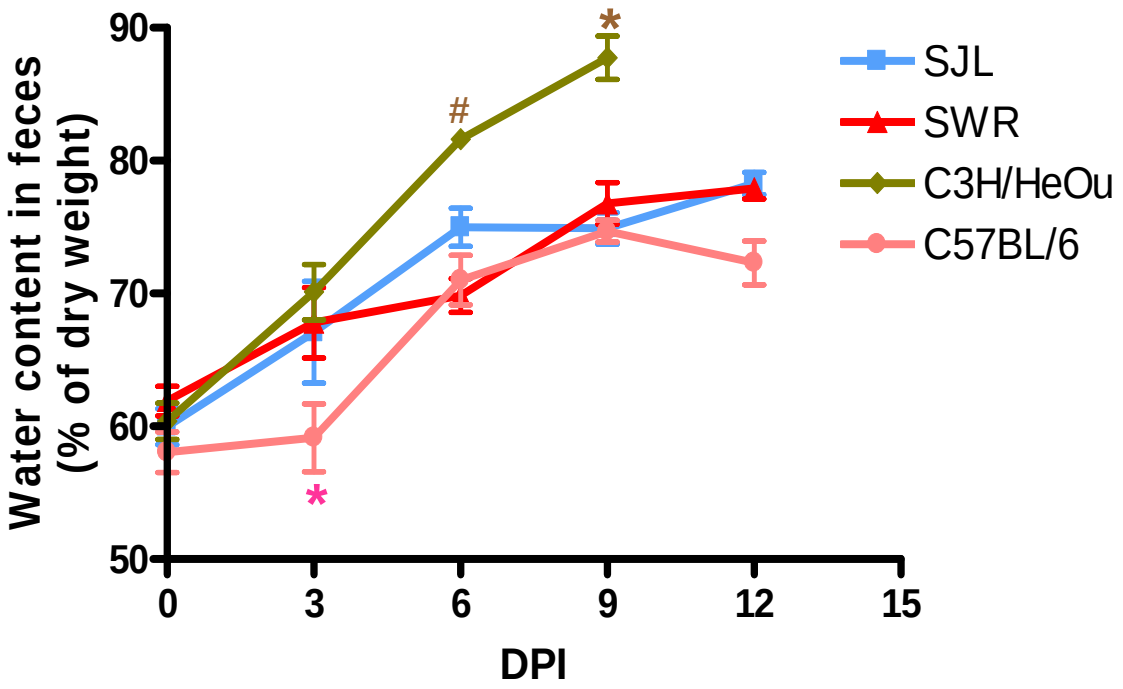

Figure 4-6. Development of diarrhea in *C. rodentium*-infected animals.
C3H mice demonstrated rapid increase in fecal water content by 9 DPI ($p<0.0001$ by two-way ANOVA). The stool water content was not analyzed in FVB mice due to lack of well-formed feces in majority of moribund animals, which indicated development of severe diarrhea in this strain.
Data presented as mean ± SEM.
*, $p<0.05$ by Bonferroni posttest compared with the rest of the groups.
#, $p<0.05$ by Bonferroni posttest compared with SJL mice.

A.

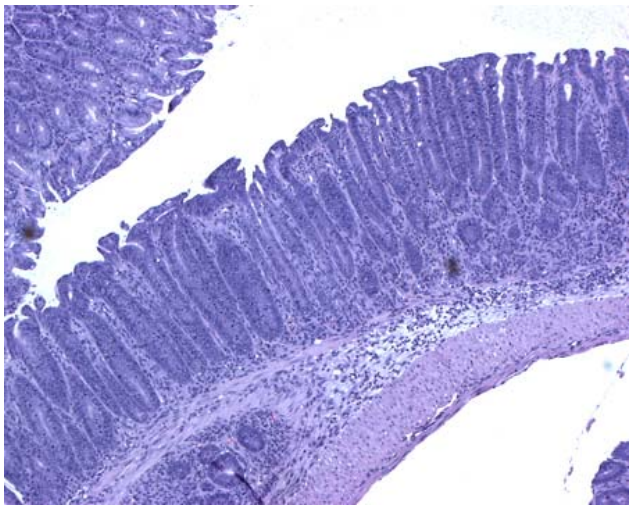

B.

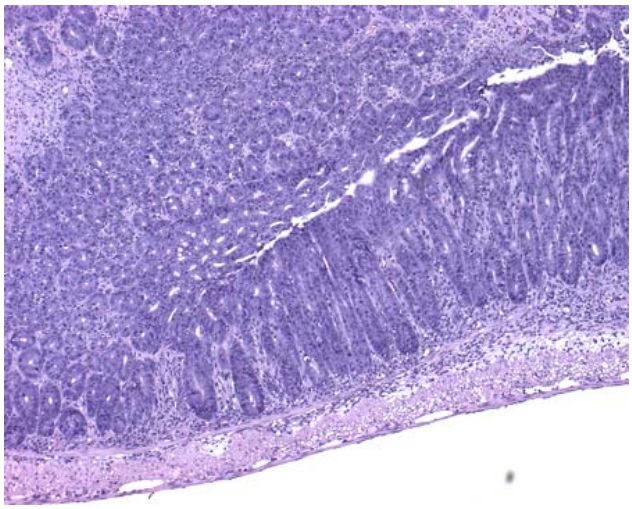

C.

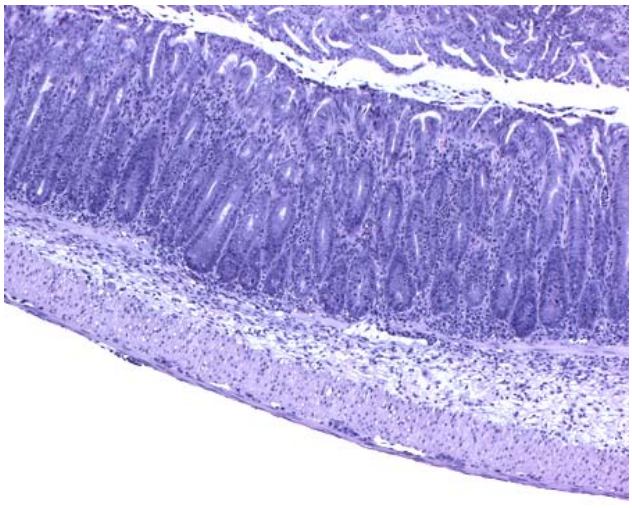

Figure 4-7. Histopathology of distal colon in *C. rodentium*-infected inbred Swiss mice. Comparable lesions were observed in FVB/NJ (**A**), SJL/J (**B**), and SWR/J (**C**) mice at 13-14 dpi. H&E staining. Original magnification x100.

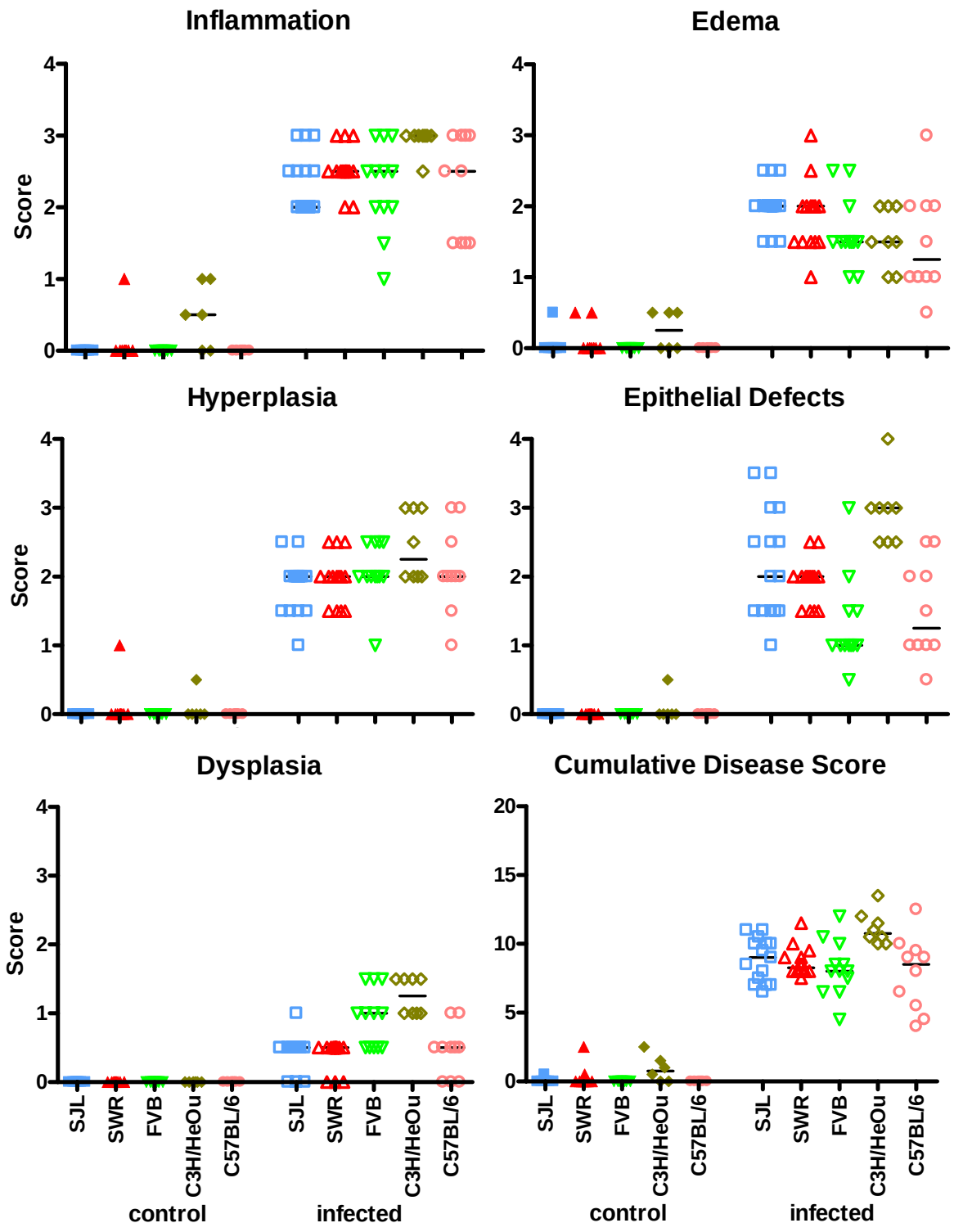

Figure 4-8. Colonic pathology in *C. rodentium*-infected inbred mice.
No significant differences in intestinal pathology were found between the groups.
Each dot represents one animal. Lines indicate group median.

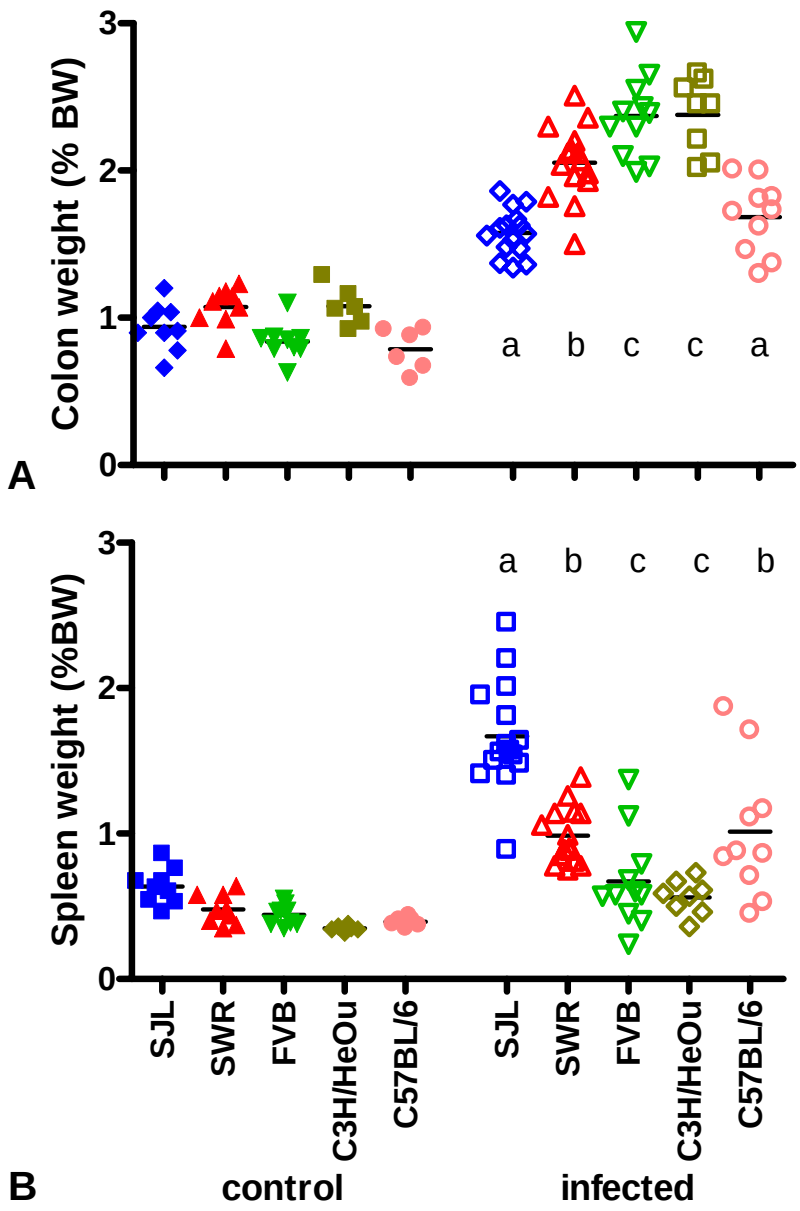

Figure 4-9. Organ weight in inbred mice infected with *C. rodentium.*

- **A.** Colon weight, as a measure of intestinal pathology, was increased in all the infected animals, but to highest extent in C3H and FVB mice ($p<0.0001$ by one-way ANOVA).
- **B.** Significant splenomegaly was observed in infected SJL mice, mild splenomegaly was found in infected SWR and C57BL/6 mice, whereas no change in spleen weight was detected in C3H and FVB mice infected with *C. rodentium* ($p<0.0001$ by one-way ANOVA).

Data was calculated as % of body weight. Each dot represents one animal. Lines indicate group means. Letters indicate significant differences as detected by post-hoc *t* test.

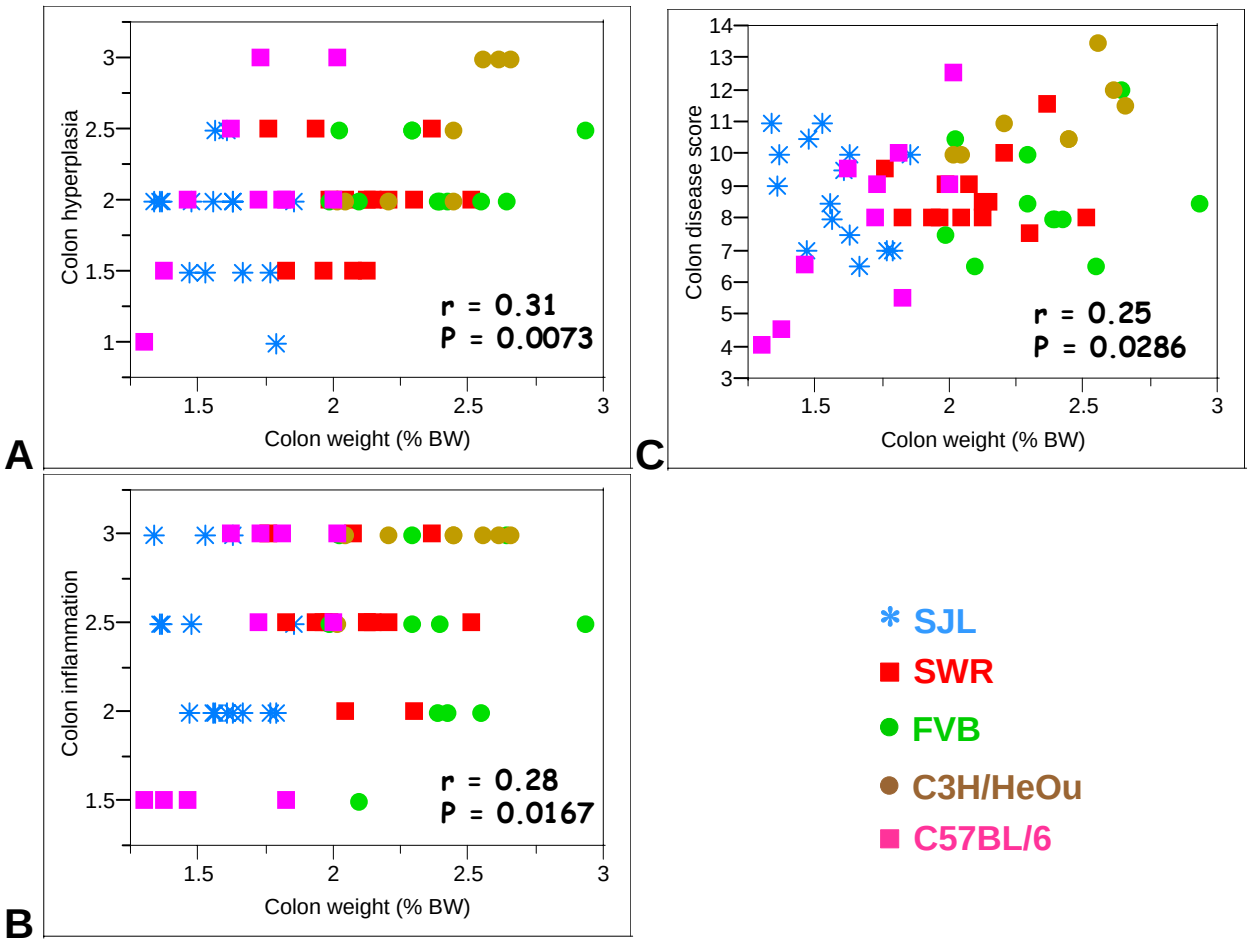

Figure 4-10. Correlation of colon lesions with colon weight in *C. rodentium*-infected inbred mice. Positive association between colon weight and hyperplasia (**A**), inflammation (**B**), and cumulative disease score (**C**) in distal colon of infected mice was found by Spearman correlation test (r and p values are given). Each dot represents one animal.

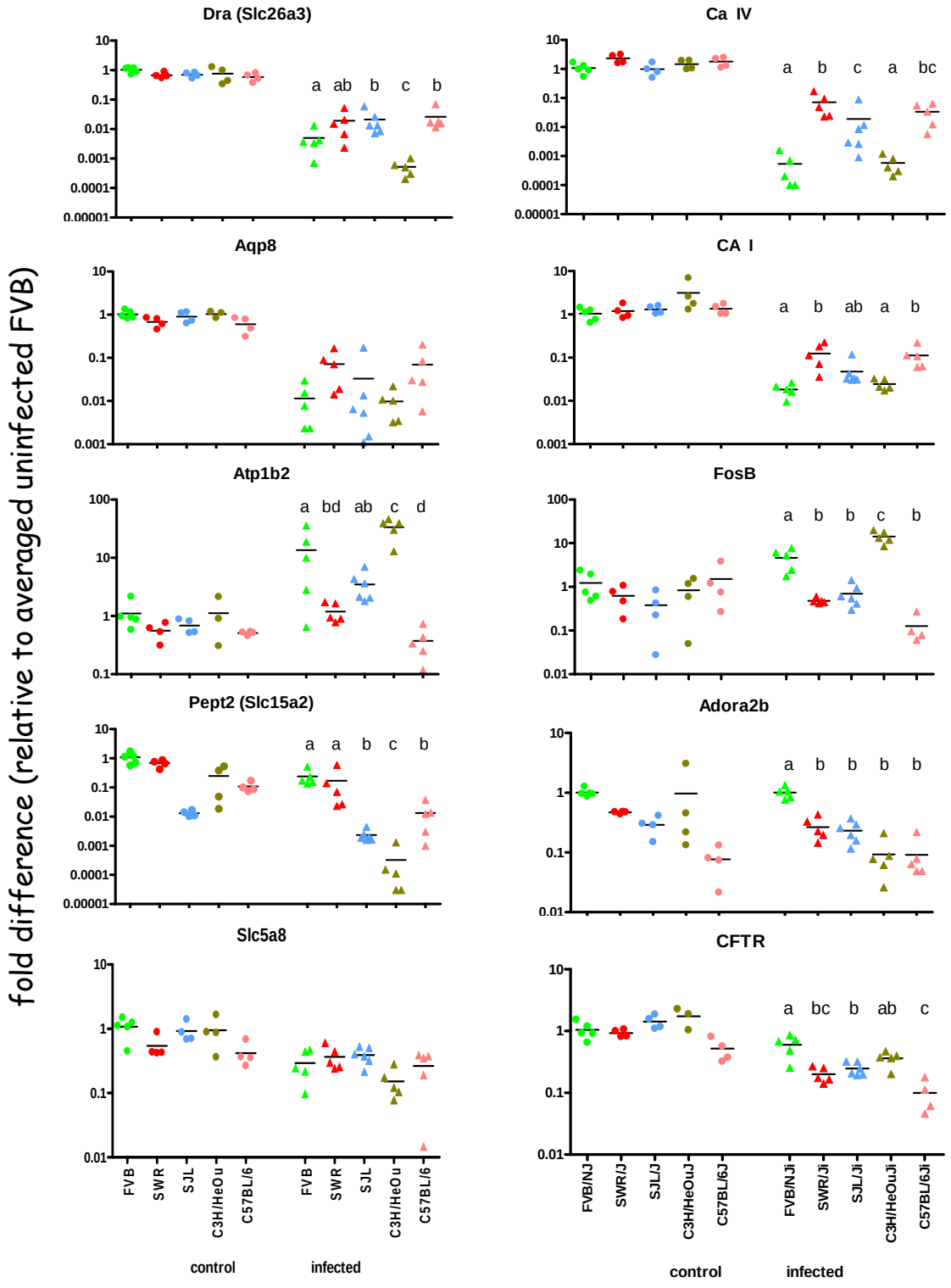

Figure 4-11. Quantitative real-time PCR (TaqMan) analysis of genes involved in intestinal ion transport that were identified by microarray analysis (Chapter 3).
The expression of genes was normalized to uninoculated FVB mice. Each dot represents one animal. Lines indicate group means. For genes with $p<0.0001$ by ANOVA, Tukey's posttest was applied (statistically significant differences are indicated by letters).

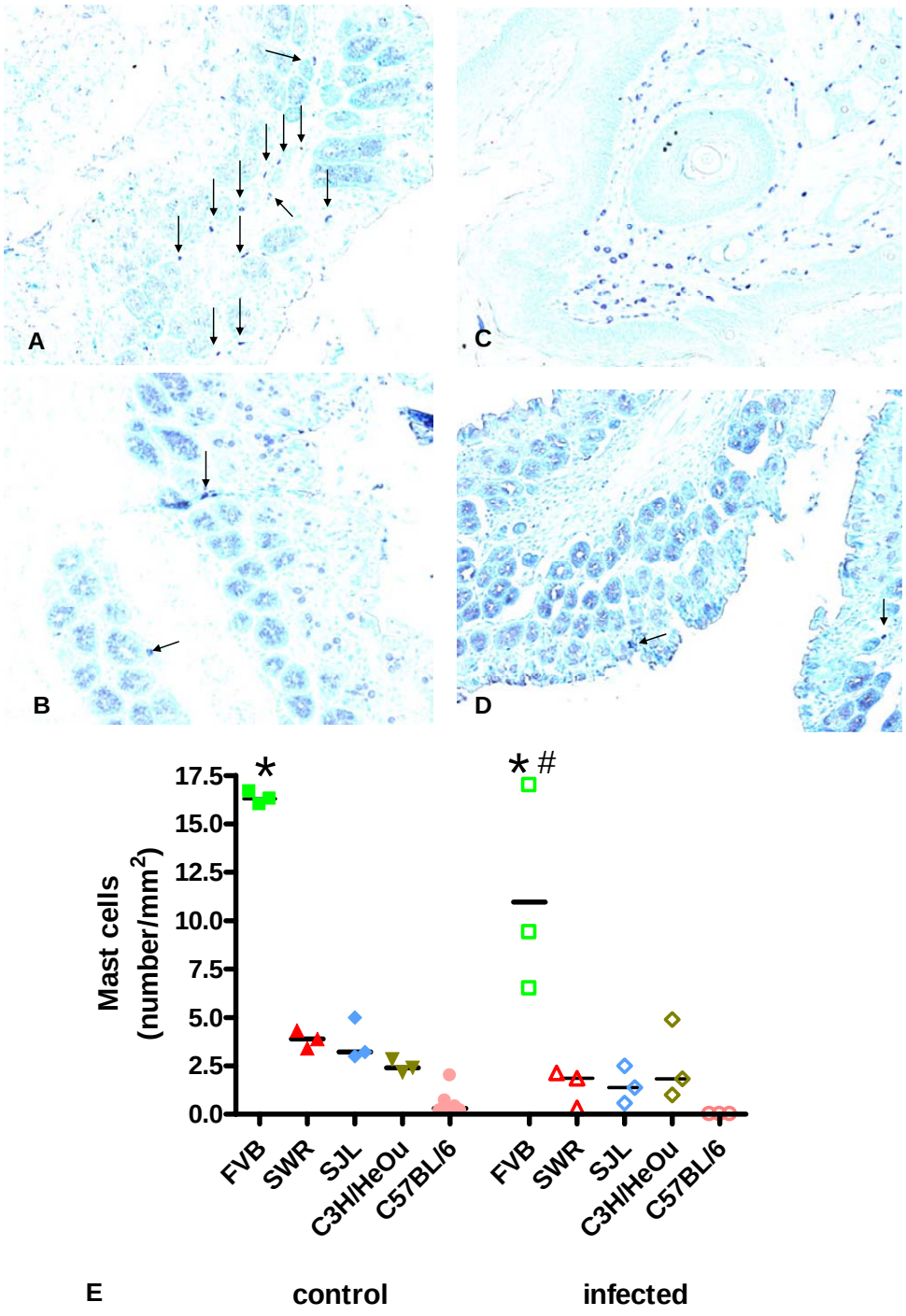

Figure 4-12. Identification of mast cells in colon tissues from *C. rodentium*-infected mice by toluidine staining. Mast cells were frequently found in colorectal area in FVB mice, but rare in other inbred strains. The images show representative areas of distal colon in uninoculated FVB (**A**), SWR (**B**), and SJL (**C, D**) mice (toluidine-positive cells are indicated by arrows). Mast cells identified in rectal epidermis are shown as positive control (C). Original magnification 200x.
The quantified levels of mast cells in each strain and condition are presented in panel E ($p<0.0001$by ANOVA). Each dot represents one animal. Lines indicate group means.
*, $p<0.001$ by post-hoc *t* test compared with the rest of the groups.
#, $p<0.01$ by post-hoc *t* test compared with uninoculated mice.

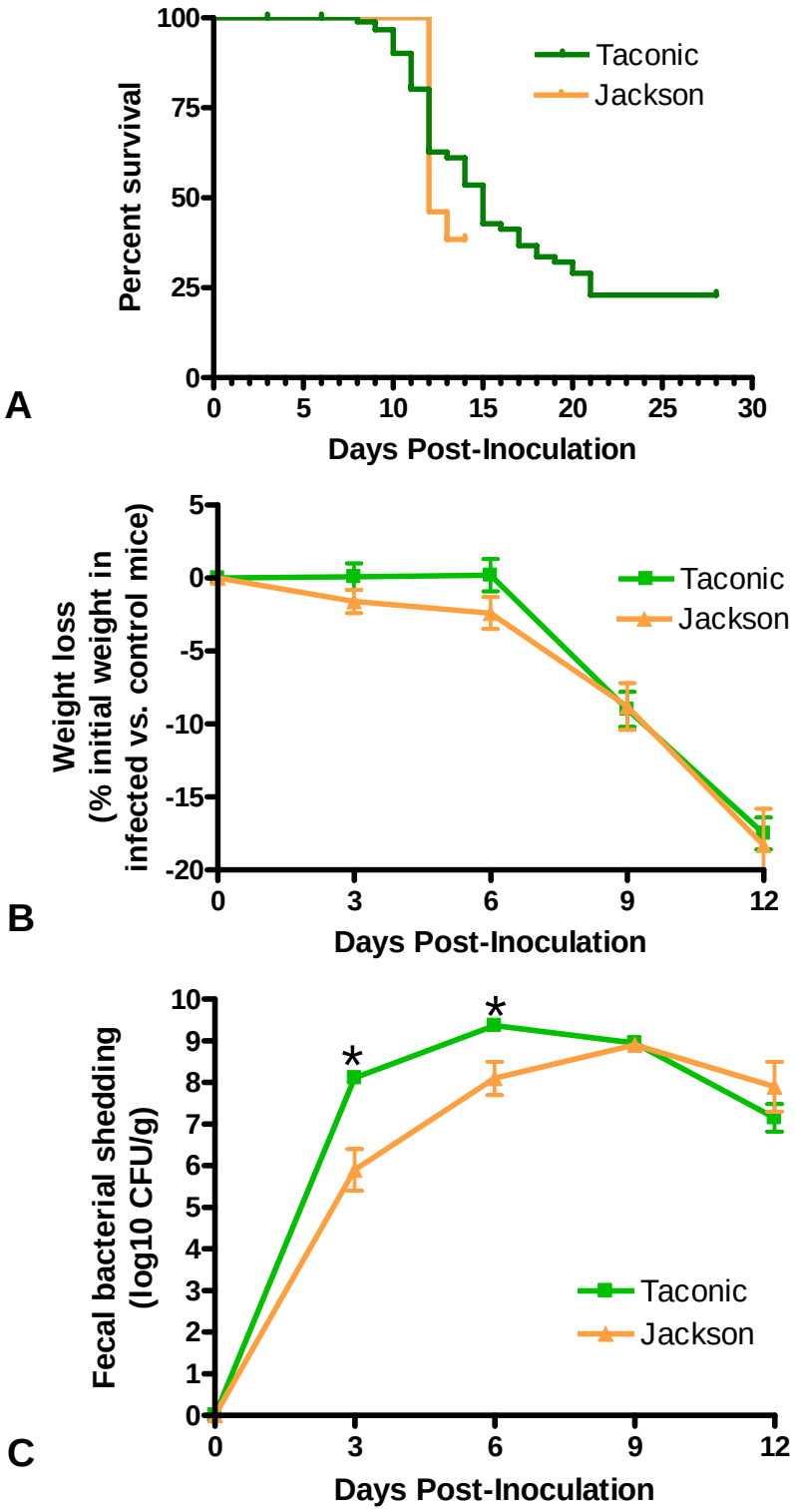

Figure 4-13. Comparison of *C. rodentium* infection in FVB mice supplied by different vendors. Mortality (**A**) and body weight loss (**B**) were comparable in FVB mice obtained from The Jackson Laboratories or from Taconic Laboratories. However, FVB/NTac demonstrated higher fecal bacterial counts at 3 and 6 DPI (**C**) (*, $p<0.0001$ by *t* test).

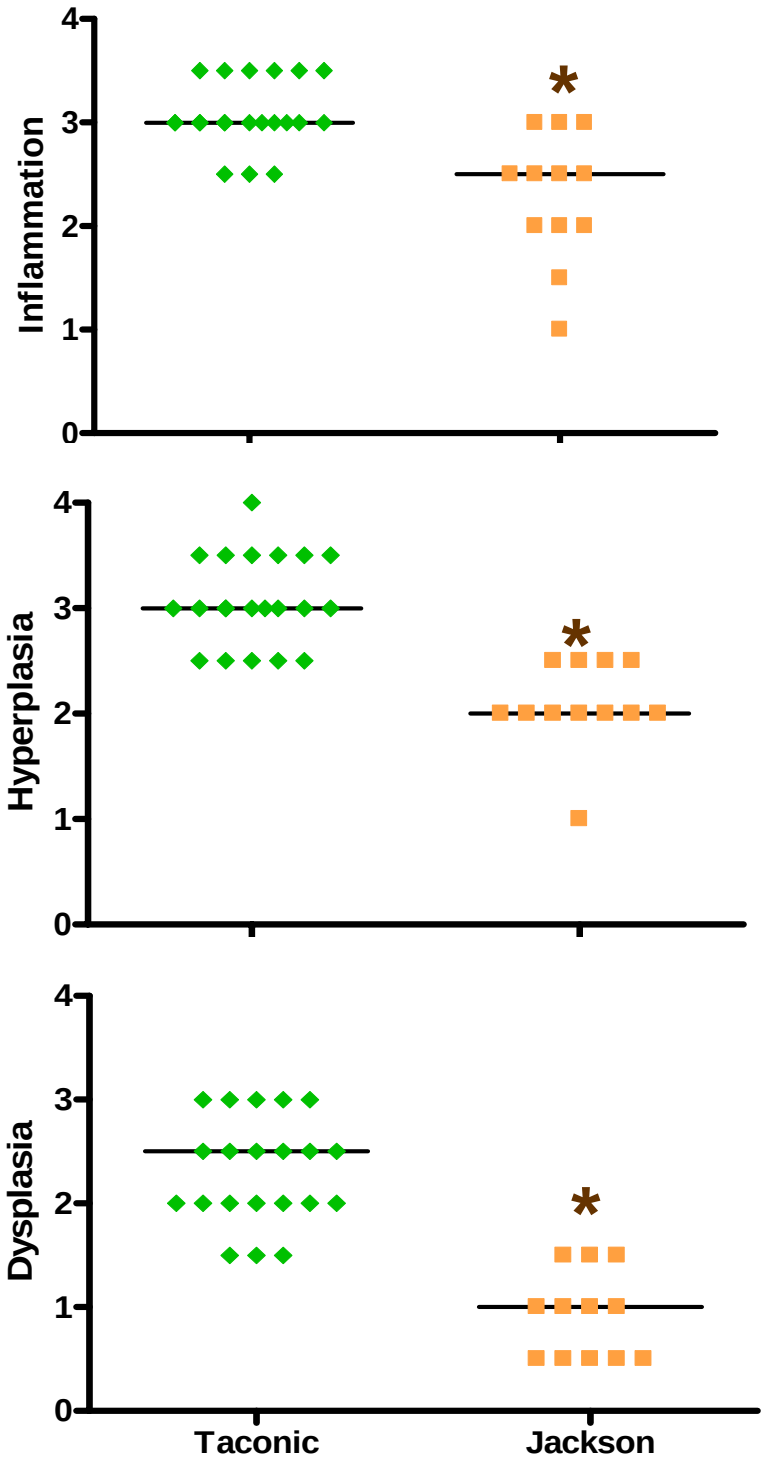

Figure 4-14. Comparison of *C. rodentium* induced-lesions in FVB mice supplied by different vendors. FVB/NTac developed more severe lesions in response to *C. rodentium* compared with FVB/NJ at 12 DPI ($p<0.0005$ by Mann-Whitney test). Data from the FVB/NTac mice presented in Chapter 2 was used for comparison. Lines indicate group median.

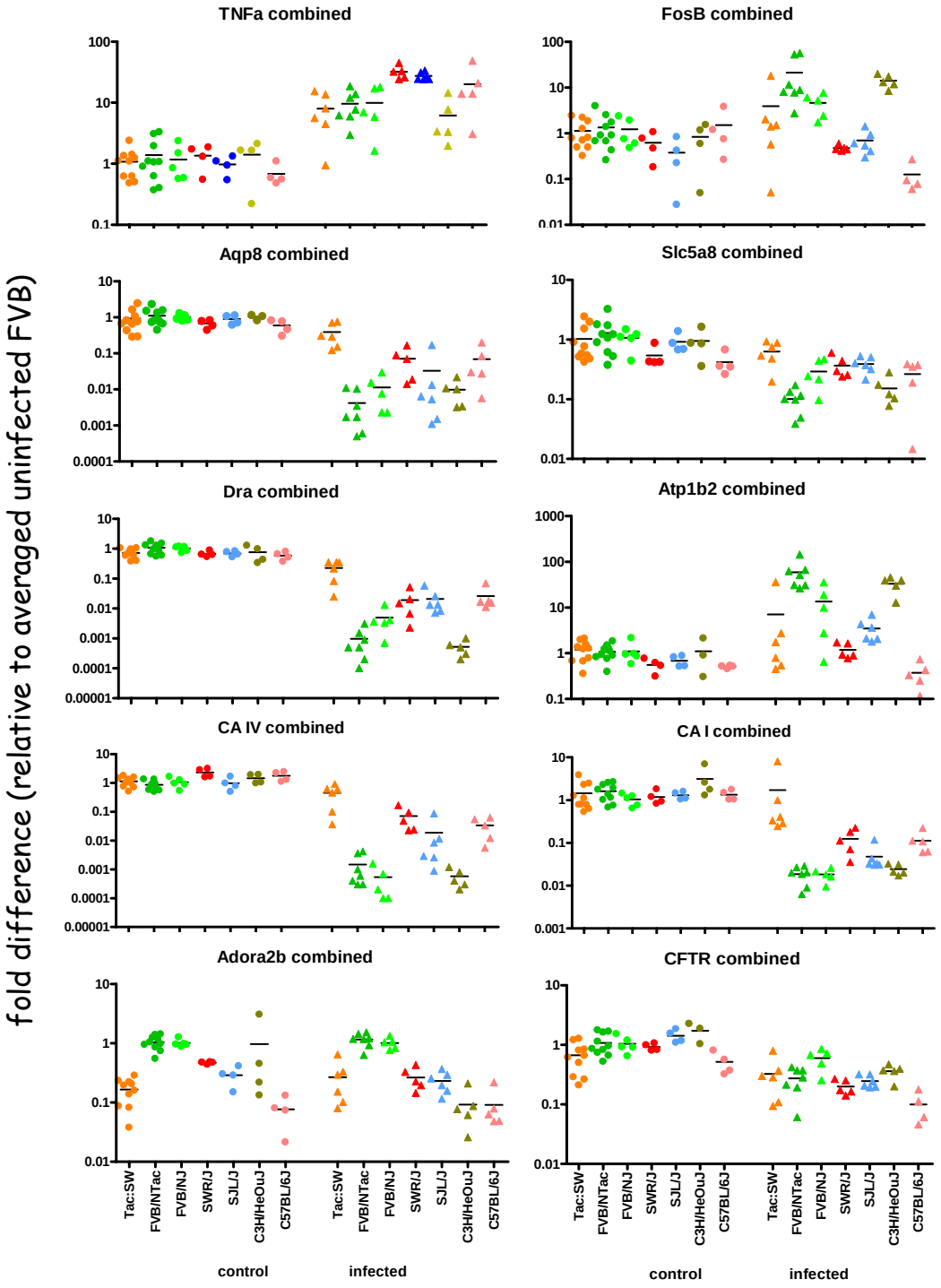

Figure 4 Supplemental 1. Combined quantitative real-time PCR (TaqMan) analysis of gene expression from microarray study (Chapter 3) and Swiss study (Chapter 4). Tissues were collected at 9 DPI for Tac:SW, FVB/NTac, and C3H/HeOuJ mice, at 12-14 DPI for FVB/NJ mice, and at 14 DPI for SWR/J, SJL/J, and C57BL/6J mice. The expression of genes was normalized to uninoculated FVB mice. Each dot represents one animal. Lines indicate group means. Expression of *Tnf-α* was used as a control for temporal changes.

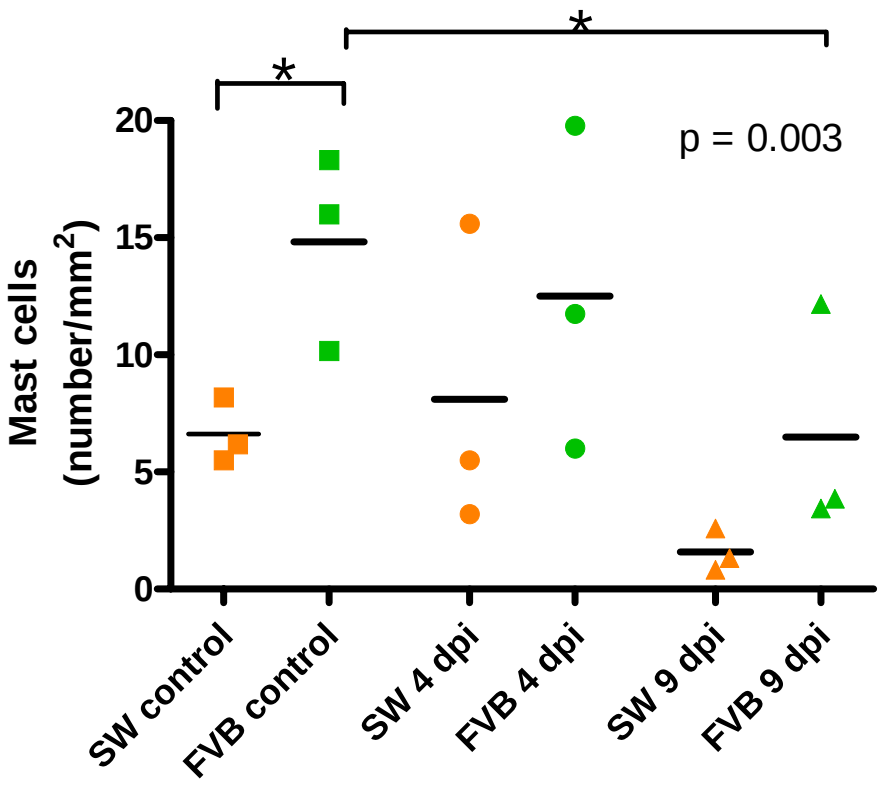

Figure 4 Supplemental 2. Identification of mast cells by toluidine staining in colon tissues from *C. rodentium*-infected Swiss Webster and FVB/NTac mice (from Chapter 3).
The number of mast cells in FVB/NTac was higher than in Swiss Webster mice ($p<0.005$ by ANOVA) and comparable to the levels in FVB/NJ mice (Figure 4-11).
Each dot represents one animal. Lines indicate group means.
*, $p<0.001$ by post-hoc *t* test compared with the rest of the groups.

Chapter 5: Conclusions and future work

C. rodentium is the only known murine pathogen causing attaching and effacing (A/E) lesions. Because human A/E pathogens do not readily infect laboratory mice [Frankel et al., 1996; Klapproth et al., 2005; Mundy et al., 2006], *C. rodentium* serves as the only murine model for human infections with pathogenic *E. coli*, EPEC and EHEC. Both pathogens are among the most important bacterial causes of acute diarrheal illness (ADI) worldwide. EPEC infection leads to the deaths of hundreds of thousands of children each year in developing countries, while EHEC, the causal agent of hemolytic uremic syndrome, is a growing health threat in North America and Europe, causing sporadic diarrheal outbreaks and deaths. For many years, studies elucidating the pathogenesis of *C. rodentium* have focused on signal transduction, host immune responses, and intestinal proliferation, neglecting the potential of this microorganism to affect intestinal ion homeostasis. Studies presented in this thesis strongly suggest that *C. rodentium* infection is able to disrupt ion transport in the distal colon leading to development of severe diarrhea, dehydration and fatal disease in affected animals. The discovery of susceptible and resistant lines of mice with very similar genetic backgrounds facilitated identification of host factors responsible for the outcome of the infection, thereby shedding important insight into the pathogenesis of *C. rodentium*. While the work described here was in the final stages, a few laboratories reported *C. rodentium*-induced disruption of tight junctions, mislocalization of aquaporins and interaction of bacterial effectors with host regulators of ion channels [Guttman et al., 2006a; Guttman et al., 2006b; Guttman et al., 2007; Ma et al., 2006; Simpson et al., 2006]. This indicates growing interest of researchers in diarrhea-inducing effects of *C. rodentium*.

In order to explore the role of the host factors in susceptibility to *C. rodentium* infection, the infection was examined in FVB mice, whose response to the pathogen was never characterized before. Inbred FVB mice belong to the same genealogic tree as Swiss Webster (SW) mice, well known for their resistance to *C .rodentium*. Investigating the infection in mice with similar genetic background will help to avoid “genetic polymorphism” bias in interpreting results. Our data show that adult FVB mice develop profound mortality and colitis when infected with *C. rodentium*, making it the second inbred strain (in addition to C3H mice) with extreme

susceptible to this pathogen. These results are especially important because FVB mice are widely used to create transgenic animals [Barthold, 2002]. Several studies characterizing this model suggested hypovolemia as the cause of death. We attempted to achieve amelioration of the disease by different methods (see Appendixes), but only preventive fluid therapy was successful. This is the first report demonstrating the protective effect of fluid therapy intervention in this animal model of diarrhea and intestinal ion imbalance. It remains to be determined if this approach will effectively prevent fatal disease in other *C. rodentium*-susceptible mice, such as young, immunodeficient animals and substrains of C3H mice.

To elucidate the genetic basis for high mortality of *C. rodentium*-infected FVB mice compared with cognate outbred animals, a microarray approach using full-genome Affymetrix DNA chips was applied. It has to be mentioned that although global genomic and proteomic responses of the host to EPEC were previously reported [de Grado et al., 2001; Hardwidge et al., 2004; Zyrek et al., 2006], these studies were performed in cell lines, such as HeLa, Caco-2 and T84 cells, and cannot reproduce the full spectrum of the disease. Therefore, our study is the first report of global gene expression analysis of host response to infection with an A/E pathogen *in vivo*. This led to a discovery of important potential candidates for susceptibility to *C. rodentium*-induced mortality. Strikingly, genes significantly different between the susceptible and resistant mice were more enriched for transporter activity than for immune response. Predicted by microarray analysis, misbalanced water and ion transport in infected colon of FVB mice was confirmed by serum electrolyte levels. This study extended our knowledge of *C. rodentium* pathogenesis and suggested that infected FVB mice can be used for modeling fatal diarrhea.

Future work should include validation of microarray results at the transcriptional level. Protein expression encoded by target genes should be verified by Western blotting and by immunohistochemical analysis. In addition, *ex vivo* techniques, i.e. Ussing chambers, and measuring electrolyte contents in stool, will be helpful in elucidating the relative impact of *C. rodentium* infection on certain intestinal ion transport pathways. For example, increased chloride content in stool may indicate that impairment of chloride absorption exceeds sodium transport disturbances, and vice versa.

Notably, many mice with ion transporter deficiencies, such as *NHE2*$^{-/-}$, *NHE3*$^{-/-}$, *cHKA*$^{-/-}$, *Aqp4*$^{-/-}$ and *Aqp8*$^{-/-}$ mice [Bachmann et al., 2004; Meneton et al., 1998; Schultheis et al., 1998a;

Schultheis et al., 1998b; Wang et al., 2000; Yang et al., 2005], develop minimal if any diarrhea and no serum electrolyte abnormalities, suggesting the existence of compensatory mechanisms when only a single gene is deleted. In that regard, *C. rodentium*-induced cumulative changes in intestinal ion transporters and their regulators may represent a better model for studying pathogenesis of diarrhea and development of new remedies for this life-threatening condition. Nevertheless, ion transporter-deficient mice on the resistant C57BL/6 background can be used for biological validation of genes identified by expression profiling. For example, it can be determined if *C. rodentium* infection in these animals will result in greater susceptibility to disease. In addition, inhibitors of different targets, i.e. carbonic anhydrases and ion transporters, can be applied in resistant mice in order to increase their susceptibility. Moreover, a number of genes identified by microarray analysis are known to be regulated during postnatal development. In light of the high susceptibility of infants and young mice to infection-induced diarrhea, exploring the regulation of these genes in development may lead to the identification of new therapies for this fatal disease.

The discovery of genes potentially responsible for mortality in infected animals may also facilitate research on molecular pathogenic determinants of *C. rodentium* and other A/E bacteria. First, similar changes in gene expression need to be confirmed in primary intestinal cells or cell lines used in gastrointestinal *in vitro* studies upon encounter with the pathogen. Then, infecting the cells with a panel of bacterial mutants may be used to identify pathogen effectors mediating diarrheal responses in host. Such studies will also be helpful to find changes in signal transduction and protein expression that could be involved in severe diarrheal response but were not captured by our global gene expression analysis.

The effects of *C. rodentium* on additional inbred strains from Swiss genealogical tree were investigated. SWR and SJL strains, widely used in biomedical research, survived through *C. rodentium* infection and developed minimal if any clinical signs, demonstrating their resistance to the disease. Because SWR mice show high degree of relatedness to FVB mice [Taketo et al., 1991], they may serve as a good control strain in future studies exploring host susceptibility to *C. rodentium*.

Notably, our data demonstrated that C3H mice, the only other inbred strain highly susceptible to *C. rodentium*, develop remarkable diarrhea. Furthermore, using a panel of genes

identified by microarray analysis as contributing to susceptibility, we showed that expression changes in C3H mice were comparable to FVB mice. These results indicate that disturbances in intestinal ion transport contribute to the development of fatal diarrhea in both susceptible strains, FVB and C3H mice, and suggest the existence of common pathogenic mechanisms. These observations are in contrast to the hypothesis that disseminated infection causes mortality in *C. rodentium*-infected C3H mice [Vallance et al., 2003]. Future work is necessary to validate our theory. Treatment of C3H mice with fluid therapy may clarify the role of fluid and electrolyte homeostasis in susceptibility of that strain to *C. rodentium* infection.

Strikingly, susceptible FVB mice demonstrated unique responses to *C. rodentium* as well. High level of expression of *Adora2b*, the adenosine receptor in cells, was found in FVB mice but not in the rest of inbred and outbred mice tested in this thesis. Because adenosine is one of the mast cell mediators and because mastocytosis is a known factor implicated in inflammatory or allergen-associated diarrhea, we explored the possibility of mast cells association with the susceptibility to *C. rodentium* infection. We found remarkably higher number of mast cells in colorectal areas of FVB mice only, indicating that at least some aspects of *C. rodentium*-induced diarrhea can be different between susceptible C3H and FVB mice. This discovery opens a new direction in studying mechanisms of susceptibility of FVB mice to *C. rodentium*. Further characterization of this pathway should include evaluation the role of IgE, histamine and serotonin in infected FVB mice. Depletion of mast cells with neutralizing antibodies prior to infection will help to shed a light on the role of this immune compartment in fatal infectious diarrhea.

In a summary, ADI, which is a major problem worldwide today, is not well studied due to ethical issues of conducting research in humans and lack of appropriate small animal models. Although *C. rodentium* has been useful for studying hyperplasia, colitis, and host immune response for many years, alterations in transport have been overlooked or underappreciated. The expression profile analysis, serum electrolyte results, and fluid therapy intervention demonstrate the utility of *C. rodentium* infection in FVB mice as a good model for ADI. This work adds FVB mice to the short list of known susceptible inbred strains, but also presents a new paradigm for susceptibility to fatal infectious diarrhea.

Appendix 1: General Methods

Media, bacterial strains, and growth conditions. Lennox L broth (LB) and LB agar (Difco Laboratories, Detroit, Michigan) were used for routine cultivation of bacteria. MacConkey lactose agar (Difco) supplemented with 40 μg/ml kanamycin was used for bacterial detection in feces and tissues. Kanamycin resistant *C. rodentium* strain DBS120 (pCRP1::Tn*5*) [Schauer and Falkow, 1993b], was used for infections.

Mouse infections. Specific pathogen free mice obtained from Taconic Laboratories (Germantown, N.Y), The Jackson Laboratory (Bar Harbor, Maine) or bred within MIT animal facilities. Animals were housed in polycarbonate microisolator cages within a facility approved by the Association for Assessment and Accreditation of Laboratory Animal Care. Animals were housed in a barrier facility and were viral antibody-free for 11 murine viruses and negative for enteric *Helicobacter* spp., *Salmonella* spp., and *Citrobacter rodentium*, as well as endoparasites and ectoparasites. The animals were maintained on pelleted rodent diet (LabDiet, Purina Mills, Inc., Richmond, Indiana) and water *ad libitum*. All experiments were approved by the MIT Animal Care and Use Committee. Mice were inoculated by oral gavage with 100 μl of a bacterial culture grown overnight and concentrated 1:10 in LB broth or 3% (w/v) sodium bicarbonate $NaHCO_3$ (approximately 3-5 x 10^9 CFU/mouse as determined by plate counts on MacConkey lactose agar). The control mice were inoculated with 100 μl of sterile vehicle. Mice were weighed prior to infection and body weight changes were calculated as a percent of initial body weight. Mice were checked daily for morbidity or signs of C. rodentium infections, such as coat ruffling, diarrhea, hunched posture, reluctance to move, and recumbancy. Animals with these signs were euthanized and necropsied prior to end-time point. At designated time points, fecal shedding of *C. rodentium* was determined by plating serial dilutions of feces from individual animals on MacConkey lactose agar supplemented with kanamycin. The lower limit of detection was 1 CFU/mg of feces.

Necropsy and histopathology. Animals were euthanized with CO_2 at different time points or when moribund. At necropsy, the entire colon and cecum of each mouse was collected aseptically and cleared of feces. The most distal 5 mm of the descending colon and the cecum were removed, homogenized in PBS and used for culturing bacteria by plating serial dilutions as described above. The rest of the tissues were snap-frozen in liquid nitrogen or fixed in neutral-buffered formalin for 24-48 hours, processed routinely, paraffin embedded, sectioned at 5 μm, and stained with hematoxylin and eosin (H&E). Frozen tissues were used for immunofluorescent staining or for DNA/RNA isolations as described below. H&E-stained colonic sections were scored for pathological lesions by a veterinary pathologist blinded to experimental groups. The lesions were graded on a scale of 0 to 4 with ascending severity as previously described [Erdman et al., 2005; Luperchio et al., 2000], where 0 corresponded to none, 1 to minimal, 2 to mild, 3 to moderate, and 4 to severe. In some studies, the cumulative disease index was calculated. The detailed grading system is provided in Appendix 1 supplemental materials.

Real-time quantitative RT-PCR. Total RNA was prepared from frozen distal colon using Trizol reagent according to the recommendations of the manufacturer (Invitrogen, Carlsbad, CA). Five micrograms of total RNA were used to generate cDNA using SuperScriptII RT (Invitrogen) as recommended by manufacturer. One hundred ng of resultant cDNA was amplified in a 25 μl reaction volume with Applied Biosystems predesigned primers and probes (TaqMan Gene Expression Assays) in an ABI Prism Sequence Detection System 7700 (Applied Biosystem, Branchburg, New Jersey, USA) using standard TaqMan protocols. Transcript levels were normalized to the endogenous control glyceraldehyde-3-phosphate dehydrogenase (GAPDH), and expressed as fold change relative to averaged uninoculated FVB group, which were set at 1, using the Comparative Ct method [PE Applied Biosystems, User Bulletin no. 2]. Each reaction was carried out in duplicates.

Statistics. All data are presented as mean values $\pm$ the standard error of mean (SEM) unless otherwise indicated. Statistical analyses were performed with either GraphPad PRISM version 4.0 (GraphPad Software, Inc., San Diego, CA) or JMP 5.0.1 software (SAS Institute Inc., Cary, NC). The survival Kaplan-Meier curves were analyzed by logrank test and χ^2 analysis to determine median survival time. When two groups were compared, *t* test and Mann Whitney U

test were applied for parametric and nonparametric data, respectively. For more than 3 groups, statistical differences were determined by using nonparametric Kruskal-Wallis test followed by Dunn's Multiple Comparison Test or with one-way ANOVA followed by Student's *t*-test or Tukey's Multiple Comparison Test. In some cases, differences were evaluated using two-way ANOVA test (for mouse group and time post-inoculation) followed by Bonferroni post-tests. Whenever Bartlett's test showed unequal variances, analysis of gene expression was performed on transformed data. A p value of < 0.05 was regarded as statistically significant.

A1. Supplemental protocols - Lower bowel lesion scoring criteria

Inflammation

0: Normal
1: Multifocal aggregates of submucosal leukocytes
2: Diffuse submucosal inflammatory infiltrates & edema
3: Extension of inflammation into mucosa and/or muscularis; prominent lymphoid follicles
4: Transmural inflammation

Hyperplasia

0: Normal
1: ~1.5 X normal
2: ~2 X; +/- mitotic figures 1/3 way up to surface
3: ~3 X; +/- mitotic figures 1/2 way up to surface
4: ~4X+; +/- mitotic figures >1/2 way up to surface

Dysplasia/Neoplasia

0: Normal
1: Aberrant crypt foci, dysplasia characterized by epithelial cell pleomorphism, plump & attenuated forms, gland malformation with splitting, branching, and infolding
2: Low-grade gastrointestinal intraepithelial neoplasia (GIN): polyploid hyperplasia/dysplasia, moderate dysplasia characterized by pleomorphism, early cellular & nuclear atypia, piling & infolding, occasional cystic dilation, bulging towards muscularis mucosae & projection into lumen, loss of normal glandular, mucous, or goblet cells
3: Adenomatous and/or sessile hyperplasia/dysplasia; high-grade GIN or carcinoma *in situ*, marked dysplasia confined to mucosa, features as above but greater severity, frequent & sometimes bizarre mitoses
3.5: Intramucosal carcinoma (extension of severely dysplastic regions into muscularis mucosae)
4: Invasive carcinoma: Submucosal invasion (differentiate from herniation) or any demonstrated invasion into blood or lymphatic vessels, regional nodes, or other metastasis.

Crypt atrophy/fibrosis

0: Normal
1: Scattered decreased crypts with thin fibrous connective tissue (CT) replacement (<10%)
2: Multifocal prominent loss of crypts with up to 25% replacement by CT
3: Markedly depleted crypts with loose fibrous CT comprising up to 50% of mucosa
4: Severe loss of crypts with >50% fibrous CT comprising mucosa

Epithelial defects

0: None
1: Focally dilated glands and/or attenuated surface epithelium, decreased goblet cells
2: Focally extensive gland dilation and/or surface epithelial attenuation. Shallow surface erosions and/or marked epithelial sloughing & mucus (catarrhal enteritis)
3: Erosions (mucosal necrosis terminating above muscularis mucosae)
4: Ulceration (full-thickness mucosal necrosis extending into submucosa or deeper)

Appendix 2: Effects of chronic infection with *Helicobacter hepaticus* on the progress of *C. rodentium* infection in FVB mice.

Diana Borenshtein, Hilda Holcombe, Prashant R. Nambiar, David B. Schauer.

Biological Engineering Division, Division of Comparative Medicine, Massachusetts Institute of Technology, Cambridge, MA, 02139.

A2.1 Introduction

The impact of the microbiota on *C. rodentium* infection has long been recognized [Bathold et al., 1977; Itoh et al., 1978; Itoh et al., 1979; Itoh et al., 1980]. Itoh and coworkers have shown that specific pathogen free DDD and CF1 mice rapidly succumb to infection compared with animals maintained conventionally [Itoh et al., 1979]. On the other hand, germ free mice of different inbred strains do not develop clinical disease and mortality despite having high bacterial burden and disseminated infection [Barthold et al., 1976; Itoh et al., 1978]. Antibiotics pretreatment [Luperchio and Schauer, 2001], as well as coinfections with helminths [Chen et al., 2005a; Chen et al., 2006], exacerbate TMCH, whereas probiotics administration ameliorates the disease in *C. rodentium*-infected mice [Chen et al., 2005b; D'Arienzo et al., 2006; Johnson-Henry et al., 2005; Varcoe et al., 2003]. Results from our lab demonstrated attenuated response to *C. rodentium* in *Rag2*$^{-/-}$ mice with concurrent chronic *H. hepaticus* infection [Holcombe and Schauer, unpublished data]. We therefore tested the hypothesis that FVB mice infected with both *H. hepaticus* and *C. rodentium* will have ameliorated disease outcome.

A2.2 Results

All mice inoculated with *H. hepaticus* at 5-week old age, were positive by PCR at 5 WPI (data not shown). *H. hepaticus* infection did not have any effects on mortality, growth rate and intestinal pathology in FVB mice and were undistinguishable from uninoculated mice (Figures A2-1 and A2-3). No gender effect was found in any experimental group (data not shown).

Consistent with our previous results (Chapters 2, 3, and 4), FVB mice infected with *C. rodentium* developed high mortality ($p<0.0001$ by Logrank test compared to uninfected animals; Figure A2-1A). The latent period was longer in mice infected with both *C. rodentium* and *H. hepaticus* (median survival 13.5 versus 16 days in single- compared to double-infected mice). However, the difference did not reach statistical significance. Both *C. rodentium*-infected groups lost weight compared with uninoculated animals ($p<0.0001$ by two-way ANOVA; Figure A2-1B), but the response was delayed in double-infected mice at 13 DPI ($p<0.01$ by Bonferroni post-test).

The increase in fecal *C. rodentium* counts was faster in single infected mice, though did not reach statistical significance (Figure A2-2A). On the other hand, delayed *C. rodentium*

clearance in double-infected mice was observed at 16 DPI ($p<0.05$ by *t* test). Higher *C. rodentium* levels were found in tissues obtained from double-infected animals at 16 DPI, though statistically significant in cecum and spleen only ($p<0.05$ by *t* test; Figure A2-2B).

Mice infected with *C. rodentium* developed remarkable pathology in distal colon at 16 DPI ($p<0.0001$ by Kruskal-Wallis test, Figure A2-3) independent of *H. hepaticus*-infection status.

A2.3 Discussion

Our results indicate that, although chronic infection of mice with *H. hepaticus* resulted in increase latency in appearance of clinical signs and mortality, it did not prevent high susceptibility and development of colonic lesions in FVB mice infected with *C. rodentium*. The attenuation of clinical disease, as well as delayed clearance of *C .rodentium* from feces and tissues at 16 DPI, can be explained by slower increase in *C. rodentium* colonization of FVB mice preinfected with *H. hepaticus*. This may indicate reprogramming of immune response in double-infected animals, though needs further evaluation. However, due to high mortality in FVB mice infected with *C. rodentium* the experiments had to be terminated and no further characterization was performed.

A2.4 Experimental Design

Five-week old 20 male and 20 female FVB/NTac mice were inoculated with *Helicobacter hepaticus* as previously described [Young et al. 2004]. *H. hepaticus* was harvested after 48 h of growth on agar plates and resuspended in a small volume of tryptic soy broth. The optical density at 600 nm of the inoculum was measured, and 10-fold serial dilutions of the inoculum were plated to quantify the CFU used for infection. Mice were inoculated with a suspension of bacteria with an optical density of 1.0 at 600 nm ($\sim 10^8$ CFU) in a volume of 0.2 ml. Bacteria were introduced directly into the stomach with a 24-gauge ball-tipped gavage needle. Mice were challenged with a total of three doses of bacteria on three alternating days. Control mice were inoculated with sterile tryptic soy broth.

The *H. hepaticus* infection was confirmed five weeks thereafter by PCR amplification of DNA isolated from fecal pellets using Qiagen DNA kit as recommended by manufacturer. PCR amplification was performed using the *Helicobacter*-specific primers 5'-ACT TCA CCC CAG

TCG CTG-3' (C05) and 5'-GCT ATG ACG GGT ATC C-3' (C97), which produce a 1200-bp amplicon [Fox et al., 1998]. *H. hepaticus* and water was used as positive and negative controls for PCR reactions respectively. PCR was performed with 5 µl of the template at approximately 250 ng/µl. Each 25-µl PCR mixture contained 20 pmol of each primer, a 200 µM concentration of each deoxynucleoside triphosphate, and 1.5 U of Taq DNA polymerase in a solution of 10 mM Tris-HCl, 50 mM KCl, and 1.5 mM $MgCl_2$ (final concentrations; Ready To Go PCR beads; Amersham Pharmacia Biotech, Piscataway, N.J.). Cycling conditions included 30 cycles of denaturation at 94°C for 1 minute, annealing at 55°C for 2½ minutes, and elongation at 72°C for 3 minutes. PCR products were visualized by agarose gel electrophoresis.

At 6 weeks post *H. hepaticus* infection, half of each *H. hepaticus*-negative or –positive groups were infected with ~10^9 CFU of o/n culture of DBS120, resulting in 4 groups of n = 10 (5 of each gender) mice used in the study. Animal monitoring, necropsy and samples collection was done as described in Appendix 1: General Methods.

A2.5 Figures

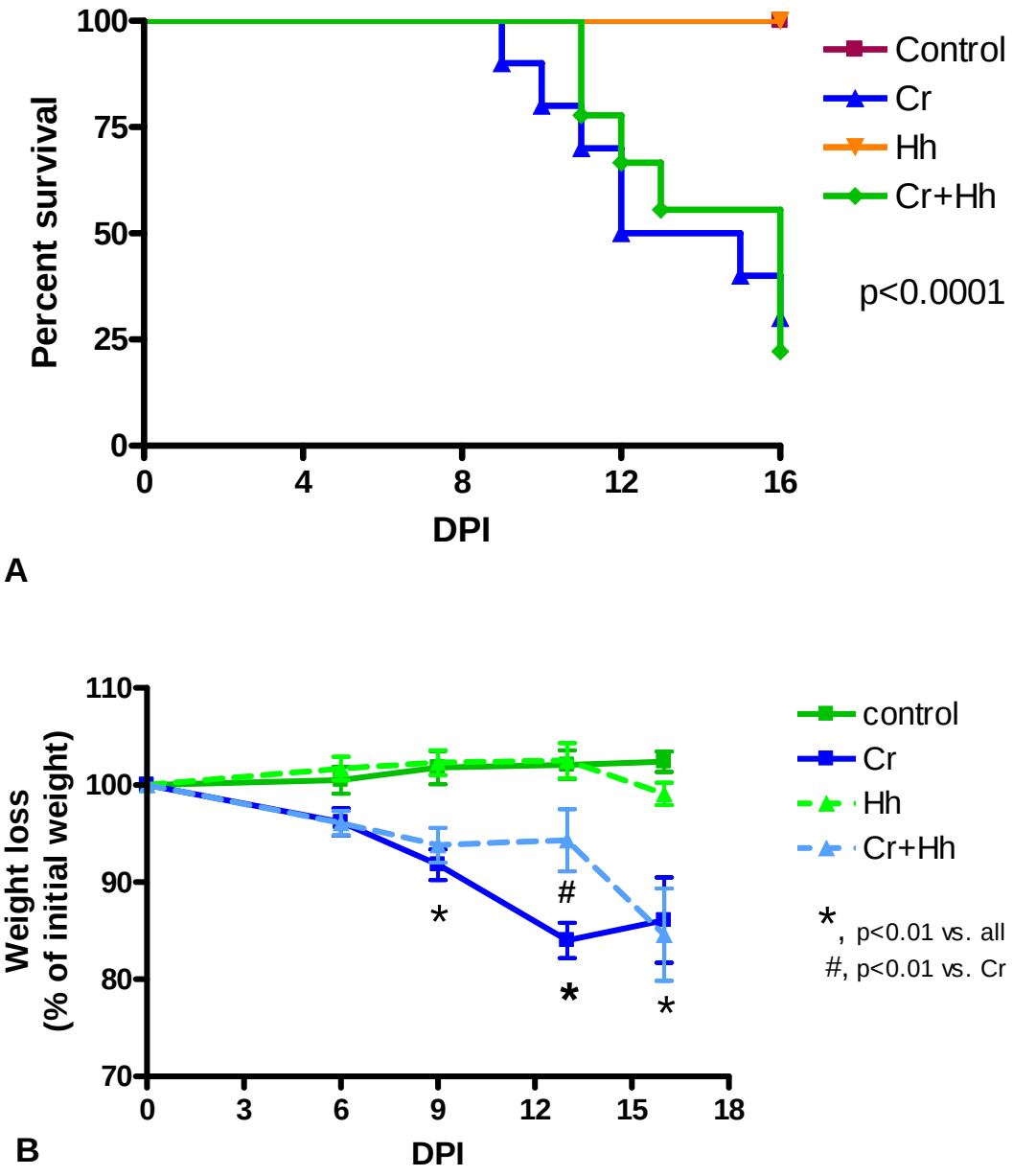

Figure A2-1. *C. rodentium* infection with or without concurrent infection with *H. hepaticus.*

A. *C. rodentium* infection resulted in high mortality rate in FVB mice regardless of *H. hepaticus* infection status ($p<0.0001$ by Logrank test). Although median survival was higher in mice infected with both pathogens, the difference did not reach statistical significance.

B. The decrease in body weight was delayed in mice infected with *C. rodentium* and *H. hepaticus* at 13 DPI.

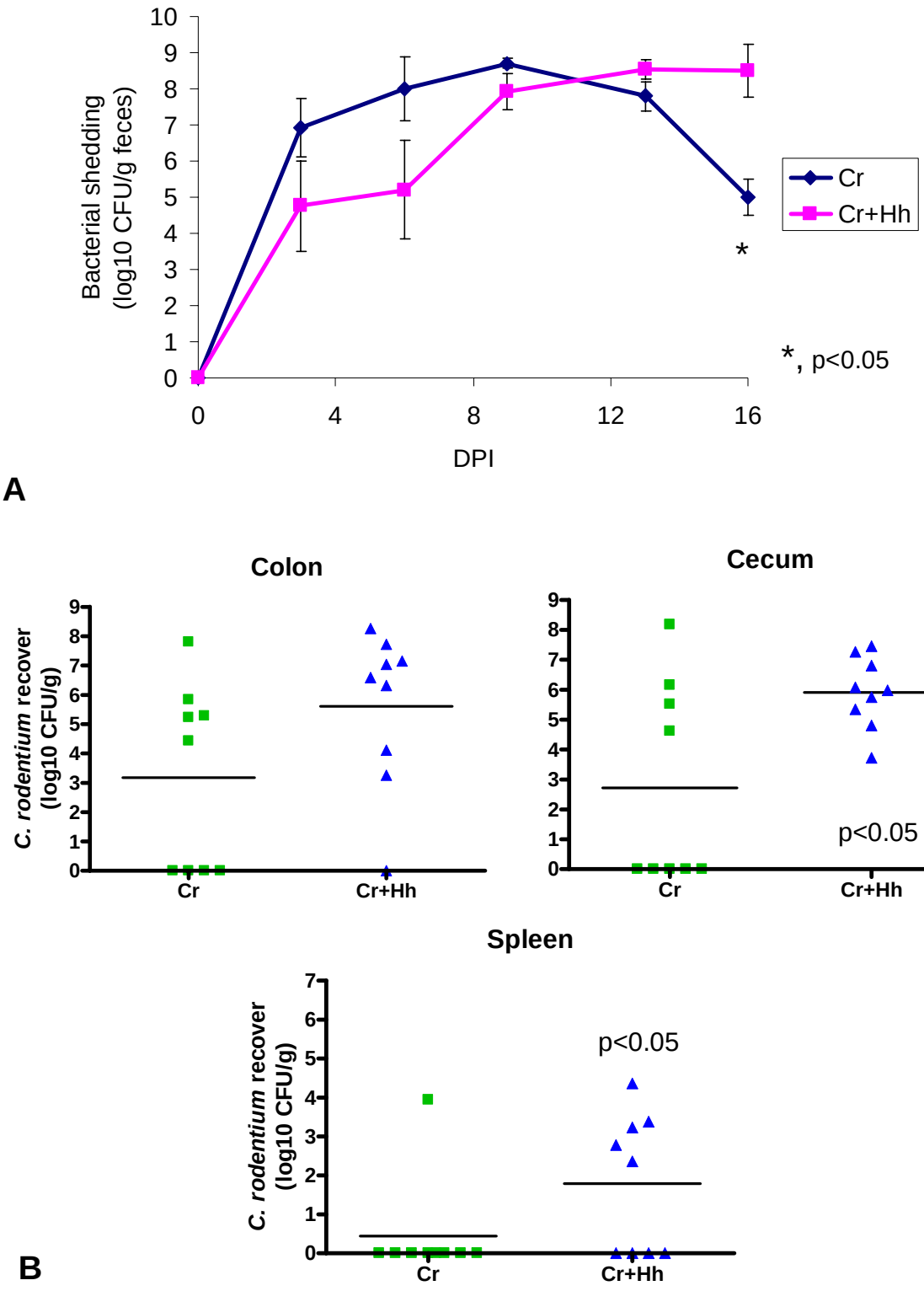

Figure A2-2. *C. rodentium* recovery from tissues.

A. Changes in fecal bacterial shedding were affected by concurrent *H. hepaticus* infection ($p<0.05$ by *t* test).

B. Recovery of *C. rodentium* was higher in cecum and spleen of double-infected mice at 16 DPI ($p<0.05$ by *t* test).

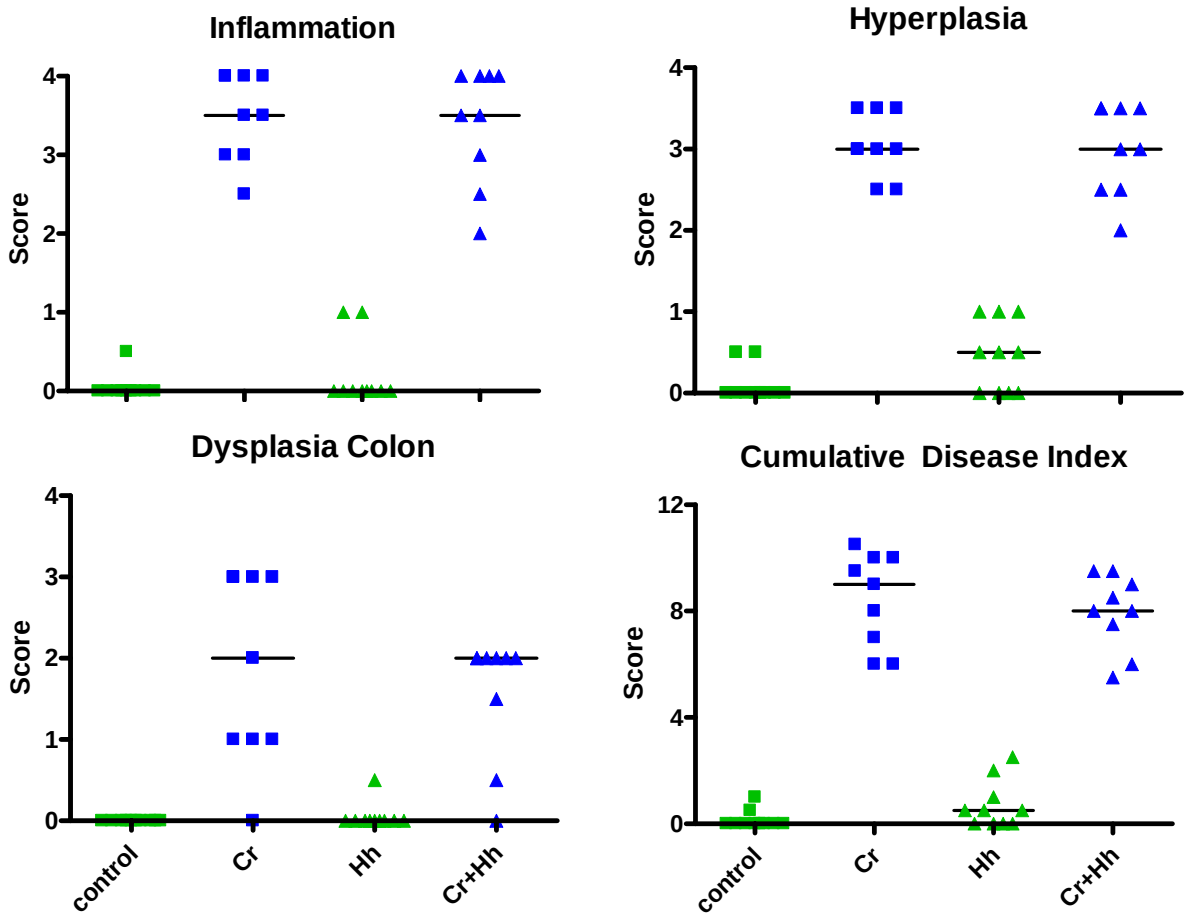

Figure A2-3. Histopathology in *C. rodentium*-infected mice with or without concurrent infection with *H. hepaticus. C. rodentium* infection was associated with the development of moderate to severe inflammation and hyperplasia, and mild to moderate dysplasia ($p<0.0001$ by Kruskal-Wallis test). Chronic infection with *H. hepaticus* did not affect the histopathology in *C. rodentium*-infected FVB mice. Lines indicate group median.

Appendix 3: Effects of dietary intervention with anti-inflammatory triterpenoids on the progress of *C. rodentium* infection in FVB mice.

Diana Borenshtein[1], Michael B. Sporn[3], Prashant R. Nambiar[2], David B. Schauer[1,2].

[1]Biological Engineering Division, [2]Division of Comparative Medicine, Massachusetts Institute of Technology, Cambridge, MA, 02139; [3]Dartmouth Medical School, Hanover, NH, 03755.

A3.1 Introduction

Synthetic triterpenoids, the most known of which is 2-cyano-3,12-dioxooleana-1,9-dien-28-oic acid (CDDO), are steroid-like analogs of oleanolic or ursolic acid with potent antiproliferative, differentiating, and anti-inflammatory activities [Dinkova-Kostova et al., 2005; Liby et al.,2005; Minns et al., 2004; Place et al., 2003; Suh et al.,1998] (Figure A3-1). They were shown to inhibit proliferation and induce apoptosis at nanomolar concentrations. These compounds also suppress oxidative stress *in vitro* and *in vivo* mainly by effecting NO production and iNOS and COX-2 expression. The exact mechanism is unknown, but the involvement of transcription factor Nrf2 regulating expression of a number of antioxidant and detoxification proteins has been exhibited. The protection was associated with increased expression of the cytoprotective heme oxygenase-1 (HO-1) enzyme and decrease in NF-kB [Dinkova-Kostova et al., 2005; Liby et al., 2005; Suh et al., 1998]. Furthermore, CDDO suppresses development of ileitis in *Toxoplasma gondii*-infected mice in TGF-β-dependent manner [Minns et al., 2004].

The profound inflammation observed in FVB mice infected with *C. rodentium* prompted us to seek for interventions allowing FVB mice to resist deleterious effects of infection. We, therefore, supplemented FVB mice with dietary triterpenoids ethyl 2-carboxy-3,12-dioxooleana-1,9(11)-dien-28-oate (NSC #D722320, TP-222). TP-222 (Figure A3-1) is a derivative of CDDO synthesized in laboratory of Dr. Michael B. Sporn from Darmouth Medical School to overcome pharmacokinetic limitations (low bioavailability) of CDDO *in vivo*. TP-222 has shown a promising *in vivo* activity [Sporn, personal communication].

A3.2 Results

Administration of TP-222 in diet did not ameliorate *C. rodentium*-induced disease in FVB mice; infected mice fed TP-222 exhibited higher mortality ($p<0.05$ by Logrank test) and more severe weight loss ($p<0.01$ by two-way ANOVA) (Figure A3-2). Moreover, substantial weight loss was observed in uninoculated TP-222-administrated mice.

Administration of triterpenoids was associated with delayed clearance of infection and high translocation of *C. rodentium* to spleen, whereas none of the infected animals on control diet had spleen bacterial counts (Figure A3-3).

Majority of histopathological parameters were comparable between the infected groups on different dietary regimes. Tendency to higher ulceration and submucosal lesions, as well as colonica dysplasia, in TP-222-fed infected FVB mice was not statistically significant (Figure A3-4).

A3.3 Discussion

Opposite to the expected, no benefits to the TP-222 containing diet were observed. The weight loss in TP-222-fed *C. rodentium*- infected mice happened faster and was more severe than in mice on the control diet, leading to a forced termination of the experiment after 12 dpi. Tendency to marked ulceration, submucosal lesions and higher dysplasia, though not statistically significant, correlated with more severe disease outcome in infected mice treated with triterpenoids. Furthermore, the uninfected mice on the TP-222 diet also lost the weight during the first week. This is consistent with few animal studies, in which toxicity associated with triterpenoids administration was characterized by weight loss [Hyer et al., 2005; Place et al., 2003; Yates et al., 2006]. In those studies, the use of the drug despite toxicity was approved due to significant efficacy in lowering tumor burden [Place et al., 2003; Yates et al., 2006]. Although in some cases, the weight loss was transient and mice recovered after 1 to 2 weeks from the beginning of triterpenoid treatment [Hyer et al., 2005], weight loss early during *C. rodentium* infection can be detrimental in FVB mice. It is not clear why FVB mice on triterpenoid diet are more susceptible to the effect of the pathogen. However, one possible explanation may be a sustained and disseminated infection characterized by higher bacterial counts in feces and spleen of TP-222-fed animals. In addition, CDDO injected in high-doses to mice was associated with swelling of the small bowel [Minns et al., 2004]. Although the exact mechanism of such an effect was not addressed, it may indicate changes in intestinal ion and fluid transport and resultant diarrhea. This could further exacerbate *C. rodentium*-induced effects in FVB mice. Since the main goal (attenuation of *C. rodentium* infection in FVB mice) was not achieved, further mechanistic characterization of the observed effects of dietary triterpenoids was not pursued.

A3.4 Experimental Design

Thirty 10-week-old female FVB/NTac mice were divided randomly into the following groups: mice on control diet inoculated with 0.1 ml bicarbonate (control, n=5); mice on TP-222 diet inoculated with 0.1 ml bicarbonate (TP-222 alone, n=5); mice on control diet inoculated with 10^9 CFU DBS120 (*C. rodentium* alone, n=10); and mice on TP-222 diet inoculated with 10^9 CFU DBS120 (*C. rodentium* + TP-222, n=10). The concentration of TP-222 in diet was 800 mg/kg. Considering and averaged food consumption of 4 g/d in mice, the daily dose of triterpenoids was ~3.2 mg/d. Animal maintenance, necropsies and sample collection was performed as described in Appendix 1: General Methods.

A3.5 Figures

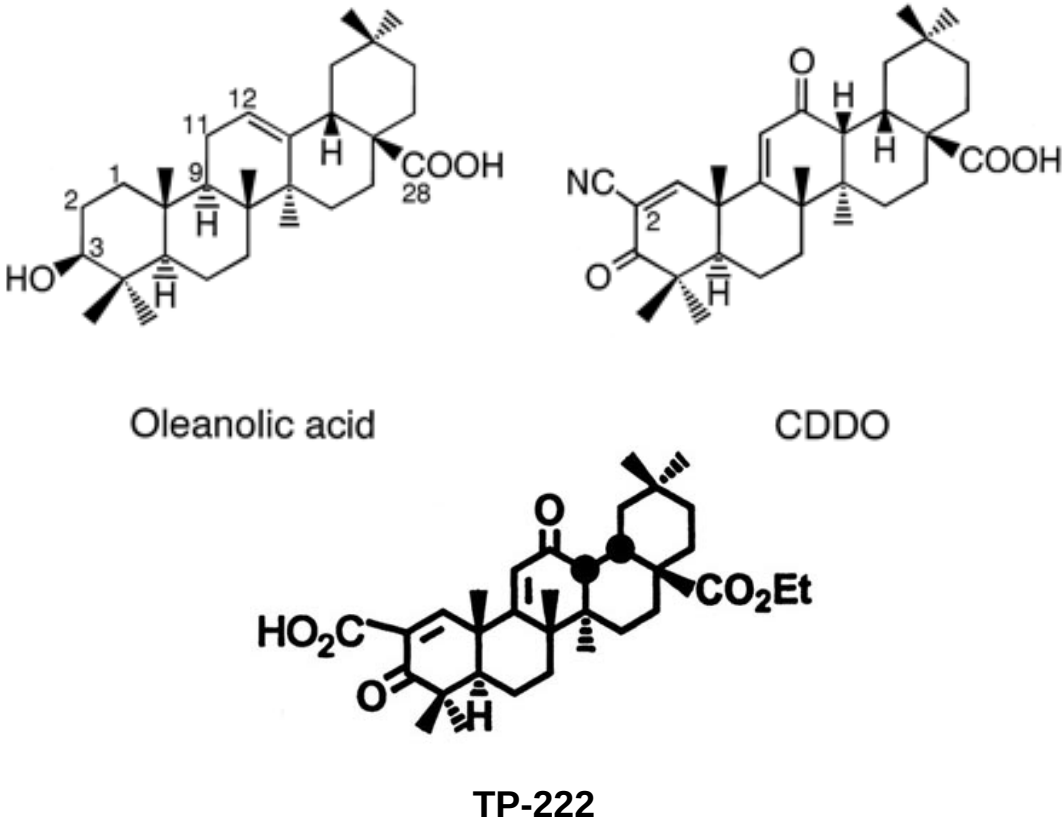

Figure A3-1. Structure of natural (OA) and synthetic (CDDO aka TP-151 and TP-222) triterpenoids. Adapted from [Dinkova-Kostova et al., 2005; Suh et al.,1998]

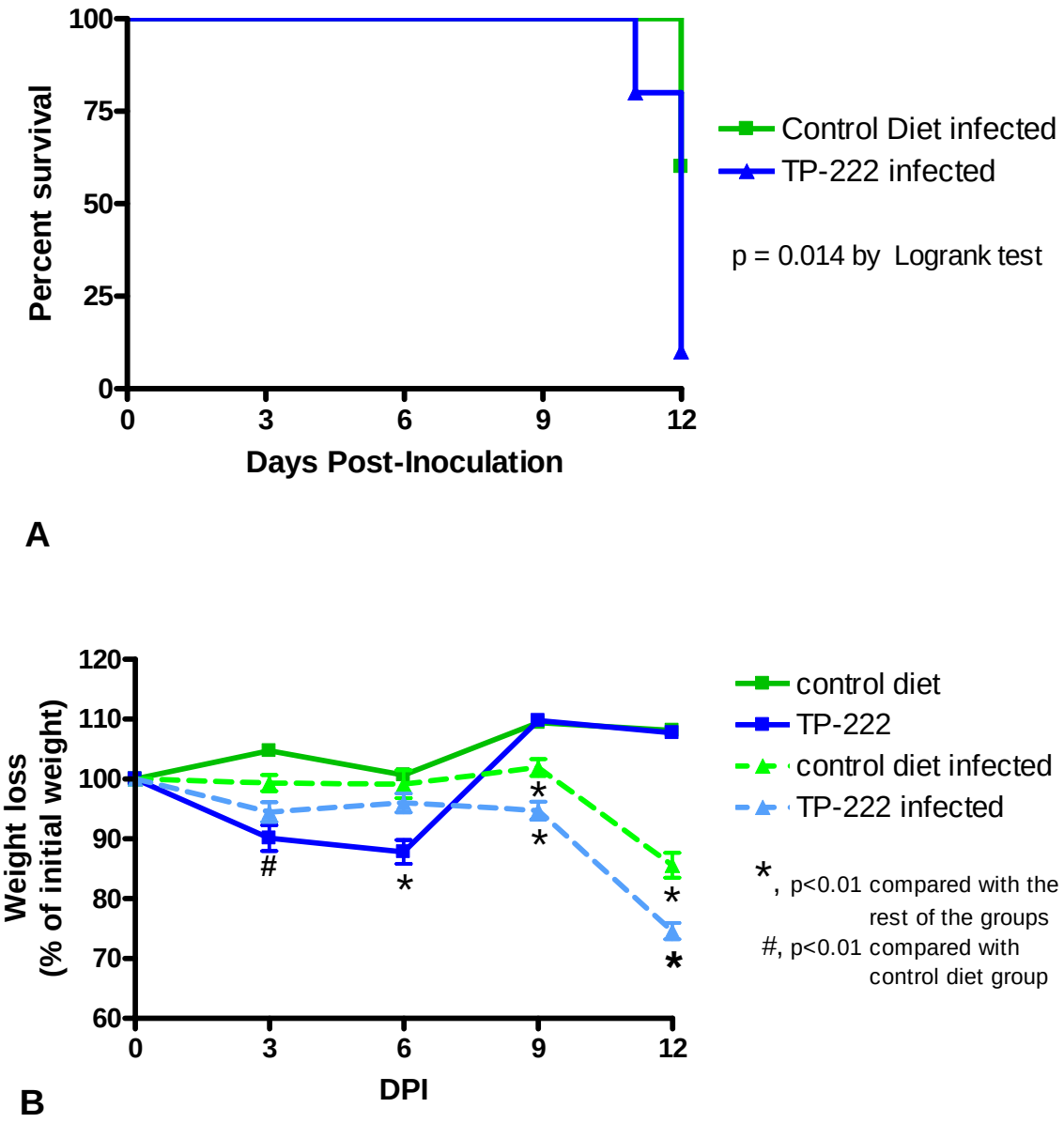

Figure A3-2. Dietary administration of triterpenoids augments *C. rodentium*-induced disease in FVB mice.

A. Development of higher mortality in infected mice supplemented with TP-222 ($p<0.05$ by Logrank test).

B. TP-222 treated animals had retarded growth rate with or without *C. rodentium* administration ($p<0.01$ by two-way ANOVA with Bonferroni post-test).

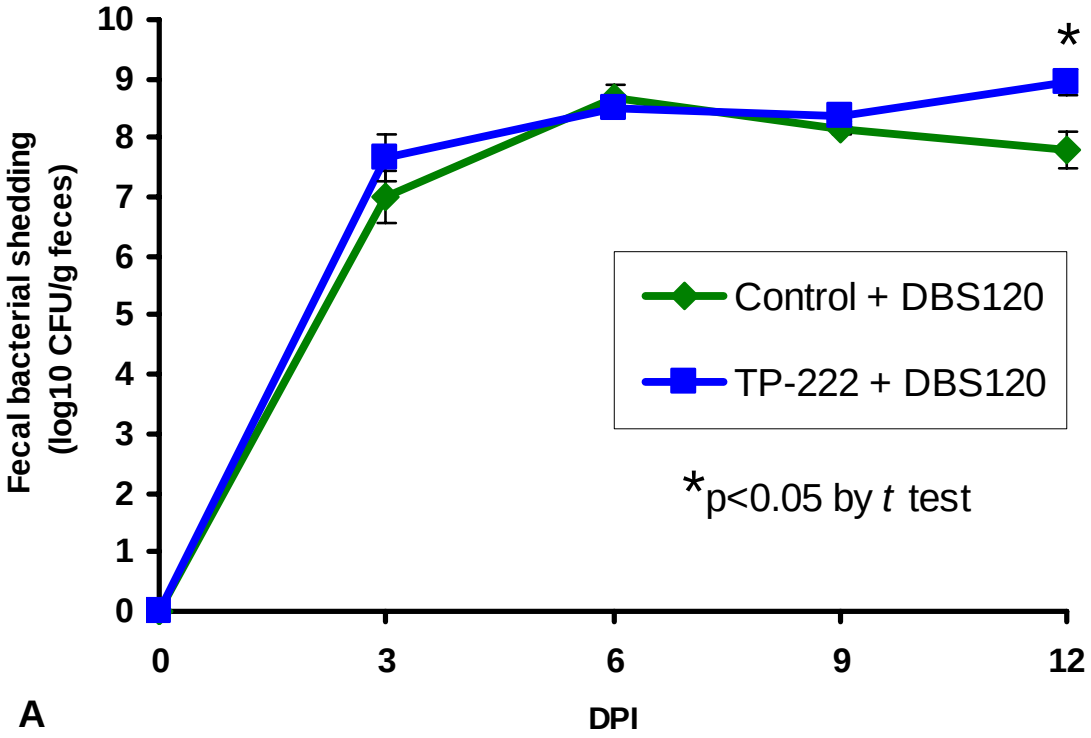

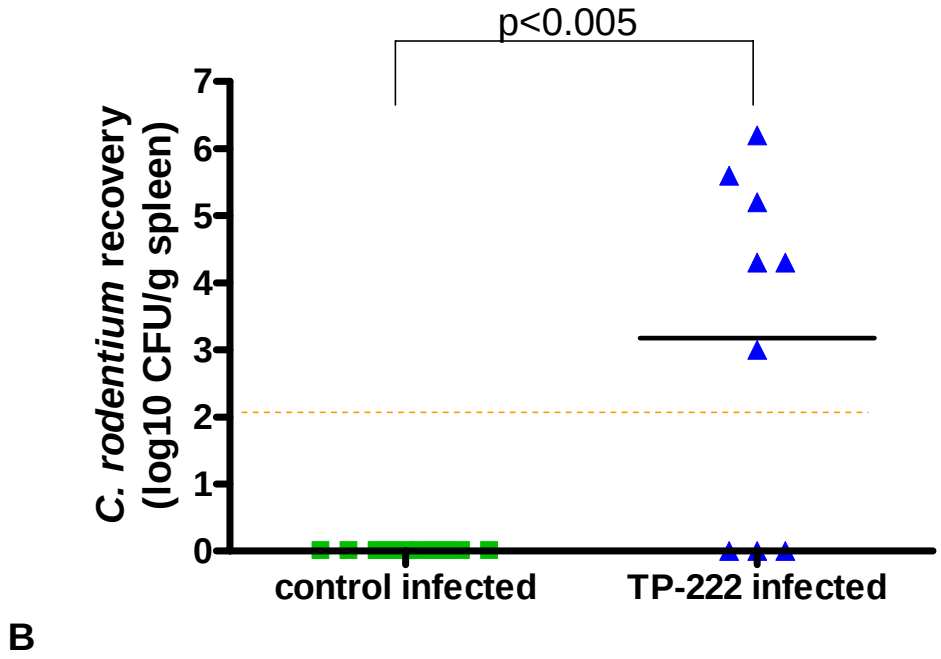

Figure A3-3. Impairment of *C. rodentium* infection in FVB mice treated with triterpenoids.

A. Delayed bacterial clearance in infected mice supplemented with dietary triterpenoids ($p<0.05$ by *t* test).

B. Increased bacterial translocation to extraintestinal tissues, i.e. spleen, in mice supplemented with TP-222 ($p<0.005$ by *t* test).

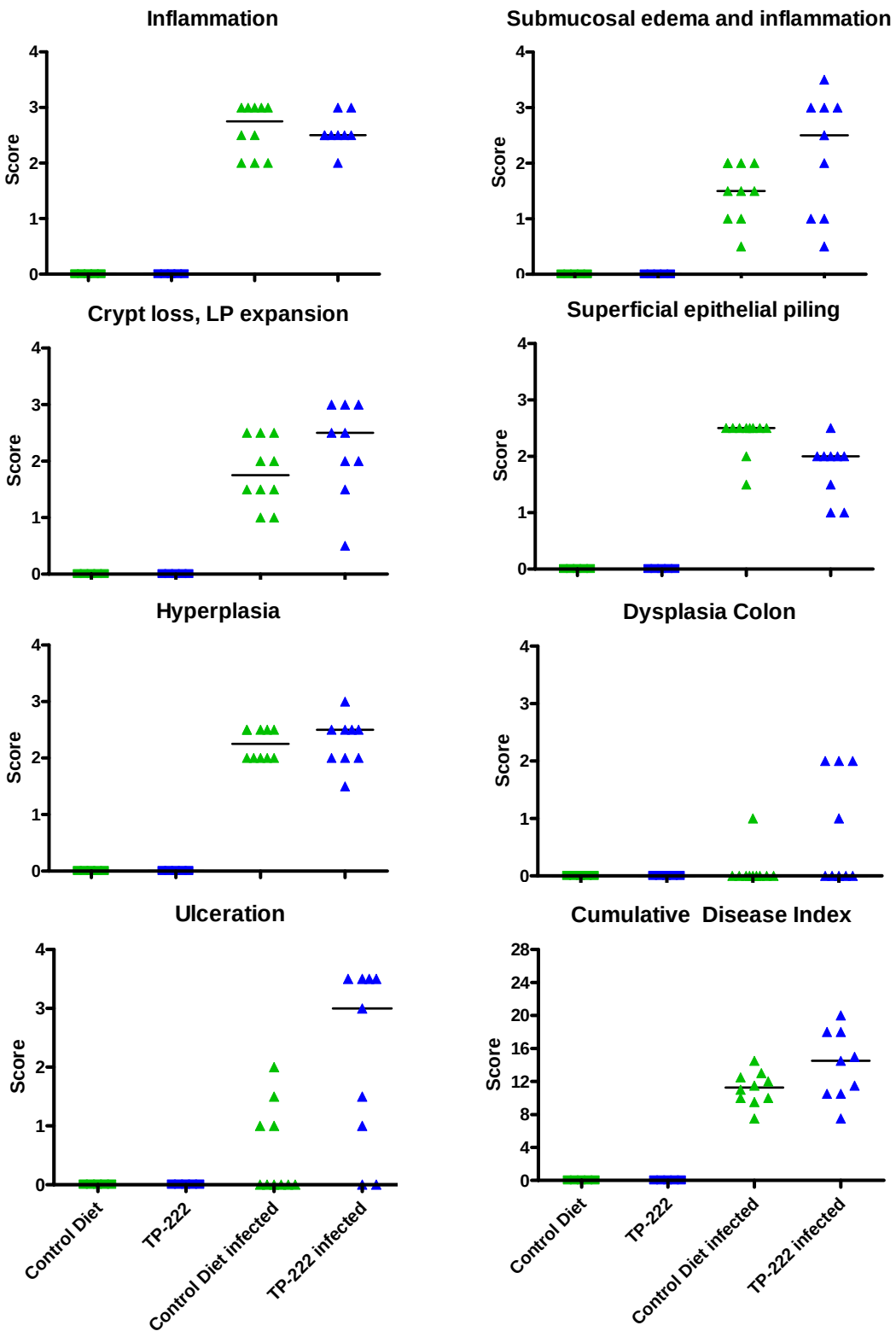

Figure A3-4. Pathology in *C. rodentium*-infected FVB mice supplemented with or without dietary triterpenoids. No significant differences were observed between the groups as indicated by Kruskal-Wallis test. Lines indicate group median.

Appendix 4: Evaluation of genomic instability in *C. rodentium*-infected FVB mice.

Diana Borenshtein, Elena V. Gostjeva, David B. Schauer.

Biological Engineering Division, Massachusetts Institute of Technology, Cambridge, MA, 02139.

A4.1 Introduction

As discussed in the Chapter 1: Introduction, *C. rodentium* exhibit pro-carcenogenic potential and can promote tumor formation in $Apc^{Min/+}$ mice or DMH-treated animals [Barthold and Beck, 1980; Barthold and Jonas, 1977; Newman *et al*., 2001]. Alterations in β-catenin pathway [Sellin et al., 2001] and 8-fold increase in mutation rate [Sohn, 2005] in distal colon of affected mice can contribute to this process. There is growing evidence that genomic instability (GI) plays an important role in development of human colorectal cancers (CRCs). The two main types of genomic abnormalitites in CRCs are chromosomal instability (CIN) and microsatellite instability (MSI), accounting for 85 and 15% of sporadic CRCs, respectively [Itzkowitz and Yio, 2004; Lengauer et al., 1998; Lindblom, 2001]. Chromosomal instability, the predominant form, causes abnormal segregation of chromosomes and abnormal DNA content (aneuploidy). As a consequence, loss of heterozygosity (LOH) may result in loss of function of key tumor suppressor genes such as adenomatous polyposis coli (*APC*) and *p53*. CIN considered to be an early event during carcinogenesis and mainly affects distal colon [Ilyas et al., 1999; Lengauer et al., 1997; Nowak et al., 2002; Shih et al., 2001]. The second form of GI is microsatellite instability (MSI) which is commonly found in hereditary non-polyposis colorectal cancer (HNPCC) but rare (~15%) in sporadic CRCs. MSI arises from the progressive accumulation of somatic alterations in the length of simple repeat nucleotide sequences known as microsatellites. MSI is characterized by diploidy and normal rate of chromosomal change, mainly affects proximal colon and is a marker for underlying DNA mismatch repair defects [Itzkowitz and Yio, 2004; Lengauer et al., 1998; Lindblom, 2001]. As was shown in Chapter 2, FVB mice infected with *C. rodentium* developed marked dysplasia. We, therefore, were interested in studying genetic instability in these animals.

A4.2 Results

Chromosomal instability was examined by unequal DNA segregation determined with Feulgen microdensitometry. Feulgen densitometry is *in situ* method, based on the reactions of free aldehyde groups in DNA molecule (released by strong acid) with aromatic amines, which results in development of color in a direct proportion to the amount of present DNA [Hardie et al., 2002]. Such an approach allowed us to localize and characterize the nature of the

chromosomal instability events in each individual crypt from the *C. rodentium*-infected whole tissue specimen.

Dividing cell in uninoculated mice were confined, as expected, to the lower part of the crypt, and spread though the whole crypt in infected animals. To analyze chromosomal instability, we assumed that variability in DNA content of daughter nuclei in anaphase/telophase cells within the 5% variation range means equal DNA segregation. More than 5% variation indicates unequal DNA segregation. Both infected and uninfected mice had mitoses with unequal DNA segregation, but the nature of it was different between experimental groups. Thus, unequal DNA segregation was observed at the bottom of normal crypts (Figure A4-1a), but was found along most of the axis in hyperpalstic crypts (Figure A4-1d,e). In many cases, mitoses in infected colons were characterized by non-disjunction of the daughter chromosomes (Figure A4-1b,c) and few apoptotic cells were found in the bottom of hyperplastic crypts (data not shown). Although the absolute number of mitoses with unequal DNA segregation was higher in colon from infected mice, the fractions were comparable between the groups and comprised of 24.0 + 0.6 % in uninoculated FVB mice and 25.0 + 0.7 % in *C. rodentium*-infected animals ($p>0.05$).

The accepted cell positional scoring technique (Figure A4-2A, [Renehan et al., 2002]) which relies on well-oriented crypts lined by monolayer of epithelium, was no longer appropriate in whole tissue specimen (Figure A4-2B). We, therefore, developed a new system for crypt cell positional analysis by dividing the crypt into layers assuming binomial division of cells (Figure A4-2C). In that schematic representation, first few layers (A through D) build the bottom part of the crypt and layer E represent the rest of the cells in the crypt. Consistent with that system of scoring, approximately 250 cells were found to populate the normal crypts (layers A through E), which is in agreement with reports by others [Booth and Potten 2000], and approximately 500 cells were counted in hyperplastic crypts (layers A through F). Using this scoring method, we were able to find the differences in positional distribution of unequally segregated DNA between the experimental groups. Thus, in control animals proliferating cells residing in levels B through D displayed unequal DNA segregation (Figure A4-3, upper panel). The variability in DNA content between the daughter nuclei was not high achieving maximum of 12% difference (Figure A4-3, lower panel). In infected animals, on the other hand, mitotic cells with unequal DNA segregation were observed in levels A through E, with the highest fraction (73%) found in the very bottom of hyperplastic crypts. Furthermore, cells proliferating in levels A and B had high

levels of divergence in DNA content up to 40-60% difference between daughter nuclei (Figure A4-3).

Microsatellites are short, tandemly repeated DNA sequences from 1 to 6 base pairs in length, distributed throughout genome. One mononucleotide and five dinucleotide repeats, previously associated with murine colonic tumors [Guda et al., 2004; Kohonen-Corish et al., 2002; Lipkin et al., 2000; Sohn et al., 2001] (Table A4-1) were used for detection of microsatellite instability (Table A4-1). MSI, defined as change in length of microsatellite allele due to either insertion or deletion of repeating units, was analyzed by fluorescence polymerase chain reaction on DNA isolated from mouse tissues (Figure A4-4). Distal and proximal colons were compared with liver samples as non-target tissue representing negative control. Allelic size variations were not detected in any of those markers in tissues from *C. rodentium*-infected FVB mice.

A4.3 Discussion

In this experiment we aimed to characterize genomic changes in mouse colon as potential mechanism for tumor promotion by murine pathogen *C. rodentium*. Because genomic instability can developed by two independent mechanisms, we examined both chromosomal and microsatellite instability in colon from untreated or *C. rodentium*-infected FVB mice.

To evaluate changes at the chromosomal level, we applied Feulgen densitometry in whole colonic tissues. The proliferating cells in normal mouse colon were confounded to the lower parts of the crypt, consistent with the current concepts on epithelial proliferation in normal intestine [Booth and Potten 2000; Renehan et al., 2002]. Surprisingly, approximately 25% of those cells exhibited unequal DNA segregation, though the differences in DNA content between daughter nuclei were not drastic (up to 12%). Interestingly, none of the dividing cells at the very bottom of the crypt (layer A) displayed that feature, indicating preservation of DNA content within this population of cells. The nature of those observations is not clear. Considering accepted hypotheses on stem cell hierarchy of the intestinal crypt [Booth and Potten 2000; Renehan et al., 2002], we can speculate that proliferating cells in the level A represent actual stem cells, whereas the portion of dividing cells in the rest of the layers in normal colon (B

through D) represents clonogenic stem cells, in which unequal DNA segregation is part of differentiation process.

Analysis of anaphase/telophase cells in distal colons revealed changes in positional distribution and regional alterations of chromosomal instability in colonic crypts of infected animals. *C. rodentium*-infected mice displayed remarkable increase in fraction of dividing cells with DNA unequal segregation and higher aneuploidy in the basal levels of the hyperplastic crypts, where the stem cells reside [Booth and Potten 2000; Renehan et al., 2002]. Because *C. rodentium* infection is not sufficient for colon tumorigenesis (Chapter 2) but does exhibit co-carcinogenic effects [Barthold and Beck, 1980; Barthold and Jonas, 1977; Newman et al., 2001], clonogenic, but not actual, stem cells may be potential target during infection. It is likely that massive lesions, such as epithelial hyperplasia, erosions, ulcers, loss of differentiation, in the infected colons induce regenerative responses that result in activation of clonogenic stem cells attempting to repopulate damaged crypt. Despite those novel observations, the overall rate of unequal DNA distribution during mitosis was similar in control and infected mice indicating the still existing steady state. This may explain the reversibility of dysplastic changes in FVB mice upon resolution of infection and inflammation in long-term studies (Chapter 2). One of the possible explanations could be removal of affected cells by apoptosis which was more frequently found in infected crypts and colocalized with chromosomal instability-exhibiting cells. These hypotheses require further evaluation and other karyotype analyses are needed to confirm CIN phenotype in colons from *C. rodentium*-infected FVB mice.

Another type of genomic abnormalities addressed here is instability at the nucleotide level. MSI was found in few animal models of intestinal tumors, including colitis-associated tumors [Guda et al., 2004; Kohonen-Corish et al., 2002; Lipkin et al., 2000; Sohn et al., 2001]. However, many other reports failed to observe MSI [Edelmann et al., 1997; Engle et al., 1999; Qin et al., 2000; Song et al., 2000; Sturlan et al., 2001], consistent with the rare observation of MSI in sporadic CRCs in human [Itzkowitz and Yio, 2004; Lengauer et al., 1998; Lindblom, 2001]. Allelic size variations were not detected in any of the analyzed MSI markers in proximal or distal colon of *C. rodentium*-infected FVB mice. Although possibility of microsatellite instability in other genomic markers cannot be excluded, out results suggest that *C. rodentium* infection does not induce widespread MSI, at least in those fragments frequently found in murine colonic tumors.

Because we saw an evidence of chromosomal abnormalities in *C. rodentium*-affected tissues, and due to existence of inverse relationship between CIN and MSI [Lengauer et al., 1998], CIN can be considered as more dominant effect in colon of FVB mice infected with the pathogen. However these changes are not sufficient for development of colon tumor in *C. rodentium*-infected mice and other factors, such as chemical initiation or chronic inflammation may be required.

A4.4 Experimental Design

FVB mice infected with *C. rodentium* for 12 DPI from Chapter 2 were subjected to GI analysis.

Analysis of genomic instability (aneuploidy). Distal colons were cleaned from feces and longitudinally dissected into halves. One half was fixed in neutral-buffered formalin and used for histopathological analysis (Chapter 2) or MSI analysis (see below). The other half was cut into 2 mm pieces, fixed in freshly prepared 4°C Carnoy's fixative and processed for Feulgen staining of DNA as described elsewhere [Gostjeva et al., 2006]. The DNA content of nuclei in anaphase-telophase cells was detected by KS-400 Image Analysis System (version 3.0; Carl Zeiss Jena GmbH, Jena, Germany). More than 5% difference in DNA content between the daughter nuclei was considered as unequal DNA segregation (aneuploidy).

Microsatellite instability analysis. DNA was isolated from formalin-fixed paraffin-embedded tissue samples (liver, proximal colon, and distal colon) using QIAamp DNA kit (Qiagen) as recommended by manufacturer. Fluorigenic PCR amplification was performed using microsatellite primer sets as indicated in table A4-1. Primer sequences for 5 dinucleotide markers were obtained from the Whitehead Institute for Genome Research database (Cambridge, MA) and sequence for mononucleotide *uPAR* marker was as in ref. [Kohonen-Corish et al., 2002]. One primer from each primer pair was synthesized with a 5’ fluorescent tag (HEX, 6-FAM, or TET). PCR was performed with 1 µl of the template at 25 to 100 ng/µl concentration. Each 25-µl PCR mixture contained 20 pmol of each primer, a 200 µM concentration of each deoxynucleoside triphosphate, and 1.5 U of Taq DNA polymerase in a solution of 10 mM Tris-HCl, 50 mM KCl, and 1.5 mM $MgCl_2$ (final concentrations; Ready To Go PCR beads; Amersham Pharmacia Biotech, Piscataway, N.J.). Water was used as negative control. PCR

amplification was initiated by denaturation at 94ºC for 4 minutes, followed by 35 cycles of 94ºC for 30 seconds, 58ºC for 30 seconds, 72ºC for 30 seconds, with a final 5 minutes 72ºC extension step. PCR products were purified using QIAquick PCR purification Kit as recommended. The purified samples were pooled in 1:1:2 concentration for 6-Fam:Tet:Hex labeled PCR products. Two μl of pooled samples (duplicates) or water were mixed with 0.5 μl GS350-TAMRA standards (Northern Biotechnology) and 12 μl Hi Di Formamide (Applied Biosystems), denaturated at 95ºC for 5 min, immediately cooled and subjected to electrophoresis in ABI 310 Sequencer. Default settings for GS POP4 polymer and matrix C virtual filter, except for 24 min of electrophoresis time, were used. The data was analyzed with GeneScan and Genotyper software. Colon samples were compared with liver samples as negative tissue control.

A4.5 Figures

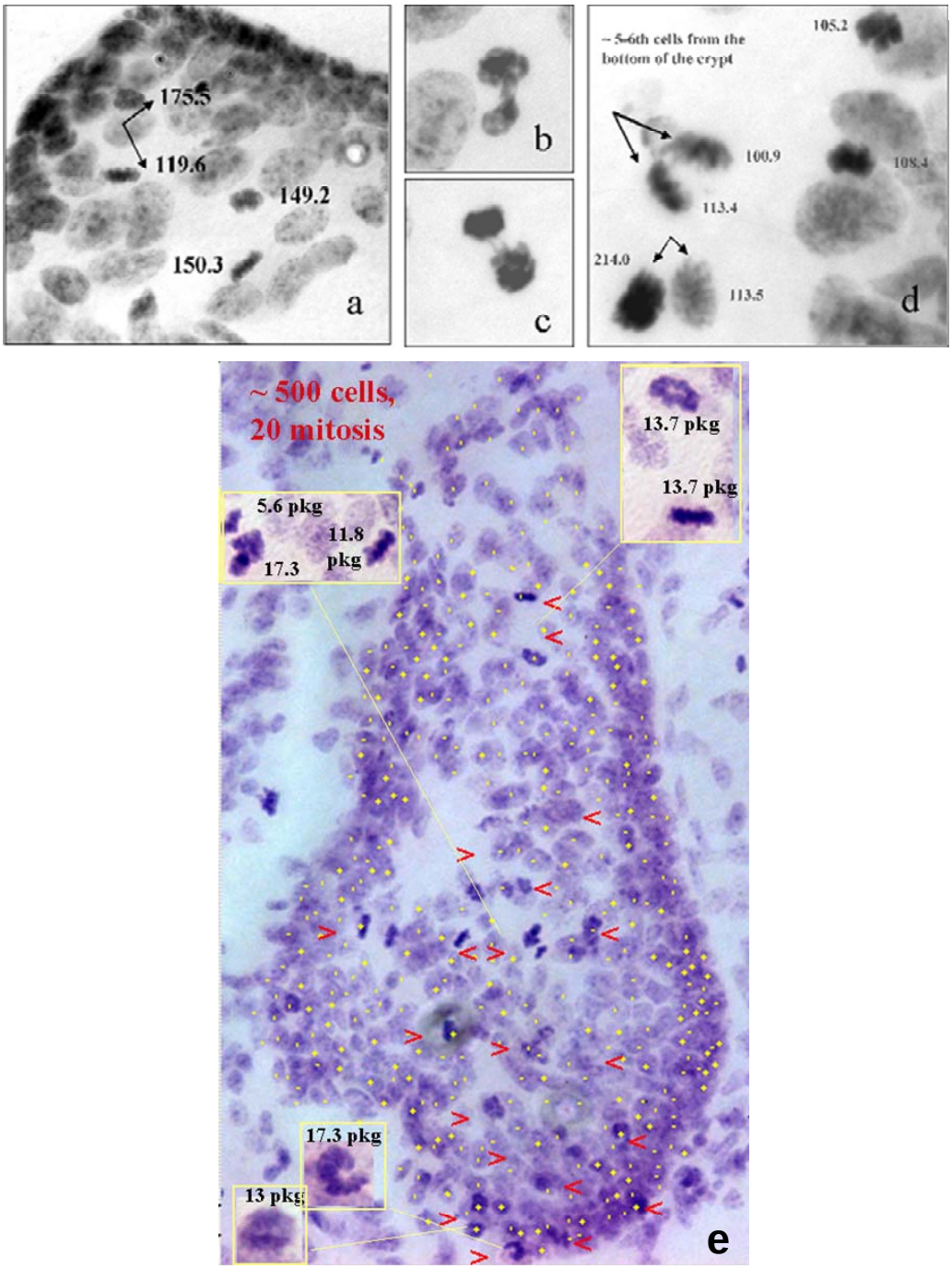

Figure A4-1. Representative images from analysis of anaphase/telophase cells by Feulgen microdensitometry. Chromosomal instability observed in normal mouse colonic crypt (**a**) and in hyperplastic crypts 12 DPI (**b-e**). Unequal DNA segregation was observed only at the bottom of the crypts. Panels **a** and **d** show daughter nuclei dividing unequally (arrowed) and equally. The numbers represent integrated optical density (absorbance). Panels **b** and **c** represent examples of non-disjunction during segregation. Panel **e** shows an example of whole hyperplastic crypt with extension of proliferative zone, approximately 20 mitoses (arrowheads), and higher position of unequally dividing cells along the crypt axis. While the absolute number of unequally dividing cells goes up in *C. rodentium*-induced hyperplasia, the fraction of such cells in a crypt remains constant (see Figure A4-3).

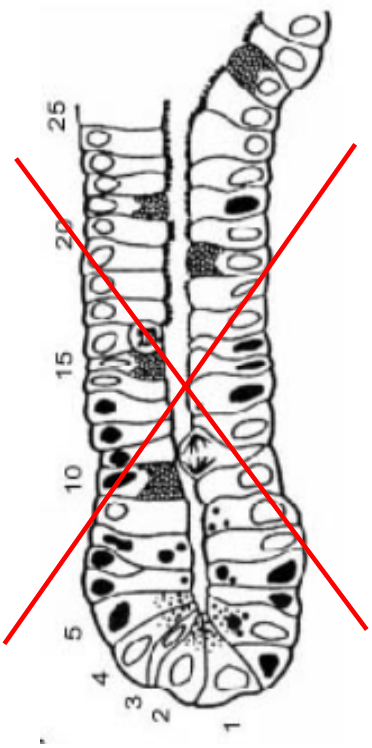

A

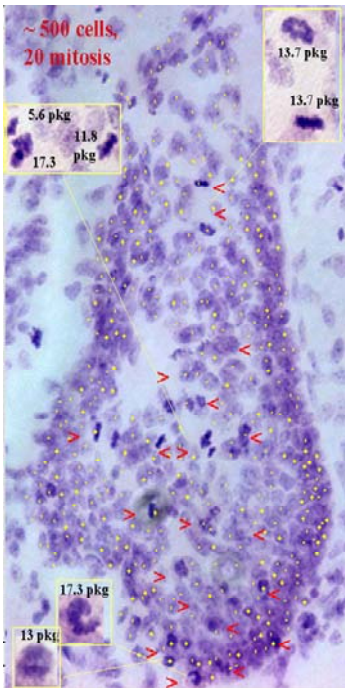

B

Designation of position of anaphase-telophase nuclei undergoing binomial division in normal (256 cells) crypt

2^7 Terminal Cells ? = 128 (E)	Within last 128 cells:	IOD/DNAs:
2^6 ? = 64 (D)	Within next 64 cells:	IOD/DNAs:
2^5 ? = 32 (C)	Within next 32 cells:	IOD/DNAs:
2^4 ? = 16 (B)	Within next 16 cells:	IOD/DNAs:
2^3 2^2 2^1 ? = 16 (A) 2^0 2^0 Stem Cell	Within first 16 cells: Bottom of the crypt	IOD/DNAs:

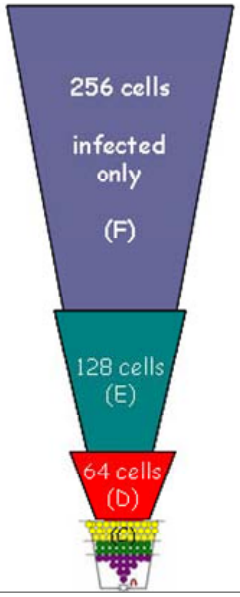

C

Figure A4-2. Analysis of colonic crypts in whole tissue sections.
Classical crypt cell positional analysis [**A**, from Renehan et al., 2002] in longitudinal section of an intestinal crypt illustrates how the position of events up the crypt axis can be determined (position 1 being at the crypt base). This method no longer valid in whole tissue sections which do not posses monolayer of epithelium lining the crypt (**B**). Therefore, we developed new method for analysis of spatial distribution of cells in a whole crypt (**C**) based on the binomial cell division. Normal crypts are divided into 5 areas (A through E), whereas hyperplastic crypts have additional layer of cells (F).

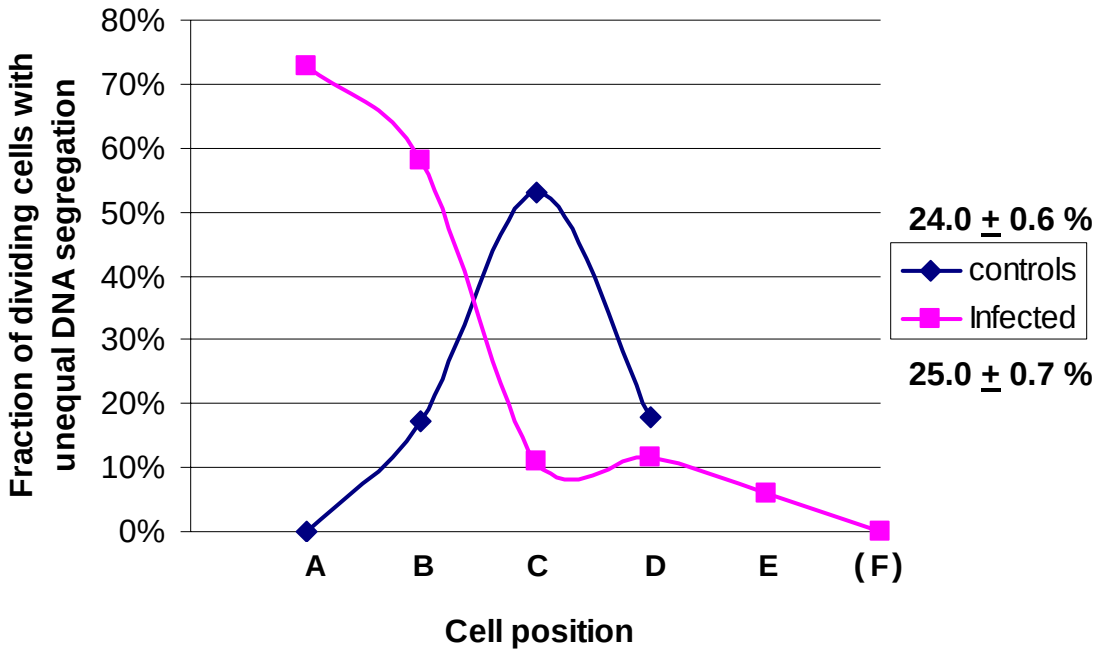

Level of the crypt	# of cells in the levels (total # cells accumulated up to this level)	% differences in DNA content Mean (range)	
		Controls	Infected
F (infected only)	256 (526)		**0.90** (0 – 3.3)
E	128 (258)		**2.42** (0 – 8.4)
D	64 (128)	**2.31** (0 – 10)	**2.75** (0 – 9.6)
C	32 (64)	**4.89** (0 – 12)	**3.01** (0 – 6.4)
B	16 (32)	**2.85** (0 – 11)	**9.83** (0 – **40**)
A (bottom, includes Stem Cells)	16 (16)	**0.89** (0 – 4.5)	**11.32** (0 – **60**)

Figure A4-3. Effect of *C. rodentium* infection on chromosomal instability in distal colon of FVB mice. Positional distribution of dividing cells with unequal DNA segregation (**upper panel**). While the overall rate of chromosomal instability is similar in both groups, the higher fraction of unequal DNA segregation was observed in the basal levels of hyperplastic crypts. Hyperplasia was also characterized by a higher aneuploidy in the basal levels of the crypt than in controls (**lower panel**). The difference of less than 5% in DNA content of daughter nuclei of anaphase/telophase cells was considered as equal DNA segregation. Numbers in red indicate unequal DNA segregation in dividing cells.

Table A4-1. Primers used for fluorigenic PCR amplification of MSI markers

MSI marker		Primers	Amplicon size[a], (bp)	Reference[b]
d15mit93	F	5'-**HEX**-AAG AAT TGG GGT GGG TAA GG-3'	168-170	Kohonen-Corish et
	R	5'-CAT GTG CAG AAT ACT TAC ACA TAT GC-3'	Black (Yellow)	al., 2002
				Guda et al., 2004
d17mit72	F	5'-GGC TTG GCG ACA TTC TAA TC-3'	209-211	Kohonen-Corish et
	R	5'-**6-FAM**-CAG CAA ATT AAC TTT CCC ATC A-3'	Blue	al., 2002
				Guda et al., 2004
d19mit36	F	5'-**TET**-ATA AGA CTT GAG GTT GAC CTC TGG-3'	192-194	Sohn et al., 2001
	R	5'-CTG TAA CAA TGG GAA CTG TAG GG-3'	Green	
d7mit91	F	5'-**6-FAM**-TCT TGC TTG CAT ACA CTC ACG-3'	162-164	Sohn et al., 2001
	R	5'-GAG ACA AAC CGC AGT CTC CT-3'	Blue	
d10mit2	F	5'- **TET**-CTG CTC ACA ACC CAT TCC TT-3'	147-149	Guda et al., 2004
	R	5'-GTT CAT TTG AGG CAC AAG CA-3'	Green	
uPAR	F	5'-GCT CAT CTT CGT TCC CTG TC-3'	101-103	Kohonen-Corish et
	R	5'- **HEX**-CAT TCG GTG GAA AGC TCT GA-3'	Black	al., 2002

a, amplicon size as detected for FVB mice in this study
b, reference studies in which MSI marker was associated with the development of colorectal tumors in mice

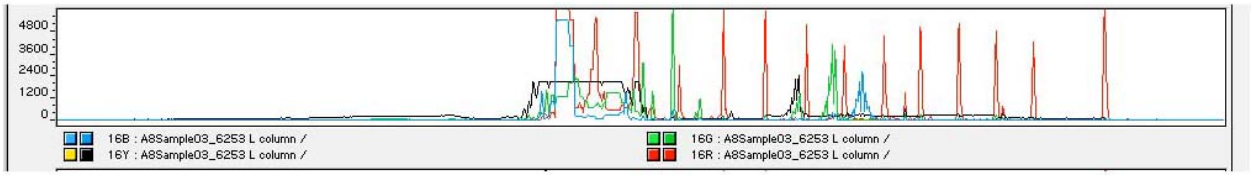

A.

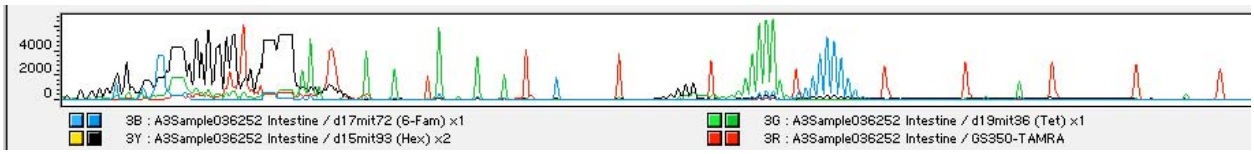

B.

Figure A4-4. Examples of size detection of fluorescently labeled PCR-amplified DNA from liver (**A**) and distal colon (**B**). Each true microsatellite peak is surrounded by stutter peaks of lower intensity with the appropriate delta (2 bases for dinucleotide repeats in this case) from the dominant peak. Peaks without stutter were considered to be non specific amplicons and were disregarded. Stutter peaks are considered a signature of amplification of a repetitive element lying within a forward and reverse primer set. DNA amplified with d15mit93 primers (Hex labeled) are shown in Black, d19mit36 primers (Tet labeled) in Green, and d17mit72 primers (6-Fam labeled) in Blue, and correspond to 168-170 bp, 192-194 bp, and 209-211 bp peaks, respectively. GS350 standards (TAMRA labeled) are shown in Red and have 13 ssDNA fragments from 50 to 350 nucleotides with 25 nt spacing.

Appendix 5: *C. rodentium* infection in mice with abnormal DNA damage repair.

Diana Borenshtein, Lisiane B. Meira, Barry H. Rickman, Prashant R. Nambiar, Leona D. Samson, David B. Schauer.

Biological Engineering Division, Center for Environmental Health Sciences, Division of Comparative Medicine, Massachusetts Institute of Technology, Cambridge, MA, 02139.

Portions of this work were submitted to PNAS

A5.1 Introduction

Bacterial interaction with epithelial cells may lead to the recruitment and activation of inflammatory cells, which in turn release potentially mutagenic products, such as nitric oxide (NO·) and hydroxyl radical (OH·) [Balkwill and Mantovani, 2001; Jaiswal et al., 2001]. These reactive species can directly damage DNA, leading to mutations, DNA strand breaks, and shortening of telomeres. Alkylated DNA bases are primarily recognized and repaired via the actions of two kinds of repair proteins; O^6-methylguanine DNA methyltransferases and 3-methyladenine (3MeA) DNA glycosylases. Methyltransferases, the main of which is encoded by *MGMT* in humans and *Mgmt* in mice, directly remove alkyl groups from O^6-alkylguanines (and to a lesser extent from O^4-alkylthymines), toxic lesions generated by most chemotherapeutic alkylating agents [Glassner et al., 1999]. 3MeA DNA glycosylase, encoded by *AAG*/*MPG/ANPG* in humans and *Aag*/*Mpg/Anpg* in mice, initiates the base excision repair pathway and serves as major DNA glycosylase for repair of 3MeA, hypoxanthine, and ethenoadenine (εA) DNA lesions [Engelward et al., 1996; Engelward et al., 1997]. Evidence from animal and human studies implicate the importance of both AAG and MGMT in colorectal carcinogenesis [Hofseth et al., 2003; Jackson et al., 2003; Povey et al., 2002; Wali et al., 1999]. As an example, increased levels of lipid peroxidation-derived etheno-adducts εA, εG and εC are found in the DNA of chronically inflammed tissues, including from colitis patients [Bartsch and Nair, 2006]. UC is associated with increases in AAG and apurinic/apyrimidinic endonuclease activity [Hofseth et al., 2003]. Recent studies from our laboratories indicate increased susceptibility to colitis and facilitated tumorigenesis in dextran sodium sulfate (DSS)-treated $Aag^{-/-}$ mice [Green et al., submitted]. In addition, nitric oxide inhibits and inactivates O^6-alkylguanine transferases, including O^6-methylguanine (O^6-MeG) DNA methyl-transferase (MGMT), by the formation of *S*-nitrosylcysteine adducts at the active site [Laval and Wink, 1994; Liu et al., 2002]. O^6-MeG adducts due to deficient MGMT activity most frequently occur in the normal mucosa of the distal colon and rectum [Jass et al., 2002; Povey et al., 2002], as well as in DMH-induced tumors in mice [Jackson et al., 2003]. Accumulation of unrepaired DNA damage can result in mutations and lead to development of colon cancer.

Considering pro-inflammatory and co-carcinogenic potential of *C. rodentium* (discussed in Chapter 1: Introduction), we were interested in investigating the effects of *C. rodentium* infection in mice deficient for DNA damage repair, namely $Aag^{-/-}$ and $Mgmt^{-/-}$ mice. Both models

were developed in laboratory of Dr. Leona Samson, and showed normal phenotype when no treatment was applied [Engelward et al., 1996; Engelward et al., 1997; Glassner et al., 1999]. In addition, similar approach was applied in C57BL6-Tg(*Aag*) mice (shortly tg-AAG) overexpressing 3MeA glycosylase.

A5.2 Results

C. rodentium infection does not cause overt disease in *Aag*$^{-/-}$ *and Mgmt*$^{-/-}$ mice.

C. rodentium infection was typical in both genotypes lacking DNA repair enzymes. Thus, differences in body weight between the infected and uninfected mice were comparable among all genotypes (Figure A5-1A, and A5-3A). Likewise, alterations in fecal bacterial shedding were similar in wild type and knockout mice (Figure A5-1B, and A5-3B). Splenomegaly was observed in C57BL/6 mice at 14-18 dpi (Figure A5-1C, and A5-3C), and to a lesser extent in *Aag*$^{-/-}$ mice. The trend to higher spleen weight was not significant in *Mgmt*$^{-/-}$ mice at 14 DPI. By 29 DPI, spleen weight was comparable to that of wild type and uninfected animals. In accordance with those results, no difference in colonic pathology was observed between different genotypes (Figure A5-2, and A5-4).

C. rodentium infection is attenuated in mice overexpressing *Aag*.

Based on the lack of obvious phenotype in *C. rodentium*-infected *Aag*$^{-/-}$ mice and reported association of increased AAG activity and protein levels with microsatellite instability in ulcerative colitis [Hofseth et al., 2003], we investigated the effects of the pathogen in mice overexpressing *Aag*. We proposed in the working hypothesis that transgenic mice will be sensitized to hyperproliferative effect of the *C. rodentium*.

Surprisingly, overexpression of *Aag* resulted in attenuated phenotype in infected mice. Thus, transgenic animals continued to grow whereas wild type mice had retarded growth rate in response to *C. rodentium* (Figure A5-5A). In addition, 3 out of 12 transgenic mice had very low fecal shedding at 4 dpi resulting in diminished increase in bacterial load compared with C57BL/6 mice (Figure A5-5B). Consistent with that, increase in colon weight, used as a marker for pathology, was attenuated in transgenic mice (Figure A5-5C). Histological scoring confirmed trends to lower pathology, which were statistically significant for epithelial defects and cumulative pathology index (Figure A5-6).

The results were confounded by contamination of mice from transgenic colony with *Helicobacter* spp (Figure A5-7), which could contribute to delayed infectivity as we showed in Appendix 2. Therefore, the attenuated phenotype of *C. rodentium* infection in tg-AAG mice cannot be truly attributed to overexpression of AAG.

A5.3 Discussion

Our data indicate that mice lacking DNA damage repair system, like AAG and MGMT, have normal classical response to *C. rodentium* infection which is not different form that demonstrated by wild type animals. None of the groups developed considerable dysplasia, suggesting that *C. rodentium* does not posses co-carcinogenic potential in those models, possibly due to compensatory effect of other repair mechanisms. In this case, dual-knockouts of *Aag* and *Mgmt* with each other or other participants in DNA damage repair may have a different outcome in response to the pathogen. In addition, the acute nature of infection and associated colitis may also play a role. Thus, treatment with 5 cycles of DSS, used to model chemical-induced colitis, did not lead to tumor formation and substantial dysplasia in $Aag^{-/-}$ mice despite profound inflammation and epithelial damage in those animals [Green et al., submitted]. Only when longer administration of DSS was applied to promote augmentation of chronic colitis, tumor incidence has increased in *Aag*-deficient animals and the differences between the genotypes become more obvious. Moreover, single administration of DSS resulted in no phenotype in $Aag^{-/-}$ mice [Green, Meira, and Samson, unpublished results], consistent with our observations and suggesting that chronic inflammation is required for tumor promotion in that model.

The most interesting result was attenuated response to *C. rodentium* infection in mice overexpressing *Aag*. While amelioration in pathology can be explained by better regenerative capacity of transgenic mice, delayed infectivity and subclinical disease was unexpected in those animals. Further studies are needed to understand the mechanisms of such effects. However, possible contribution of *Helicobacter* spp contamination to the observed phenotype should be considered and needs further clarification. In addition, studies in transgenic mice on susceptible background (FVB) will be helpful to clarify the role of AAG on susceptibility to *C. rodentium* infection.

A5.4 Experimental Design and selected Methods

Four to five-weeks-old *Aag*$^{-/-}$, *Mgmt*$^{-/-}$, C57BL6-Tg(*Aag*) and C57BL/6Tac or wild type littermates mice of both genders were inoculated with ~10^9 CFU of DBS120 and 0.1 ml LB or 3% (w/v) sodium bicarbonate as described in Appendix 1: General Methods. Number of mice was n = 6-20 for wild type, n = 6-13 for *Aag*$^{+/-}$ mice, and n = 4-16 for *Aag*$^{-/-}$ mice and followed for 18 or 29 DPI. For *Mgmt*$^{-/-}$ study, n = 6-8 wild type and n = 4-6 knockout animals for 14 DPI were used. Mice were monitored daily for morbidity and necropsied by CO_2 overdose at designated time points. Sample collection was processed routinely as described in Appendix 1. The animals were screened for the *Helicobacter* spp. contamination by amplification of isolated DNA with *Helicobacter*-specific primers C05 and C97 creating a 1.2kb PCR product (Appendix 2, [Fox et al., 1998]). *H. bilis* and water were used as positive and negative controls for PCR reactions, respectively.

A5.5 Figures

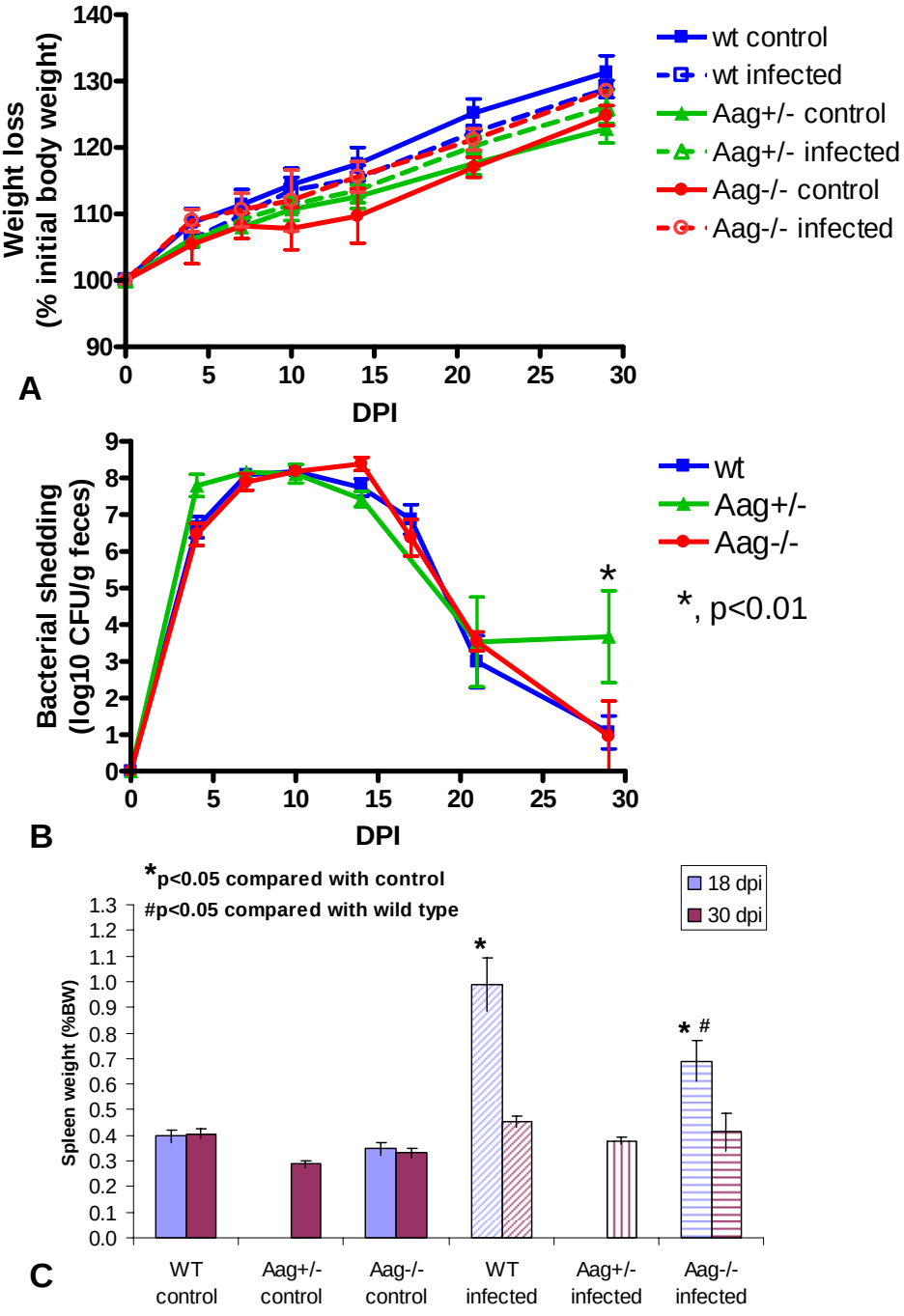

Figure A5-1. *C .rodentium* infection in mice with *Aag* deficiency.

A. Comparable clinical disease in wild type and *Aag-/-* deficient mice.

B. Comparable fecal bacterial shedding ($p<0.01$ for $Aag^{+/-}$ mice at 29 DPI by two-way ANOVA followed with Bonferroni post-test).

C. Splenomegaly was more significant in wild type animals at 18 DPI, but returned to normal levels at 29 DPI ($p<0.05$ by ANOVA and post-hoc *t* test).

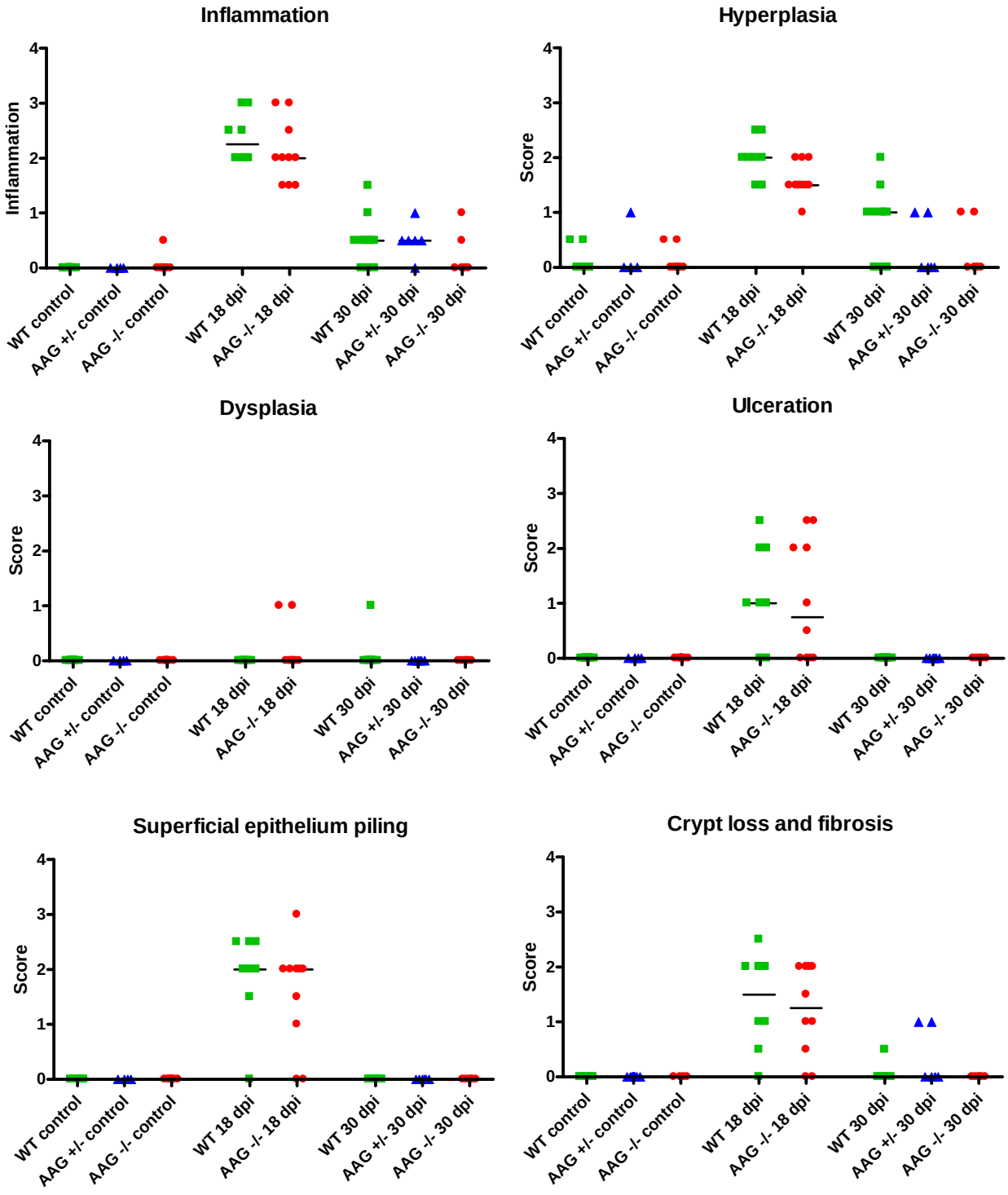

Figure A5-2. Pathology in *Aag*$^{-/-}$ mice infected with *C. rodentium*.
None of the histological parameters were different between the groups. Lines indicate group median.

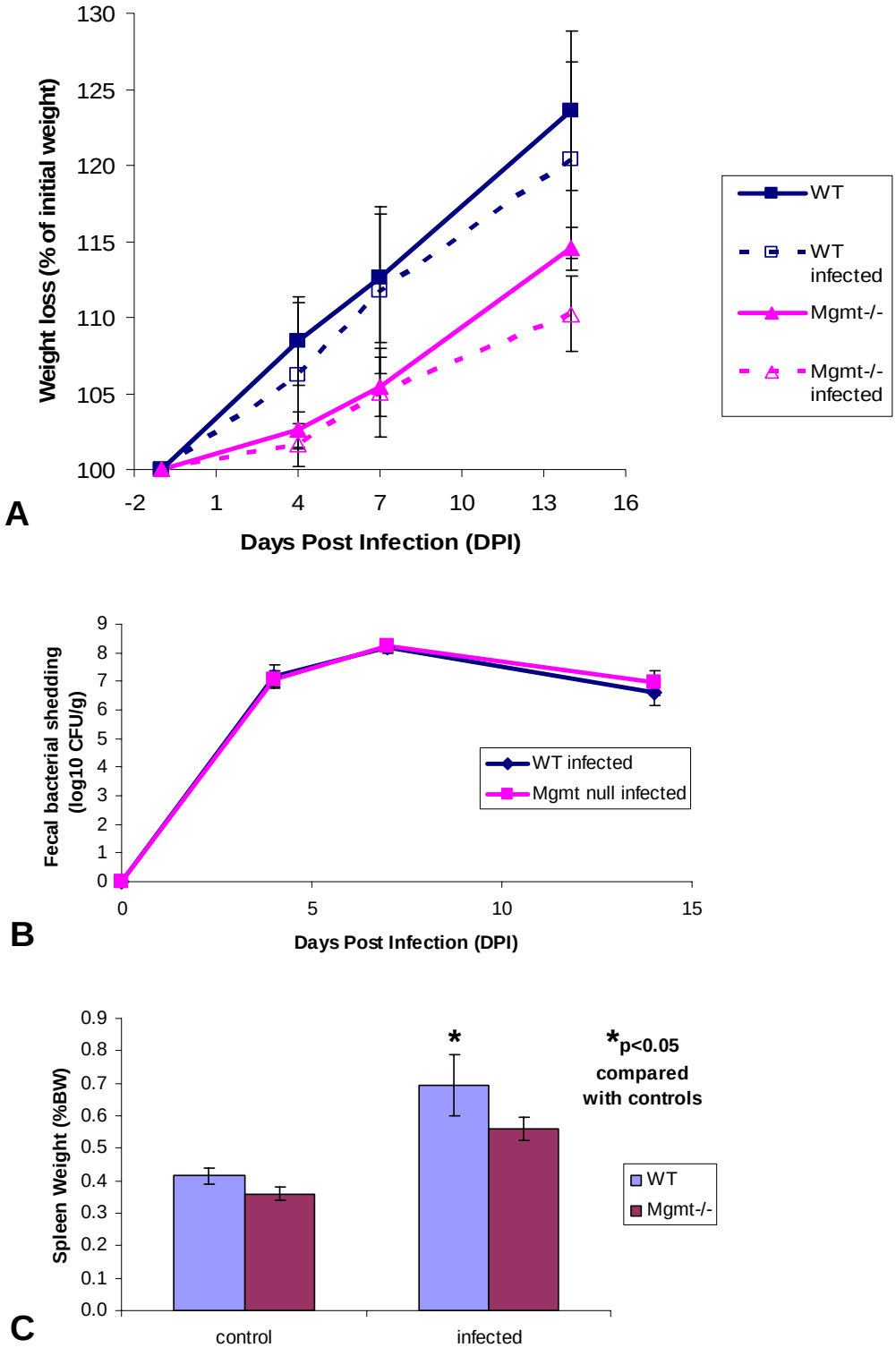

Figure A5-3. *C. rodentium* infection in mice *Mgmt* deficiency.

A. Comparable clinical disease in wild type and *Mgmt-/-*deficient mice.

B. Comparable fecal bacterial shedding.

C. Splenomegaly was more significant in wild type animals than in *Mgmt-/-*deficient mice at 14 DPI ($p<0.05$ by ANOVA and post-hoc *t* test).

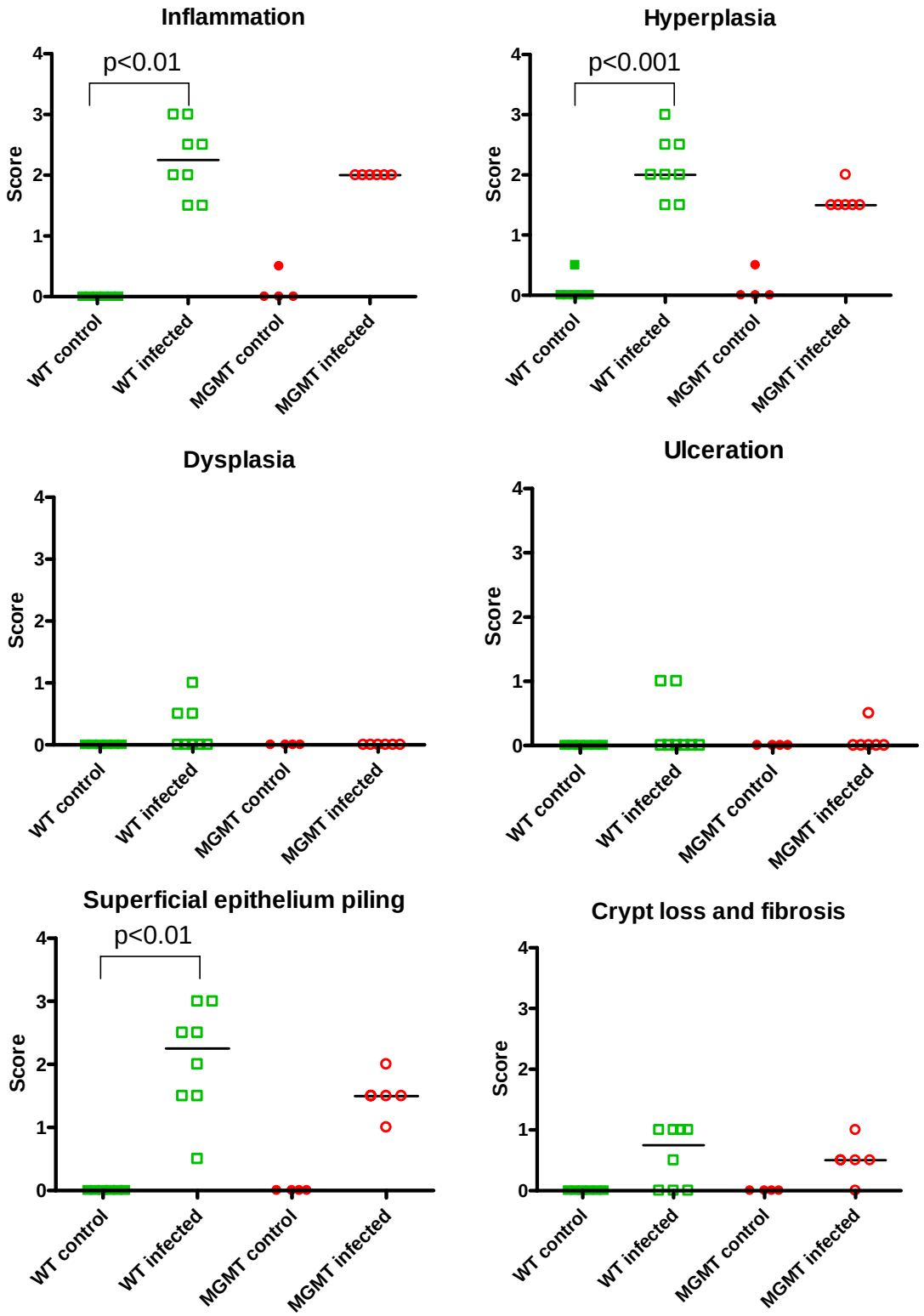

Figure A5-4. Pathology in *Mgmt*$^{-/-}$ mice infected with *C. rodentium*.
None of the histological parameters were different between the genotypes. Significant increases in inflammation, hyperplasia and piled epithelium in response to infection were observed in wild type group only ($p<0.01$ by Kruskal-Wallis test followed by Dunn's Multiple Comparison Test).

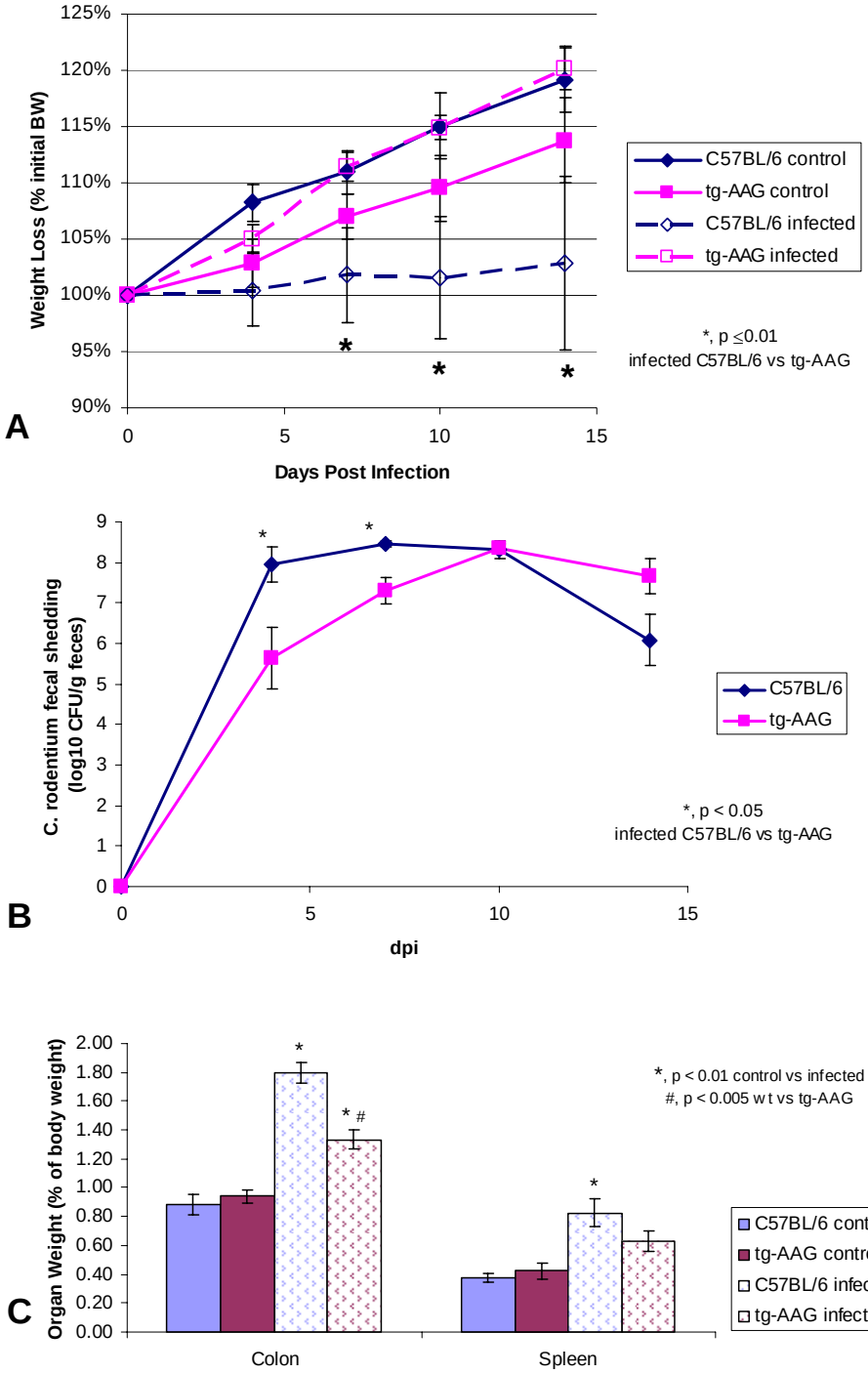

Figure A5-5. Mice overexpressing *Aag* are protected from deleterious effects of *C. rodentium* infection.

- **A.** Experimental inoculation of mice with *C. rodentium* impairs weight gain in wild type, but not transgenic animals beginning by 7 dpi ($p<0.01$ by two-way ANOVA followed by Bonferroni post-test).
- **B.** Increase in fecal bacterial shedding was delayed in 25% of transgenic mice resulting in attenuated response in *Aag* overexpressing animals ($p<0.05$ by Student's *t* test).
- **C.** Infection resulted in significant increase in colon and spleen weights in wild type mice at 14 dpi. The increase in organ weight in infected tg-AAG mice was attenuated and reached statistical significance for colon weight only ($p<0.01$ by ANOVA and post-hoc *t* test).

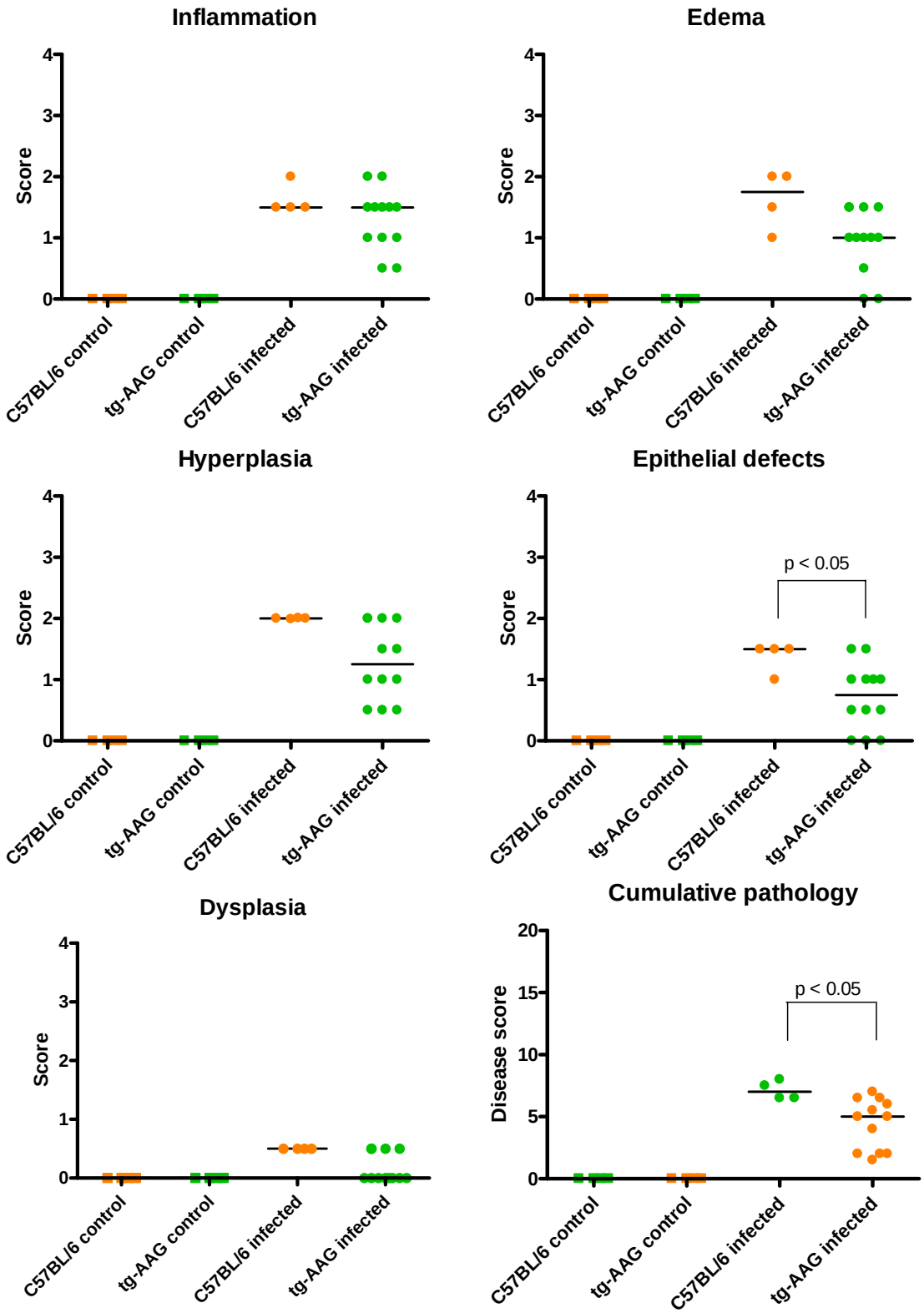

Figure A5-6. Intestinal pathology in *C. rodentium*-infected mice overexpressing *Aag*.
Although transgenic mice tended to develop less *C. rodentium*-induced pathology at 14 dpi, the statistical significance was reached for epithelial defects and cumulative disease score only ($p<0.01$ by Kruskal-Wallis test followed by Dunn's Multiple Comparison Test).

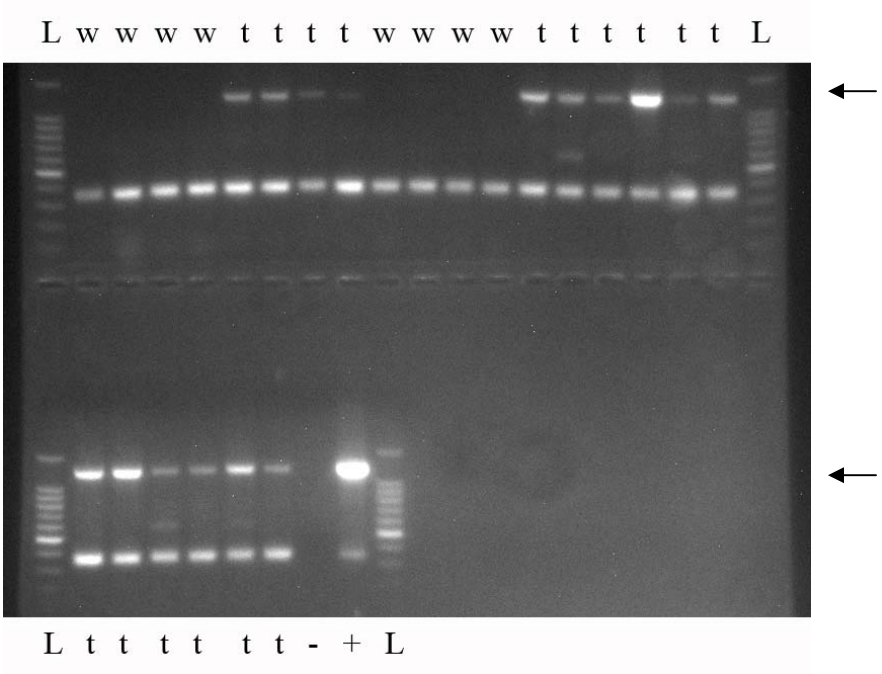

Figure A5-7. *Helicobacter* spp. contamination of mice overexpressing *Aag*.
All the transgenic animals were positive for *Helicobacter* spp as indicated by PCR.
L,100 bp ladder; w, wild type mice; t, transgenic mice; -, negative control; +, positive control.

Appendix 6: Abbreviations

ε	Etheno
3MeA	3-methyladenine
AAG, *Aag*	alkyladenine glycosylase, 3-methyladenine DNA glycosylase (also known as MPG, N-methylpurine-DNA glycosylase)
ADI	acute diarrheal illness
A/E	attaching and effacing
CD	Crohn's disease
CFU	colony forming units
DMH	1,2-dimethylhydrazine
DPI , dpi	days post-inoculation
DSS	dextran sodium sulfate
EHEC	enterohemorrhagic *E. coli*
EPEC	enteropathogenic *E. coli*
FVB	FVB/N mice
H&E	hemotoxylin and eosin
IBD	inflammatory bowel disease
IFN	interferon
IL	interleukin
LB	Lennox L broth
LEE	locus of enterocyte effacement
MLN	mesenteric lymph nodes
PBS	phosphate buffered saline
PCR	polymerase chain reaction
qRT-PCR	quantitative real-time reverse-transcriptase polymerase chain reaction
SEM	standard error of mean
SW	Swiss Webster mice
tg-AAG	C57BL/6-Tg(*Aag*) mice overexpressing AAG
TMCH	transmissible murine colonic hyperplasia
TNF	tumor necrosis factor
UC	Ulcerative colitis
WPI	weeks post-inoculation
wt	wild type

Appendix 7: References

1. Alfonso-Jaume MA, Bergman MR, Mahimkar R, Cheng S, Jin ZQ, Karliner JS, Lovett DH. Cardiac ischemia-reperfusion injury induces matrix metalloproteinase-2 expression through the AP-1 components FosB and JunB. Am J Physiol Heart Circ Physiol 2006; 291: H1838-46.
2. Allen KP, Randolph MM, Fleckenstein JM. Importance of heat-labile enterotoxin in colonization of the adult mouse small intestine by human enterotoxigenic *Escherichia coli* strains. Infect Immun 2006; 74: 869-75.
3. Alleva DG, Johnson EB, Wilson J, Beller DI, Conlon PJ. SJL and NOD macrophages are uniquely characterized by genetically programmed, elevated expression of the IL-12(p40) gene, suggesting a conserved pathway for the induction of organ-specific autoimmunity. J Leukoc Biol 2001; 69: 440-8.
4. Al-Majali AM, Asem EK, Lamar CH, Robinson JP, Freeman MJ, Saeed AM. Studies on the mechanism of diarrhoea induced by *Escherichia coli* heat-stable enterotoxin (STa) in newborn calves. Vet Res Commun 2000; 24: 327-38.
5. Al-Shahrour F, Diaz-Uriarte R, Dopazo J. Discovering molecular functions significantly related to phenotypes by combining gene expression data and biological information. Bioinformatics. 2005; 21: 2988-93.
6. Al-Shahrour F, Diaz-Uriarte R, Dopazo J. FatiGO: a web tool for finding significant associations of Gene Ontology terms with groups of genes. Bioinformatics 2004; 20: 578-80.
7. Alvarez BV, Loiselle FB, Supuran CT, Schwartz GJ, Casey JR. Direct extracellular interaction between carbonic anhydrase IV and the human NBC1 sodium/bicarbonate co-transporter. Biochemistry 2003; 42: 12321-9.
8. Anderle P, Rakhmanova V, Woodford K, Zerangue N, Sadee W. Messenger RNA expression of transporter and ion channel genes in undifferentiated and differentiated Caco-2 cells compared to human intestines. Pharm Res 2003; 20: 3-15.
9. Bachmann O, Riederer B, Rossmann H, Groos S, Schultheis PJ, Shull GE, Gregor M, Manns MP, Seidler U. The Na+/H+ exchanger isoform 2 is the predominant NHE isoform in murine colonic crypts and its lack causes NHE3 upregulation. Am J Physiol Gastrointest Liver Physiol 2004; 287: G125-33.
10. Baker AM, Grekova MC, Richert JR. EAE susceptibility in FVB mice. J Neurosci Res 2000; 61: 140-5.
11. Balkwill F, Mantovani A. Inflammation and cancer: back to Virchow? Lancet 2001; 357: 539-45.
12. Baqar S, Burg E, Murphy JR. Mouse models of *Campylobacter jejuni* infection. *In:* Zak O, Sande MA, eds. Handbook of animal models of infection. Experimental models in antimicrobial chemotherapy. San Diego: Academic Press, 2000: 223-40.
13. Barmeyer C, Harren M, Schmitz H, Heinzel-Pleines U, Mankertz J, Seidler U, Horak I, Wiedenmann B, Fromm M, Schulzke JD. Mechanisms of diarrhea in the interleukin-2-deficient mouse model of colonic inflammation. Am J Physiol Gastrointest Liver Physiol 2004; 286: G244-52.
14. Barrett KE, Bigby TD. Involvement of arachidonic acid in the chloride secretory response of intestinal epithelial cells. Am J Physiol 1993; 264: C446-52.
15. Barrett KE, Cohn JA, Huott PA, Wasserman SI, Dharmsathaphorn K. Immune-related intestinal chloride secretion. II. Effect of adenosine on T84 cell line. Am J Physiol 1990; 258: C902-12.
16. Barrett KE, Keely SJ. Chloride secretion by the intestinal epithelium: molecular basis and regulatory aspects. Annu Rev Physiol 2000; 62: 535-72.
17. Barrett KE. Immune-related intestinal chloride secretion. III. Acute and chronic effects of mast cell mediators on chloride secretion by a human colonic epithelial cell line. J Immunol 1991; 147: 959-64.
18. Barthold SW, Beck D. Modification of early dimethylhydrazine carcinogenesis by colonic mucosal hyperplasia. Cancer Res 1980; 40: 4451-5.

19. Barthold SW, Coleman GL, Bhatt PN, Osbaldiston GW, Jonas AM. The etiology of transmissible murine colonic hyperplasia. Lab Anim Sci 1976; 26: 889-94.
20. Barthold SW, Coleman GL, Jacoby RO, Livestone EM, Jonas AM. Transmissible murine colonic hyperplasia. Vet Pathol 1978; 15: 223-36.
21. Barthold SW, Jonas AM. Morphogenesis of early 1, 2-dimethylhydrazine-induced lesions and latent period reduction of colon carcinogenesis in mice by a variant of *Citrobacter freundii*. Cancer Res 1977; 37: 4352-60.
22. Barthold SW, Osbaldiston GW, Jonas AM. Dietary, bacterial, and host genetic interactions in the pathogenesis of transmissible murine colonic hyperplasia. Lab Anim Sci 1977; 27: 938-45.
23. Barthold SW. "Muromics": genomics from the perspective of the laboratory mouse. Comp Med 2002; 52: 206-23.
24. Barthold SW. Autoradiographic cytokinetics of colonic mucosal hyperplasia in mice. Cancer Res 1979; 39: 24-9.
25. Barthold SW. The microbiology of transmissible murine colonic hyperplasia. Lab Anim Sci 1980; 30: 167-73.
26. Bartsch H, Nair J. Chronic inflammation and oxidative stress in the genesis and perpetuation of cancer: role of lipid peroxidation, DNA damage, and repair. Langenbecks Arch Surg 2006; 391: 499-510.
27. Bates MD, Erwin CR, Sanford LP, Wiginton D, Bezerra JA, Schatzman LC, Jegga AG, Ley-Ebert C, Williams SS, Steinbrecher KA, Warner BW, Cohen MB, Aronow BJ. Novel genes and functional relationships in the adult mouse gastrointestinal tract identified by microarray analysis. Gastroenterology 2002; 122: 1467-82.
28. Beck JA, Lloyd S, Hafezparast M, Lennon-Pierce M, Eppig JT, Festing MF, Fisher EM. Genealogies of mouse inbred strains. Nat Genet 2000; 24: 23-5.
29. Bekku S, Mochizuki H, Takayama E, Shinomiya N, Fukamachi H, Ichinose M, Tadakuma T, Yamamoto T. Carbonic anhydrase I and II as a differentiation marker of human and rat colonic enterocytes. Res Exp Med (Berl) 1998; 198: 175-85.
30. Berkes J, Viswanathan VK, Savkovic SD, Hecht G. Intestinal epithelial responses to enteric pathogens: effects on the tight junction barrier, ion transport, and inflammation. Gut 2003; 52: 439-51.
31. Bernstein CN, Blanchard JF, Kliewer E, Wajda A. Cancer risk in patients with inflammatory bowel disease: a population-based study. Cancer 2001; 91: 854-62.
32. Beutner U, Launois P, Ohteki T, Louis JA, MacDonald HR. Natural killer-like T cells develop in SJL mice despite genetically distinct defects in NK1.1 expression and in inducible interleukin-4 production. Eur J Immunol 1997; 27: 928-34.
33. Birkenkamp-Demtroder K, Olesen SH, Sorensen FB, Laurberg S, Laiho P, Aaltonen LA, Orntoft TF. Differential gene expression in colon cancer of the caecum versus the sigmoid and rectosigmoid. Gut 2005; 54: 374-84.
34. Bischoff SC, Wedemeyer J, Herrmann A, Meier PN, Trautwein C, Cetin Y, Maschek H, Stolte M, Gebel M, Manns MP. Quantitative assessment of intestinal eosinophils and mast cells in inflammatory bowel disease. Histopathology 1996; 28: 1-13.
35. Blumberg RS, Saubermann LJ, Strober W. Animal models of mucosal inflammation and their relation to human inflammatory bowel disease. Curr Opin Immunol 1999; 11: 648-56.
36. Boivin GP, Washington K, Yang K, Ward JM, Pretlow TP, Russell R, Besselsen DG, Godfrey VL, Doetschman T, Dove WF, Pitot HC, Halberg RB, Itzkowitz SH, Groden J, Coffey RJ. Pathology of mouse models of intestinal cancer: consensus report and recommendations. Gastroenterology 2003; 124: 762-77.
37. Boll M, Herget M, Wagener M, Weber WM, Markovich D, Biber J, Clauss W, Murer H, Daniel H. Expression cloning and functional characterization of the kidney cortex high-affinity proton-coupled peptide transporter. Proc Natl Acad Sci U S A 1996; 93: 284-9.
38. Booth C, Potten CS. Gut instincts: thoughts on intestinal epithelial stem cells. J Clin Invest. 2000; 105: 1493-9.
39. Borenshtein D, Nambiar PR, Groff EB, Fox JG, Schauer DB. Development of fatal colitis in FVB mice infected with *Citrobacter rodentium*. Submitted.
40. Borthakur A, Gill RK, Hodges K, Ramaswamy K, Hecht G, Dudeja PK. Enteropathogenic *Escherichia coli* inhibits butyrate uptake in Caco-2 cells by altering the apical membrane MCT1

level. Am J Physiol Gastrointest Liver Physiol 2006; 290: G30-5.
41. Boshuizen JA, Reimerink JH, Korteland-van Male AM, van Ham VJ, Koopmans MP, Buller HA, Dekker J, Einerhand AW. Changes in small intestinal homeostasis, morphology, and gene expression during rotavirus infection of infant mice. J Virol 2003; 77: 13005-16.
42. Brandt EB, Strait RT, Hershko D, Wang Q, Muntel EE, Scribner TA, Zimmermann N, Finkelman FD, Rothenberg ME. Mast cells are required for experimental oral allergen-induced diarrhea. J Clin Invest 2003; 112: 1666-77.
43. Brennan PC, Fritz TE, Flynn RJ, Poole CM. *Citrobacter freundii* associated with diarrhea in a laboratory mice. Lab Anim Care 1965; 15:266-75.
44. Bry L, Brenner MB. Critical role of T cell-dependent serum antibody, but not the gut-associated lymphoid tissue, for surviving acute mucosal infection with *Citrobacter rodentium*, an attaching and effacing pathogen. J Immunol 2004; 172: 433-41.
45. Bry L, Brigl M, Brenner MB. CD4+-T-cell effector functions and costimulatory requirements essential for surviving mucosal infection with *Citrobacter rodentium*. Infect Immun 2006; 74: 673-81.
46. Cahill RJ, Foltz CJ, Fox JG, Dangler CA, Powrie F, Schauer DB. Inflammatory bowel disease: an immunity-mediated condition triggered by bacterial infection with *Helicobacter hepaticus*. Infect Immun 1997; 65: 3126-31.
47. Casburn-Jones AC, Farthing MJ. Management of infectious diarrhoea. Gut 2004; 53: 296-305.
48. Cenac N, Cellars L, Steinhoff M, Andrade-Gordon P, Hollenberg MD, Wallace JL, Fiorucci S, Vergnolle N. Proteinase-activated receptor-1 is an anti-inflammatory signal for colitis mediated by a type 2 immune response. Inflamm Bowel Dis 2005; 11: 792-8.
49. Chapman JM, Knoepp SM, Byeon MK, Henderson KW, Schweinfest CW. The colon anion transporter, down-regulated in adenoma, induces growth suppression that is abrogated by E1A. Cancer Res 2002; 62: 5083-8.
50. Charney AN, Alexander-Chacko J, Gummaconda R, Egnor RW. Non-catalytic role of carbonic anhydrase in rat intestinal absorption. Biochim Biophys Acta 2002; 1573: 141-8.
51. Charney AN, Dagher PC. Acid-base effects on colonic electrolyte transport revisited. Gastroenterology 1996; 111: 1358-68.
52. Charney AN, Egnor RW, Henner D, Rashid H, Cassai N, Sidhu GS. Acid-base effects on intestinal Cl- absorption and vesicular trafficking. Am J Physiol Cell Physiol 2004; 286: C1062-70.
53. Chen CC, Louie S, McCormick B, Walker WA, Shi HN. Concurrent infection with an intestinal helminth parasite impairs host resistance to enteric *Citrobacter rodentium* and enhances *Citrobacter*-induced colitis in mice. Infect Immun 2005a; 73: 5468-81.
54. Chen CC, Louie S, McCormick BA, Walker WA, Shi HN. Helminth-primed dendritic cells alter the host response to enteric bacterial infection. J Immunol 2006; 176: 472-83.
55. Chen CC, Louie S, Shi HN, Walker WA. Preinoculation with the probiotic *Lactobacillus acidophilus* early in life effectively inhibits murine *Citrobacter rodentium* colitis. Pediatr Res 2005b; 58: 1185-91.
56. Chen F, Ma L, Al-Ansari N, Shneider B. The role of AP-1 in the transcriptional regulation of the rat apical sodium-dependent bile acid transporter. J Biol Chem 2001; 276: 38703-14.
57. Chernova MN, Jiang L, Shmukler BE, Schweinfest CW, Blanco P, Freedman SD, Stewart AK, Alper SL. Acute regulation of the SLC26A3 congenital chloride diarrhoea anion exchanger (DRA) expressed in *Xenopus* oocytes. J Physiol 2003; 549: 3-19.
58. Chia R, Achilli F, Festing MF, Fisher EM. The origins and uses of mouse outbred stocks. Nat Genet 2005; 37: 1181-6.
59. Clarke LL, Harline MC. Dual role of CFTR in cAMP-stimulated HCO3- secretion across murine duodenum. Am J Physiol 1998; 274: G718-26.
60. Cobb BR, Ruiz F, King CM, Fortenberry J, Greer H, Kovacs T, Sorscher EJ, Clancy JP. A(2) adenosine receptors regulate CFTR through PKA and PLA(2). Am J Physiol Lung Cell Mol Physiol 2002; 282: L12-25.
61. Collington GK, Booth IW, Knutton S. Rapid modulation of electrolyte transport in Caco-2 cell monolayers by enteropathogenic *Escherichia coli* (EPEC) infection. Gut 1998; 42:200-7.
62. Collins JF, Kiela PR, Xu H, Zeng J, Ghishan FK. Increased NHE2 expression in rat intestinal epithelium during ontogeny is transcriptionally mediated. Am J Physiol 1998; 275: C1143-50.

63. Collins JF, Xu H, Kiela PR, Zeng J, Ghishan FK. Functional and molecular characterization of NHE3 expression during ontogeny in rat jejunal epithelium. Am J Physiol 1997; 273: C1937-46.
64. Coombes BK, Hardwidge PR, Finlay BB. Interpreting the host-pathogen dialogue through microarrays. Adv Appl Microbiol 2004; 54: 291-331.
65. Crane JK, Olson RA, Jones HM, Duffey ME. Release of ATP during host cell killing by enteropathogenic E. coli and its role as a secretory mediator. Am J Physiol Gastrointest Liver Physiol 2002; 283: G74-86.
66. Croner RS, Foertsch T, Brueckl WM, Guenther K, Siebenhaar R, Stremmel C, Matzel KE, Papadopoulos T, Kirchner T, Behrens J, Klein-Hitpass L, Stuerzl M, Hohenberger W, Reingruber B. Common denominator genes that distinguish colorectal carcinoma from normal mucosa. Int J Colorectal Dis 2005; 20: 353-62.
67. Crowe SE, Luthra GK, Perdue MH. Mast cell mediated ion transport in intestine from patients with and without inflammatory bowel disease. Gut 1997; 41: 785-92.
68. Crowe SE, Perdue MH. Functional abnormalities in the intestine associated with mucosal mast cell activation. Reg Immunol 1992; 4: 113-7.
69. D'Arienzo R, Maurano F, Mazzarella G, Luongo D, Stefanile R, Ricca E, Rossi M. *Bacillus subtilis* spores reduce susceptibility to *Citrobacter rodentium*-mediated enteropathy in a mouse model. Res Microbiol 2006; 157: 891-7.
70. de Grado M, Rosenberger CM, Gauthier A, Vallance BA, Finlay BB. Enteropathogenic *Escherichia coli* infection induces expression of the early growth response factor by activating mitogen-activated protein kinase cascades in epithelial cells. Infect Immun. 2001; 69: 6217-24.
71. Dean P, Maresca M, Schuller S, Phillips AD, Kenny B. Potent diarrheagenic mechanism mediated by the cooperative action of three enteropathogenic *Escherichia coli*-injected effector proteins. Proc Natl Acad Sci U S A 2006; 103: 1876-81.
72. Deng W, Li Y, Vallance BA, Finlay BB. Locus of enterocyte effacement from *Citrobacter rodentium*: sequence analysis and evidence for horizontal transfer among attaching and effacing pathogens. Infect Immun 2001; 69: 6323-35.
73. Deng W, Puente JL, Gruenheid S, Li Y, Vallance BA, Vazquez A, Barba J, Ibarra JA, O'Donnell P, Metalnikov P, Ashman K, Lee S, Goode D, Pawson T, Finlay BB. Dissecting virulence: systematic and functional analyses of a pathogenicity island. Proc Natl Acad Sci U S A 2004; 101: 3597-602.
74. Deng W, Vallance BA, Li Y, Puente JL, Finlay BB. *Citrobacter rodentium* translocated intimin receptor (Tir) is an essential virulence factor needed for actin condensation, intestinal colonization and colonic hyperplasia in mice. Mol Microbiol 2003; 48: 95-115.
75. Dinkova-Kostova AT, Liby KT, Stephenson KK, Holtzclaw WD, Gao X, Suh N, Williams C, Risingsong R, Honda T, Gribble GW, Sporn MB, Talalay P. Extremely potent triterpenoid inducers of the phase 2 response: correlations of protection against oxidant and inflammatory stress. Proc Natl Acad Sci U S A 2005; 102: 4584-9.
76. Edelmann W, Yang K, Umar A, Heyer J, Lau K, Fan K, Liedtke W, Cohen PE, Kane MF, Lipford JR, Yu N, Crouse GF, Pollard JW, Kunkel T, Lipkin M, Kolodner R, Kucherlapati R. Mutation in the mismatch repair gene *Msh6* causes cancer susceptibility. Cell 1997; 91: 467-77.
77. Ediger RD, Kovatch RM, Rabstein MM. Colitis in mice with a high incidence of rectal prolapse. Lab Anim Sci 1974; 24: 488-94.
78. Eliason BC, Lewan RB. Gastroenteritis in children: principles of diagnosis and treatment. Am Fam Physician 1998; 58: 1769-76.
79. Elson CO, Cong Y, McCracken VJ, Dimmitt RA, Lorenz RG, Weaver CT. Experimental models of inflammatory bowel disease reveal innate, adaptive, and regulatory mechanisms of host dialogue with the microbiota. Immunol Rev 2005; 206: 260-76.
80. Engelward BP, Dreslin A, Christensen J, Huszar D, Kurahara C, Samson L. Repair-deficient 3-methyladenine DNA glycosylase homozygous mutant mouse cells have increased sensitivity to alkylation-induced chromosome damage and cell killing. EMBO J 1996; 15: 945-52.
81. Engelward BP, Weeda G, Wyatt MD, Broekhof JL, de Wit J, Donker I, Allan JM, Gold B, Hoeijmakers JH, Samson LD. Base excision repair deficient mice lacking the *Aag* alkyladenine DNA glycosylase. Proc Natl Acad Sci U S A 1997; 94: 13087-92.

82. Engle SJ, Hoying JB, Boivin GP, Ormsby I, Gartside PS, Doetschman T. Transforming growth factor beta1 suppresses nonmetastatic colon cancer at an early stage of tumorigenesis. Cancer Res 1999; 59: 3379-86.
83. Erdman SE, Sohn JJ, Rao VP, Nambiar PR, Ge Z, Fox JG, Schauer DB. CD4+CD25+ regulatory lymphocytes induce regression of intestinal tumors in *Apc*$^{Min/+}$ mice. Cancer Res 2005; 65: 3998-4004.
84. Favaloro FG Jr, Honda T, Honda Y, Gribble GW, Suh N, Risingsong R, Sporn MB. Design and synthesis of tricyclic compounds with enone functionalities in rings A and C: a novel class of highly active inhibitors of nitric oxide production in mouse macrophages. J Med Chem 2002; 45: 4801-5.
85. Festing MFW; Inbred strains of mice. Mouse Genome Informatics, The Jackson Laboratory, Bar Harbor, Maine. World Wide Web (www.informatics.jax.org).
86. Field M. Intestinal ion transport and the pathophysiology of diarrhea. J Clin Invest 2003; 111: 931-43.
87. Fischer H, Stenling R, Rubio C, Lindblom A. Differential expression of aquaporin 8 in human colonic epithelial cells and colorectal tumors. BMC Physiol 2001; 1: 1.
88. Flach CF, Lange S, Jennische E, Lonnroth I. Cholera toxin induces expression of ion channels and carriers in rat small intestinal mucosa. FEBS Lett 2004; 561: 122-6.
89. Fleming RE, Crouch EC, Ruzicka CA, Sly WS. Pulmonary carbonic anhydrase IV: developmental regulation and cell-specific expression in the capillary endothelium. Am J Physiol 1993; 265: L627-35.
90. Fonti R, Latella G, Caprilli R, Frieri G, Marcheggiano A, Sambuy Y. Carbonic anhydrase I reduction in colonic mucosa of patients with active ulcerative colitis. Dig Dis Sci 1998; 43: 2086-92.
91. Fox JG, Dewhirst FE, Shen ZL, Feng Y, Taylor NS, Paster BJ, Ericson RL, Lau CN, Correa P, Araya JC, Roa I. Hepatic *helicobacter* species identified in bile and gallbladder tissue from Chileans with chronic cholecystitis. Gastroenterology 1998; 114: 755–63.
92. Frankel G, Phillips AD, Novakova M, Field H, Candy DC, Schauer DB, Douce G, Dougan G. Intimin from enteropathogenic Escherichia coli restores murine virulence to a *Citrobacter rodentium eae*A mutant: induction of an immunoglobulin A response to intimin and EspB. Infect Immun 1996; 64: 5315-25.
93. Frankel G, Phillips AD, Rosenshine I, Dougan G, Kaper JB, Knutton S. Enteropathogenic and enterohaemorrhagic *Escherichia coli*: more subversive elements. Mol Microbiol 1998; 30: 911-21.
94. Garmendia J, Frankel G, Crepin VF. Enteropathogenic and enterohemorrhagic *Escherichia coli* infections: translocation, translocation, translocation. Infect Immun 2005; 73: 2573-85.
95. Ge Z, Feng Y, Taylor NS, Ohtani M, Polz MF, Schauer DB, Fox JG. Colonization dynamics of altered Schaedler flora is influenced by gender, aging, and *Helicobacter hepaticus* infection in the intestines of Swiss Webster mice. Appl Environ Microbiol 2006; 72: 5100-3.
96. George JW, Lerche NW. Electrolyte abnormalities associated with diarrhea in rhesus monkeys: 100 cases (1986-1987). J Am Vet Med Assoc 1990; 196: 1654-8.
97. Ghaem-Maghami M, Simmons CP, Daniell S, Pizza M, Lewis D, Frankel G, Dougan G. Intimin-specific immune responses prevent bacterial colonization by the attaching-effacing pathogen *Citrobacter rodentium*. Infect Immun 2001; 69: 5597-605.
98. Glassner BJ, Weeda G, Allan JM, Broekhof JL, Carls NH, Donker I, Engelward BP, Hampson RJ, Hersmus R, Hickman MJ, Roth RB, Warren HB, Wu MM, Hoeijmakers JH, Samson LD. DNA repair methyltransferase (*Mgmt*) knockout mice are sensitive to the lethal effects of chemotherapeutic alkylating agents. Mutagenesis 1999; 14: 339-47.
99. Goldfarb DS, Sly WS, Waheed A, Charney AN. Acid-base effects on electrolyte transport in CA II-deficient mouse colon. Am J Physiol Gastrointest Liver Physiol 2000; 278: G409-15.
100. Goncalves NS, Ghaem-Maghami M, Monteleone G, Frankel G, Dougan G, Lewis DJ, Simmons CP, MacDonald TT. Critical role for tumor necrosis factor alpha in controlling the number of lumenal pathogenic bacteria and immunopathology in infectious colitis. Infect Immun 2001; 69: 6651-9.
101. Gostjeva EV, Zukerberg L, Chung D, Thilly WG. Bell-shaped nuclei dividing by symmetrical and asymmetrical nuclear fission have qualities of stem cells in human colonic embryogenesis and carcinogenesis. Cancer Genet Cytogenet 2006; 164: 16-24.

102. Grasl-Kraupp B, Ruttkay-Nedecky B, Koudelka H, Bukowska K, Bursch W, Schulte-Hermann R. *In situ* detection of fragmented DNA (TUNEL assay) fails to discriminate among apoptosis, necrosis, and autolytic cell death: a cautionary note. Hepatology 1995; 21: 1465-8.
103. Greeley T, Shumaker H, Wang Z, Schweinfest CW, Soleimani M. Downregulated in adenoma and putative anion transporter are regulated by CFTR in cultured pancreatic duct cells. Am J Physiol Gastrointest Liver Physiol 2001; 281: G1301-8.
104. Green SB, Meira LB, Bugni JM, Borenshtein D, Rickman BH, Rogers AB, Moroski CA, Schauer DB, Samson LD. Alkyl Adenine DNA Glycosylase (Aag) suppresses colon carcinogenesis associated with chronic inflammation, *submitted to PNAS*.
105. Gruenheid S, Sekirov I, Thomas NA, Deng W, O'Donnell P, Goode D, Li Y, Frey EA, Brown NF, Metalnikov P, Pawson T, Ashman K, Finlay BB. Identification and characterization of NleA, a non-LEE-encoded type III translocated virulence factor of enterohaemorrhagic *Escherichia coli* O157:H7. Mol Microbiol 2004; 51: 1233-49.
106. Guda K, Upender MB, Belinsky G, Flynn C, Nakanishi M, Marino JN, Ried T, Rosenberg DW. Carcinogen-induced colon tumors in mice are chromosomally stable and are characterized by low-level microsatellite instability. Oncogene 2004; 23: 3813-21.
107. Guttman JA, Li Y, Wickham ME, Deng W, Vogl AW, Finlay BB. Attaching and effacing pathogen-induced tight junction disruption *in vivo*. Cell Microbiol 2006a; 8: 634-45.
108. Guttman JA, Samji FN, Li Y, Deng W, Lin A, Finlay BB. Aquaporins contribute to diarrhoea caused by attaching and effacing bacterial pathogens. Cell Microbiol 2006b *In press*.
109. Guttman JA, Samji FN, Li Y, Vogl AW, Finlay BB. Evidence that tight junctions are disrupted due to intimate bacterial contact and not inflammation during attaching and effacing pathogen infection *in vivo*. Infect Immun. 2006c; 74: 6075-84.
110. Guyton AC, ed. Textbook of medical physiology. 8th ed. Philadelphia, W.B. Saunders Company, 1991: 264-8.
111. Hahm KB, Im YH, Parks TW, Park SH, Markowitz S, Jung HY, Green J, Kim SJ. Loss of transforming growth factor beta signalling in the intestine contributes to tissue injury in inflammatory bowel disease. Gut 2001; 49: 190-8.
112. Haila S, Saarialho-Kere U, Karjalainen-Lindsberg ML, Lohi H, Airola K, Holmberg C, Hastbacka J, Kere J, Hoglund P. The congenital chloride diarrhea gene is expressed in seminal vesicle, sweat gland, inflammatory colon epithelium, and in some dysplastic colon cells. Histochem Cell Biol 2000; 113: 279-86.
113. Halaihel N, Lievin V, Alvarado F, Vasseur M. Rotavirus infection impairs intestinal brush-border membrane Na(+)-solute cotransport activities in young rabbits. Am J Physiol Gastrointest Liver Physiol 2000a; 279: G587-96.
114. Halaihel N, Lievin V, Ball JM, Estes MK, Alvarado F, Vasseur M. Direct inhibitory effect of rotavirus NSP4(114-135) peptide on the Na(+)-D-glucose symporter of rabbit intestinal brush border membrane. J Virol 2000b; 74: 9464-70.
115. Hardie DC, Gregory TR, Hebert PD. From pixels to picograms: a beginners' guide to genome quantification by Feulgen image analysis densitometry. J Histochem Cytochem 2002; 50: 735-49.
116. Hardin JA, Wallace LE, Wong JF, O'Loughlin EV, Urbanski SJ, Gall DG, MacNaughton WK, Beck PL. Aquaporin expression is downregulated in a murine model of colitis and in patients with ulcerative colitis, Crohn's disease and infectious colitis. Cell Tissue Res 2004; 318: 313-23.
117. Hardwidge PR, Rodriguez-Escudero I, Goode D, Donohoe S, Eng J, Goodlett DR, Aebersold R, Finlay BB. Proteomic analysis of the intestinal epithelial cell response to enteropathogenic *Escherichia coli*. J Biol Chem. 2004; 279: 20127-36.
118. Hecht G, Hodges K, Gill RK, Kear F, Tyagi S, Malakooti J, Ramaswamy K, Dudeja PK. Differential regulation of Na+/H+ exchange isoform activities by enteropathogenic *E. coli* in human intestinal epithelial cells. Am J Physiol Gastrointest Liver Physiol 2004; 287: G370-8.
119. Hecht G. Innate mechanisms of epithelial host defense: spotlight on intestine. Am J Physiol 1999; 277: C351-8.
120. Hendrickson BA, Gokhale R, Cho JH. Clinical aspects and pathophysiology of inflammatory bowel disease. Clin Microbiol Rev 2002; 15: 79-94.
121. Higgins LM, Frankel G, Douce G, Dougan G, MacDonald TT. *Citrobacter rodentium* infection in mice elicits a mucosal Th1 cytokine response and lesions similar to those in murine inflammatory bowel disease. Infect Immun 1999; 67: 3031-9.

122. Ho SB. Cytoskeleton and other differentiation markers in the colon. J Cell Biochem Suppl 1992; 16G: 119-28.
123. Hofseth LJ, Khan MA, Ambrose M, Nikolayeva O, Xu-Welliver M, Kartalou M, Hussain SP, Roth RB, Zhou X, Mechanic LE, Zurer I, Rotter V, Samson LD, Harris CC. The adaptive imbalance in base excision-repair enzymes generates microsatellite instability in chronic inflammation. J Clin Invest 2003; 112: 1887-94.
124. Hoglund P, Haila S, Socha J, Tomaszewski L, Saarialho-Kere U, Karjalainen-Lindsberg ML, Airola K, Holmberg C, de la Chapelle A, Kere J. Mutations of the Down-regulated in adenoma (DRA) gene cause congenital chloride diarrhoea. Nat Genet 1996; 14: 316-9.
125. Holmberg C, Perheentupa J, Launiala K. Colonic electrolyte transport in health and in congenital chloride diarrhea. J Clin Invest 1975; 56: 302-10.
126. Hyer ML, Croxton R, Krajewska M, Krajewski S, Kress CL, Lu M, Suh N, Sporn MB, Cryns VL, Zapata JM, Reed JC. Synthetic triterpenoids cooperate with tumor necrosis factor-related apoptosis-inducing ligand to induce apoptosis of breast cancer cells. Cancer Res 2005; 65: 4799-808.
127. Iimura M, Gallo RL, Hase K, Miyamoto Y, Eckmann L, Kagnoff MF. Cathelicidin mediates innate intestinal defense against colonization with epithelial adherent bacterial pathogens. J Immunol 2005; 174: 4901-7.
128. Ilyas M, Straub J, Tomlinson IP, Bodmer WF. Genetic pathways in colorectal and other cancers. Eur J Cancer 1999; 35: 1986-2002.
129. Irizarry RA, Bolstad BM, Collin F, Cope LM, Hobbs B, Speed TP. Summaries of Affymetrix genechip probe level data. Nucleic Acids Res 2003; 31: e15.
130. Ishibashi Y, Maita H, Yano M, Koike N, Tamai K, Ariga H, Iguchi-Ariga SM. Pim-1 translocates sorting nexin 6/TRAF4-associated factor 2 from cytoplasm to nucleus. FEBS Lett 2001; 506: 33-8.
131. Itoh K, Maejima K, Ueda K, Fujiwara K. Difference in susceptibility of mice raised under barrier-sustained (SPF) or conventional conditions to infectious megaenteron. Microbiol Immunol 1979; 23: 909-13.
132. Itoh K, Maejima K, Ueda K, Fujiwara K. Effect of intestinal flora on megaenteron of mice. Microbiol Immunol 1978; 22: 661-72.
133. Itoh K, Matsui T, Tsuji K, Mitsuoka T, Ueda K. Genetic control in the susceptibility of germfree inbred mice to infection by *Escherichia coli* O115a,c:K(B). Infect Immun 1988; 56: 930-5.
134. Itoh K, Ueda K, Fujiwara K. Susceptibility of germ-free mice to infectious megaenteron. Microbiol Immunol 1980; 24: 281-90.
135. Itzkowitz SH, Yio X. Inflammation and cancer IV. Colorectal cancer in inflammatory bowel disease: the role of inflammation. Am J Physiol Gastrointest Liver Physiol 2004; 287: G7-17.
136. Jackson PE, O'Connor PJ, Cooper DP, Margison GP, Povey AC. Associations between tissue-specific DNA alkylation, DNA repair and cell proliferation in the colon and colon tumour yield in mice treated with 1,2-dimethylhydrazine. Carcinogenesis 2003; 24: 527-33.
137. Jaiswal M, LaRusso NF, Gores GJ. Nitric oxide in gastrointestinal epithelial cell carcinogenesis: linking inflammation to oncogenesis. Am J Physiol Gastrointest Liver Physiol 2001; 281: G626-34.
138. Jakate S, Demeo M, John R, Tobin M, Keshavarzian A. Mastocytic enterocolitis: increased mucosal mast cells in chronic intractable diarrhea. Arch Pathol Lab Med 2006; 130: 362-7.
139. Jass JR, Whitehall VL, Young J, Leggett BA. Emerging concepts in colorectal neoplasia. Gastroenterology 2002; 123: 862-76.
140. Johnson E, Barthold SW. The ultrastructure of transmissible murine colonic hyperplasia. Am J Pathol 1979; 97: 291-313.
141. Johnson-Henry KC, Nadjafi M, Avitzur Y, Mitchell DJ, Ngan BY, Galindo-Mata E, Jones NL, Sherman PM. Amelioration of the effects of *Citrobacter rodentium* infection in mice by pretreatment with probiotics. J Infect Dis 2005; 191: 2106-17.
142. Kelly M, Hart E, Mundy R, Marches O, Wiles S, Badea L, Luck S, Tauschek M, Frankel G, Robins-Browne RM, Hartland EL. Essential role of the type III secretion system effector NleB in colonization of mice by *Citrobacter rodentium*. Infect Immun 2006; 74: 2328-37.

143. Khan MA, Ma C, Knodler LA, Valdez Y, Rosenberger CM, Deng W, Finlay BB, Vallance BA. Toll-like receptor 4 contributes to colitis development but not to host defense during *Citrobacter rodentium* infection in mice. Infect Immun 2006; 74: 2522-36.
144. Klapproth JM, Sasaki M, Sherman M, Babbin B, Donnenberg MS, Fernandes PJ, Scaletsky IC, Kalman D, Nusrat A, Williams IR. *Citrobacter rodentium lifA/efa1* is essential for colonic colonization and crypt cell hyperplasia *in vivo*. Infect Immun 2005; 73: 1441-51.
145. Klapproth JM, Scaletsky IC, McNamara BP, Lai LC, Malstrom C, James SP, Donnenberg MS. A large toxin from pathogenic *Escherichia coli* strains that inhibits lymphocyte activation. Infect Immun 2000; 68: 2148-55.
146. Knoops L, Louahed J, Van Snick J, Renauld JC. IL-9 promotes but is not necessary for systemic anaphylaxis. J Immunol 2005; 175: 335-41.
147. Ko SB, Shcheynikov N, Choi JY, Luo X, Ishibashi K, Thomas PJ, Kim JY, Kim KH, Lee MG, Naruse S, Muallem S. A molecular mechanism for aberrant CFTR-dependent HCO(3)(-) transport in cystic fibrosis. EMBO J 2002; 21: 5662-72.
148. Ko SB, Zeng W, Dorwart MR, Luo X, Kim KH, Millen L, Goto H, Naruse S, Soyombo A, Thomas PJ, Muallem S. Gating of CFTR by the STAS domain of SLC26 transporters. Nat Cell Biol 2004; 6: 343-50.
149. Kohonen-Corish MR, Daniel JJ, te Riele H, Buffinton GD, Dahlstrom JE. Susceptibility of *Msh2*-deficient mice to inflammation-associated colorectal tumors. Cancer Res 2002; 62: 2092-7.
150. Kolachala V, Asamoah V, Wang L, Obertone TS, Ziegler TR, Merlin D, Sitaraman SV. TNF-alpha upregulates adenosine 2b (A2b) receptor expression and signaling in intestinal epithelial cells: a basis for A2bR overexpression in colitis. Cell Mol Life Sci 2005a; 62: 2647-57.
151. Kolachala V, Asamoah V, Wang L, Srinivasan S, Merlin D, Sitaraman SV. Interferon-gamma down-regulates adenosine 2b receptor-mediated signaling and short circuit current in the intestinal epithelia by inhibiting the expression of adenylate cyclase. J Biol Chem 2005b; 280: 4048-57.
152. Kordasti S, Istrate C, Banasaz M, Rottenberg M, Sjovall H, Lundgren O, Svensson L. Rotavirus infection is not associated with small intestinal fluid secretion in the adult mouse. J Virol 2006; 80: 11355-61
153. Kosek M, Bern C, Guerrant RL. The global burden of diarrhoeal disease, as estimated from studies published between 1992 and 2000. Bull World Health Organ 2003; 81: 197-204.
154. Kunzelmann K, Mall M. Electrolyte transport in the mammalian colon: mechanisms and implications for disease. Physiol Rev 2002; 82: 245-89.
155. Lamprecht G, Heil A, Baisch S, Lin-Wu E, Yun CC, Kalbacher H, Gregor M, Seidler U. The down regulated in adenoma (dra) gene product binds to the second PDZ domain of the NHE3 kinase A regulatory protein (E3KARP), potentially linking intestinal Cl-/HCO3- exchange to Na+/H+ exchange. Biochemistry 2002; 41: 12336-42.
156. Lamprecht G, Schaefer J, Dietz K, Gregor M. Chloride and bicarbonate have similar affinities to the intestinal anion exchanger DRA (down regulated in adenoma). Pflugers Arch 2006a; 452: 307-15.
157. Lamprecht G, Seidler U. The emerging role of PDZ adapter proteins for regulation of intestinal ion transport. Am J Physiol Gastrointest Liver Physiol 2006b; 291: G766-77.
158. Laval F, Wink DA. Inhibition by nitric oxide of the repair protein, O6-methylguanine-DNA-methyltransferase. Carcinogenesis 1994; 15: 443-7.
159. Lawrance IC, Fiocchi C, Chakravarti S. Ulcerative colitis and Crohn's disease: distinctive gene expression profiles and novel susceptibility candidate genes. Hum Mol Genet 2001; 10: 445-56.
160. Lengauer C, Kinzler KW, Vogelstein B. Genetic instabilities in human cancers. Nature. 1998; 396: 643-9.
161. Li C, Wong WH. DNA-Chip Analyzer (dChip). *In:* The analysis of gene expression data: methods and software. Parmigiani G, Garrett ES, Irizarry R, Zeger SL, eds. Springer, 2003.
162. Li C, Wong WH. Model-based analysis of oligonucleotide arrays: expression index computation and outlier detection. Proc Natl Acad Sci U S A. 2001a; 98(1):31-6.
163. Li C, Wong WH. Model-based analysis of oligonucleotide arrays: model validation, design issues and standard error application. Genome Biol 2001b; 2: research0032.1-11
164. Li CK, Pender SL, Pickard KM, Chance V, Holloway JA, Huett A, Goncalves NS, Mudgett JS, Dougan G, Frankel G, MacDonald TT. Impaired immunity to intestinal bacterial infection in stromelysin-1 (matrix metalloproteinase-3)-deficient mice. J Immunol 2004; 173: 5171-9.

165. Liby K, Hock T, Yore MM, Suh N, Place AE, Risingsong R, Williams CR, Royce DB, Honda T, Honda Y, Gribble GW, Hill-Kapturczak N, Agarwal A, Sporn MB. The synthetic triterpenoids, CDDO and CDDO-imidazolide, are potent inducers of heme oxygenase-1 and Nrf2/ARE signaling. Cancer Res 2005; 65: 4789-98.
166. Lindblom A. Different mechanisms in the tumorigenesis of proximal and distal colon cancers. Curr Opin Oncol 2001; 13: 63-9.
167. Lipkin SM, Wang V, Jacoby R, Banerjee-Basu S, Baxevanis AD, Lynch HT, Elliott RM, Collins FS. MLH3: a DNA mismatch repair gene associated with mammalian microsatellite instability. Nat Genet 2000; 24: 27-35.
168. Liu L, Xu-Welliver M, Kanugula S, Pegg AE. Inactivation and degradation of O(6)-alkylguanine-DNA alkyltransferase after reaction with nitric oxide. Cancer Res 2002; 62: 3037-43.
169. Lopez AD, Mathers CD, Ezzati M, Jamison DT, Murray CJ. Global and regional burden of disease and risk factors, 2001: systematic analysis of population health data. Lancet 2006; 367: 1747-57.
170. Luperchio SA, Newman JV, Dangler CA, Schrenzel MD, Brenner DJ, Steigerwalt AG, Schauer DB. *Citrobacter rodentium*, the causative agent of transmissible murine colonic hyperplasia, exhibits clonality: synonymy of *C. rodentium* and mouse-pathogenic *Escherichia coli*. J Clin Microbiol 2000; 38: 4343-50.
171. Luperchio SA, Schauer DB. Molecular pathogenesis of *Citrobacter rodentium* and transmissible murine colonic hyperplasia. Microbes Infect 2001; 3: 333-40.
172. Ma C, Wickham ME, Guttman JA, Deng W, Walker J, Madsen KL, Jacobson K, Vogl WA, Finlay BB, Vallance BA. *Citrobacter rodentium* infection causes both mitochondrial dysfunction and intestinal epithelial barrier disruption *in vivo*: role of mitochondrial associated protein (Map). Cell Microbiol 2006; 8: 1669-86.
173. Ma T, Verkman AS. Aquaporin water channels in gastrointestinal physiology. J Physiol 1999; 517: 317-26.
174. Maaser C, Housley MP, Iimura M, Smith JR, Vallance BA, Finlay BB, Schreiber JR, Varki NM, Kagnoff MF, Eckmann L. Clearance of *Citrobacter rodentium* requires B cells but not secretory immunoglobulin A (IgA) or IgM antibodies. Infect Immun 2004; 72: 3315-24.
175. MacDonald TT, Frankel G, Dougan G, Goncalves NS, Simmons C. Host defences to *Citrobacter rodentium*. Int J Med Microbiol 2003; 293: 87-93.
176. Madara JL, Patapoff TW, Gillece-Castro B, Colgan SP, Parkos CA, Delp C, Mrsny RJ. 5'-adenosine monophosphate is the neutrophil-derived paracrine factor that elicits chloride secretion from T84 intestinal epithelial cell monolayers. J Clin Invest 1993; 91: 2320-5.
177. Maggio-Price L, Nicholson KL, Kline KM, Birkebak T, Suzuki I, Wilson DL, Schauer D, Fink PJ. Diminished reproduction, failure to thrive, and altered immunologic function in a colony of T-cell receptor transgenic mice: possible role of *Citrobacter rodentium*. Lab Anim Sci 1998; 48: 145-55.
178. Makela S, Kere J, Holmberg C, Hoglund P. SLC26A3 mutations in congenital chloride diarrhea. Hum Mutat 2002; 20: 425-38.
179. Malstrom C, James S. Inhibition of murine splenic and mucosal lymphocyte function by enteric bacterial products. Infect Immun 1998; 66: 3120-7.
180. Mariadason JM, Nicholas C, L'Italien KE, Zhuang M, Smartt HJ, Heerdt BG, Yang W, Corner GA, Wilson AJ, Klampfer L, Arango D, Augenlicht LH. Gene expression profiling of intestinal epithelial cell maturation along the crypt-villus axis. Gastroenterology 2005; 128: 1081-8.
181. Marquardt DL, Gruber HE, Wasserman SI. Adenosine release from stimulated mast cells. Proc Natl Acad Sci U S A 1984; 81: 6192-6.
182. Matsuzaki T, Tajika Y, Ablimit A, Aoki T, Hagiwara H, Takata K. Aquaporins in the digestive system. Med Electron Microsc 2004; 37: 71-80.
183. McDermott JR, Bartram RE, Knight PA, Miller HR, Garrod DR, Grencis RK. Mast cells disrupt epithelial barrier function during enteric nematode infection. Proc Natl Acad Sci U S A 2003; 100: 7761-6.
184. McSwine RL, Musch MW, Bookstein C, Xie Y, Rao M, Chang EB. Regulation of apical membrane Na+/H+ exchangers NHE2 and NHE3 in intestinal epithelial cell line C2/bbe. Am J Physiol 1998; 275: C693-701.
185. Mello PM, Sharma VK, Dellinger RP. Shock overview. Semin Respir Crit Care Med 2004; 25: 619-28.

186. Melvin JE, Park K, Richardson L, Schultheis PJ, and Shull GE. Mouse down-regulated in adenoma (DRA) is an intestinal Cl-/ exchanger and is up-regulated in colon of mice lacking the NHE3 Na+/H+ exchanger. J Biol Chem 1999; 274: 22855-61.
187. Meneton P, Schultheis PJ, Greeb J, Nieman ML, Liu LH, Clarke LL, Duffy JJ, Doetschman T, Lorenz JN, Shull GE. Increased sensitivity to K+ deprivation in colonic H,K-ATPase-deficient mice. J Clin Invest 1998; 101: 536-42.
188. Meredith D, Boyd CA. Structure and function of eukaryotic peptide transporters. Cell Mol Life Sci 2000; 57: 754-78.
189. Minns LA, Buzoni-Gatel D, Ely KH, Rachinel N, Luangsay S, Kasper LH. A novel triterpenoid induces transforming growth factor beta production by intraepithelial lymphocytes to prevent ileitis. Gastroenterology 2004; 127: 119-26.
190. Mizoguchi E, Xavier RJ, Reinecker HC, Uchino H, Bhan AK, Podolsky DK, Mizoguchi A. Colonic epithelial functional phenotype varies with type and phase of experimental colitis. Gastroenterology 2003; 125: 148-61.
191. Morris AP, Scott JK, Ball JM, Zeng CQ, O'Neal WK, Estes MK. NSP4 elicits age-dependent diarrhea and Ca(2+)mediated I(-) influx into intestinal crypts of CF mice. Am J Physiol 1999; 277: G431-44.
192. Muller T, Wijmenga C, Phillips AD, Janecke A, Houwen RH, Fischer H, Ellemunter H, Fruhwirth M, Offner F, Hofer S, Muller W, Booth IW, Heinz-Erian P. Congenital sodium diarrhea is an autosomal recessive disorder of sodium/proton exchange but unrelated to known candidate genes. Gastroenterology 2000; 119:1506–13
193. Mundy R, Girard F, Fitzgerald AJ, Frankel G. Comparison of colonization dynamics and pathology of mice infected with enteropathogenic *Escherichia coli*, enterohaemorrhagic *E. coli* and *Citrobacter rodentium*. FEMS Microbiol Lett 2006.
194. Mundy R, MacDonald TT, Dougan G, Frankel G, Wiles S. *Citrobacter rodentium* of mice and man. Cell Microbiol 2005; 7: 1697-706.
195. Mundy R, Pickard D, Wilson RK, Simmons CP, Dougan G, Frankel G. Identification of a novel type IV pilus gene cluster required for gastrointestinal colonization of *Citrobacter rodentium*. Mol Microbiol 2003; 48: 795-809.
196. Muto T, Nakagawa M, Isobe Y, Saito M, Nakano T. Infectious megaenteron of mice. I. Manifestation and pathological observation. Jpn J Med Sci Biol 1969; 22: 363-74.
197. Nagai T, Abe A, Sasakawa C. Targeting of enteropathogenic *Escherichia coli* EspF to host mitochondria is essential for bacterial pathogenesis: critical role of the 16th leucine residue in EspF. J Biol Chem 2005; 280: 2998-3011.
198. Nakagawa M, Sakazaki R, Muto T, Saito M, Hagiwara T. Infectious megaenteron of mice. II. Detection of coliform organisms of an unusual biotype as the primary cause. Jpn J Med Sci Biol 1969; 22:375-82.
199. Nataro JP, Kaper JB. Diarrheagenic *Escherichia coli*. Clin Microbiol Rev 1998; 11: 142-201.
200. Nestler EJ, Hyman SE. Regulation of gene expression. *In*: Fifth Generation of Progress. Davis KL, Charney DS, Coyle JT, Nemeroff C, eds. New York: Lippincott Williams and Wilkins, 2002: 217-28.
201. Newman JV, Kosaka T, Sheppard BJ, Fox JG, Schauer DB. Bacterial infection promotes colon tumorigenesis in Apc(Min/+) mice. J Infect Dis 2001; 184: 227-30.
202. Newman JV, Zabel BA, Jha SS, Schauer DB. *Citrobacter rodentium* espB is necessary for signal transduction and for infection of laboratory mice. Infect Immun 1999; 67: 6019-25.
203. Nowak MA, Komarova NL, Sengupta A, Jallepalli PV, Shih IeM, Vogelstein B, Lengauer C. The role of chromosomal instability in tumor initiation. Proc Natl Acad Sci U S A 2002; 99: 16226-31.
204. Okuda J, Fukumoto M, Takeda Y, Nishibuchi M. Examination of diarrheagenicity of cytolethal distending toxin: suckling mouse response to the products of the cdtABC genes of *Shigella dysenteriae*. Infect Immun 1997; 65: 428-33.
205. Okutani A, Tobe T, Sasakawa C, Nozu R, Gotoh K, Takakura A, Itoh T, Miyamoto Y, Itoh K. Comparison of bacteriological, genetic and pathological characters between *Escherichia coli* O115a,c:K(B) and *Citrobacter rodentium*. Exp Anim 2001; 50: 183-6.
206. Pang T, Su X, Wakabayashi S, Shigekawa M. Calcineurin homologous protein as an essential cofactor for Na+/H+ exchangers. J Biol Chem 2001; 276:17367–72

207. PE Applied Biosystems: ABI Prism 7700 Sequence Detection System: Relative quantitation of gene expression. User bulletin #2 Norwalk, CT Perkin-Elmer Corp., 1997: 36.
208. Place AE, Suh N, Williams CR, Risingsong R, Honda T, Honda Y, Gribble GW, Leesnitzer LM, Stimmel JB, Willson TM, Rosen E, Sporn MB. The novel synthetic triterpenoid, CDDO-imidazolide, inhibits inflammatory response and tumor growth *in vivo*. Clin Cancer Res 2003; 9: 2798-806.
209. Povey AC, Badawi AF, Cooper DP, Hall CN, Harrison KL, Jackson PE, Lees NP, O'Connor PJ, Margison GP. DNA alkylation and repair in the large bowel: animal and human studies. J Nutr 2002; 132: 3518S-21S.
210. Powrie F. Immune regulation in the intestine: a balancing act between effector and regulatory T cell responses. Ann N Y Acad Sci 2004; 1029: 132-41.
211. Purkerson JM, Schwartz GJ. Expression of membrane-associated carbonic anhydrase isoforms IV, IX, XII, and XIV in the rabbit: induction of CA IV and IX during maturation. Am J Physiol Regul Integr Comp Physiol 2005; 288: R1256-63.
212. Qin X, Shibata D, Gerson SL. Heterozygous DNA mismatch repair gene *PMS2*-knockout mice are susceptible to intestinal tumor induction with N-methyl-N-nitrosourea. Carcinogenesis 2000; 21: 833-8.
213. Reichling T, Goss KH, Carson DJ, Holdcraft RW, Ley-Ebert C, Witte D, Aronow BJ, Groden J. Transcriptional profiles of intestinal tumors in Apc(Min) mice are unique from those of embryonic intestine and identify novel gene targets dysregulated in human colorectal tumors. Cancer Res 2005; 65: 166-76.
214. Renehan AG, O'Dwyer ST, Haboubi NJ, Potten CS. Early cellular events in colorectal carcinogenesis. Colorectal Dis 2002; 4: 76-89.
215. Renes IB, Verburg M, Van Nispen DJ, Taminiau JA, Buller HA, Dekker J, Einerhand AW. Epithelial proliferation, cell death, and gene expression in experimental colitis: alterations in carbonic anhydrase I, mucin MUC2, and trefoil factor 3 expression. Int J Colorectal Dis 2002; 17: 317-26.
216. Riddell RH, Goldman H, Ransohoff DF, Appelman HD, Fenoglio CM, Haggitt RC, Ahren C, Correa P, Hamilton SR, Morson BC, Sommers SC, Yardley JH. Dysplasia in inflammatory bowel disease: standardized classification with provisional clinical applications. Hum Pathol 1983; 14: 931-68.
217. Rijnierse A, Koster AS, Nijkamp FP, Kraneveld AD. Critical role for mast cells in the pathogenesis of 2,4-dinitrobenzene-induced murine colonic hypersensitivity reaction. J Immunol 2006; 176: 4375-84.
218. Rosati B, Grau F, Kuehler A, Rodriguez S, McKinnon D. Comparison of different probe-level analysis techniques for oligonucleotide microarrays. Biotechniques 2004; 36: 316-22.
219. Rutter M, Saunders B, Wilkinson K, Rumbles S, Schofield G, Kamm M, Williams C, Price A, Talbot I, Forbes A. Severity of inflammation is a risk factor for colorectal neoplasia in ulcerative colitis. Gastroenterology 2004; 126: 451-9.
220. Sandle GI. Pathogenesis of diarrhea in ulcerative colitis: new views on an old problem. J Clin Gastroenterol 2005; 39: S49-52.
221. Santos RL, Tsolis RM, Baumler AJ, Adams LG. Pathogenesis of *Salmonella*-induced enteritis. Braz J Med Biol Res 2003; 36: 3-12.
222. Sartor RB. Review article: How relevant to human inflammatory bowel disease are current animal models of intestinal inflammation? Aliment Pharmacol Ther 1997; 11: 89-96.
223. Savkovic SD, Villanueva J, Turner JR, Matkowskyj KA, Hecht G. Mouse model of enteropathogenic *Escherichia coli* infection. Infect Immun 2005; 73: 1161-70.
224. Schauer DB, Falkow S. Attaching and effacing locus of a *Citrobacter freundii* biotype that causes transmissible murine colonic hyperplasia. Infect Immun 1993a; 61: 2486-92.
225. Schauer DB, Falkow S. The eae gene of *Citrobacter freundii* biotype 4280 is necessary for colonization in transmissible murine colonic hyperplasia. Infect Immun. 1993b; 61: 4654-61.
226. Schuermann M, Jooss K, Muller R. fosB is a transforming gene encoding a transcriptional activator. Oncogene 1991; 6: 567-76.
227. Schultheis PJ, Clarke LL, Meneton P, Harline M, Boivin GP, Stemmermann G, Duffy JJ, Doetschman T, Miller ML, Shull GE. Targeted disruption of the murine Na+/H+ exchanger

isoform 2 gene causes reduced viability of gastric parietal cells and loss of net acid secretion. J Clin Invest 1998a; 101: 1243-53.
228. Schultheis PJ, Clarke LL, Meneton P, Miller ML, Soleimani M, Gawenis LR, Riddle TM, Duffy JJ, Doetschman T, Wang T, Giebisch G, Aronson PS, Lorenz JN, Shull GE. Renal and intestinal absorptive defects in mice lacking the NHE3 Na+/H+ exchanger. Nat Genet 1998b; 19: 282-5.
229. Schweinfest CW, Spyropoulos DS, Henderson KW, Ho-Kim J, Chapman JM, Barone S, Worrell RT, Wang Z, Soleimani M. SLC26a3 (DRA) deficient mice display chloride losing diarrhea, enhanced colonic proliferation and distinct upregulation of ion transporters in the colon. J Biol Chem 2006; 281: 37962-71.
230. Seidler U, Lenzen H, Cinar A, Tessema T, Bleich A, Riederer B. Molecular mechanisms of disturbed electrolyte transport in intestinal inflammation. Ann N Y Acad Sci 2006; 1072: 262-75.
231. Sellin JH, Umar S, Xiao J, Morris AP. Increased beta-catenin expression and nuclear translocation accompany cellular hyperproliferation *in vivo*. Cancer Res 2001; 61: 2899-906.
232. Shen H, Smith DE, Brosius FC 3rd. Developmental expression of PEPT1 and PEPT2 in rat small intestine, colon, and kidney. Pediatr Res 2001; 49: 789-95.
233. Shifflett DE, Clayburgh DR, Koutsouris A, Turner JR, Hecht GA. Enteropathogenic *E. coli* disrupts tight junction barrier function and structure in vivo. Lab Invest 2005; 85: 1308-24.
234. Shih IM, Zhou W, Goodman SN, Lengauer C, Kinzler KW, Vogelstein B. Evidence that genetic instability occurs at an early stage of colorectal tumorigenesis. Cancer Res 2001; 61: 818-22.
235. Shimamura T, Tazume S, Hashimoto K, Sasaki S. Experimental cholera in germfree suckling mice. Infect Immun 1981; 34: 296-8.
236. Silverman J, Chavannes JM, Rigotty J, Ornaf M. A natural outbreak of transmissible murine colonic hyperplasia in A/J mice. Lab Anim Sci 1979; 29: 209-13.
237. Simmons CP, Clare S, Ghaem-Maghami M, Uren TK, Rankin J, Huett A, Goldin R, Lewis DJ, MacDonald TT, Strugnell RA, Frankel G, Dougan G. Central role for B lymphocytes and CD4+ T cells in immunity to infection by the attaching and effacing pathogen *Citrobacter rodentium.* Infect Immun 2003; 71: 5077-86.
238. Simmons CP, Goncalves NS, Ghaem-Maghami M, Bajaj-Elliott M, Clare S, Neves B, Frankel G, Dougan G, MacDonald TT. Impaired resistance and enhanced pathology during infection with a noninvasive, attaching-effacing enteric bacterial pathogen, *Citrobacter rodentium*, in mice lacking IL-12 or IFN-gamma. J Immunol 2002; 168: 1804-12.
239. Simpson JE, Gawenis LR, Walker NM, Boyle KT, Clarke LL. Chloride conductance of CFTR facilitates basal Cl-/HCO3- exchange in the villous epithelium of intact murine duodenum. Am J Physiol Gastrointest Liver Physiol 2005; 288: G1241-51.
240. Simpson N, Shaw R, Crepin VF, Mundy R, FitzGerald AJ, Cummings N, Straatman-Iwanowska A, Connerton I, Knutton S, Frankel G. The enteropathogenic *Escherichia coli* type III secretion system effector Map binds EBP50/NHERF1: implication for cell signalling and diarrhoea. Mol Microbiol 2006; 60: 349-63.
241. Singer M, Sansonetti PJ. IL-8 is a key chemokine regulating neutrophil recruitment in a new mouse model of *Shigella*-induced colitis. J Immunol 2004; 173: 4197-206.
242. Smyth GK Limma: Linear models for microarray data. *In:* Gentleman R, Carey V, Dudoit S, Irizarry RA, Huber W, eds. Bioinformatics and computational biology solutions using R and bioconductor. New York: Springer, 2005: 397.
243. Sohn JJ. Intestinal cancer: linking infection, inflammation and neoplasia. Ph.D thesis, Massachusetts Institute of Technology, Cambridge, MA, United States, 2005.
244. Sohn KJ, Shah SA, Reid S, Choi M, Carrier J, Comiskey M, Terhorst C, Kim YI. Molecular genetics of ulcerative colitis-associated colon cancer in the interleukin 2- and beta(2)-microglobulin-deficient mouse. Cancer Res 2001; 61: 6912-7.
245. Song J, Sohn KJ, Medline A, Ash C, Gallinger S, Kim YI. Chemopreventive effects of dietary folate on intestinal polyps in Apc+/-Msh2-/- mice. Cancer Res 2000; 60: 3191-9.
246. Spahn TW, Maaser C, Eckmann L, Heidemann J, Lugering A, Newberry R, Domschke W, Herbst H, Kucharzik T. The lymphotoxin-beta receptor is critical for control of murine *Citrobacter rodentium*-induced colitis. Gastroenterology 2004; 127: 1463-73.
247. Spicer Z, Clarke LL, Gawenis LR, Shull GE. Colonic H(+)-K(+)-ATPase in K(+) conservation and electrogenic Na(+) absorption during Na(+) restriction. Am J Physiol Gastrointest Liver Physiol 2001; 281: G1369-77.

248. Stadelmann C, Lassmann H. Detection of apoptosis in tissue sections. Cell Tissue Res 2000; 301: 19-31.
249. Sterling D, Alvarez BV, Casey JR. The extracellular component of a transport metabolon. Extracellular loop 4 of the human AE1 Cl-/HCO3- exchanger binds carbonic anhydrase IV. J Biol Chem 2002; 277: 25239-46.
250. Stewart AK, Boyd CA, Vaughan-Jones RD. A novel role for carbonic anhydrase: cytoplasmic pH gradient dissipation in mouse small intestinal enterocytes. J Physiol 1999; 516: 209-17.
251. Strohmeier GR, Reppert SM, Lencer WI, Madara JL. The A2b adenosine receptor mediates cAMP responses to adenosine receptor agonists in human intestinal epithelia. J Biol Chem 1995; 270: 2387-94.
252. Sturlan S, Oberhuber G, Beinhauer BG, Tichy B, Kappel S, Wang J, Rogy MA. Interleukin-10-deficient mice and inflammatory bowel disease associated cancer development. Carcinogenesis 2001; 22: 665-71.
253. Suh N, Honda T, Finlay HJ, Barchowsky A, Williams C, Benoit NE, Xie QW, Nathan C, Gribble GW, Sporn MB. Novel triterpenoids suppress inducible nitric oxide synthase (iNOS) and inducible cyclooxygenase (COX-2) in mouse macrophages. Cancer Res 1998; 58: 717-23.
254. Taketo M, Schroeder AC, Mobraaten LE, Gunning KB, Hanten G, Fox RR, Roderick TH, Stewart CL, Lilly F, Hansen CT, et al. FVB/N: an inbred mouse strain preferable for transgenic analyses. Proc Natl Acad Sci U S A 1991; 88: 2065-9.
255. Tang JC, Ho FC, Chan AC, Srivastava G. Clonality of lymphomas at multiple sites in SJL mice. Lab Invest 1998; 78: 205-12.
256. Tatsuno I, Mundy R, Frankel G, Chong Y, Phillips AD, Torres AG, Kaper JB. The lpf gene cluster for long polar fimbriae is not involved in adherence of enteropathogenic *Escherichia coli* or virulence of *Citrobacter rodentium*. Infect Immun 2006; 74: 265-72.
257. Thwaites DT, Ford D, Glanville M, Simmons NL. H(+)/solute-induced intracellular acidification leads to selective activation of apical Na(+)/H(+) exchange in human intestinal epithelial cells. J Clin Invest 1999; 104: 629-35.
258. Tobe T, Beatson SA, Taniguchi H, Abe H, Bailey CM, Fivian A, Younis R, Matthews S, Marches O, Frankel G, Hayashi T, Pallen MJ. An extensive repertoire of type III secretion effectors in *Escherichia coli* O157 and the role of lambdoid phages in their dissemination. Proc Natl Acad Sci U S A 2006; 103: 14941-6.
259. Toivola DM, Krishnan S, Binder HJ, Singh SK, Omary MB. Keratins modulate colonocyte electrolyte transport via protein mistargeting. J Cell Biol 2004; 164: 911-21.
260. Turi JL, Jaspers I, Dailey LA, Madden MC, Brighton LE, Carter JD, Nozik-Grayck E, Piantadosi CA, Ghio AJ. Oxidative stress activates anion exchange protein 2 and AP-1 in airway epithelial cells. Am J Physiol Lung Cell Mol Physiol 2002; 283: L791-8.
261. Ullman T, Croog V, Harpaz N, Sachar D, Itzkowitz S. Progression of flat low-grade dysplasia to advanced neoplasia in patients with ulcerative colitis. Gastroenterology 2003; 125: 1311-9.
262. Umar S, Morris AP, Kourouma F, Sellin JH. Dietary pectin and calcium inhibit colonic proliferation *in vivo* by differing mechanisms. Cell Prolif 2003; 36: 361-75.
263. Umar S, Scott J, Sellin JH, Dubinsky WP, Morris AP. Murine colonic mucosal hyperproliferation. I. Elevated CFTR expression and enhanced cAMP-dependent Cl-secretion. Am J Physiol Gastrointest Liver Physiol 2000; 278: G753-64.
264. Vallance BA, Deng W, De Grado M, Chan C, Jacobson K, Finlay BB. Modulation of inducible nitric oxide synthase expression by the attaching and effacing bacterial pathogen *Citrobacter rodentium* in infected mice. Infect Immun 2002a; 70: 6424-35.
265. Vallance BA, Deng W, Jacobson K, Finlay BB. Host Susceptibility to the Attaching and Effacing Bacterial Pathogen *Citrobacter rodentium*. Infect Immun 2003; 71: 3443-53.
266. Vallance BA, Deng W, Knodler LA, Finlay BB. Mice lacking T and B lymphocytes develop transient colitis and crypt hyperplasia yet suffer impaired bacterial clearance during *Citrobacter rodentium* infection. Infect Immun 2002b; 70: 2070-81.
267. Vallance BA, Finlay BB. Exploitation of host cells by enteropathogenic *Escherichia coli*. Proc Natl Acad Sci U S A 2000; 97: 8799-806.
268. Varcoe JJ, Krejcarek G, Busta F, Brady L. Prophylactic feeding of *Lactobacillus acidophilus* NCFM to mice attenuates overt colonic hyperplasia. J Food Prot 2003; 66: 457-65.
269. Vidyasagar S, Barmeyer C, Geibel J, Binder HJ, Rajendran VM. Role of short-chain fatty acids in

colonic HCO(3) secretion. Am J Physiol Gastrointest Liver Physiol 2005; 288: G1217-26.
270. Wali RK, Skarosi S, Hart J, Zhang Y, Dolan ME, Moschel RC, Nguyen L, Mustafi R, Brasitus TA, Bissonnette M. Inhibition of O(6)-methylguanine-DNA methyltransferase increases azoxymethane-induced colonic tumors in rats. Carcinogenesis 1999; 20: 2355-60.
271. Wang KS, Ma T, Filiz F, Verkman AS, Bastidas JA. Colon water transport in transgenic mice lacking aquaporin-4 water channels. Am J Physiol Gastrointest Liver Physiol 2000; 279: G463-70.
272. Wang L, Kolachala V, Walia B, Balasubramanian S, Hall RA, Merlin D, Sitaraman SV. Agonist-induced polarized trafficking and surface expression of the adenosine 2b receptor in intestinal epithelial cells: role of SNARE proteins. Am J Physiol Gastrointest Liver Physiol 2004; 287: G1100-7.
273. Wei OL, Hilliard A, Kalman D, Sherman M. Mast cells limit systemic bacterial dissemination but not colitis in response to *Citrobacter rodentium*. Infect Immun 2005; 73: 1978-85.
274. Wheat VJ, Shumaker H, Burnham C, Shull GE, Yankaskas JR, Soleimani M. CFTR induces the expression of DRA along with Cl(-)/HCO(3)(-) exchange activity in tracheal epithelial cells. Am J Physiol Cell Physiol 2000; 279: C62-71.
275. Whitehead GS, Walker JK, Berman KG, Foster WM, Schwartz DA. Allergen-induced airway disease is mouse strain dependent. Am J Physiol Lung Cell Mol Physiol 2003; 285: L32-42.
276. WHO. The world health report 1999: making a difference. Geneva: World Health Organization, 1999. http://www.who.int/whr/1999/en/index.html
277. Wieler LH, Vieler E, Erpenstein C, Schlapp T, Steinruck H, Bauerfeind R, Byomi A, Baljer G. Shiga toxin-producing *Escherichia coli* strains from bovines: association of adhesion with carriage of eae and other genes. J Clin Microbiol 1996; 34: 2980-4.
278. Wiles S, Clare S, Harker J, Huett A, Young D, Dougan G, Frankel G. Organ specificity, colonization and clearance dynamics *in vivo* following oral challenges with the murine pathogen *Citrobacter rodentium*. Cell Microbiol 2004; 6: 963-72.
279. Yang B, Song Y, Zhao D, Verkman AS. Phenotype analysis of aquaporin-8 null mice. Am J Physiol Cell Physiol 2005; 288: C1161-70.
280. Yates MS, Kwak MK, Egner PA, Groopman JD, Bodreddigari S, Sutter TR, Baumgartner KJ, Roebuck BD, Liby KT, Yore MM, Honda T, Gribble GW, Sporn MB, Kensler TW. Potent protection against aflatoxin-induced tumorigenesis through induction of Nrf2-regulated pathways by the triterpenoid 1-[2-cyano-3-,12-dioxooleana-1,9(11)-dien-28-oyl]imidazole. Cancer Res 2006; 66: 2488-94.
281. Yoon T, Kim M, Lee K. Inhibition of Na,K-ATPase-suppressive activity of translationally controlled tumor protein by sorting nexin 6. FEBS Lett 2006; 580: 3558-64.
282. Yoshimoto T, Bendelac A, Hu-Li J, Paul WE. Defective IgE production by SJL mice is linked to the absence of CD4+, NK1.1+ T cells that promptly produce interleukin 4. Proc Natl Acad Sci U S A 1995; 92: 11931-4.
283. Young VB, Knox KA, Pratt JS, Cortez JS, Mansfield LS, Rogers AB, Fox JG, Schauer DB. In vitro and in vivo characterization of Helicobacter hepaticus cytolethal distending toxin mutants. Infect Immun 2004; 72: 2521-7.
284. Yun CH, Oh S, Zizak M, Steplock D, Tsao S, Tse CM, Weinman EJ, Donowitz M. cAMP-mediated inhibition of the epithelial brush border Na+/H+ exchanger, NHE3, requires an associated regulatory protein. Proc Natl Acad Sci USA 1997; 94: 3010–15.
285. Zachos NC, Tse M, Donowitz M. Molecular physiology of intestinal Na+/H+ exchange. Annu Rev Physiol 2005; 67: 411-43.
286. Zhang S, Kingsley RA, Santos RL, Andrews-Polymenis H, Raffatellu M, Figueiredo J, Nunes J, Tsolis RM, Adams LG, Baumler AJ. Molecular pathogenesis of *Salmonella enterica* serotype typhimurium-induced diarrhea. Infect Immun 2003; 71: 1-12.
287. Zyrek AA, Cichon C, Helms S, Enders C, Sonnenborn U, Schmidt MA. Molecular mechanisms underlying the probiotic effects of *Escherichia coli* Nissle 1917 involve ZO-2 and PKCzeta redistribution resulting in tight junction and epithelial barrier repair. Cell Microbiol 2006.